

AD-766 932

THE ANALYSIS AND DESIGN OF COMPOSITE
MATERIAL BONDED JOINTS UNDER STATIC
AND FATIGUE LOADINGS

W. James Renton, et al

Delaware University

Prepared for:

Air Force Office of Scientific Research

August 1973

DISTRIBUTED BY:

NTIS

National Technical Information Service
U. S. DEPARTMENT OF COMMERCE
5285 Port Royal Road, Springfield Va. 22151

AFOSR SCIENTIFIC REPORT

MAE TR 169

AFOSR **AFOSR - TR - 78 - 1627**

AD 766933

THE ANALYSIS AND DESIGN OF
COMPOSITE MATERIAL BONDED JOINTS
UNDER STATIC AND FATIGUE LOADINGS

W. James Renton

Jack R. Vinson

DEPARTMENT OF MECHANICAL AND AEROSPACE ENGINEERING
UNIVERSITY OF DELAWARE
NEWARK, DELAWARE

August 1973

Reproduced by
NATIONAL TECHNICAL
INFORMATION SERVICE
US Department of Commerce
Springfield, VA 22151



AIR FORCE OFFICE OF SCIENTIFIC RESEARCH

UNITED STATES AIR FORCE

Grant
~~CONTRACT~~ NUMBER AFOSR - 1760-69

Approved for public release; distribution unlimited

Qualified requestors may obtain additional copies from the Defense Documentation Center, all others should apply to the National Technical Information Service

ACCESSION FOR	
NTIS	Write Service <input checked="" type="checkbox"/>
DDC	B.I. Service <input type="checkbox"/>
UNAN ORDER	<input type="checkbox"/>
JCS/IN/DO	
BY	
DISTRIBUTION AVAILABILITY CODES	
Dist	A. I. L. 222 54 SPECIAL
A	

Conditions of Reproduction

Reproduction, translation, publication, use and disposal in whole or in part by or for the United States Government is permitted.

UNCLASSIFIED

Security Classification

AD-766 932

DOCUMENT CONTROL DATA - R & D

(Security classification of title, body of abstract and indexing annotation must be entered when the overall report is classified)

1. ORIGINATING ACTIVITY (Corporate author)		2a. REPORT SECURITY CLASSIFICATION	
UNIVERSITY OF DELAWARE DEPT OF MECHANICAL & AEROSPACE ENGINEERING NEWARK, DELAWARE 19711		UNCLASSIFIED	
3. REPORT TITLE		2b. GROUP	
THE ANALYSIS AND DESIGN OF COMPOSITE MATERIAL BONDED JOINTS UNDER STATIC AND FATIGUE LOADING			
4. DESCRIPTIVE NOTES (Type of report and inclusive dates)			
Interim			
5. AUTHOR(S) (First name, middle initial, last name)			
W J RENTON J R VINSON			
6. REPORT DATE		7a. TOTAL NO. OF PAGES	7b. NO. OF REFS
August 1973		445-443	65
8a. CONTRACT OR GRANT NO		9a. ORIGINATOR'S REPORT NUMBER(S)	
AFOSR 1760-69		MAE TR 169	
b. PROJECT NO		9b. OTHER REPORT NO(S) (Any other numbers that may be assigned this report)	
9782-01		AFOSR - TR - 73 - 1627	
c.			
61102F			
d.			
681307			
10. DISTRIBUTION STATEMENT			
Approved for public release; distribution unlimited.			
11. SUPPLEMENTARY NOTES		12. SPONSORING MILITARY ACTIVITY	
		AF Office of Scientific Research (NAM) 1400 Wilson Boulevard Arlington, Virginia 22209	
13. ABSTRACT			
<p>Extensive research was conducted providing analysis methods and design methodology for bonded joints in structures of laminated composite materials under static and fatigue loads. An analytical closed form solution has been developed for stresses and deformations in the adhesive joint and the adherends, including transverse shear deformations and normal strain, adherend anisotropy, and adhesive properties. A digital program provides rapid design and analysis; an inclusive parameter study provides trends and methodology. Static tests have been developed providing shear and extensional stiffnesses and ultimate stresses of the adhesive in the joint configurations. Fatigue tests were conducted for various geometries, loadings, and adherend materials.</p>			

i d

DD FORM 1473
1 NOV 65

UNCLASSIFIED

Security Classification

Security Classification

AD-766 932

14

Security Classification

THE ANALYSIS AND DESIGN OF
COMPOSITE MATERIAL BONDED JOINTS
UNDER STATIC AND FATIGUE LOADINGS*

by

W. James Renton**

and

Jack R. Vinson***

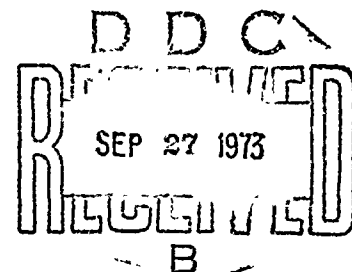
DEPARTMENT OF MECHANICAL AND AEROSPACE ENGINEERING
UNIVERSITY OF DELAWARE

August 1973

* Research sponsored by the Air Force Office of Scientific Research, ~~Office of Aerospace Research~~, United States Air Force, Grant Number AFOSR-1760-69. This document has been approved for public release; distribution is unlimited.

** Research Associate

*** Professor and Chairman



ABSTRACT

To more clearly understand the many parameters which influence the ultimate and fatigue capacity of composite material bonded joints, the enclosed theoretical and analytical program was initiated. Presently a lack of understanding in this area has impeded the wide spread use of the high strength, light weight fibrous material systems presently available.

Using the Goland-Reissner bonded lap joint analysis as a starting point, an elaborate analysis including the effects of transverse shear and normal strain is presented. Moreover, the analysis allows one to look at the various stress distribution through the thickness of the adherend and to analyze anisotropic material systems and unsymmetrical lap joints. Using this analysis an extensive parametric study is presented indicating ways to maximize the strength of a bonded joint under ultimate and fatigue loadings. Good agreement with the Goland-Reissner theory is also shown.

Excellent correlation between ultrasonic and destructive test modulus measurements is shown. In

addition, two new test methods are advanced to measure the shear and tensile properties of the adhesive as they exist within the joint. The influence of ply orientation, adhesive thickness and overlap length on the true tensile and shear moduli are ascertained.

Ultimate and fatigue test results of 1002-S fiberglass adherends bonded with Hysol EA951 Film are presented. It is shown that the shear proportional limit stress of the adhesive is an important fatigue life parameter, as is overlap length and ply orientation in the adherends. An adhesive with a high ratio of ultimate strength to modulus in shear and tension is found to be a definite advantage in maximizing the capability of the joint. The all 0° adherend specimens failed in the adhesive, for both ultimate and fatigue loadings, while the $45^{\circ}/0^{\circ}/-45^{\circ}/0^{\circ}$ specimens failed primarily in the adhesive for ultimate loading and in the 45° ply adjacent to the adhesive for fatigue loading. This was explained through the use of the Bond 3 analysis routine.

An electron scanning microscope was used to examine and offer insight into what precipitated the failures in the adhesive. A fatigue and ultimate design methodology of bonded single lap joints is presented.

A continuing, non-uniform loading fatigue test program is underway.

TABLE OF CONTENTS

	Page
NOMENCLATURE	ix
ABSTRACT	xi
CHAPTER I	
A. INTRODUCTION	1
B. REVIEW OF LITERATURE	5
C. COMPOSITE TO COMPOSITE AND COMPOSITE TO METAL BONDED JOINTS	10
D. PROPOSED RESEARCH PROGRAM	26
CHAPTER II SOLUTION OF THE PROBLEM OF A SINGLE LAP JOINT WITH ANISOTROPIC ADHERENDS	30
A. INTRODUCTION	30
B. ANALYSIS LIMITATIONS	32
C. FORMULATION OF THE PROBLEM	34
D. DETERMINATION OF THE MOMENT, SHEAR AND AXIAL LOAD RELATIONS OF THE ADHERENDS	35
E. DEVELOPMENT OF ADHESIVE STRESS-STRAIN AND FORCES EQUILIBRIUM EQUATIONS	97
F. SOLUTION OF THE GOVERNING DIFFERENTIAL EQUATIONS OF PARTS (1) AND (4)	120
G. BOUNDARY CONDITIONS	125
H. DETERMINATION OF \bar{w}^0	129

Table of Contents - Continued	Page
I. BOUNDARY CONDITIONS	132
J. CALCULATION OF M_1 AND V_1	136
K. GENERAL SOLUTION OF THE GOVERNING EQUATIONS FOR PARTS (2) AND (3)	139
L. TWO LAMINATES OF EQUAL THICKNESS AND MATERIAL PROPERTIES	151
M. TWO LAMINATES OF UNEQUAL THICKNESS AND/OR UNEQUAL MATERIAL PROPERTIES	174
CHAPTER III - A STUDY OF CERTAIN PARAMETERS INVOLVING JOINTS WITH IDENTICAL ADHERENDS	195
CHAPTER IV -	
A. ELASTIC MODULUS MEASUREMENTS ON 1002-S FIBERGLASS MATERIAL	242
B. ULTIMATE STRENGTH AND STRESS STRAIN DATA OF THE ADHEREND MATERIAL	255
C. SHEAR MODULUS TESTS	263
D. ADHESIVE TENSILE TESTS	302
CHAPTER V -	
A. ULTIMATE LOAD TESTS	333
B. FATIGUE TEST RESULTS OF BONDED SINGLE LAP JOINTS	359
C. ALL 0° ADHEREND FATIGUE TEST RESULTS	366
D. ANGLE PLY FATIGUE TEST RESULTS	394
REFERENCES	423
APPENDIX A	430

NOMENCLATURE

- A_{ij} = terms of the lamina compliance matrix referred to the principle material axes.
- \bar{A}_{ij} = terms of the lamina compliance matrix referred to an arbitrary set of axes.
- h = thickness of the laminate.
- H_{K+1} = distance from the geometrical mid-plane of the laminate to a particular point where lamina (K) and (K+1) have their common interface.
- Q_{ij} = terms of the lamina stiffness matrix referred to the principle material axes.
- \bar{Q}_{ij} = terms of the lamina stiffness matrix referred to an arbitrary set of axes.
- T = applied axial load.
- $[T']$ = transformation matrix.
- u^o = the laminate mid-plane longitudinal displacement in the direction of the applied axial load.
- w^o = the laminate mid-plane lateral displacement.
- z = thickness of a given lamina.

ϵ_i = normal strains.

ϵ_{ij} = shear strains.

σ_i = normal stresses.

τ_{ij} = shear stresses.

CHAPTER I

A. INTRODUCTION

The application of fibrous composites to various space and aircraft vehicles has opened up a whole new area of analysis and design technology. The material system is generally anisotropic and quasi-homogeneous in make-up. These materials offer significant advantages over the more conventional metallic materials in common use. Namely, they offer the advantages of a high strength-to-weight ratio, a system flexible enough to give one the elastic properties he desires for given loadings and orientation and increased structural efficiency in the design of a specific item.

With the increased use of these filamentary material systems structural theories relating to homogeneous, isotropic materials must and in some instances have been modified to account for the anisotropic nature of these materials. However, due to the large ratio of the in-plane elastic moduli to the shear modulus the effects of transverse shear and normal strain have in numerous instances proven to be important in obtaining a good analytical result vs. experimental works.

The work I have performed and am reporting on in

this manuscript will concern itself with filamentary composites composed of fibers embedded in a matrix supporting system. The primary load path is along the direction of the fibers while the matrix acts to carry shear loads and constrain the fibers to a specific orientation once the system is cured. In general a structural part is composed of several plies or lamina and it is the orientation of these plies with respect to each other that gives one the desired elastic properties in a specific direction. If the laminate--several lamina--has three mutually perpendicular planes of material property symmetry, one has a specially orthotropic material system with nine independent elastic constants. It is this type system I will consider throughout this work.

At present the biggest drawback to the widespread use of composite material systems is the predictable joining of one part to another. Theoretically, one could rivet, bolt or bond two parts together to withstand static and fatigue loads. However, presently it is the failure of technology to establish an accurate, reliable analysis for joining components together under "real-life" loading conditions by any of the above methods which has impeded the widespread use of composite material systems.

The objective of this work is to develop an adequate and a satisfactory method of static and fatigue analysis and design of a single lap joint involving composite material adherends. The anisotropic properties of the adherends ply orientation, adhesive thickness, lap length and the mechanical properties of the adhesive as they exist in the lap joint will be studied for their respective effects on the response of the lap joint to static and dynamic loads.

More specifically, it is proposed to investigate fatigue strength trends and failure modes for the lap joint involving a study of the response of the joint as the adhesive is loaded above and below its proportional limit stress. This will be done while employing certain significant joint parametric variations under ambient temperature and humidity conditions.

To accomplish this goal the study has embodied the following:

1. Static and ultrasonic mechanical property tests
2. Static strength tests of single lap joints
3. Constant amplitude fatigue tests of single lap joints

4. Tests involving programmed variations in the constant amplitude loading spectrum to isolate the damage characteristics of certain variations in the fatigue loading spectrum. These variations would introduce stresses both above and below the proportional limit stress of the adhesive.
5. Development of a closed form solution which substantiates the test results of item 2.
6. Development of a semi-empirical approach to the data obtained in items 3 and 4.
7. Reduction of the results to guidelines for simple analytical and design procedures for lap joints in fatigue.
8. Screening tests using a PRD49 material system to view the possibility of extending the information found during the glass testing to this new material system.

B. REVIEW OF LITERATURE

Fatigue of metallic and non-metallic materials has been a constant source of challenge and concern for the researcher and practicing engineer for many years. A multitude of fatigue damage theories have been proposed, none of which have been consistently reliable. In general the approach to a fatigue damage theory has been as given in References 1 and 3.

1. For each cycle of load $x(t)$ a response $y(t)$ of the structure is measured. It is assumed that this $y(t)$ inflicts an increment of damage to the structure which depends on the peak amplitude of the response. Failure will occur when the accumulated total damage equals 100 per cent.
2. It has been further hypothesized that under a given load--response history, a given structure sees many small dislocations and localized plastic deformations. Microscopic cracks begin and grow with each load cycle. Eventually one of the cycles causes rapid crack growth and rupture of the structure

occurs.

In most approaches to establishing a fatigue damage theory and correlating it with test results, a constant amplitude alternating stress about a given mean stress is prescribed. However, this is a very special load history and in most cases far from reality for use in the design of an actual structure. A much more realistic fatigue response by a given material can be obtained by a random loading approach. Under such an approach a continually varying alternating stress amplitude is used which assumes each cycle does an amount of damage in proportion to the peak amplitude of the excursion. Again failure is hypothesized to occur when the accumulated damage equals 100%. Such a procedure has been used with metal structure subjected to certain load spectra (i.e. a ground-air-ground load spectrum for an aircraft). However, the Palmgren/Miner hypothesis gave accumulated total damage predictions both greater than and less than 100%, dependent on which test results in the literature were observed. Very little work using other than constant amplitude alternating stresses has been done in composites.

A summary of the work done in fatigue is found in References 6 to 19.

Some of the parameters which were studied for their effect on the fatigue properties of composites were:

1. moisture and temperature
2. resin content
3. mean stress
4. angle of load to the material principal axes
5. ply stacking sequence
6. notch effects
7. effect of high amplitude-low cycle and low amplitude-high cycle load
8. effect of cross-ply mixed with uni-ply to form a complex laminate
9. effect of shear loading
10. effect of loading the matrix beyond its elastic range (i.e. .2% offset)
11. effect of matrix porosity
12. hysteresis of the load cycle
13. complex load history.

Many of these parameters have been investigated for glass cloth and uni-glass materials while a minimal amount of work has been generated to establish the fatigue characteristics of boron or carbon composites.

SUMMARY

Some tentative conclusions to be drawn from the preceding References as concerns glass uni-directional material are:

1. Axial fatigue strength decreases with increasing moisture and/or temperature, especially for a porous matrix.
2. Compression fatigue is a realistic damage criterion.
3. Resin content has a nominal effect on the axial fatigue strength of glass-epoxy systems.
4. As the mean stress level increases the allowable alternating stress decreases for a given number of cycles.
5. A $\pm 5^\circ$ angle ply laminate exhibits superior fatigue strength for glass-epoxy systems.
6. The ply stacking sequence effects the S-N curve shape.
7. The fatigue strength is most notch sensitive when load is applied parallel to the fibers.
8. High initial cyclic loading especially beyond the proportional limit stress of the matrix causes damage and premature failure of the

component.

9. Miner's Rule has proven unreliable in predicting the life of components under constant-amplitude loading.
10. Hysteresis effects due to rapid cycling of the load can degrade glass fatigue properties.
11. Knowledge concerning the response of composite material systems to a random type load is lacking both theoretically and experimentally.

c. COMPOSITE TO COMPOSITE AND COMPOSITE TO METAL
BONDED JOINTS

1. Static Loading Characteristics - The purpose of a joint is usually to join several discrete parts into a complete load carrying structure. There are basically three methods utilized by a joint in transferring load. These are shear, tension (compression) and bending. There are two basic categories of joints, namely bonded joints or mechanically fastened joints. It is the intent here to pursue the relevant facts of bonded joints only.

To evaluate objectively the response of bonded joints under a system of loads one must have an appreciation for the rheology of the hardened adhesive layer of the manufactured joint. DeBruyne (Ref. 24) gives a concise and meaningful presentation on this subject. Summarily he states that an adhesive substance shows greater tensile and shear properties in the joint vs. those it possesses in a bulk quantity. Also, for thinner adhesives (i.e. 80 microns or less) the strength of the joint is inversely proportional to its thickness, while for thick adhesive joints (i.e. thicker than 80 microns) no appreciable thickness-to-strength relation

is evident. DeBruyne hypothesizes that part of the reason for this phenomenon is that as the thickness of the adhesive increases the probability of flaws in the adhesive increases. Moreover, tangential stresses in the adhesive increase as thickness increases especially for a non-yielding adhesive. These are due to adhesive shrinkage or swelling brought on by a response of the adhesive to its environment or the difference in thermal expansion between the adhesive and the adherend material. Thus the negating effects of a thick adhesive overcome its intended benefit.

DeBruyne also points out the relative merits of various type adhesives as evaluated by numerous researchers. It is believed that a highly viscous adhesive is desirable for deformable adherends. Such adhesives are forgiving and as tangential stresses build up they can negate such stress raisers by flowing. However, for structures under continuous loading permanent deformation may occur and be untenable. Also in temperature extremes viscous adhesives in general perform poorly.

Highly elastic adhesives of moderate breaking strength have the advantage of being stable under prolonged loads below certain levels. This in turn relieves borderline stress raisers and makes the joint

more suitable under a random type load.

In general a more efficient joint exists if the elastic modulus of the adhesive is less than the elastic modulus of the adherend.

Tiezzi and Doyle (Ref. 56) have also looked at adhesives, particularly in a lap joint involving their response under various loadings. Also, Tetelman (Ref. 50) has looked at the fracture process of both the adhesive and fibers which compose a composite material system.

Lehman et. al. (Ref 22) in an extensive study of bonded joints using metal (titanium, aluminum and steel) boron and S-994 glass adherends in various joint configurations with Shell 951 adhesive established the most important bonded joint parameters. These were (1) the strength and stiffness properties of the adhesive, (2) lap length, (3) adherend thickness and (4) fiber orientation adjacent to the adhesives. Kutscha in (Ref. 30) substantiated this. However, in (Ref. 42) test results of a Narmco 5505 adherend and MB 329 adhesive system showed no significant effect on the ultimate load capacity of the joint by adjusting the orientation of the ply adjacent to the bond surface. Hawley and Ashizawa

(Ref. 35) in work related to (Ref. 22) and the two basic adherend patterns used ($0^\circ/\pm 45^\circ/0^\circ$ and $+ 45^\circ/0^\circ/-45^\circ$) predicted failure in the adhesive for the 0° ply next to the bond while anticipating a resin failure of the adherend when the 45° ply was adjacent to the adhesive for the double lap joint. This is primarily the result of the difference in shear stress distribution in the resin for the two patterns analyzed. A similar result indicating earlier damage for angle ply vs. uniply once its proportional limit was exceeded (the proportional limit is usually lower for angle ply laminates) was observed by McGarry (Ref. 38) for E-glass/epoxy in a balanced $0^\circ/90^\circ$ laminate and by Waddoups (Ref. 39) for a $0^\circ/90^\circ$ Boron reinforced composite.

Numerous trends have been observed in the literature (Refs. 22 and 46) which show that composite single lap joints usually fail under static load in any one of five possible modes depending on the length of overlap to thickness of adherend ratio (L/t). For an $(L/t) \approx 12.5$ failure usually occurred by (1) cohesive failure of the adhesive or (2) adhesive failure of the resin-adhesive interface or (3) adhesive failure at resin-fiber interface at the first layer of the lamina. Moreover, interlaminar shear failure in the adherend occurred for

an (L/t) = 25 while if L/t = 50 then the adherends failed in tension (compression). References 22 and 36 specify that for isotropic elastic adherends and adhesives, lap joints are theoretically stronger for (1) short overlap, (2) a thick adhesive layer (Ref.22 found that a relatively thick adhesive had a negligible effect on the ultimate strength of a composite double lap joint), (3) low adhesive/adherend stiffness ratio. Item (3) most probably results from the increased ductility of low modulus adhesives which tend to be more forgiving of the strain incompatibility between the adherend and the adhesive especially in a single lap joint. Also, the more ductile adhesives will yield and thus better cope with the stress concentration before failing.

Moreover, it has been found in most of the literature, especially References 22 and 34, that the strongest bonded joints (single and double lap) occur when the extensional stiffness of the adherends is equal. Discrete element analysis has verified this by showing that the peak stress at each end of the joint is at a minimum when this is true. In addition bonded joints with lap lengths in excess of approximately one inch are less efficient since the stress distribution in the joint shows that little load is transferred in the midportion of the joint.

Kutscha and Hofer (Ref. 44) specify that in thick adherends the load transfer to the joint occurs in the first 3 or 4 layers adjacent to the adhesive before shear failure occurs in the laminate (usually a cross-ply lamina) while for very thin laminates the ultimate strength of the adherend in tension (compression) is achieved. Thus for an efficient joint whereby the adherend and adhesive are loaded efficiently, proper selection of the (L/t) ratio for the load to be carried is important for a minimum weight design. Reference 43 studied the effects of outside adherend taper on single lap joints and found it to be an insignificant variable. However, an inside adhesive taper which increased adhesive thickness at the ends of the joint in the region of high stress concentration factors does have a significant effect. Basically it reduces the stress level at the end of the joint by the addition of this extra adhesive locally. Such a joint looks especially promising as a good fatigue joint as it has been observed that exceeding the proportional limit stress of the adhesive in fatigue (static loading to a lesser degree) leads to rapid deterioration of the joint.

Additional problem areas which may influence the reliability of predicting the allowable strength of full

scale bonded joints (Ref. 22) are the residual thermal stresses induced if the adherend and the adhesive have widely different coefficients of thermal expansion. Also Refs. 22 and 37 state that the results of one inch wide lap joint test specimens may yield data (25-30%) in excess of that obtained from wider specimens. In addition Refs. 22 and 46 found bonded joints to be weight-efficient vs. bolted joints and recommended them for all permanent joint applications while composite-to-composite joints can give comparable strength vs. composite-to-metal joints.

A number of individuals have developed analytical techniques to determine the load and stress distribution in isotropic adhesive bonded joints. The "classic" work in the field is that by Goland and Reissner for single lap joints while the work of Cornell, Volkersen, Szepe, Sherrer, DeBruyne, Hahn and Fouser, Goodwin, Erdogan, Ratwani, Korbacher, Pahoja and Niskanen have made significant contributions to the "state of the art".

The basic approach to analyzing adhesive joints has been to idealize the joint in terms of a mathematical model whereby the material properties and joint geometry are related to the applied loads resulting in a higher order differential equation which is solved to

determine the stress distribution in the joint which in turn must result in physically realistic distributions. References 21, 22, 23, 24, 25, 27, 28, 30, 34, 53, and 54 have for the most part the following assumptions in their analysis: (1) all elements are linearly elastic, (2) the stress is uniform across the width of the lap (usually assumed one inch wide) and through the thickness of the adhesive, (3) the adherends behave as plates, (4) the adhesive is adequately bonded to the adherend, (5) adhesive properties are uniform throughout the joint, (6) the adhesive is in a state of plane stress or plane strain, (7) linear small deflection theory is valid. Moreover, as pointed out by Goland and Reissner (Ref. 23), dependent on the relative magnitude of the physical properties of the adhesive vs. the adherend the adhesive at times can be neglected in the analysis. Also, in double lap joints bending effects on the joint's capacity are usually neglected. However, with the ductile adhesives and resins in use today exhibiting non-linear behavior (plasticity) at relatively low percentages of their ultimate strength and the anisotropic nature of composite materials adding further complexities, the traditional analytical techniques available have become less reliable. A realistic approach to this problem has been advanced in Refs. 22 and 41,

among others by using linear and nonlinear (plasticity) discrete element analysis of the joint. The results in general have given good test-theory correlation for bonded composite and composite-to-metal joints while the analysis of Volkersen and Goland and Reissner have predicted results approximately twice that of the discrete element analysis. This discrepancy is partly the result of the composite material adhesive joints exhibiting lower stress concentration factors experimentally than predicted by theoretical methodology.

Several analytical methods will be enlarged upon. In 1944 Goland and Reissner (Ref. 23) determined the stresses in a single lap joint for a relatively inflexible cement layer ($\frac{\text{thickness adherend}}{\text{elastic modulus adherend}} \gg \frac{\text{thickness adhesive}}{\text{elastic modulus adhesive}}$) in which the cement layer is ignored and for a relatively flexible cement layer where- by the properties of the cement are taken into account in the analysis. He assumed the joint acted as a cylindrically bent plate of variable cross section and neutral plane.

In a 1953 article Cornell (Ref. 25) used a brittle lacquer and photoelastic stress analysis to experimentally verify his analytical formulation of a single lap brazed joint in terms of a 10th order differential

equation. In general he found the brazed stress distribution became more uniform as the braze modulus decreased and the braze thickness increased. In 1962 Hahn and Fouser (Ref. 28) analyzed the bending of the adherends (ignoring the adhesive) in a lap joint assuming they act as cylindrically bent plates (analogous to the Goland and Reissner solution). The second part of the article considered the differential straining in a double lap joint (bending neglected) and determined the shear stress distribution in the adhesive.

Goodwin (Ref. 29) studied brazed joints in sandwich panels using a theory-test correlation approach. He studied the effect of ten parameters (i.e. ratio of the elastic modulus of the braze to the adherend, ratio of braze thickness to sheet thickness) on the static, fatigue and creep strength of the joint. Most, important, he developed an analysis method, which included plastic effects and produced results in good agreement with his static and fatigue test results.

2. Fatigue Loading Characteristics - The inherent nature of composite materials makes bonded joints much more efficient than mechanical fasteners for transferring loads between components. Moreover, composite materials appli-

cation to space vehicles, aircraft, etc. complicates the problem by introducing a random loading spectrum to such joints during their service life. These loads are primarily the result of aerodynamic and inertial effects.

To date the few isolated studies of composite-to-composite or composite-to-metal adherend bonded joints have been conducted under constant-amplitude cyclic loading, while no generally accepted cumulative damage theories have evolved. Lehman et al. in (Ref. 22) have performed fatigue testing of single lap, double lap and scarf joints with the variables being lap length and lamina orientation. (A similar series of tests are presently being conducted by the Lockheed-Georgia Company.) Results in general showed failure was in the adhesive or in the resin adjacent to the adhesive.

From these results and the observations made by Grimes in (Ref. 49) it has been hypothesized that if you exceed the proportional limit stress of the adhesive or resin in the high stress concentration areas of the joint, micromechanical cracking occurs which effectively alters the joint geometry and accelerates failure of the joint. Moreover, reference is made to observations using microscopic photography of these cracks occurring once the proportional limit stress of the

adhesive was exceeded. In addition, fatigue testing reported in Ref. 22 showed no failures in testing to 10^6 cycles when the maximum shear stress of the adhesive did not exceed its proportional limit.

Realizing that the magnitude of the stress concentration factor is the limiting factor in joint strength in many instances, several studies were conducted on the sensitivity of the adhesive joint to the magnitude of the stress concentration factor. Ref. 34 cites an analytical study of single and double lap joints which found the fatigue strength of the joint to be more sensitive to stress concentration factors than for static loading. In turn, they believed the most efficient way to lower the magnitude of the stress concentration factor was to increase the adhesive thickness. In addition, Ref. 22 cites that one may possibly improve the adhesive's fatigue capability by using more ductile adhesives or by local adhesive thickness increases in the areas of peak stress.

Several inroads into the analytical prediction of fatigue failure of bonded joints under constant-amplitude loading have been advanced. In Ref. 22 the results of fatigue tests of boron and glass bonded joints using fatigue loads of 60-80 percent of ultimate

showed that a peak shear stress concept could be used to evaluate the fatigue life of the joint for an adhesive failure using a linear discrete element approach.

In addition, Wang (Ref. 20) in 1964 investigated the fatigue strength of adhesive bonded joints using aluminum adherends and in particular studying the effects of adherend and adhesive mechanical properties and joint geometry (lap vs. scarf vs. butt) under constant amplitude loading. He found that Metalbond 4021, a highly ductile adhesive performed superior to FM-47 a more brittle adhesive even though FM-47 had a higher ultimate strength. It was felt the more ductile adhesive exhibited a more uniform shear stress in the joint resulting in a longer life joint. Qualitatively the equations of Reissner verified this result.

In 1966 Szepe (Ref. 21) used a semi-empirical approach to determine the stress distribution in a bonded double lap joint in terms of two constants. These were the adhesive spring constant (c) and the adhesive average ultimate shear strength as the length of overlap approached zero (τ_0). He also established that (c) and (τ_0) decreased in magnitude with increasing temperature resulting in a similar decrease in joint

strength.

Moreover he extended his semi-empirical equations for bonded joints to include constant-amplitude loadings. He established that (τ_0) decreased in magnitude with number of cycles while (c) remained approximately constant in the elastic range. From these results he was able to determine the characteristic S-N curve shape for a given length of overlap. Also, he was able to determine the fatigue strength of joints at other overlap lengths for any number of cycles (N) once he had the fatigue strength of the new joint at a given number of cycles by using these constants in a proportionality relationship.

It is felt by the author that a further analysis of this work might relate these constants (τ_0) and (c) to the viscoelastic shift factors of such type materials for temperature, nonuniform loading and stress levels as exemplified by Halpin and Polley in (Ref. 32).

SUMMARY:

Some tentative conclusions to be drawn from the preceding discussion as concerns composite bonded joints are:

1. A significant joint parameter is the pro-

portional limit stress of the adhesive.

2. Thick adhesive joints are not stronger than thin adhesive joints for similar adherends.
3. Composite bonded joints do not necessarily respond under load as isotropic and elastic material joints.
4. The strongest bonded joints occur (statically) when the extensional stiffness of the adherends are equal.
5. The static and fatigue strength of a bonded joint may be improved by increasing the local adhesive thickness at the ends of the joint.
6. In fatigue joints appear to be more sensitive to stress concentrations than they are under static loading.
7. The resin shear strength of the lamina adds a new parameter to joint analysis.
8. A ductile low modulus adhesive seems to be most desirable.
9. The visco-elastic response of the adhesive is important in the fatigue strength of the joint and should be accounted for in any analysis.
10. Knowledge of the response of composite bonded joints to a random type load is lacking both

theoretically and experimentally.

D. PROPOSED RESEARCH PROGRAM

It is seen from reviewing the enclosed reference list that only eighteen in-depth articles were found which have been concerned with adhesive bonded composite joints under static loads. Moreover, only three articles are concerned with constant-amplitude fatigue loading of this type joint, while no articles have yet been found concerning the fatigue aspects of bonded joints subjected to random loading.

From the scarcity of articles on fatigue loading of bonded composite adherend joints it is obvious that:

1. Only initial attempts to analyze and experimentally to verify the fatigue loading response of adhesive bonded composite joints has been undertaken.
2. A methodology for a random type loading of bonded composite joints is lacking as is a methodology to account for the fatigue phenomena under such loads.
3. Experimental response data of bonded composite joints under random type loading is absent.

4. No simple analytical or design procedure for fatigue of bonded composite joints under real life loading conditions exist.

Thus, this research program will attempt to provide initial information to enlighten us in the four areas mentioned above as concerns the lap joint.

The research program will be conducted at ambient temperature humidity conditions. It will include:

1. Continued literature survey.
2. Design of the bonded lap joint.
 - a. Selection of the resin and adhesive systems to be employed accounting for:
 - (1) Temperature and pressure requirements of the cure cycle.
 - (2) The ductility of the resin and/or adhesive.
 - (3) Thermal expansion coefficients of the adhesive and adherend to insure compatibility.
 - b. Conduct material properties tests including those of the adherend material and the adhesive properties as they exist in the joint configuration, using the ap-

propriate specifications.

- c. Establish the lap joint geometry - this includes selection of laminate patterns, length-to-thickness ratios, adherend thickness, adhesive thicknesses and the extensional stiffnesses of the adherends.
 - d. Development of the necessary static and dynamic methods of analysis.
3. Static testing of the joints and correlation with theory. This would include determination of the number of tests needed to acquire reliable results and a statistical analysis of these data points.
4. Fatigue loading program:
- a. To study the effects of exceeding the proportional limit stress of the adhesive and/or resin system, as evidence in the literature indicates that this is of significant importance on the life of the joint under certain fatigue loads. This will be accomplished by determining the proportional limit stress of the adhesive and running constant-amplitude and programmed variation fatigue tests above and below the proportional limit stress.

- b. Correlation of the test results vs. theory.
- 5. Presentation of results and conclusions including the relation of the static characteristics to the fatigue characteristics of the material.

CHAPTER II

SOLUTION OF THE PROBLEM OF A SINGLE LAP JOINT WITH ANISOTROPIC ADHERENDS

A. INTRODUCTION

The objective of this dissertation is to determine the stress field in a bonded joint composed of anisotropic adherends and an isotropic adhesive system. The problem, originally solved by Reissner and Goland (Ref. 23) for a completely isotropic material system, is treated as two problems in one within this dissertation. The problems to be solved are:

1. To determine the load relations in the anisotropic adherends. Then, using linear plate theory, to determine the joint edge loads, as needed.
2. To determine the normal and shear stresses in the adhesive by solving an eighth order linear ordinary differential equation. The complete solution of this part of the problem requires the use of twenty-six boundary conditions. The solution incorporates the effects of

transverse shear and tranverse normal strain.

B. ANALYSIS LIMITATIONS

The analysis within has assumed a laminate, structured such that the bending-stretching coupling matrix (B_{ij}) is zero. This was assumed to be a realistic limitation as in few practically designed structures is such coupling tolerable.

A second limitation of the analysis involves the stretching-shearing coupling introduced when the "16" and "26" terms of the in-plane stiffness matrix (A_{ij}) are not equal to zero. A problem could arise based on the fact that while assuming plane strain is valid a check of the strain-stress relations on page (43) would indicate that if the A_{16} , A_{26} terms were not zero a strain ϵ_{xy} in violation of the plane strain assumption could be induced. The only time this could cause concern would be for an adherend composed of an odd number of lamina, few in number (i.e. $+45^\circ/-45^\circ/+45^\circ$). In most cases it is summarized that the " A_{16} " " A_{26} " terms would equal zero as in the case of 0° and 90° lamina and for adherends where for every lamina of a plus (θ) orientation one has another lamina of the same orthotropic properties and thickness in the negative (θ) direction.

Moreover, if this is not the case but an adherend is composed of six plys or more the coupling effect will usually be minimal. For the $45^{\circ}/0^{\circ}/-45^{\circ}/0^{\circ}$ ply orientation pattern used in this report a secondary effect is evident.

C. FORMULATION OF THE PROBLEM

Given two rectangular sheets of anisotropic material; sheet one has length $(L_1 + L_2)$ and thickness (h_1) , sheet two has length $(L_2 + L_4)$ and thickness (h_2) . The thickness of the adhesive (η) is small compared to (h_1) and (h_2) . The far ends of the sheet are clamped and are loaded in tension by a force of (T) lbs/unit width (Figure 1).

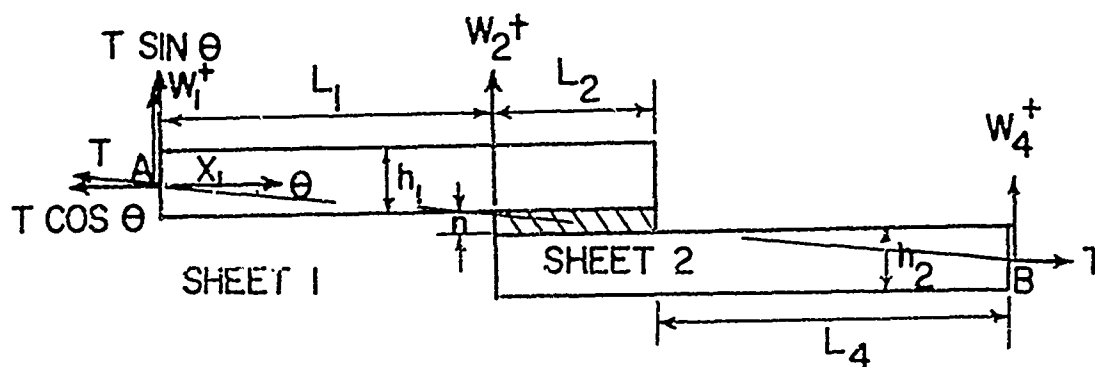


FIGURE (2-1)

D. DETERMINATION OF THE MOMENT, SHEAR AND AXIAL
LOAD RELATIONS OF THE ADHERENDS

Assumptions:

1. Plane strain exists (i.e. variations in y-direction are neglected)
2. The material system has (3) planes of elastic symmetry (i.e. 9 independent elastic constants in a three-dimensional solid).
3. Each adherend's lamina are layed-up symmetric about it's geometrical mid-plane.
4. Effect of adhesive materials elastic properties are accounted for.
5. The transverse shear stress distribution is parabolic in the elastic range.
6. Both shear and normal stresses are accounted for in the adhesive.
7. The moment, shear and axial load relations are equally valid for material axes non-coincident with the geometrical axes as they are when the axes are coincident.
8. Deformation of the sheets is due to bending and tensile strains plus the deformation due

to transverse shear and normal strain.

9. The normal stress σ_x in the adhesive is neglected.
10. The shear stress and transverse normal stresses in the adhesive do not vary over the thickness of the adhesive.
11. The glue thickness is assumed to be much smaller than the adherend thicknesses.

Definitions and Sign Convention:

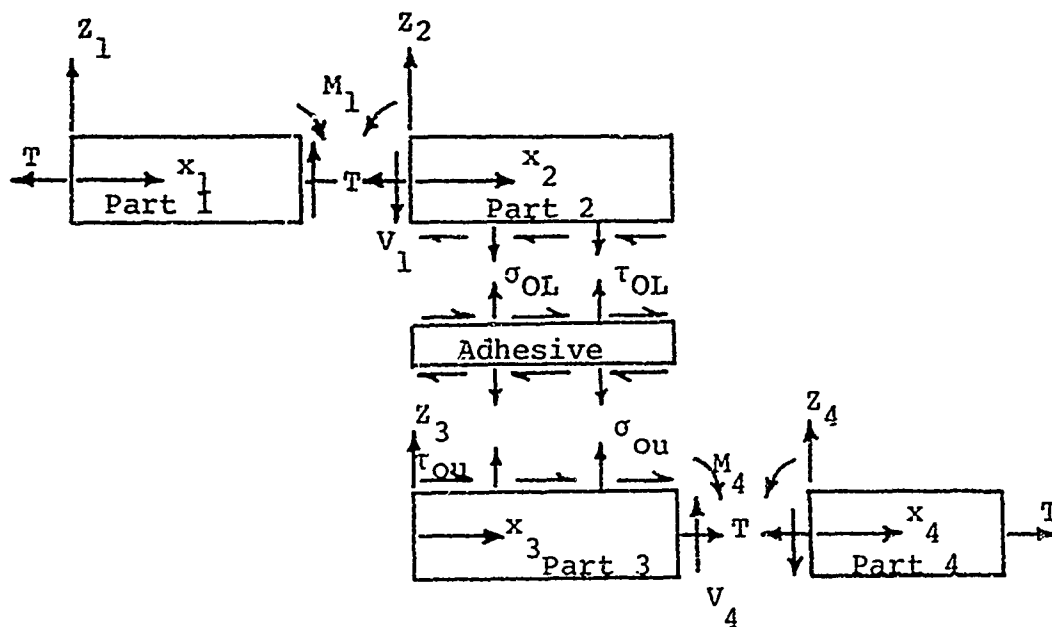


FIGURE (2-2)

The structure is divided into four parts for ease of analysis. Moment, shear and axial load relations for each part will be found. All loadings will subscribe to

the sign convention detailed in Figure 2.

Material System and Equivalent Stiffness Matrix

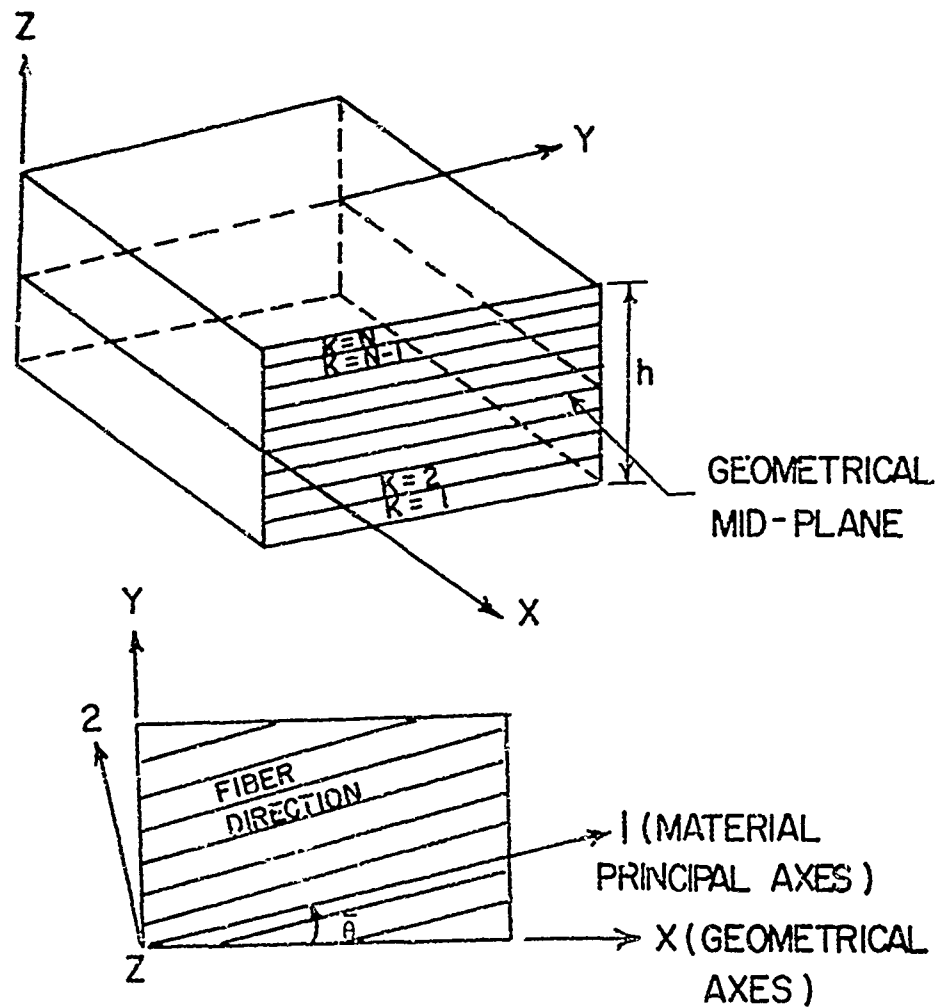


FIGURE (2-3)

The material system is assumed to be of an anisotropic nature with three planes of elastic symmetry (nine independent elastic constants). The k^{th} lamina's principal directions (1-2 axes) are related to the geometri-

cal axes (x-y) by the angle $(\bar{\theta})$, in Figure 3. The lamina are numbered in ascending order from the lower to the upper laminate surface.

The constitutive relation for the k^{th} lamina is:

$$\begin{bmatrix} \sigma_1 \\ \sigma_2 \\ \sigma_3 \\ \tau_{23} \\ \tau_{13} \\ \tau_{12} \end{bmatrix}_K = \begin{bmatrix} Q_{11} & Q_{12} & Q_{13} & 0 & 0 & 0 \\ Q_{12} & Q_{22} & Q_{23} & 0 & 0 & 0 \\ Q_{13} & Q_{23} & Q_{33} & 0 & 0 & 0 \\ 0 & 0 & 0 & 2Q_{44} & 0 & 0 \\ 0 & 0 & 0 & 0 & 2Q_{55} & 0 \\ 0 & 0 & 0 & 0 & 0 & 2Q_{66} \end{bmatrix} \begin{bmatrix} \epsilon_1 \\ \epsilon_2 \\ \epsilon_3 \\ \epsilon_{23} \\ \epsilon_{13} \\ \epsilon_{12} \end{bmatrix}_K \quad (2.1)$$

The transformation matrix relating the material properties and/or the stresses and strains along the (x-y) axes to those along the (1-2) axes by rotating from the (x-y) axes to the (1-2) axes a $(+\bar{\theta})$ degrees is:

$$[T] = \begin{bmatrix} M^2 & N^2 & 0 & 0 & 0 & 2MN \\ N^2 & M^2 & 0 & 0 & 0 & -2MN \\ 0 & 0 & 1 & 0 & 0 & 0 \\ 0 & 0 & 0 & M & -N & 0 \\ 0 & 0 & 0 & N & M & 0 \\ -MN & MN & 0 & 0 & 0 & M^2 - N^2 \end{bmatrix} \quad (2.2)$$

where:

$$M = \cos \bar{\theta}$$

$$N = \sin \bar{\theta} \quad .$$

Thus, the stress and strain transformation relations are:

$$\begin{bmatrix} \sigma_1 \\ \sigma_2 \\ \sigma_3 \\ \tau_{23} \\ \tau_{13} \\ \tau_{12} \end{bmatrix} = [T] \begin{bmatrix} \sigma_x \\ \sigma_y \\ \sigma_z \\ \tau_{yz} \\ \tau_{xz} \\ \tau_{xy} \end{bmatrix} \quad \text{and} \quad \begin{bmatrix} \epsilon_1 \\ \epsilon_2 \\ \epsilon_3 \\ \epsilon_{23} \\ \epsilon_{13} \\ \epsilon_{12} \end{bmatrix} = [T] \begin{bmatrix} \epsilon_x \\ \epsilon_y \\ \epsilon_z \\ \epsilon_{yz} \\ \epsilon_{xz} \\ \epsilon_{xy} \end{bmatrix} \quad (2.3)$$

Moreover, if one transforms the constitutive relation given by equation (2.1) through an angle ($\bar{\theta}$), the stress-strain relations along the (x-y) axes for the K^{th} lamina are:

$$\begin{bmatrix} \sigma_x \\ \sigma_y \\ \sigma_z \\ \tau_{yz} \\ \tau_{xz} \\ \tau_{xy} \end{bmatrix}_K = \begin{bmatrix} \bar{Q}_{11} & \bar{Q}_{12} & \bar{Q}_{13} & 0 & 0 & \bar{Q}_{16} \\ \bar{Q}_{21} & \bar{Q}_{22} & \bar{Q}_{23} & 0 & 0 & \bar{Q}_{26} \\ \bar{Q}_{31} & \bar{Q}_{32} & \bar{Q}_{33} & 0 & 0 & \bar{Q}_{36} \\ 0 & 0 & 0 & \bar{Q}_{44} & \bar{Q}_{45} & 0 \\ 0 & 0 & 0 & \bar{Q}_{45} & \bar{Q}_{55} & 0 \\ \bar{Q}_{61} & \bar{Q}_{62} & \bar{Q}_{63} & 0 & 0 & \bar{Q}_{66} \end{bmatrix}_K \begin{bmatrix} \epsilon_x \\ \epsilon_y \\ \epsilon_z \\ \epsilon_{yz} \\ \epsilon_{xz} \\ \epsilon_{xy} \end{bmatrix}_K \quad (2.4)$$

where:

$$[\bar{Q}_{ij}]_K = [T]^{-1} [Q_{ij}]_K [T] \quad (2.5)$$

In expanded form the $[\bar{Q}_{ij}]_K$ terms are:

$$\bar{Q}_{11} = M^2(M^2Q_{11} + N^2Q_{12}) + N^2(M^2Q_{12} + N^2Q_{22}) + 4M^2N^2Q_{66}$$

$$\bar{Q}_{12} = N^2(M^2Q_{11} + N^2Q_{12}) + M^2(M^2Q_{12} + N^2Q_{22}) - 4M^2N^2Q_{66}$$

$$\bar{Q}_{31} = \bar{Q}_{13} = M^2Q_{13} + N^2Q_{23}$$

$$\bar{Q}_{14} = \bar{Q}_{15} = \bar{Q}_{24} = \bar{Q}_{25} = \bar{Q}_{34} = \bar{Q}_{35} = \bar{Q}_{46} = \bar{Q}_{56} = 0$$

$$\bar{Q}_{16} = 2MN(M^2Q_{11} + N^2Q_{12}) - 2MN(M^2Q_{12} + N^2Q_{22}) - 4MN(M^2 - N^2)Q_{66}$$

$$\bar{Q}_{21} = \bar{Q}_{12}$$

$$\bar{Q}_{22} = N^2(N^2Q_{11} + M^2Q_{12}) + M^2(N^2Q_{12} + M^2Q_{22}) + 4M^2N^2Q_{66}$$

$$\bar{Q}_{32} = \bar{Q}_{23} = N^2Q_{13} + M^2Q_{23}$$

$$\bar{Q}_{26} = 2MN(N^2Q_{11} + M^2Q_{12}) - 2MN(N^2Q_{12} + M^2Q_{22}) + 4MN(M^2 - N^2)Q_{66}$$

$$\bar{Q}_{33} = Q_{33}$$

$$\bar{Q}_{36} = 2MNQ_{13} - 2MNQ_{23}$$

$$\bar{Q}_{44} = M^2Q_{44} + N^2Q_{55}$$

$$\bar{Q}_{54} = \bar{Q}_{45} = -MNQ_{44} + MNQ_{55}$$

$$\bar{Q}_{55} = +N^2Q_{44} + M^2Q_{55}$$

$$\bar{Q}_{61} = M^2(MNQ_{11} - MNQ_{12}) + N^2(MNQ_{12} - MNQ_{22}) - 2MN(M^2 - N^2)Q_{66}$$

$$\bar{Q}_{62} = N^2(MNQ_{11} - MNQ_{12}) + M^2(MNQ_{12} - MNQ_{22}) + 2MN(M^2 - N^2)Q_{66}$$

$$\bar{Q}_{63} = (MNQ_{13} - MNQ_{23})$$

$$\bar{Q}_{66} = [2MN(MNQ_{11} - MNQ_{12}) - 2MN(MNQ_{12} - MNQ_{22}) + 2(M^2 - N^2)^2 Q_{66}] \quad (2.6)$$

In a similar vein the compliance matrix (A_{ij}) relates strain to stress for the K^{th} lamina per equation (2.7)

$$\begin{bmatrix} \epsilon_1 \\ \epsilon_2 \\ \epsilon_3 \\ \epsilon_{23} \\ \epsilon_{13} \\ \epsilon_{12} \end{bmatrix}_K = \begin{bmatrix} A_{11} & A_{12} & A_{13} & 0 & 0 & 0 \\ A_{21} & A_{22} & A_{23} & 0 & 0 & 0 \\ A_{31} & A_{32} & A_{33} & 0 & 0 & 0 \\ 0 & 0 & 0 & A_{44} & 0 & 0 \\ 0 & 0 & 0 & 0 & A_{55} & 0 \\ 0 & 0 & 0 & 0 & 0 & A_{66} \end{bmatrix}_K \begin{bmatrix} \sigma_1 \\ \sigma_2 \\ \sigma_3 \\ \sigma_{23} \\ \sigma_{13} \\ \sigma_{12} \end{bmatrix}_K \quad (2.7)$$

where the A_{ij} are defined in terms of material constants as:

$$A_{11} = \frac{1}{E_{11}}$$

$$A_{22} = \frac{1}{E_{22}}$$

$$A_{33} = \frac{1}{E_{33}}$$

$$A_{44} = \frac{1}{2G_{23}}$$

$$\begin{aligned}
 A_{55} &= \frac{1}{2G_{13}} \\
 A_{66} &= \frac{1}{2G_{12}} \\
 A_{12} = A_{21} &= -\frac{\nu_{21}}{E_{22}} = -\frac{\nu_{12}}{E_{11}} \\
 A_{13} = A_{31} &= -\frac{\nu_{31}}{E_{33}} = -\frac{\nu_{13}}{E_{11}} \\
 A_{23} = A_{32} &= -\frac{\nu_{32}}{E_{33}} = -\frac{\nu_{23}}{E_{22}}
 \end{aligned} \tag{2.8}$$

ν_{ij} is defined as the negative of the ratio of strain in the j direction to the strain in the i direction due to a stress in the i direction. and

$$[Q_{ij}]_K^{-1} = [A_{ij}]_K \tag{2.9}$$

Finally, the compliance matrix may be transformed from the (1-2) axes to the (x-y) axes through an angle $(\bar{\theta})$. This gives $[\bar{A}_{ij}]_K$ which in matrix notation is defined as

$$[\bar{A}_{ij}]_K = [T]^{-1} [A_{ij}]_K [T] \tag{2.10}$$

Determination of Lamina Relations for Moment, Shear and Axial Load

Assuming a state of plane strain exists ($\epsilon_y = \epsilon_{yz} = \epsilon_{xy} = \frac{\partial(\quad)}{\partial y} = 0$) the strain-stress relations for the k^{th} lamina are:

$$\begin{bmatrix} \epsilon_x \\ \epsilon_y \\ \epsilon_z \\ \epsilon_{yz} \\ \epsilon_{xz} \\ \epsilon_{xy} \end{bmatrix}_K = \begin{bmatrix} \bar{A}_{11} & \bar{A}_{12} & \bar{A}_{13} & 0 & 0 & \bar{A}_{16} \\ \bar{A}_{12} & \bar{A}_{22} & \bar{A}_{23} & 0 & 0 & \bar{A}_{26} \\ \bar{A}_{31} & \bar{A}_{32} & \bar{A}_{33} & 0 & 0 & \bar{A}_{36} \\ 0 & 0 & 0 & \bar{A}_{44} & \bar{A}_{45} & 0 \\ 0 & 0 & 0 & \bar{A}_{54} & \bar{A}_{55} & 0 \\ \bar{A}_{61} & \bar{A}_{62} & \bar{A}_{63} & 0 & 0 & \bar{A}_{66} \end{bmatrix}_K \begin{bmatrix} \sigma_x \\ \sigma_y \\ \sigma_z \\ \tau_{yz} \\ \tau_{xz} \\ \tau_{xy} \end{bmatrix}_K \quad (2.11)$$

The equilibrium equations are:

$$\frac{\partial \sigma_x}{\partial x} + \frac{\partial \tau_{xz}}{\partial z} = 0 \quad (2.12)$$

$$\frac{\partial \tau_{xz}}{\partial x} + \frac{\partial \sigma_z}{\partial z} = 0 \quad (2.13)$$

The strain-displacement relations are:

$$\epsilon_x = \frac{\partial u}{\partial x} \quad (2.14)$$

$$\epsilon_y = \frac{\partial v}{\partial y} = 0 \quad (2.15)$$

$$\epsilon_z = \frac{\partial w}{\partial z} \quad (\neq 0 \text{ as in classical plate theory}) \quad (2.16)$$

$$\epsilon_{xz} = \frac{1}{2} \left[\frac{\partial u}{\partial z} + \frac{\partial w}{\partial x} \right] \quad (2.17)$$

$$\epsilon_{yz} = \frac{1}{2} \left[\frac{\partial v}{\partial z} + \frac{\partial v}{\partial y} \right] = 0 \quad (2.18)$$

$$\epsilon_{xy} = \frac{1}{2} \left[\frac{\partial u}{\partial y} + \frac{\partial v}{\partial x} \right] = 0 \quad (2.19)$$

where:

u = displacement in the x -direction

v = displacement in the y -direction

w = displacement in the z -direction

Also, it is assumed that the u and w displacements are of the form

$$u = u(x, z) = u^0(x) + f_1(x, z) \quad (2.20)$$

$$w = w(x, z) = w^0(x) + f_2(x, z) \quad (2.21)$$

1. Transverse Shear Stress - τ_{xz}

Assume:

(a) A laminate layed-up symmetric about it's centerline with adhesive shear and normal stresses being applied at it's top and bottom surfaces (Figure 5).

(b) The boundary value constants will be evaluated for an adherend composed of an odd number of lamina. The procedure is the same for an even number of lamina.

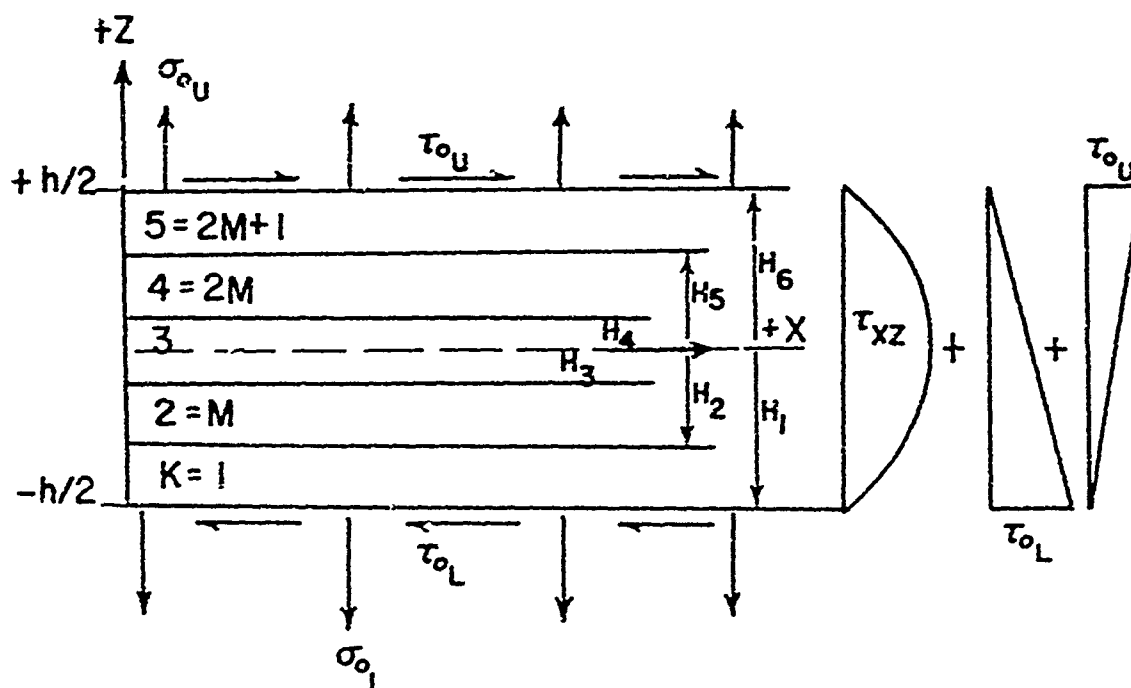


FIGURE (2-5)

K = the number of a particular lamina measured from the bottom surface (i.e. $z = -h/2$)

M = the number of the lamina below the laminates neutral surface.

(c) Superposition is valid. Thus, one can superimpose the adhesive shear stress (τ_o) upon the transverse shear stress of the laminate (τ_{xz}).

(d) It is also assumed that the adhesive thickness (η) $\ll h$. The shear stress $\tau_{xz}|_K$ will take the form defined in equation (2.22)

$$\tau_{xz}|_K = \tau_{oL} f_4(z) + \tau_{ou} f_5(z) + [Q_{55}|_K f_3(z) + b_{55}|_K] \phi x \quad (2.22)$$

where:

$f_3(z)$ is a function which characterizes the shear stress distribution through the thickness of the plate such that $f_3(\pm h/2) = 0$

$f_4(z)$ is a function so defined that for $z = -h/2$ a shear stress τ_{oL} exists, while if $z = +h/2$ the shear stress $\tau_{oL} = 0$

$f_5(z)$ is a function so defined that for $z = +h/2$ a shear stress τ_{ou} exists, while if $z = -h/2$ the shear stress $\tau_{ou} = 0$

b_{55} is a constant which guarantees the continuity of shear stress at the lamina interfaces

ϕ_x is an arbitrary function to be determined

τ_{oL} is the peak shear stress on the lower external surface of the laminate

τ_{ou} is the peak shear stress on the upper external surface of the laminate

Boundary Conditions:

The boundary conditions the transverse shear stress function must satisfy are:

$$\tau_{xz}(\frac{h}{2}) = \tau_{ou} \quad (2.23)$$

$$\tau_{xz}(-\frac{h}{2}) = \tau_{oL} \quad (2.24)$$

$$\tau_{xz}|_K^{(H_{K+1})} = \tau_{xz}|_{K+1}^{(H_{K+1})} \quad (2.25)$$

Let

$$f_3(z) = 1 - 4 \left(\frac{z}{h}\right)^2 \quad (2.26)$$

$$f_4(z) = \frac{1}{2} \left[1 - \frac{2z}{h}\right] \quad (2.27)$$

$$f_5(z) = \frac{1}{2} \left[1 + \frac{2z}{h}\right] \quad (2.28)$$

Provided $b_{55}|_1 = b_{55}|_{2M+1} = 0$ an inspection of $f_3(z)$ and $f_4(z)$ shows that boundary condition (2.23) is satisfied. A similar inspection of $f_3(z)$ and $f_5(z)$ shows boundary condition (2.24) to also be satisfied.

Thus,

$$\tau_{xz}|_K = \frac{\tau_{oL}}{2} \left[1 - \frac{2z}{h}\right] + \frac{\tau_{ou}}{2} \left[1 + \frac{2z}{h}\right] +$$

$$[\bar{Q}_{55}|_K (1 - 4 \left(\frac{z}{h}\right)^2) + b_{55}|_K] \phi_x \quad (2.29)$$

Due to the symmetrical lay-up of the lamina about the neutral axis of the laminate it can be shown that:

$$b_{55}|_K = b_{55}|_{2M+2-K} \quad (2.30)$$

$$K = 1 \rightarrow M$$

Noting the form of $f_4(z)$ and $f_5(z)$ one realizes that $b_{55}|_K$ is independent of them, being influenced only by the difference in the values of $\bar{Q}_{55}|_K$ for adjacent lamina.

To find the other values of $b_{55}|_K$ one uses boundary condition (2.25), namely:

$$\tau_{xz}|_K^{(H_{K+1})} = \tau_{xz}|_{K+1}^{(H_{K+1})}$$

Employing equation (2.29) one gets

$$\begin{aligned} \{\bar{Q}_{55}|_r f_3(H_{r+1}) + b_{55}|_r\} \phi_x &= \{\bar{Q}_{55}|_{r+1} f_3(H_{r+1}) + \\ &+ b_{55}|_{r+1}\} \phi_x \end{aligned}$$

Rearranging,

$$[\bar{Q}_{55}|_r - \bar{Q}_{55}|_{r+1}] f_3(H_{r+1}) + b_{55}|_r = b_{55}|_{r+1}$$

Thus, one can discern that $b_{55|_K}$ is related to the layers preceding it as evidenced by the $b_{55|_r}$ term above. Thus, the general expression for $b_{55|_K}$ can be written

$$b_{55|_K} = \sum_{r=1}^{K-1} f_3(H_{r+1}) [\bar{Q}_{55|_r} - \bar{Q}_{55|_{r+1}}] \quad (2.31)$$

$$K = 2 + M + 1$$

2. Calculation of σ_z from Equilibrium Equations

From equation (2.13) on page 43 one can state

$$\frac{\partial \sigma_z}{\partial z} = - \frac{\partial \tau_{xz}}{\partial x}$$

Integrating over the thickness of the lamina (z) one gets

$$\sigma_z(x, z)_K - \sigma_z(x, 0) = - \int_0^z \frac{\partial \tau_{xz}}{\partial x} dz = - \frac{\partial}{\partial x} \int_0^z \tau_{xz} dz \quad (2.32)$$

Assuming τ_{xz} and it's derivatives are continuous over the area of concern and substituting equation (2.29) into equation (2.32) and defining $d_K(x) = \sigma_z(x, 0)$ one gets

$$\begin{aligned}\sigma_z(x, z)_K = & - \frac{\partial}{\partial x} \left[\int_0^z \frac{\tau_{oL}}{2} \left(1 - \frac{2z}{h}\right) dz + \int_0^z \frac{\tau_{ou}}{2} \left(1 + \frac{2z}{h}\right) dz \right. \\ & + \int_0^z \bar{Q}_{55}|_K \left(1 - 4 \frac{z^2}{h^2}\right) \phi_x dz + \int_0^z b_{55}|_K \phi_x dz \Big] \\ & + d_K(x)\end{aligned}$$

performing the indicated integration an expression for the normal stress is attained

$$\begin{aligned}\sigma_z(x, z)_K = & - \frac{d\tau_{oL}}{dx} \left(\frac{z}{2} - \frac{z^2}{2h}\right) - \frac{d\tau_{ou}}{dx} \left(\frac{z}{2} + \frac{z^2}{2h}\right) \\ & - \bar{Q}_{55}|_K \frac{d\phi_x}{dx} \left(z - \frac{4z^3}{3h^2}\right) - b_{55}|_K \frac{d\phi_x}{dx} z + d_K(x)\end{aligned}\quad (2.33)$$

The constant $d_K(x)$ can be found by imposing certain boundary conditions on $\sigma_z(x, z)_K$. These are

$$\sigma_z(x, H_1)_1 = \sigma_{oL}(x) \quad (2.34)$$

$$\sigma_z(x, H_{2M+2})_{2M+1} = \sigma_{ou}(x) \quad (2.35)$$

$$\sigma_z|_K(x, H_{K+1}) = \sigma_z|_{K+1}(x, H_{K+1}) \quad (2.36)$$

Note that boundary condition (2.36) guarantees the continuity of σ_z through the thickness of the laminate for all (x) .

Using boundary condition (2.34) and equation (2.33) an expression for $d_1(x)$ evolves

$$\begin{aligned} \sigma_z(x, H_1)_1 = \sigma_{oL}(x) = & - \left(\frac{H_1}{2} - \frac{H_1^2}{2h} \right) \frac{d\tau_{oL}}{dx} - \left(\frac{H_1}{2} + \frac{H_1^2}{2h} \right) \frac{d\tau_{ou}}{dx} \\ & - \bar{Q}_{55}|_1 \frac{d\phi_x}{dx} \left(H_1 - \frac{4H_1^3}{3h^2} \right) - \cancel{b_{55}}^o|_1 \frac{d\phi_x}{dx} H_1 + d_1(x) \\ d_1(x) = & \sigma_{oL}(x) + \left(\frac{H_1}{2} - \frac{H_1^2}{2h} \right) \frac{d\tau_{oL}}{dx} + \left(\frac{H_1}{2} + \frac{H_1^2}{2h} \right) \frac{d\tau_{ou}}{dx} \\ & + \bar{Q}_{55}|_1 \frac{d\phi_x}{dx} \left(H_1 - \frac{4H_1^3}{3h^2} \right) \end{aligned} \quad (2.37)$$

Using boundary condition (2.36) and equation (2.33) a general expression for $d_K(x)$ will be developed.

$$\begin{aligned} \sigma_z|_1(x, H_2) = \sigma_z|_2(x, H_2) \\ = \left(\frac{H_2}{2} - \frac{H_2^2}{2h} \right) \frac{d\tau_{oL}}{dx} - \left(\frac{H_2}{2} + \frac{H_2^2}{2h} \right) \frac{d\tau_{ou}}{dx} - \bar{Q}_{55}|_1 \frac{d\phi_x}{dx} \left(H_2 - \frac{4H_2^3}{3h^2} \right) \\ - b_{55}|_1 \frac{d\phi_x}{dx} H_2 + d_1(x) = - \left(\frac{H_2}{2} - \frac{H_2^2}{2h} \right) \frac{d\tau_{oL}}{dx} \end{aligned}$$

$$- \left(\frac{H_2}{2} + \frac{H_2^2}{2h} \right) \frac{d\tau_{ou}}{dx} - \bar{Q}_{55}|_2 \frac{d\phi_x}{dx} \left(H_2 - \frac{4H_2^3}{3h^2} \right)$$

$$- b_{55}|_2 \frac{d\phi_x}{dx} H_2 + d_2(x) = 0$$

Solving for $d_2(x)$ and using equation (2.37)

$$\begin{aligned} d_2(x) = & \{ (\bar{Q}_{55}|_2 - \bar{Q}_{55}|_1) \left(H_2 - \frac{4H_2^3}{3h^2} \right) + (b_{55}|_2 - \cancel{b_{55}|_1}) H_2 \} \frac{d\phi_x}{dx} \\ & + \sigma_{oL}(x) + \left(\frac{H_1}{2} - \frac{H_1^2}{2h} \right) \frac{d\tau_{oL}}{dx} + \left(\frac{H_1}{2} + \frac{H_1^2}{2h} \right) \frac{d\tau_{ou}}{dx} \\ & + \bar{Q}_{55}|_1 \frac{d\phi_x}{dx} \left(H_1 - \frac{4H_1^3}{3h^2} \right) \end{aligned}$$

However, $H_1 = -h/2$, thus rearranging terms one gets

$$\begin{aligned} d_2(x) = & \{ (\bar{Q}_{55}|_2 - \bar{Q}_{55}|_1) \left(H_2 - \frac{4H_2^3}{3h^2} \right) + (b_{55}|_2 - b_{55}|_1) H_2 \\ & - \bar{Q}_{55}|_1 \frac{h}{3} \} \frac{d\phi_x}{dx} + \sigma_{oL} - \frac{3h}{8} \frac{d\tau_{oL}}{dx} - \frac{h}{8} \frac{d\tau_{ou}}{dx} \quad (2.38) \end{aligned}$$

Now to find $d_K(x)$ one sums from $d_1(x)$ to $d_K(x)$.

Thus, a general relationship exists for $d_K(x)$. It is

$$d_K(x) = [\alpha_K - \bar{Q}_{55}|_1 \frac{h}{3}] \frac{d\phi_x}{dx} + \sigma_{oL} - \frac{3h}{8} \frac{d\tau_{oL}}{dx} - \frac{h}{8} \frac{d\tau_{ou}}{dx} \quad (2.39)$$

$$K = 1 \rightarrow 2M + 1$$

where

$$\begin{aligned} \alpha_K = & \sum_{r=1}^{K-1} \{ \bar{Q}_{55}|_{r+1} - \bar{Q}_{55}|_r \} [H_{r+1} - \frac{4H_{r+1}^3}{3h^2}] \\ & + [b_{55}|_{r+1} - b_{55}|_r] H_{r+1} \end{aligned} \quad (2.40)$$

$$K = 2 \rightarrow 2M + 1$$

It is not obvious that boundary condition (2.35) is satisfied. However, for a symmetrical lay-up it is shown in Appendix A that using equation (2.33), with $K = 2M+1$, will result in boundary condition (2.35) being satisfied. Namely, that $\sigma_z(x, H_{2M+2})_{2M+1} = \sigma_{ou}(x)$.

3. Calculation of In-Plane Displacement due to Curvature of the Lamina- $u(x,z)_K$

From equation (2.17), for the K^{th} lamina

$$\epsilon_{xz}|_K = \frac{1}{2} \left(\frac{\partial u}{\partial z} + \frac{\partial w}{\partial x} \right)_K$$

From the strain-stress relations on page 43

$$\epsilon_{xz}|_K = \bar{A}_{54} \tau_{yz}|_K + \bar{A}_{55} \tau_{xz}|_K \quad (2.41)$$

$$\epsilon_{yz}|_K = 0 = \bar{A}_{44} \tau_{yz}|_K + \bar{A}_{45} \tau_{xz}|_K$$

Therefore,

$$\tau_{yz}|_K = - \frac{\bar{A}_{45}}{\bar{A}_{44}} \tau_{xz}|_K \quad (2.42)$$

substituting equation (2.42) into equation (2.41) one gets

$$\epsilon_{xz}|_K = - \frac{\bar{A}_{54} \bar{A}_{45}}{\bar{A}_{44}} \tau_{xz}|_K + \bar{A}_{55} \tau_{xz}|_K$$

$$\text{Let } \Delta_K = - \frac{\bar{A}_{54} \bar{A}_{45}}{\bar{A}_{44}}$$

$$\epsilon_{xz}|_K = (\Delta + \bar{A}_{55}) \tau_{xz}|_K \quad (2.43)$$

substituting equation (2.22) into (2.43) will give an expression for the shear strain ϵ_{xz} in terms of the transverse shear stress in the lamina

$$\begin{aligned} \epsilon_{xz}|_K &= (\Delta + \bar{A}_{55})_K [\tau_{oL} f_4(z) + \tau_{ou} f_5(z)] \\ &+ \{ (\Delta + \bar{A}_{55})_K \bar{Q}_{55}|_K f_3(z) + (\Delta + \bar{A}_{55})_K b_{55}|_K \} \phi_x \end{aligned}$$

Rearranging terms gives

$$\begin{aligned} \varepsilon_{xz}|_K &= (\Delta + \bar{A}_{55})_K [\tau_{oL} f_4(z) + \tau_{ou} f_5(z)] \\ &+ \{(1 + \Delta \bar{Q}_{55})_K f_3(z) + (\Delta + \bar{A}_{55})_K b_{55}|_K\} \phi_x \end{aligned} \quad (2.44)$$

Note that $\Delta \rightarrow 0$ if the material axes coincide with the geometrical axes of the laminate, since in that case

$$\bar{A}_{45} = \bar{A}_{54} = 0.$$

Rearranging equation (2.17) one gets

$$\frac{\partial u}{\partial z}|_K = - \frac{\partial w}{\partial x}|_K + 2\varepsilon_{xz}|_K \quad (2.45)$$

substituting equations (2.29) and (2.44) into (2.45) an expression for $\frac{\partial u}{\partial z}$ in terms of the transverse shear stress is obtained.

$$\begin{aligned} \frac{\partial u}{\partial z}|_K &= - \frac{\partial w}{\partial x}|_K + (\Delta + \bar{A}_{55})_K \left[\tau_{oL} \left(1 - \frac{2z}{h}\right) + \tau_{ou} \left(1 + \frac{2z}{h}\right) \right] \\ &+ 2(1 + \Delta \bar{Q}_{55})_K \left(1 - \frac{4z^2}{h^2}\right) \phi_x + 2(\Delta + \bar{A}_{55})_K b_{55}|_K \phi_x \end{aligned} \quad (2.46)$$

Integrating once over the thickness (z) of the lamina gives the expression for in-plane displacement $u(x,z)_K$ of the lamina.

$$\begin{aligned}
 u(x,z)_K \Big|_0^z = & - \int_0^z \frac{\partial w}{\partial x} \Big|_K dz + (\Delta + \bar{A}_{55})_K \left[\tau_{OL} \left(z - \frac{z^2}{h} \right) \Big|_0^z \right. \\
 & + \tau_{Ou} \left(z + \frac{z^2}{h} \right) \Big|_0^z \Big] + 2(1 + \Delta \bar{Q}_{55})_K \left(z - \frac{4z^3}{3h^2} \right) \Big|_0^z \phi_x \\
 & + 2(\Delta + \bar{A}_{55})_K b_{55} \Big|_K \phi_x z \Big|_0^z \\
 u(x,z)_K = & u(x,0) - \int_0^z \frac{\partial w}{\partial x} \Big|_K dz + (\Delta + \bar{A}_{55})_K \left[\tau_{OL} \left(z - \frac{z^2}{h} \right) \right. \\
 & + \tau_{Ou} \left(z + \frac{z^2}{h} \right) \Big] + 2(1 + \Delta \bar{Q}_{55})_K \left(z - \frac{4z^3}{3h^2} \right) \phi_x \\
 & + 2(\Delta + \bar{A}_{55})_K b_{55} \Big|_K \phi_x z
 \end{aligned} \tag{2.47}$$

Equation (2.47) gives one the expression for in-plane displacement due to curvature effects.

4. Transverse Normal Strain

Unlike most theoretical work performed today,

it will be assumed that $\epsilon_z \neq 0$. This, in turn will give one an expression for $\int_0^z \frac{\partial w}{\partial x} dz$ in terms of σ_z and τ_{xz} .

From equation (2.16) on page 43

$$\epsilon_z|_K = \frac{\partial w(x, z)}{\partial z}|_K$$

differentiating with respect to (x)

$$\frac{\partial \epsilon_z}{\partial x}|_K = \frac{\partial^2 w}{\partial x \partial z}|_K \quad (2.48)$$

From the strain stress relations on page 43.

$$\epsilon_z|_K = \bar{A}_{13} \sigma_x|_K + \bar{A}_{33} \sigma_z|_K \quad (2.49)$$

$$\epsilon_{xy}|_K = 0 = \bar{A}_{61} \sigma_x + \bar{A}_{63} \sigma_z + \bar{A}_{66} \tau_{xy}$$

Mention should be made of the fact that the $\bar{A}_{32} \sigma_y$ and $\bar{A}_{62} \sigma_y$ terms have been neglected. This assumption is felt to be valid since for the construction limitation outlined on page 32 the terms \bar{A}_{32} and \bar{A}_{62} would be small with the resulting values of $\bar{A}_{32} \sigma_y$ and $\bar{A}_{62} \sigma_y$ being at least an order of magnitude smaller than the terms retained. Thus,

$$\tau_{xy}|_K = - \frac{\bar{A}_{61}}{\bar{A}_{66}} \sigma_x|_K - \frac{\bar{A}_{63}}{\bar{A}_{66}} \sigma_z|_K \quad (2.50)$$

differentiating equation (2.49) with respect to (x).

$$\frac{\partial \epsilon_z}{\partial x}|_K = \bar{A}_{13} \frac{\partial \sigma_x}{\partial x}|_K + \bar{A}_{33} \frac{\partial \sigma_z}{\partial x}|_K \quad (2.51)$$

From equilibrium condition (2.12) on page 43

$$\frac{\partial \sigma_x}{\partial x}|_K = - \frac{\partial \tau_{xz}}{\partial z}|_K \quad (2.52)$$

Also, differentiate equation (2.32) on page 49 with respect to (x) one obtains

$$\frac{\partial \sigma_z}{\partial x}|_K = - \frac{2}{\partial x^2} \int_0^z \tau_{xz} dz + \frac{d \sigma_z}{d x} (x, 0)_K \quad (2.53)$$

Letting

$$\frac{d \sigma_z}{d x} (x, 0)_K = \frac{d d_K(x)}{d x}$$

and combining equations (2.48), (2.51), (2.52) and (2.53)

the expression for $\frac{\partial \epsilon_z}{\partial x}$ becomes

$$\frac{\partial^2 \epsilon_z}{\partial x^2}|_K = - \bar{A}_{13} \frac{\partial \tau_{xz}}{\partial z}|_K - \bar{A}_{33}|_K \frac{\partial^2}{\partial x^2} \int_0^z \tau_{xz} dz$$

$$+ \bar{A}_{33}|_K \frac{d\bar{d}_K(x)}{dx} \quad (2.54)$$

differentiating equation (2.29) with respect to (z)

$$\frac{\partial \tau_{xz}}{\partial z}|_K = - \frac{\tau_{oL}}{h} + \frac{\tau_{ou}}{h} - \frac{8 \bar{Q}_{55}|_K}{h^2} z \phi_x \quad (2.55)$$

If one now substitutes equation (2.39) into equation (2.33) and differentiates equation (2.33) with respect to (x) one will get

$$\begin{aligned} \frac{\partial \sigma_z}{\partial x}|_K = & - \frac{d^2 \tau_{oL}}{dx^2} \left(\frac{z}{2} - \frac{z^2}{2h} \right) - \frac{d^2 \tau_{ou}}{dx^2} \left(\frac{z}{2} + \frac{z^2}{2h} \right) \\ & - \bar{Q}_{55}|_K \left(z - \frac{4z^3}{3h^2} \right) \frac{d^2 \phi_x}{dx^2} - b_{55}|_K z \frac{d^2 \phi_x}{dx^2} \\ & + [\alpha_K - \bar{Q}_{55}|_1 \frac{h}{3}] \frac{d^2 \phi_x}{dx^2} + \frac{d\sigma_{oL}}{dx} - \frac{3h}{8} \frac{d^2 \tau_{oL}}{dx^2} \\ & - \frac{h}{8} \frac{d^2 \tau_{ou}}{dx^2} \end{aligned} \quad (2.56)$$

Substituting equations (2.55) and (2.56) into (2.54) gives

$$\frac{\partial^2 w}{\partial x \partial z}|_K = \bar{A}_{13}|_K \frac{\tau_{oL}}{h} - \bar{A}_{13}|_K \frac{\tau_{ou}}{h} + \frac{8 \bar{A}_{13} \bar{Q}_{55}|_K}{h^2} z \phi_x$$

$$\begin{aligned}
 & - \frac{\bar{A}_{33}|_K}{2} \left(z - \frac{z^2}{h} \right) \frac{d^2 \tau_{oL}}{dx^2} - \frac{\bar{A}_{33}|_K}{2} \left(z + \frac{z^2}{h} \right) \frac{d^2 \tau_{ou}}{dx^2} \\
 & - \bar{A}_{33} \bar{Q}_{55}|_K \left(z - \frac{4z^3}{3h^2} \right) \frac{d^2 \phi_x}{dx^2} - \bar{A}_{33} b_{55}|_K z \frac{d^2 \phi_x}{dx^2} \\
 & + \bar{A}_{33}|_K \left(\alpha_K - \bar{Q}_{55}|_1 \frac{h}{3} \right) \frac{d^2 \phi_x}{dx^2} + \bar{A}_{33}|_K \frac{d\sigma_{oL}}{dx} \\
 & - \frac{3h \bar{A}_{33}|_K}{8} \frac{d^2 \tau_{oL}}{dx^2} - \frac{h \bar{A}_{33}|_K}{8} \frac{d^2 \tau_{ou}}{dx^2} \quad (2.57)
 \end{aligned}$$

Collecting terms and integrating over the thickness (z) of the lamina gives

$$\begin{aligned}
 \frac{\partial w}{\partial x} (x, z)_K - \frac{dw}{dx} (x, 0)_K &= \frac{\bar{A}_{13}|_K}{h} [\tau_{oL} - \tau_{ou}] z \\
 & - \frac{\bar{A}_{33}|_K}{2} \left[\frac{z^2}{2} - \frac{z^3}{3h} + \frac{3zh}{4} \right] \frac{d^2 \tau_{oL}}{dx^2} \\
 & - \frac{\bar{A}_{33}|_K}{2} \left[\frac{z^2}{2} + \frac{z^3}{3h} - \frac{zh}{4} \right] \frac{d^2 \tau_{ou}}{dx^2} \\
 & + \frac{4\bar{A}_{13} \bar{Q}_{55}|_K}{h^2} z^2 \phi_x - A_{33}|_K [\bar{Q}_{55}|_K \left(\frac{z^2}{2} - \frac{z^4}{3h^2} \right) \\
 & - \alpha_K z + \bar{Q}_{55}|_1 \frac{hz}{3} + b_{55}|_K \frac{z^2}{2}] \frac{d^2 \phi_x}{dx^2}
 \end{aligned}$$

$$+ \bar{A}_{33}|_K \frac{d\sigma_{oL}}{dx} z \quad (2.58)$$

Integrating once again w/R the thickness (z) will give us the desired relation for $\int_0^z \frac{\partial w}{\partial x} dz$. Namely,

$$\begin{aligned} \int_0^z \frac{\partial w}{\partial x} (x, z)_K dz &= z \frac{dw^o}{dx} + \frac{\bar{A}_{13}|_K}{2h} [\tau_{oL} - \tau_{ou}] z^2 \\ &- \frac{\bar{A}_{33}|_K}{2} \left[\frac{z^3}{6} - \frac{z^4}{12h} + \frac{3z^2h}{8} \right] \frac{d^2 \tau_{oL}}{dx^2} \\ &- \frac{\bar{A}_{33}|_K}{2} \left[\frac{z^3}{6} + \frac{z^4}{12h} - \frac{hz^2}{8} \right] \frac{d^2 \tau_{ou}}{dx^2} \\ &+ 4 \frac{\bar{A}_{13} \bar{Q}_{55}|_K}{3h^2} z^3 \phi_x - \bar{A}_{33}|_K [\bar{Q}_{55}]_K \left(\frac{z^3}{6} - \frac{z^5}{15h^2} \right) \\ &- \frac{\alpha_K z^2}{2} + \bar{Q}_{55}|_1 \frac{hz^2}{6} + b_{55}|_K \left[\frac{z^3}{6} \right] \frac{d^2 \phi_x}{dx^2} \\ &+ \bar{A}_{33}|_K \frac{d\sigma_{oL}}{dx} \frac{z^2}{2} \end{aligned} \quad (2.59)$$

If one substitutes equation (2.59) into equation (2.47) and adds on the in-plane strain component $u_o(x)$ one gets the final relationship for the axial displacement in a lamina under shear, axial and normal loadings.

$$\begin{aligned}
 u(x,z)_K = & u^0(x) + C_K(x) - z \frac{dw^0}{dx} + \left[-\frac{\bar{A}_{13}|_K}{2h} z^2 \right. \\
 & + (\Delta + \bar{A}_{55})_K \left(z - \frac{z^2}{h} \right) \tau_{oL} + \left[-\frac{\bar{A}_{13}|_K}{2h} z^2 \right. \\
 & + (\Delta + \bar{A}_{55})_K \left(z + \frac{z^2}{h} \right) \tau_{ou} + \frac{\bar{A}_{33}|_K}{2} \left[\frac{z^3}{6} \right. \\
 & - \frac{z^4}{12h} + \frac{3z^2 h}{8} \left. \right] \frac{d^2 \tau_{oL}}{dx^2} + \frac{\bar{A}_{33}|_K}{2} \left[\frac{z^3}{6} \right. \\
 & + \frac{z^4}{12h} - \frac{hz^2}{8} \left. \right] \frac{d^2 \tau_{ou}}{dx^2} + \left[(2 + 2\Delta \bar{Q}_{55})_K \left(z - \frac{4z^3}{3h^2} \right) \right. \\
 & + (2\Delta + 2\bar{A}_{55})_K b_{55}|_K z - \frac{4\bar{A}_{13} \bar{Q}_{55}|_K}{3h^2} z^3 \left. \right] \phi_x \\
 & + \bar{A}_{33}|_K \left[\bar{Q}_{55}|_K \left(\frac{z^3}{6} - \frac{z^5}{15h^2} \right) - \frac{\alpha_K z^2}{2} + \bar{Q}_{55}|_1 \frac{hz^2}{6} \right. \\
 & \left. + b_{55}|_K \frac{z^3}{6} \right] \frac{d^2 \phi_x}{dx^2} - \bar{A}_{33}|_K \frac{d\sigma_{oL}}{dx} \frac{z^2}{2} \quad (2.60)
 \end{aligned}$$

To calculate the boundary continuity constants $C_K(x)$ one must employ the boundary conditions $u(x,z)_K$ must satisfy, namely,

$$u(x, z=0)_{M+1} = u^0(x) \quad (2.61)$$

$$u_K(H_K+1) = u_{K+1}(H_K+1) \quad (2.62)$$

Boundary condition (2.61) implies an anti-symmetric bending displacement distribution about the x-axis, namely that curvature effects at the geometric mid-plane are zero.

Boundary condition (2.62) guarantees continuity of in-plane displacements between adjacent lamina.

Using Equation (2.60) and boundary condition (2.61) one gets

$$C_{M+1} = 0$$

Using boundary condition (2.62) and beginning with $K = M+1$, one can readily see a general relationship for $C_K(x)$ evolve.

Using equation (2.62) with $K = M+1$ one gets

$$u_{M+1}(H_{M+2}) = u_{M+2}(H_{M+2})$$

Substituting into this relation using equation (2.60) gives

$$\begin{aligned}
 u^0(x) + C_{M+1}(x) - H_{M+2} \frac{dw^0}{dx} + \left[-\frac{\bar{A}_{13}|_{M+1}}{2h} H_{M+2}^2 \right. \\
 + (\Delta + \bar{A}_{55})_{M+1} \left(H_{M+2} - \frac{H_{M+2}^2}{h} \right) \tau_{oL} + \left[-\frac{\bar{A}_{13}|_{M+1}}{2h} H_{M+2}^2 \right. \\
 + (\Delta + \bar{A}_{55})_{M+1} \left(H_{M+2} + \frac{H_{M+2}^2}{h} \right) \tau_{ou} + \frac{\bar{A}_{33}|_{M+1}}{2} \left[-\frac{H_{M+2}^3}{6} \right. \\
 - \frac{H_{M+2}^4}{12h} - \frac{3H_{M+2}^2}{8} h \left. \right] \frac{d^2 \tau_{oL}}{dx^2} + \frac{\bar{A}_{33}|_{M+1}}{2} \left[-\frac{H_{M+2}^3}{6} \right. \\
 + \frac{H_{M+2}^4}{12h} - \frac{hH_{M+2}^2}{8} \left. \right] \frac{d^2 \tau_{ou}}{dx^2} + [(2 + 2\Delta \bar{Q}_{55})_{M+1} (H_{M+2} \\
 - \frac{4H_{M+2}^3}{3h^2} + (2\Delta + 2\bar{A}_{55})_{M+1} b_{55}|_{M+1} H_{M+2} \\
 - \frac{4\bar{A}_{13}}{3h^2} \bar{Q}_{55}|_{M+1} H_{M+2}^3] \phi_x + \bar{A}_{33}|_{M+1} [\bar{Q}_{55}|_{M+1} (\frac{H_{M+2}^3}{6} \\
 - \frac{H_{M+2}^5}{15h^2}) - \frac{\alpha_{M+1} H_{M+2}^2}{2} + \bar{Q}_{55}|_1 \frac{hH_{M+2}^2}{6} \\
 + b_{55}|_{M+1} \frac{H_{M+2}^3}{6}] \frac{d^2 \phi_x}{dx^2} - \bar{A}_{33}|_{M+1} \frac{d\sigma_{oL}}{dx} \frac{H_{M+2}^2}{2} \\
 = u^0(x) + C_{M+2}(x) - H_{M+2} \frac{dw^0}{dx} + \left[-\frac{\bar{A}_{13}|_{M+2}}{2h} H_{M+2}^2 \right.
 \end{aligned}$$

$$\begin{aligned}
 & + (\Delta + \bar{A}_{55})_{M+2} (H_{M+2} - \frac{H_{M+2}^2}{h}) \tau_{OL} \\
 & + [\bar{A}_{13}]_{M+2} \frac{H_{M+2}^2}{2h} + (\Delta + \bar{A}_{55})_{M+2} (H_{M+2} + \frac{H_{M+2}^2}{h}) \tau_{Ou} \\
 & + \frac{\bar{A}_{33}|_{M+2}}{2} \left[\frac{H_{M+2}^3}{6} - \frac{H_{M+2}^4}{12h} - \frac{3H_{M+2}^2 h}{8} \right] \frac{d^2 \tau_{OL}}{dx^2} \\
 & + \frac{\bar{A}_{33}|_{M+2}}{2} \left[\frac{H_{M+2}^3}{6} + \frac{H_{M+2}^4}{12h} - \frac{hH_{M+2}^2}{8} \right] \frac{d^2 \tau_{Ou}}{dx^2} \\
 & + [(2 + 2\Delta \bar{Q}_{55})_{M+2} (H_{M+2} - \frac{4H_{M+2}^3}{3h^2}) + (2\Delta + 2\bar{A}_{55})_{M+2} b_{55}|_{M+2} H_{M+2} \\
 & - \frac{4\bar{A}_{13}}{3h^2} \bar{Q}_{55}|_{M+2} H_{M+2}^3] \phi_x + \bar{A}_{33}|_{M+2} [\bar{Q}_{55}|_{M+2} (\frac{H_{M+2}^3}{6} \\
 & - \frac{H_{M+2}^5}{15h^2}) - \frac{\alpha_{M+2} H_{M+2}^2}{2} + \bar{Q}_{55}|_1 \frac{hH_{M+2}^2}{6} + b_{55}|_{M+2} \frac{H_{M+2}^3}{6}] \\
 & \frac{d^2 \phi_x}{dx^2} - \bar{A}_{33}|_{M+2} \frac{d\sigma_{OL}}{dx} \frac{H_{M+2}^2}{2}
 \end{aligned}$$

Rearranging the terms in relation to $\frac{d^n}{dx^n}$ and realizing that for the most general $C_K(x)$ a sum of such terms evolves, the general expression for $C_K(x)$ can be written as

$$C_K(x) = D_K \frac{d^2 \phi_x}{dx^2} + E_K \phi_x + F_K \frac{d^2 \tau_{oL}}{dx^2} + \bar{F}_K \frac{d^2 \tau_{ou}}{dx^2} \\ + G_K \tau_{oL} + \bar{G}_K \tau_{ou} + H_K \frac{d\sigma_{oL}}{dx} \quad (2.63)$$

$$K = M + 2 \rightarrow 2M + 1$$

where

$$D_K = \sum_{r=M+1}^{K-1} \{ [\bar{A}_{33}|_r (\bar{Q}_{55}|_r + b_{55}|_r) - \bar{A}_{33}|_{r+1} (\bar{Q}_{55}|_{r+1} \\ + b_{55}|_{r+1})] \frac{H_{r+1}^3}{6} + (\bar{A}_{33} \bar{Q}_{55})_{r+1} - \bar{A}_{33} \bar{Q}_{55}|_r \frac{H_{r+1}^5}{15h^2} \\ + (\bar{A}_{33}|_{r+1} \alpha|_{r+1} - \bar{A}_{33} \alpha|_r) \frac{H_{r+1}^2}{2} \\ + (\bar{A}_{33}|_r - \bar{A}_{33}|_{r+1}) \bar{Q}_{55}|_1 \frac{hH_{r+1}^2}{6} \} \quad (2.64)$$

$$E_K = \sum_{r=M+1}^{K-1} \{ (\bar{A}_{13} \bar{Q}_{55}|_{r+1} - \bar{A}_{13} \bar{Q}_{55}|_r) \frac{4H_{r+1}^3}{3h^2} \\ + (2\Delta \bar{Q}_{55})_r - 2\Delta \bar{Q}_{55}|_{r+1} \} H_{r+1} + (8\Delta \bar{Q}_{55}|_{r+1} \\ - 8\Delta \bar{Q}_{55}|_r) \frac{H_{r+1}^3}{3h^2} + ((2\Delta + 2\bar{A}_{55})_r b_{55}|_r \\ - (2\Delta + 2\bar{A}_{55})_{r+1} b_{55}|_{r+1}) H_{r+1} \} \quad (2.65)$$

$$\bar{F}_K = \sum_{r=M+1}^{K-1} \left\{ \left(\frac{\bar{A}_{33}|_r}{2} - \frac{\bar{A}_{33}|_{r+1}}{2} \right) \left(\frac{H_{r+1}^3}{6} + \frac{H_{r+1}^4}{12h} - \frac{3hH_{r+1}^2}{8} \right) \right\} \quad (2.66)$$

$$F_K = \sum_{r=M+1}^{K-1} \left\{ \left(\frac{\bar{A}_{33}|_r}{2} - \frac{\bar{A}_{33}|_{r+1}}{2} \right) \left(\frac{H_{r+1}^3}{6} - \frac{H_{r+1}^4}{12h} + \frac{3hH_{r+1}^2}{8} \right) \right\} \quad (2.67)$$

$$G_K = \sum_{r=M+1}^{K-1} \left\{ (\bar{A}_{13}|_{r+1} - \bar{A}_{13}|_r) \frac{H_{r+1}^2}{2h} + [(\Delta + \bar{A}_{55})_r - (\Delta + \bar{A}_{55})_{r+1}] \left[H_{r+1} - \frac{H_{r+1}^2}{h} \right] \right\} \quad (2.68)$$

$$\bar{G}_K = \sum_{r=M+1}^{K-1} \left\{ (\bar{A}_{13}|_r - \bar{A}_{13}|_{r+1}) \frac{H_{r+1}^2}{2h} + [(\Delta + \bar{A}_{55})'_r - (\Delta + \bar{A}_{55})_{r+1}] \left[H_{r+1} + \frac{H_{r+1}^2}{h} \right] \right\} \quad (2.69)$$

$$H_K = \sum_{r=M+1}^{K-1} (\bar{A}_{33}|_{r+1} - \bar{A}_{33}|_r) \frac{H_{r+1}^2}{2} \quad (2.70)$$

Let us check to see if this general expression for $C_K(x)$ holds for $K = M + 1$. Using boundary condition (2.62) and setting $K = M$

$$u_M(H_{M+1}) - u_{M+1}(H_{M+1}) = 0$$

Substituting into this relation using equation (2.60) gives

$$\begin{aligned}
 C_M - C_{M+1} - H_{M+1} \frac{dw^0}{dx} + H_{M+1} \frac{dw^0}{dx} + [(-\bar{A}_{13}|_M \\
 + \bar{A}_{13}|_{M+1}) \frac{H_{M+1}^2}{2h} + ((\Delta + \bar{A}_{55})_M - (\Delta + \bar{A}_{55})_{M+1}) (H_{M+1} \\
 - \frac{H_{M+1}^2}{h}) \tau_{oL} + (\bar{A}_{13}|_M - \bar{A}_{13}|_{M+1}) \frac{H_{M+1}^2}{2h} \\
 + [(\Delta + \bar{A}_{55})_M - (\Delta + \bar{A}_{55})_{M+1}] [H_{M+1} + \frac{H_{M+1}^2}{h}] \tau_{ou} \\
 + [\frac{\bar{A}_{33}|_M}{2} - \frac{\bar{A}_{33}|_{M+1}}{2}] [\frac{H_{M+1}^3}{6} - \frac{H_{M+1}^4}{12h} - \frac{3hH_{M+1}^2}{8}] \frac{d^2 \tau_{oL}}{dx^2} \\
 + [\frac{\bar{A}_{33}|_M}{2} - \frac{\bar{A}_{33}|_{M+1}}{2}] [\frac{H_{M+1}^3}{6} + \frac{H_{M+1}^4}{12h} - \frac{hH_{M+1}^2}{8}] \frac{d^2 \tau_{ou}}{dx^2} \\
 + \{[(2 + 2\Delta \bar{Q}_{55})_M - (2 + 2\Delta \bar{Q}_{55})_{M+1}] (H_{r+1} - \frac{4H_{r+1}^3}{3h^2}) \\
 + \{(2\Delta + 2\bar{A}_{55})_M b_{55}|_M - (2\Delta + \bar{A}_{55})_{M+1} b_{55}|_{M+1}\} H_{r+1} \\
 + (\bar{A}_{13} \bar{Q}_{55}|_{M+1} - \bar{A}_{13} \bar{Q}_{55}|_M) \frac{4H_{M+1}^3}{3h^2} \} \phi_x
 \end{aligned}$$

$$\begin{aligned}
 & + [(\bar{A}_{33} \bar{Q}_{55}|_M - \bar{A}_{33} \bar{Q}_{55}|_{M+1}) (\frac{H^3_{r+1}}{6} - \frac{H^5_{r+1}}{15h^2}) \\
 & + (\bar{A}_{33} \alpha|_{M+1} - \bar{A}_{33} \alpha|_M) \frac{H^2_{M+1}}{2} + (\bar{A}_{33}|_M - \bar{A}_{33}|_{M+1}) \\
 & \bar{Q}_{55}|_1 \frac{hH^2_{M+1}}{6} + (\bar{A}_{33}|_M b_{55}|_M - \bar{A}_{33}|_{M+1} b_{55}|_{M+1}) \frac{H^3_{r+1}}{6}] \frac{d^2 \phi_x}{dx^2} \\
 & + [\bar{A}_{33}|_{M+1} - \bar{A}_{33}|_M] \frac{d\sigma_{OL}}{dx} \frac{H^2_{r+1}}{2}
 \end{aligned}$$

Now visually checking these constants vs. those
for $C_K(x)$ already defined there results:

$$\underline{K = M + 1}$$

$$- D_K$$

$$- E_K$$

$$- F_K$$

$$- G_K$$

$$- H_K$$

$$\underline{K = M + 2 \rightarrow 2M + 1}$$

$$D_K$$

$$E_K$$

$$F_K$$

$$G_K$$

$$H_K$$

Thus the lamina below the mid-plane lamina have the
same general constant relationships but with new limits.
Thus for lamina $K = M + 1$ the following constants are
valid

$$\begin{aligned}
 D_K = & \sum_{r=M+1}^2 \{ [A_{33}|_r (Q_{55}+b_{55})_r - A_{33}|_{r-1} (Q_{55}+b_{55})_{r-1}] \frac{H_r^3}{6} \\
 & + (A_{33} Q_{55}|_{r-1} - \bar{A}_{33} Q_{55}|_r) \frac{H_r^5}{15h^2} \\
 & + (\bar{A}_{33}|_{r-1} \alpha_{r-1} - \bar{A}_{33}|_r \alpha_r) \frac{H_r^2}{2} \\
 & + (\bar{A}_{33}|_r - \bar{A}_{33}|_{r-1}) \bar{Q}_{55}|_1 \frac{hH_r^2}{6} \} \quad (2.71)
 \end{aligned}$$

$$\begin{aligned}
 E_K = & \sum_{r=M+1}^2 \{ (\bar{A}_{13} \bar{Q}_{55}|_{r-1} - \bar{A}_{13} \bar{Q}_{55}|_r) \frac{4H_r^3}{3h^2} \\
 & + (2\Delta \bar{Q}_{55}|_r - 2\Delta \bar{Q}_{55}|_{r-1}) H_r + (8\Delta \bar{Q}_{55}|_{r-1} - 8\Delta \bar{Q}_{55}|_r) \frac{H_r^3}{3h^2} \\
 & + ((\Delta + \bar{A}_{55})_r b_{55}|_r - (\Delta + \bar{A}_{55})_{r-1} b_{55}|_{r-1}) 2H_r \} \quad (2.72)
 \end{aligned}$$

$$\begin{aligned}
 F_K = & \sum_{r=M+1}^2 \{ (\bar{A}_{33}|_r - \bar{A}_{33}|_{r-1}) \frac{H_r^3}{12} + (\bar{A}_{33}|_{r-1} - \bar{A}_{33}|_r) \frac{H_r^4}{24h} \\
 & + (\bar{A}_{33}|_r - \bar{A}_{33}|_{r-1}) \frac{3h H_r^2}{16} \} \quad (2.73)
 \end{aligned}$$

$$\bar{F}_K = \sum_{r=M+1}^2 \left\{ \left(\frac{\bar{A}_{33}|_r}{2} - \frac{\bar{A}_{33}|_{r-1}}{2} \right) \left(\frac{H_r^3}{6} + \frac{H_r^4}{12h} - \frac{h H_r^2}{8} \right) \right\} \quad (2.74)$$

$$G_K = \sum_{r=M+1}^2 \{ (\bar{A}_{13}|_{r-1} - \bar{A}_{13}|_r) \frac{H_r^2}{2h} + [(\Delta + \bar{A}_{55})_r - (\Delta + \bar{A}_{55})_{r-1}] [H_r - \frac{H_r^2}{h}] \} \quad (2.75)$$

$$\bar{G}_K = \sum_{r=M+1}^2 \{ (\bar{A}_{13}|_r - \bar{A}_{13}|_{r-1}) \frac{H_r^2}{2h} + [(\Delta + \bar{A}_{55})_r - (\Delta + \bar{A}_{55})_{r-1}] [H_r + \frac{H_r^2}{h}] \} \quad (2.76)$$

$$H_K = \sum_{r=M+1}^2 \{ (\bar{A}_{33}|_{r-1} - \bar{A}_{33}|_r) \frac{H_r^2}{2} \} \quad (2.77)$$

Thus having evaluated all constants the general relationship for $u(x, z)_K$ can be written:

$$u(x, z)_K = u^0(x) - \frac{zdw^0}{dx} + [-\frac{\bar{A}_{13}|_K}{2h} z^2 + (\Delta + \bar{A}_{55})_K (z - \frac{z^2}{h}) + G_K] \tau_{oL} + [\frac{A_{13}|_K}{2h} z^2 + (\Delta + \bar{A}_{55})_K (z + \frac{z^2}{h}) + \bar{G}_K] \tau_{ou} + \{ \frac{\bar{A}_{33}|_K}{2} [\frac{z^3}{6}$$

$$\begin{aligned}
 & - \frac{z^4}{12h} + \frac{3zh^2}{8} + F_K \} \frac{d^2 \tau_{oL}}{dx^2} + \left\{ \frac{\bar{A}_{33}|_K}{2} \left[\frac{z^3}{6} \right. \right. \\
 & + \left. \frac{z^4}{12h} - \frac{hz^2}{8} \right] + \bar{F}_K \} \frac{d^2 \tau_{ou}}{dx^2} + [(2+2\Delta \bar{Q}_{55})_K (z - \frac{4z^3}{3h^2}) \\
 & + (2\Delta + 2\bar{A}_{55})_K b_{55}|_K z - \frac{4\bar{A}_{13}}{3h^2} \bar{Q}_{55}|_K z^3 + E_K] \phi_x \\
 & + \{ \bar{A}_{33}|_K [\bar{Q}_{55}|_K (\frac{z^3}{6} - \frac{z^5}{15h^2} - \frac{a_K z^2}{2} + Q_{55}|_1 \frac{hz^2}{6} \\
 & + b_{55}|_K \frac{z^3}{6}] + D_K \} \frac{d^2 \phi_x}{dx^2} + (- \bar{A}_{33}|_K \frac{z^2}{2} + H_K) \frac{d\sigma_{oL}}{dx} \\
 & \hspace{15em} (2.78)
 \end{aligned}$$

5. Calculation of the Resultant Axial Load, Moment and Transverse Shear Relations for a Plate:

By definition

$$\epsilon_x(x, z)_K = \frac{\partial u(x, z)_K}{\partial x} \quad (2.79)$$

Also, from the stress-strain relations on page 39

$$\sigma_x(x, z)_K = \bar{Q}_{11}|_K \epsilon_x|_K + \bar{Q}_{13}|_K \epsilon_z|_K \quad (2.80)$$

Neglect per page 57

By definition, in laminated plate theory the resultant moment over the thickness of the plate is defined as

$$M_x = \sum_{K=1}^N \int_{H_{K-1}}^{H_K} \sigma_x \cdot z \, dz \quad (2.81)$$

In a similar vein the resultant axial load acting over the thickness of the plate is defined as

$$N_x = \sum_{K=1}^N \int_{H_{K-1}}^{H_K} \sigma_x \, dz \quad (2.82)$$

Finally the transverse shear resultant through the thickness of the plate is defined as

$$Q_x = \sum_{K=1}^N \int_{H_{K-1}}^{H_K} \tau_{xz} \, dz \quad (2.83)$$

Employing equations (2.78-2.80) the general relationship for $\sigma_x(x, z)_K$ is

$$\begin{aligned} \sigma_x(x, z)_K = & \bar{Q}_{11}|_K \left\{ \frac{du^o}{dx} - z \frac{d^2 w^o}{dx^2} + \left[-\frac{\bar{A}_{13}|_K}{2h} z^2 \right. \right. \\ & + (\Delta + \bar{A}_{55})_K \left(z - \frac{z^2}{h} \right) + G_K \left. \right] \frac{d\tau_{oL}}{dx} + \left[\frac{\bar{A}_{13}|_K}{2h} z^2 \right. \\ & + (\Delta + \bar{A}_{55})_K \left(z + \frac{z^2}{h} \right) + \bar{G}_K \left. \right] \frac{d\tau_{ou}}{dx} + \left\{ \frac{\bar{A}_{33}|_K}{2} \left[\frac{z^3}{6} \right. \right. \end{aligned}$$

$$\begin{aligned}
 & - \frac{z^4}{12h} - \frac{3z^2h}{8} + F_K \} \frac{d^3 \tau_{OL}}{dx^3} + \left\{ \frac{\bar{A}_{33}|_K}{2} \left[\frac{z^3}{6} + \frac{z^4}{12h} \right. \right. \\
 & \left. \left. - \frac{hz^2}{8} \right] + \bar{F}_K \right\} \frac{d^3 \tau_{OL}}{dx^3} + [(2+2\Delta\bar{Q}_{55})_K \left(z - \frac{4z^3}{3h^2} \right) \\
 & + (2\Delta+2\bar{A}_{55})_K b_{55}|_K z - \frac{4\bar{A}_{13}\bar{Q}_{55}|_K}{3h^2} z^3 + E_K] \frac{d\phi_x}{dx} \\
 & + \{ \bar{A}_{33}|_K [\bar{Q}_{55}|_K \left(\frac{z^3}{6} - \frac{z^5}{15h^2} \right) - \frac{\alpha_K z^2}{2} + \bar{Q}_{55}|_1 \frac{hz^2}{6} \\
 & + b_{55}|_K \frac{z^3}{6} + D_K \} \frac{d^3 \phi_x}{dx^3} + (-\bar{A}_{33}|_K \frac{z^2}{2} + H_K) \frac{d^2 \sigma_{OL}}{dx^2} \} \\
 & \hspace{15em} (2.84)
 \end{aligned}$$

Final relations for moment, axial load, and shear, will now be stated. The reader should realize that for a laminate symmetric w/R to it's mid-surface the relations marked (0) would equal zero.

Employing equations (2.81) and (2.84) a general expression for M_x is calculated.

$$\begin{aligned}
 M_x = & \sum_{K=1}^N \left\{ \int_{H_{K-1}}^{H_K} \bar{Q}_{11}|_K \frac{du^0}{dx} z dz - \int_{H_{K-1}}^{H_K} \bar{Q}_{11}|_K \frac{d^2 w^0}{dx^2} z^2 dz \right. \\
 & + \left[\int_{H_{K-1}}^{H_K} \frac{\bar{Q}_{11}\bar{A}_{13}|_K}{2h} z^3 dz + \int_{H_{K-1}}^{H_K} \bar{Q}_{11} (\Delta+\bar{A}_{55})_K \left(z^2 - \frac{z^3}{h} \right) dz \right. \\
 & \left. \left. \left. \begin{array}{c} \nearrow 0 \\ \nearrow 0 \end{array} \right. \right. \right.
 \end{aligned}$$

$$\begin{aligned}
 & + \int_{H_{K-1}}^{H_K} \bar{Q}_{11}|_K G_K z dz \left[\frac{d\tau_{oL}}{dx} + \left[\int_{H_{K-1}}^{H_K} \frac{\bar{Q}_{11} \bar{A}_{13}|_K}{2h} z^3 dz \right. \right. \\
 & + \int_{H_{K-1}}^{H_K} \bar{Q}_{11} (\Delta + \bar{A}_{55})_K (z^2 + \frac{z^3}{h}) dz + \int_{H_{K-1}}^{H_K} \bar{Q}_{11}|_K G_K z dz \left. \right] \frac{d\tau_{ou}}{dx} \\
 & + \left[\int_{H_{K-1}}^{H_K} \bar{Q}_{11} \bar{A}_{33}|_K (\frac{z^4}{12} dz - \frac{z^5}{24h} + \frac{3z^3}{16}) dz \right. \\
 & + \int_{H_{K-1}}^{H_K} \bar{Q}_{11} \bar{A}_{33}|_K F_K z dz \left. \right] \frac{d^3 \tau_{oL}}{dx^3} + \left[\int_{H_{K-1}}^{H_K} \bar{Q}_{11} \bar{A}_{33}|_K (\frac{z^4}{12} \right. \\
 & + \frac{z^5}{24h} - \frac{hz}{16}) dz + \int_{H_{K-1}}^{H_K} \bar{Q}_{11}|_K \bar{A}_{33}|_K F_K z dz \left. \right] \frac{d^3 \tau_{oL}}{dx^3} \\
 & + \left[\int_{H_{K-1}}^{H_K} \bar{Q}_{11}|_K (2+2\Delta \bar{Q}_{55})_K z^2 dz - \int_{H_{K-1}}^{H_K} \bar{Q}_{11}|_K (2+2\Delta \bar{Q}_{55})_K \frac{4z^4}{3h^2} dz \right. \\
 & + \int_{H_{K-1}}^{H_K} \bar{Q}_{11}|_K (2\Delta + 2\bar{A}_{55})_K b_{55}|_K z^2 dz - \int_{H_{K-1}}^{H_K} \frac{4\bar{Q}_{11} \bar{A}_{13} \bar{Q}_{55}|_K}{3h^2} z^4 dz \\
 & + \int_{H_{K-1}}^{H_K} \bar{Q}_{11}|_K E_K z dz \left. \right] \frac{d\phi_x}{dx} + \left[\int_{H_{K-1}}^{H_K} \bar{Q}_{11} \bar{A}_{33} \bar{Q}_{55}|_K (\frac{z^4}{6} - \right. \\
 & - \frac{z^6}{15h^2}) dz - \int_{H_{K-1}}^{H_K} \bar{A}_{33} \bar{Q}_{11}|_K \alpha_K \frac{z^3}{2} dz + \int_{H_{K-1}}^{H_K} \bar{Q}_{11} \bar{A}_{33}|_K \bar{Q}_{55}|_K \frac{hz^3}{6} dz \\
 & + \int_{H_{K-1}}^{H_K} \bar{A}_{33} \bar{Q}_{11}|_K b_{55}|_K \frac{z^4}{6} dz + \int_{H_{K-1}}^{H_K} \bar{Q}_{11}|_K D_K z dz \left. \right] \frac{d^3 \phi_x}{dx^3}
 \end{aligned}$$

$$+ \left[- \int_{H_{K-1}}^{H_K} \bar{Q}_{11} \bar{A}_{33} \Big|_K \frac{z^3}{2} dz + \int_{H_{K-1}}^{H_K} \bar{Q}_{11} \Big|_K \frac{H_K}{z} dz \right] \frac{d^2 \sigma_{OL}}{dx^2} \quad (2.85)$$

Employing equations (2.82) and (2.84) a general expression for N_x is calculated.

$$\begin{aligned} N_x = & \sum_{K=1}^N \left\{ \int_{H_{K-1}}^{H_K} \bar{Q}_{11} \Big|_K \frac{du^o}{dx} dz - \int_{H_{K-1}}^{H_K} \bar{Q}_{11} \Big|_K \frac{d^2 w^o}{dx^2} dz \right. \\ & + \left[- \int_{H_{K-1}}^{H_K} \frac{\bar{Q}_{11} \bar{A}_{13} \Big|_K}{2h} z^2 dz + \int_{H_{K-1}}^{H_K} \bar{Q}_{11} \Big|_K (\Delta + \bar{A}_{55}) \left(z - \frac{z^2}{h} \right) dz \right. \\ & + \int_{H_{K-1}}^{H_K} \bar{Q}_{11} \Big|_K G_K dz \Big] \frac{d\tau_{OL}}{dx} + \left[\int_{H_{K-1}}^{H_K} \bar{Q}_{11} \frac{\bar{A}_{13} \Big|_K}{2h} z^2 dz \right. \\ & + \int_{H_{K-1}}^{H_K} \bar{Q}_{11} \Big|_K (\Delta + \bar{A}_{55}) \left(z + \frac{z^2}{h} \right) dz + \int_{H_{K-1}}^{H_K} \bar{Q}_{11} \Big|_K G_K^* dz \Big] \frac{d\tau_{OU}}{dx} \\ & + \left[\int_{H_{K-1}}^{H_K} \bar{Q}_{11} \bar{A}_{33} \Big|_K \left[\frac{z^3}{12} - \frac{z^4}{24h} + \frac{3z^2 h}{16} \right] dz \right. \\ & \left. + \int_{H_{K-1}}^{H_K} \bar{Q}_{11} \Big|_K F_K dz \right] \frac{d^3 \tau_{OL}}{dx^3} + \left[\int_{H_{K-1}}^{H_K} \bar{Q}_{11} \bar{A}_{33} \Big|_K \left(\frac{z^3}{12} \right. \right. \end{aligned}$$

$$\begin{aligned}
 & + \frac{z^4}{24h} - \frac{hz^2}{16} dz + \int_{H_{K-1}}^{H_K} \bar{Q}_{11}|_K F_K^* dz \Big] \frac{d^3 \tau_{oL}}{dx^3} \\
 & + \left[\int_{H_{K-1}}^{H_K} \bar{Q}_{11}|_K (2+2\Delta\bar{Q}_{55})_K \cancel{z dz} - \int_{H_{K-1}}^{H_K} \bar{Q}_{11}|_K (2+2\Delta\bar{Q}_{55})_K \right. \\
 & \quad \left. \frac{4z^3}{3h^2} dz + \int_{H_{K-1}}^{H_K} \bar{Q}_{11}|_K (2\Delta+2\bar{A}_{55})_K b_{55}|_K \cancel{z dz} \right. \\
 & \quad \left. - \int_{H_{K-1}}^{H_K} \frac{4\bar{Q}_{11} \bar{A}_{13}}{3h^2} \bar{Q}_{55}|_K \cancel{z^3 dz} + \int_{H_{K-1}}^{H_K} \bar{Q}_{11}|_K E_K dz \right] \frac{d\phi_x}{dx} \\
 & + \left[\int_{H_{K-1}}^{H_K} \bar{Q}_{11} \bar{A}_{33} \bar{Q}_{55}|_K \left(\frac{z^3}{6} - \frac{z^5}{15h^2} \right) dz - \int_{H_{K-1}}^{H_K} \bar{Q}_{11} \bar{A}_{33} \alpha|_K \frac{z^2}{2} dz \right. \\
 & \quad \left. + \int_{H_{K-1}}^{H_K} \bar{Q}_{11} \bar{A}_{33}|_K \bar{Q}_{55}|_1 \frac{hz^2}{6} dz + \int_{H_{K-1}}^{H_K} \bar{Q}_{11} \bar{A}_{33}|_K b_{55}|_K \frac{z^3}{6} dz \right. \\
 & \quad \left. + \int_{H_{K-1}}^{H_K} \bar{Q}_{11} D_K dz \right] \frac{d^3 \phi_x}{dx^3} + \left[- \int_{H_{K-1}}^{H_K} \bar{Q}_{11} \bar{A}_{33}|_K \frac{z^2}{2} dz \right. \\
 & \quad \left. + \int_{H_{K-1}}^{H_K} \bar{Q}_{11}|_K H_K dz \right] \frac{d^2 \sigma_{oL}}{dx^2} \} \quad (2.86)
 \end{aligned}$$

Employing equations (2.83-2.84) a general expression

for Q_x is calculated:

$$Q_x = \sum_{K=1}^N \left\{ \int_{H_{K-1}}^{H_K} \tau_{oL} \left(\frac{1}{2} - \frac{z}{h} \right) dz + \int_{H_{K-1}}^{H_K} \tau_{ou} \left(\frac{1}{2} + \frac{z}{h} \right) dz \right. \\ \left. + \left[\int_{H_{K-1}}^{H_K} \bar{Q}_{55} \left(1 - \frac{4z^2}{h^2} \right) dz + \int_{H_{K-1}}^{H_K} b_{55} dz \right] \phi_x \right\} \quad (2.87)$$

In summation the moment, axial load and transverse shear relations for a symmetric laminated composite plate have been developed. These equations assume a state of plane strain exists. They also include the effects of

- 1) transverse shear
- 2) normal strain
- 3) the upper and lower extreme surfaces of the laminate having a shear and normal stress applied to them.

In a condensed notation the moment, axial load and transverse shear relations can be rewritten as

$$M_x = - D_{11} \frac{d^2 w^o}{dx^2} + F \frac{d^3 \phi_x}{dx^3} + G \frac{d \phi_x}{dx} + H \frac{d^3 \tau_{oL}}{dx^3} + I \frac{d \tau_{oL}}{dx} \\ + \bar{I} \frac{d \tau_{ou}}{dx} + \bar{H} \frac{d^3 \tau_{ou}}{dx^3} \quad (2.88)$$

$$N_x = A \frac{d^3 \phi_x}{dx^3} + B \frac{d\phi_x}{dx} + C \frac{d^3 \tau_{oL}}{dx^3} + \bar{C} \frac{d^3 \tau_{ou}}{dx^3} + D \frac{d\tau_{oL}}{dx} + \bar{D} \frac{d\tau_{ou}}{dx} \\ + E \frac{d^2 \tau_{oL}}{dx^2} + \bar{A} \frac{du^o}{dx} \quad (2.89)$$

$$Q_x = \frac{h}{2} (\tau_{oL} + \tau_{ou}) + K_5 \phi_x \quad (2.90)$$

where:

$$A = \sum_{K=1}^N \left\{ - \int_{H_{K-1}}^{H_K} \bar{Q}_{11} \bar{A}_{33}|_K \alpha_K \frac{z^2}{2} dz \right. \\ \left. + \int_{H_{K-1}}^{H_K} \bar{Q}_{11} \bar{A}_{33}|_K Q_{55}|_1 \frac{h}{6} z^2 dz + \int_{H_{K-1}}^{H_K} \bar{Q}_{11}|_K D_K dz \right\} \quad (2.91)$$

$$B = \sum_{K=1}^N \int_{H_{K-1}}^{H_K} \bar{Q}_{11}|_K E_K dz \quad (2.92)$$

$$C = \sum_{K=1}^N \left\{ - \int_{H_{K-1}}^{H_K} \bar{Q}_{11} \bar{A}_{33}|_K \frac{z^4}{24h} dz + \int_{H_{K-1}}^{H_K} \bar{Q}_{11} \bar{A}_{33}|_K \frac{3h}{16} z^2 dz \right. \\ \left. + \int_{H_{K-1}}^{H_K} \bar{Q}_{11}|_K F_K dz \right\} \quad (2.93)$$

$$\bar{C} = \sum_{K=1}^N \left\{ \int_{H_{K-1}}^{H_K} \bar{Q}_{11} \bar{A}_{33}|_K \left(\frac{z^4}{24h} - \frac{hz^2}{16} \right) dz + \int_{H_{K-1}}^{H_K} \bar{Q}_{11}|_K F_K^* dz \right\} \quad (2.94)$$

$$D = \sum_{K=1}^N \left\{ - \int_{H_{K-1}}^{H_K} \bar{Q}_{11} \bar{A}_{13}|_K \frac{z^2}{2h} dz - \int_{H_{K-1}}^{H_K} \bar{Q}_{11}|_K (\Delta + \bar{A}_{55})_K \frac{z^2}{h} dz + \int_{H_{K-1}}^{H_K} \bar{Q}_{11}|_K G_K dz \right\} \quad (2.95)$$

$$\bar{D} = \sum_{K=1}^N \left\{ \int_{H_{K-1}}^{H_K} \bar{Q}_{11} \bar{A}_{13}|_K \frac{z^2}{2h} dz + \int_{H_{K-1}}^{H_K} \bar{Q}_{11}|_K (\Delta + \bar{A}_{55})_K \frac{z^2}{h} dz + \int_{H_{K-1}}^{H_K} \bar{Q}_{11}|_K G_K dz \right\} \quad (2.96)$$

$$E = \sum_{K=1}^N \left\{ - \int_{H_{K-1}}^{H_K} \bar{Q}_{11} \bar{A}_{33}|_K \frac{z^2}{2} dz + \int_{H_{K-1}}^{H_K} \bar{Q}_{11}|_K H_K dz \right\} \quad (2.97)$$

$$\bar{A} = \sum_{K=1}^N \int_{H_{K-1}}^{H_K} \bar{Q}_{11}|_K dz \quad (2.98)$$

$$D_{11} = \sum_{K=1}^N \int_{H_{K-1}}^{H_K} \bar{Q}_{11}|_K z^2 dz \quad (2.99)$$

$$F = \sum_{K=1}^N \left\{ \int_{H_{K-1}}^{H_K} \bar{Q}_{11} \bar{A}_{33} \bar{Q}_{55}|_K \frac{z^4}{6} dz - \int_{H_{K-1}}^{H_K} \bar{Q}_{11} \bar{A}_{33} \bar{Q}_{55}|_K \frac{z^6}{15h^2} dz \right\}$$

$$+ \int_{H_{K-1}}^{H_K} \bar{Q}_{11} \bar{A}_{33}|_K b_{55}|_K \frac{z^4}{6} dz \quad (2.100)$$

$$\begin{aligned} G = & \sum_{K=1}^N \left\{ - \int_{H_{K-1}}^{H_K} 4\bar{Q}_{11} \bar{A}_{13} \bar{Q}_{55}|_K \frac{z^4}{3h^2} dz \right. \\ & + \int_{H_{K-1}}^{H_K} \bar{Q}_{11}|_K (1+\Delta\bar{Q}_{55})_K 2z^2 dz - \int_{H_{K-1}}^{H_K} \bar{Q}_{11}|_K (1+\Delta\bar{Q}_{55})_K \frac{8z^4}{3h^2} dz \\ & \left. + \int_{H_{K-1}}^{H_K} \bar{Q}_{11}|_K (\Delta+\bar{A}_{55})_K b_{55}|_K 2z^2 dz \right\} \quad (2.101) \end{aligned}$$

$$H = \sum_{K=1}^N \int_{H_{K-1}}^{H_K} \bar{Q}_{11} \bar{A}_{33}|_K \frac{z^4}{12} dz \quad (2.102)$$

$$I = \sum_{K=1}^N \int_{H_{K-1}}^{H_K} \bar{Q}_{11}|_K (\Delta+\bar{A}_{55})_K z^2 dz \quad (2.103)$$

$$\bar{I} = \sum_{K=1}^N \int_{H_{K-1}}^{H_K} \bar{Q}_{11}|_K (\Delta+\bar{A}_{55})_K z^2 dz \quad (2.104)$$

$$\begin{aligned} K_5 = & \sum_{K=1}^N \left\{ \int_{H_{K-1}}^{H_K} \bar{Q}_{55}|_K dz - \int_{H_{K-1}}^{H_K} 4\bar{Q}_{55}|_K \frac{z^2}{h^2} dz \right. \\ & \left. + \int_{H_{K-1}}^{H_K} b_{55}|_K dz \right\} \quad (2.105) \end{aligned}$$

6. Reduction of Equations (2.88-2.90) to the
Governing Equations of Parts (1) and (4)

Parts (1) and (4) as defined in Figure 2, page 36 have their extreme upper and lower surfaces free of external shear and normal stresses. The governing relations for M_x , N_x , and Q_x can be found by setting τ_{oL} , τ_{ou} , σ_{oL} , and σ_{ou} to zero in equations (2.88-2.90).

The resulting relations become:

Part 1

$$M_x = -D_{111} \frac{d^2 w_1^o}{dx^2} + F \frac{d^3 \phi_{x1}}{dx^3} + G \frac{d\phi_{x1}}{dx} \quad (2.106)$$

$$N_x = A \frac{d^3 \phi_{x1}}{dx^3} + B \frac{d\phi_{x1}}{dx} + \bar{A} \frac{du_1^o}{dx} \quad (2.107)$$

$$Q_x = K_5 \phi_{x1} \quad (2.108)$$

Part 4

$$M_x = -D_{114} \frac{d^2 w_4^o}{dx^2} + F^* \frac{d^3 \phi_{x4}}{dx^3} + G^* \frac{d\phi_{x4}}{dx} \quad (2.109)$$

$$N_x = A^* \frac{d^3 \phi_{x_4}}{dx^3} + B^* \frac{d\phi_{x_4}}{dx} + \bar{A}^* \frac{du_4^o}{dx} \quad (2.110)$$

$$Q_x = K_5^* \phi_{x_4} \quad (2.111)$$

where the (*) terms are so labeled as the upper and lower adherends may be of different materials, thicknesses and/or lamina orientation. This would result in different values for the constants associated with Part 1 and Part 4, respectively.

Numerical values of the constants in equations (2.106-2.111) can be determined by using equations (2.40), (2.64-2.65), (2.71-2.72) and relations (2.91-2.105).

7. Reduction of Equations (2.88-2.90) to the Governing Equations of Part 2

Part 2 as defined in Figure 2, page 36 has it's lower surface under the influence of stresses τ_{oL} and σ_{oL} while its upper surface is free of applied stresses. The governing relations for M_x , N_x , and Q_x can be obtained by equating σ_{ou} and τ_{ou} to zero in equations (2.88-2.90).

The resulting relations become

$$M_x = - D_{11} \frac{d^2 w_2^o}{dx^2} + F \frac{d^3 \phi_{x2}}{dx^3} + G \frac{d\phi_{x2}}{dx} + H \frac{d^3 \tau_{oL}}{dx^3} + I \frac{d\tau_{oL}}{dx} \quad (2.112)$$

$$N_x = A \frac{d^3 \phi_{x2}}{dx^3} + B \frac{d\phi_x}{dx} + C \frac{d^3 \tau_{oL}}{dx^3} + D \frac{d\tau_{oL}}{dx} + E \frac{d^2 \sigma_{oL}}{dx^2} + \bar{A} \frac{du_2^o}{dx} \quad (2.113)$$

$$Q_x = \frac{h\tau_{oL}}{2} + K_5 \phi_{x2} \quad (2.114)$$

The definition of the constants in equations (2.112-2.114) can be determined as follows:

$b_{55}|_K$ is obtained using equations (2.30) and (2.31)

α_K is obtained using equation (2.40)

$C_K(x)$ is obtained from equation (2.63) by setting

$$\tau_{ou} = 0$$

Therefore,

$$C_K(x) = D_K \frac{d^2 \phi_{x_2}}{dx^2} + E_K \phi_{x_2} + F_K \frac{d^2 \tau_{oL}}{dx^2} + G_K \tau_{oL} + H_K \frac{d\sigma_{oL}}{dx} \quad (2.115)$$

$$K = 1 \rightarrow 2M + 1$$

where D_K , E_K , F_K , G_K , H_K are determined using equations (2.64-2.77).

8. Reduction of Equations (2.88-2.90) to the Governing Equations of Part 3

Part 3 as defined in Figure 2, page 36 has it's upper surface under the influence of stresses τ_{ou} and σ_{ou} while the lower surface is free of applied stresses. With this information one can readily see that Part 3 is just Part 2 rotated 180 degrees about the x-axis.

Therefore, the resultant moment, axial load and shear relations (equations 2.88-2.90) with τ_{oL} and σ_{oL} replaced by τ_{ou} and σ_{ou} , respectively, are

$$M_x = -D_{11} \frac{d^2 w_3}{dx^2} + F^* \frac{d^3 \phi_{x_3}}{dx^3} + G^* \frac{d\phi_{x_3}}{dx} + H^* \frac{d^3 \tau_{ou}}{dx^3} + I^* \frac{d\tau_{ou}}{dx} \quad (2.116)$$

$$N_x = A^* \frac{d^3 \phi_{x3}}{dx^3} + B^* \frac{d\phi_{x3}}{dx} + C^* \frac{d^3 \tau_{ou}}{dx^3} + D^* \frac{d\tau_{ou}}{dx} + E^* \frac{d^2 \tau_{ou}}{dx^2} + \bar{A}^* \frac{du_3^0}{dx} \quad (2.117)$$

$$Q_x = \frac{h_3}{2} \tau_{ou} + K_5^* \phi_{x3} \quad (2.118)$$

To determine the constants $A^* - H^*$, $D_K^* - H_K^*$, and α_K^* several changes in the formulas for these constants must be performed. These changes are necessitated by the change in sign of the second term in the function $f_4(z)$ vs. $f_5(z)$. A brief check of equations (2.27) and (2.28) will reinforce this rationale.

Therefore, the net effect on the equations used to calculate the above mentioned constants is twofold.

- 1) Replace $\bar{Q}_{55}|_1$ by $-\bar{Q}_{55}|_{2M+1}$ where necessary
- 2) Change the sign of all terms in the constants which reflect the difference of sign in function $f_4(z)$ vs. $f_5(z)$.

The net result is presented here as equations (2.119-

2.145).

$$\begin{aligned} \alpha_K^* = & \sum_{r=2M}^K \{ [\bar{Q}_{55}|_r - \bar{Q}_{55}|_{r+1}] H_{r+1} + [\bar{Q}_{55}|_{r+1} - \bar{Q}_{55}|_r] \frac{4H_{r+1}^3}{3h^2} + [b_{55}|_r - b_{55}|_{r+1}] H_{r+1} \} \\ & (2.119) \end{aligned}$$

$$K = 2M + 1$$

where:

$$\alpha_{2M+1}^* = 0 \quad (2.120)$$

$$\begin{aligned} C_K^*(x) = & D_K^* \frac{d^2 \phi_{x_3}}{dx^2} + E_K^* \phi_{x_3} + F_K^* \frac{d^2 \tau_o}{dx^2} + G_K^* \tau_o \\ & + H_K^* \frac{d\sigma_{ou}}{dx} \end{aligned} \quad (2.121)$$

$$K = 1 \rightarrow 2M + 1$$

where for the lamina $K = M + 2 \rightarrow 2M + 1$ the following relations are valid:

$$\begin{aligned}
 D_K^* = & \sum_{r=M+1}^{K-1} \{ [\bar{A}_{33} \bar{Q}_{55}|_r - \bar{A}_{33} \bar{Q}_{55}|_{r+1}] \frac{H_{r+1}^3}{6} + [\bar{A}_{33} \bar{Q}_{55}|_{r+1} \\
 & - \bar{A}_{33} \bar{Q}_{55}|_r] \frac{H_{r+1}^5}{15h_3^2} + [\bar{A}_{33} b_{55}|_r - \bar{A}_{33} b_{55}|_{r+1}] \frac{H_{r+1}^3}{6} \\
 & + [\bar{A}_{33} \alpha^*|_{r+1} - A_{33} \alpha^*|_r] \frac{H_{r+1}^2}{2} + [\bar{A}_{33}|_{r+1} - \bar{A}_{33}|_r] \\
 & \bar{Q}_{55}|_{2M+1} \frac{h_3 H_{r+1}^2}{6} \} \quad (2.122)
 \end{aligned}$$

$$\begin{aligned}
 E_K^* = & \sum_{r=M+1}^{K-1} \{ [\bar{A}_{13} \bar{Q}_{55}|_{r+1} - \bar{A}_{13} \bar{Q}_{55}|_r] \frac{4H_{r+1}^3}{3h_3^2} \\
 & + [\Delta \bar{Q}_{55}|_r - \Delta \bar{Q}_{55}|_{r+1}] 2H_{r+1} + [\Delta \bar{Q}_{55}|_{r+1} \\
 & - \Delta \bar{Q}_{55}|_r] \frac{8H_{r+1}^3}{3h_3^2} + [(\Delta + \bar{A}_{55})_r b_{55}|_r \\
 & - (\Delta + \bar{A}_{55})_{r+1} b_{55}|_{r+1}] 2H_{r+1} \} \quad (2.123)
 \end{aligned}$$

$$F_K^* = \sum_{r=M+1}^{K-1} \{ [\bar{A}_{33}|_r - \bar{A}_{33}|_{r+1}] \frac{H_{r+1}^3}{12} + [\bar{A}_{33}|_r - \bar{A}_{33}|_{r+1}] \frac{H_{r+1}^4}{24h_3} + [\bar{A}_{33}|_{r+1} - \bar{A}_{33}|_r] \frac{3h_3}{16} H_{r+1}^2 \} \quad (2.124)$$

$$G_K^* = \sum_{r=M+1}^{K-1} \{ [\bar{A}_{13}|_r - \bar{A}_{13}|_{r+1}] \frac{H_{r+1}^2}{2h_3} + [(\Delta + \bar{A}_{55})_r - (\Delta + \bar{A}_{55})_{r+1}] H_{r+1} + [(\Delta + \bar{A}_{55})_r - (\Delta + \bar{A}_{55})_{r+1}] \frac{H_{r+1}^2}{h_3} \} \quad (2.125)$$

$$H_K^* = \sum_{r=M+1}^{K-1} \{ [\bar{A}_{33}|_{r+1} - \bar{A}_{33}|_r] \frac{H_{r+1}^2}{2} \} \quad (2.126)$$

$$K = M + 2 \rightarrow 2M + 1$$

Moreover, for the lamina $K = M + 1$ the following constants are valid:

$$D_K^* = \sum_{r=M+1}^2 \{ [\bar{A}_{33} \bar{Q}_{55}|_r - \bar{A}_{33} \bar{Q}_{55}|_{r-1}] \frac{H_r^3}{6} + [\bar{A}_{33} \bar{Q}_{55}|_{r-1} + \bar{A}_{33} \bar{Q}_{55}|_r] \frac{H_r^5}{15h_3^2} \}$$

$$\begin{aligned}
 & + [\bar{A}_{33} \bar{b}_{55}|_r - \bar{A}_{33} b_{55}|_{r-1}] \frac{H_r^3}{6} + [A_{33} \alpha^*|_{r-1} \\
 & - A_{33} \alpha^*|_r] \frac{H_r^2}{2} + [\bar{A}_{33}|_{r-1} - \bar{A}_{33}|_r] \frac{h_3 \bar{Q}_{55}|_{2M+1}}{6} H_r^2 \} \\
 & (2.127)
 \end{aligned}$$

$$\begin{aligned}
 E_K^* &= \sum_{r=M+1}^2 \{ [\bar{A}_{13} \bar{Q}_{55}|_{r-1} - \bar{A}_{13} \bar{Q}_{55}|_r] \frac{4H_r^3}{3h_3} \\
 & + [\Delta \bar{Q}_{55}|_r - \Delta \bar{Q}_{55}|_{r-1}] 2H_r + [\Delta \bar{Q}_{55}|_{r-1} - \Delta \bar{Q}_{55}|_r] \frac{8H_r^3}{3h_3^2} \\
 & + [(\Delta + \bar{A}_{55})_r b_{55}|_r - (\Delta + \bar{A}_{55})_{r-1} b_{55}|_{r-1}] 2H_r \} \quad (2.128)
 \end{aligned}$$

$$\begin{aligned}
 F_K^* &= \sum_{r=M+1}^2 \{ [\bar{A}_{33}|_r - \bar{A}_{33}|_{r-1}] \frac{H_r^3}{12} + [\bar{A}_{33}|_r - \bar{A}_{33}|_{r-1}] \\
 & \frac{H_r^4}{24h_3} + [\bar{A}_{33}|_{r-1} - \bar{A}_{33}|_r] \frac{3h_3 H_r^2}{16} \} \quad (2.129)
 \end{aligned}$$

$$\begin{aligned}
 G_K^* &= \sum_{r=M+1}^2 \{ [\bar{A}_{13}|_r - \bar{A}_{13}|_{r-1}] \frac{H_r^2}{2h_3} + [(\Delta + \bar{A}_{55})_r \\
 & - (\Delta + \bar{A}_{55})_{r-1}] H_r + [(\Delta + \bar{A}_{55})_r - (\Delta + \bar{A}_{55})_{r-1}] \frac{H_r^2}{h_3} \} \quad (2.130)
 \end{aligned}$$

$$H_K^* = \sum_{r=M+1}^2 [\bar{A}_{33}|_{r-1} - \bar{A}_{33}|_r] \frac{H_r^2}{2} \quad (2.13)$$

$$K = M + 1$$

Finally, equations (2.91-2.105) are rewritten to read

$$A^* = \sum_{K=1}^N \left\{ - \int_{H_{K-1}}^{H_K} \bar{Q}_{11} \bar{A}_{33}|_K \alpha_K^* \frac{z^2}{2} dz - \int_{H_{K-1}}^{H_K} \bar{Q}_{11} \bar{A}_{33}|_K \bar{Q}_{55}|_{2M+1} \right.$$

$$\left. \frac{h_3 z^2}{6} dz + \int_{H_{K-1}}^{H_K} \bar{Q}_{11}|_K D_K^* dz \right\} \quad (2.132)$$

$$B^* = \sum_{K=1}^N \int_{H_{K-1}}^{H_K} \bar{Q}_{11}|_K E_K^* dz \quad (2.133)$$

$$C^* = \sum_{K=1}^N \left\{ - \int_{H_{K-1}}^{H_K} \bar{Q}_{11} \bar{A}_{33}|_K \frac{3h_3}{16} z^2 dz \right.$$

$$\left. + \int_{H_{K-1}}^{H_K} \bar{Q}_{11} \bar{A}_{33}|_K \frac{z^4}{24h_3} dz + \int_{H_{K-1}}^{H_K} \bar{Q}_{11}|_K F_K^* dz \right\} \quad (2.134)$$

$$D^* = \sum_{K=1}^N \left\{ \int_{H_{K-1}}^{H_K} \bar{Q}_{11} \bar{A}_{13}|_K \frac{z^2}{2h_3} dz + \int_{H_{K-1}}^{H_K} \bar{Q}_{11}|_K (\Delta + \bar{A}_{55})_K \frac{z^2}{h_3} dz \right.$$

$$\left. + \int_{H_{K-1}}^{H_K} \bar{Q}_{11}|_K G_K^* dz \right\} \quad (2.135)$$

$$E^* = \sum_{K=1}^N \left\{ - \frac{H_K}{H_{K-1}} \bar{Q}_{11} \bar{A}_{33} \Big|_K \frac{z^2}{2} dz + \frac{H_K}{H_{K-1}} \bar{Q}_{11} \Big|_K H_K^* dz \right\} \quad (2.136)$$

$$\bar{A}^* = \sum_{K=1}^N \frac{H_K}{H_{K-1}} \bar{Q}_{11} \Big|_K dz \quad (2.137)$$

$$\bar{D}_{11}^* = \sum_{K=1}^N \frac{H_K}{H_{K-1}} \bar{Q}_{11} \Big|_K z^2 dz \quad (2.138)$$

$$F^* = \sum_{K=1}^N \left\{ \frac{H_K}{H_{K-1}} \bar{Q}_{11} \bar{A}_{33} \bar{Q}_{55} \Big|_K \frac{z^4}{6} dz - \frac{H_K}{H_{K-1}} \bar{Q}_{11} \bar{A}_{33} \bar{Q}_{55} \Big|_K \frac{z^6}{15h_3^2} dz + \frac{H_K}{H_{K-1}} \bar{Q}_{11} \bar{A}_{33} \bar{Q}_{55} \Big|_K \frac{z^4}{6} dz \right\} \quad (2.139)$$

$$G^* = \sum_{K=1}^N \left\{ - \frac{H_K}{H_{K-1}} \bar{Q}_{11} \bar{A}_{13} \bar{Q}_{55} \Big|_K \frac{4z^4 dz}{3h_3^2} + \frac{H_K}{H_{K-1}} \bar{Q}_{11} \Big|_K (1 + \Delta \bar{Q}_{55})_K 2z^2 dz - \frac{H_K}{H_{K-1}} \bar{Q}_{11} \Big|_K (1 + \Delta \bar{Q}_{55})_K \frac{8z^4}{3h_3^2} dz + \frac{H_K}{H_{K-1}} \bar{Q}_{11} \Big|_K (\Delta + \bar{A}_{55})_K \bar{Q}_{55} \Big|_K 2z^2 dz \right\} \quad (2.140)$$

$$H^* = \sum_{K=1}^N \int_{H_{K-1}}^{H_K} \bar{Q}_{11} \bar{A}_{33}|_K \frac{z^4}{12} dz \quad (2.141)$$

$$I^* = \sum_{K=1}^N \int_{H_{K-1}}^{H_K} \bar{Q}_{11}|_K (\Delta + \bar{A}_{55})_K z^2 dz \quad (2.142)$$

$$K_5^* = \sum_{K=1}^N \left\{ \int_{H_{K-1}}^{H_K} Q_{55}|_K dz - \int_{H_{K-1}}^{H_K} 4\bar{Q}_{55}|_K \frac{z^2}{h_3} dz + \int_{H_{K-1}}^{H_K} b_{55}|_K dz \right\} \quad (2.143)$$

It is also desirable to specify the expressions for $\sigma_{z3}(x, z)_K$, $u_3(x, z)_K$ and $\frac{dw_3}{dx}|_K$ as they also will be modified due to the rationale elaborated on page 86. The resulting expressions become:

$$\sigma_{z3}(x, z)_K = \left[-\frac{z}{2} - \frac{z^2}{2h} \right] \frac{d\tau_{ou}}{dx} + \left[-\bar{Q}_{55}|_K z + \frac{4\bar{Q}_{55}|_K}{3} \frac{z^3}{h^2} - b_{55}|_K z \right] \frac{d\phi_{x3}}{dx} + d_K^*(x) \quad (2.144)$$

where:

$$d_K^*(x) = [\alpha_K^* + \frac{h_3}{3} \bar{Q}_{55}|_{2M+1}] \frac{d\phi_{x_3}}{dx} + \sigma_{ou} + \frac{3h}{8} \frac{d\tau_{ou}}{dx} \quad (2.145)$$

$$K = 2M + 1 + 1$$

$$u_3(x, z)_K = u_3^0 - z \frac{dw^0}{dx} + [\bar{A}_{13}|_K \frac{z^2}{2h_3} + (\Delta + \bar{A}_{55})_K z + G_K^*$$

$$+ (\Delta + \bar{A}_{55})_K \frac{z^2}{h_3}] \tau_0 + [-4\bar{A}_{13} \bar{Q}_{55}|_K \frac{z^3}{3h_3}$$

$$+ (1 + \Delta \bar{Q}_{55})_K 2z - (1 + \Delta \bar{Q}_{55})_K \frac{8z^3}{3h_3} + E_K^*$$

$$+ (\Delta + \bar{A}_{55})_K b_{55}|_K 2z] \phi_{x_3} + [\bar{A}_{33}|_K \frac{z^3}{12} + F_K^*$$

$$+ \bar{A}_{33}|_K \frac{z^4}{24h_3} - \bar{A}_{33}|_K \frac{3h_3 z^2}{16}] \frac{d^2 \tau_0}{dx^2}$$

$$+ [\bar{A}_{33} \bar{Q}_{55}|_K \frac{z^3}{6} - \bar{A}_{33} \bar{Q}_{55}|_K \frac{z^5}{15h_3} + \bar{A}_{33} b_{55}|_K \frac{z^3}{6} + D_K^*$$

$$- \bar{A}_{33} \alpha_K^* \frac{z^2}{2} - \bar{A}_{33}|_K \bar{Q}_{55}|_{2M+1} \frac{h_3 z^2}{6}] \frac{d^2 \phi_{x_3}}{dx^2}$$

$$+ [-\bar{A}_{33}|_K \frac{z^2}{2} + H_K^*] \frac{d\sigma_o}{dx} \quad (2.146)$$

$$+ \frac{\partial w_3}{\partial x} (x, z)_K - \frac{dw(x, 0)_K}{dx} = -\bar{A}_{13}|_K \tau_o \frac{z}{h_3} + 4\bar{A}_{13} Q_{55}|_K \frac{z^2}{h_3^2} \phi_{x_3}$$

$$+ \bar{A}_{33}|_K \frac{d^2 \tau_o}{dx^2} [-\frac{z^2}{4} - \frac{z^3}{6h_3}] + \bar{A}_{33}|_K \frac{d^2 \phi_{x_3}}{dx^2} [-\bar{Q}_{55}|_K \frac{z^2}{2}$$

$$+ \bar{Q}_{55}|_K \frac{z^4}{3h_3^2} - b_{55}|_K \frac{z^2}{2} + \alpha_K^* z + \frac{h_3}{3} \bar{Q}_{55}|_{2M+1} z]$$

$$+ \bar{A}_{33}|_K z \frac{d\sigma_o}{dx} + \frac{3}{8} \bar{A}_{33}|_K h_3 \frac{d^2 \tau_o}{dx^2} z \quad (2.147)$$

9. Summary

It should be noted that these moment, shear, and axial load relations are valid for any laminate subject to the restrictions mentioned on page 32. While the case for an odd number of lamina was solved in detail, these relations are valid for an even number of lamina provided the boundary value constants are adjusted to reflect this lay-up. Having these relations one could solve any number of physical problems by employing these

relations in connection with the proper force equilibrium and boundary conditions which are valid for the case in question.

It should also be noted that the relations derived give shear and normal stress distributions throughout the lamina. Thus the stresses in the resin between laminae can be determined. As is known failure very often occurs in the resin yet most present day analyses ignore this fact.

E. DEVELOPMENT OF ADHESIVE STRESS-STRAIN AND FORCE
 EQUILIBRIUM EQUATIONS

To make the problem determinant and thus solvable it is necessary that the stress-strain relations between the adhesive and the adherends be determined. Also, the force equilibrium criteria on all four sections is a prerequisite for a determinant solution. These relations will now be formulated.

1. Development of the Adhesive Stress-Strain
 Relations

Assume the adhesive is a homogeneous, isotropic material system. Set $\tau_{oL} = \tau_{ou} = \tau_o$ and $\sigma_{oL} = \sigma_{ou} = \sigma_o$. Also, set the upper laminate thickness to h_2 and the lower laminate thickness to h_3 . The stress-displacement relations can be written

$$w_2(x, -\frac{h_2}{2}) - w_3(x, \frac{h_3}{2}) = \frac{\sigma_o}{C_n} \quad (2.148)$$

$$u_2(x, -\frac{h_2}{2}) - u_3(x, \frac{h_3}{2}) = \frac{\tau_o}{C_s} \quad (2.149)$$

by definition:

$$C_n = \frac{E_{\text{adhesive}}}{\tau_{\text{adhesive}}}$$

$$C_s = \frac{G_{\text{adhesive}}}{\tau_{\text{adhesive}}}$$

where it should be noted that the E and G values here are not those measured by standard tests of the bulk material, but values determined through experiment, of the adhesive in the geometry of the joint, from the relations above.

Using the relations developed earlier for u_K and $\frac{\partial u}{\partial x}|_K$ for parts 2 and 3 one can obtain expressions relating the laminate physical properties to τ_0 and σ_0 .

(a) Equation (2.149) - Derivation of

Using equation (2.76) one gets

$$u_2(x, -\frac{h_2}{2})_1 = + \frac{h_2}{2} \frac{dw^0}{dx} + \bar{A}_{13}|_1 \frac{h_2}{8} - (\Delta + \bar{A}_{55})_1 \frac{h_3}{7}$$

$$- (\Delta + \bar{A}_{55})_1 \frac{h_2}{4} + G_1 \tau_0 + [\bar{A}_{13} \bar{Q}_{55}]_1 \frac{h_2}{6}$$

$$\begin{aligned}
 & - (1+\Delta\bar{Q}_{55})_1 h_2 + (1+\Delta\bar{Q}_{55})_1 \frac{h_2}{3} - (\Delta+\bar{A}_{55})_1 \cancel{b_{55}|_1} h_2 \\
 & + E_1] \phi_{x_2} + [-\bar{A}_{33}|_1 \frac{h_2^3}{96} - \bar{A}_{33}|_1 \frac{h_2^3}{384} \\
 & + \frac{3\bar{A}_{33}|_1}{64} h_2^3 + F_1] \frac{d^2 \tau_o}{dx^2} + [-\bar{A}_{33} \bar{Q}_{55}|_1 \frac{h_2^3}{48} \\
 & + \bar{A}_{33} \bar{Q}_{55}|_1 \frac{h_2^3}{480} - \bar{A}_{33} \cancel{b_{55}|_1} \frac{h_2^3}{48} - \bar{A}_{33} \cancel{\alpha|_1} \frac{h_2^2}{8} \\
 & + \bar{A}_{33}|_1 \bar{Q}_{55}|_1 \frac{h_2^3}{24} + D_1] \frac{d^2 \phi_{x_2}}{dx_2^2} + [-\bar{A}_{33}|_1 \frac{h_2^2}{8} \\
 & + H_1] \frac{d\sigma_o}{dx} + u_2^O(x)
 \end{aligned}$$

Upon simplifying one gets

$$\begin{aligned}
 u_2(x, -\frac{h_2}{2})_1 &= \frac{h_2}{2} \frac{dw^O}{dx} + [-\bar{A}_{13}|_1 \frac{h_2}{8} - (\Delta+\bar{A}_{55})_1 \frac{3h_2}{4} \\
 &+ G_1] \tau_o + [\bar{A}_{13} \bar{Q}_{55}|_1 \frac{h_2}{6} - (1+\Delta\bar{Q}_{55})_1 \frac{2h_2}{3}
 \end{aligned}$$

$$\begin{aligned}
 & + F_1] \phi_{x_2} + [\frac{13}{384} \bar{A}_{33}|_1 h_2^3 + F_1] \frac{d^2 \tau_o}{dx^2} \\
 & + [\frac{11}{480} \bar{A}_{33} \bar{Q}_{55}|_1 h_2^3 + D_1] \frac{d^2 \phi_{x_2}}{dx^2} \\
 & + [- \bar{A}_{33}|_1 \frac{h_2^2}{8} + H_1] \frac{d\sigma_o}{dx} + u_o^0(x) \quad (2.150)
 \end{aligned}$$

similarly using (2.146) with $K = 2M + 1$ the relation for $u_3(x, \frac{h_3}{2})$ involves

$$\begin{aligned}
 u_3(x, \frac{h_3}{2}) &= - \frac{h_3}{2} \frac{dw^o}{dx} + [\bar{A}_{13}|_{2M+1} \frac{h_3}{8} + (\Delta + \bar{A}_{55})_{2M+1} \frac{h_3}{2} \\
 &+ G_{2M+1}^* + (\Delta + \bar{A}_{55})_{2M+1} \frac{h_3}{4}] \tau_o + [- \bar{A}_{13} \bar{Q}_{55}|_{2M+1} \frac{h_3}{6} \\
 &+ (1 + \Delta \bar{Q}_{55})_{2M+1} h_3 - (1 + \Delta \bar{Q}_{55})_{2M+1} \frac{h_3}{3} + E_{2M+1}^* \\
 &+ (\Delta + \bar{A}_{55})_{2M+1} b_{55}|_{2M+1} h_3] \phi_{x_3} + [\bar{A}_{33}|_{2M+1} \frac{h_3^3}{96}
 \end{aligned}$$

$$\begin{aligned}
 & + F_{2M+1}^* + \bar{A}_{33}|_{2M+1} \frac{h_3^3}{384} - \bar{A}_{33}|_{2M+1} \frac{3h_3^3}{64} \frac{d^2 \tau_0}{dx^2} \\
 & + [\bar{A}_{33} \bar{Q}_{55}|_{2M+1} \frac{h_3^3}{48} - \bar{A}_{33} \bar{Q}_{55}|_{2M+1} \frac{h_3^3}{480} + \bar{A}_{33} b_{55}|_{2M+1} \frac{h_3^3}{48} \\
 & + D_{2M+1}^* - \bar{A}_{33} \alpha|_{2M+1} \frac{h_3^2}{8} - \bar{A}_{33} \bar{Q}_{55}|_{2M+1} \frac{h_3^3}{24} \frac{d^2 \phi_{x_3}}{dx^2} \\
 & + [- \bar{A}_{33}|_{2M+1} \frac{h_3^2}{8} + \Pi_{2M+1}^*] \frac{d\sigma_0}{dx} + u_3^0(x)
 \end{aligned}$$

Upon simplifying once again one gets

$$\begin{aligned}
 u_3(x, \frac{h_3}{2}) & = - \frac{h_3}{2} \frac{dw^0}{dx} + [\bar{A}_{13}|_{2M+1} \frac{h_3}{8} + (\Delta + \bar{A}_{55})_{2M+1} \frac{3h_3}{4} \\
 & + G_{2M+1}^*] \tau_0 + [- \bar{A}_{13} \bar{Q}_{55}|_{2M+1} \frac{h_3}{6} + (1 + \Delta \bar{Q}_{55})_{2M+1} \frac{2h_3}{3} \\
 & + E_{2M+1}^*] \phi_{x_3} + [- \bar{A}_{33}|_{2M+1} \frac{13h_3^3}{384} + F_{2M+1}^*] \frac{d^2 \tau_0}{dx^2} \\
 & + [- \frac{11}{480} \bar{A}_{33} \bar{Q}_{55}|_{2M+1} h_3^3 + D_{2M+1}^*] \frac{d^2 \phi_{x_3}}{dx^2}
 \end{aligned}$$

$$+ [-\bar{A}_{33}|_{2M+1} \frac{h_3^2}{8} + H_{2M+1}^*] \frac{d\sigma_o}{dx} + u_o^o(x) \quad (2.151)$$

Substitute equations (2.150) and (2.151) into (2.149) to get the first governing equation:

$$\begin{aligned} \frac{\tau_o}{C_s} = & u_o^o(x) - u_o^o(x) + \frac{h_2}{2} \frac{dw_o^o}{dx} + \frac{h_3}{2} \frac{dw_o^o}{dx} + [-\bar{A}_{13}|_1 \frac{h_2}{8} \\ & - \bar{A}_{13}|_{2M+1} \frac{h_3}{8} - (\Delta + \bar{A}_{55})_1 \frac{3h_2}{4} - (\Delta + \bar{A}_{55})_{2M+1} \frac{3h_3}{4} \\ & + G_1 - G_{2M+1}^*] \tau_o + \phi_{x_2} \bar{A}_{13} \bar{Q}_{55}|_1 \frac{h_2}{6} + \bar{A}_{13} \bar{Q}_{55}|_{2M+1} \frac{h_3}{6} \phi_x^3 \\ & - (1 + \Delta \bar{Q}_{55})_1 \frac{2h_2}{3} \phi_{x_2} - (1 + \Delta \bar{Q}_{55})_{2M+1} \frac{2h_3}{3} \phi_{x_3} + E_1 \phi_{x_2} \\ & - E_{2M+1}^* \phi_{x_3} + [\frac{13}{384} \bar{A}_{33}|_1 h_2^3 + \frac{13}{384} \bar{A}_{33}|_{2M+1} h_3^2 \\ & + F_1 - F_{2M+1}^*] \frac{d^2 \tau_o}{dx^2} + \frac{11}{480} \bar{A}_{33} \bar{Q}_{55}|_1 h_2^3 \frac{d^2 \phi_{x_2}}{dx^2} \end{aligned}$$

$$\begin{aligned}
 & + \frac{11}{480} \bar{A}_{33} \bar{Q}_{55}|_{2M+1} h_3^3 \frac{d^2 \phi_{x_3}}{dx^2} + D_1 \frac{d^2 \phi_{x_2}}{dx^2} - D_{2M+1}^* \frac{d^2 \phi_{x_3}}{dx^2} \\
 & + [- \bar{A}_{33}|_1 \frac{h_2^2}{8} + \bar{A}_{33}|_{2M+1} \frac{h_3^2}{8} + H_1 - H_{2M+1}^*] \frac{d\sigma_0}{dx}
 \end{aligned}$$

Upon rearranging this equation and defining several new parameters, the resulting equation is

$$\begin{aligned}
 \frac{\tau_0}{C_s} = & + u_2^0(x) - u_3^0(x) \frac{h_2}{2} \frac{dw_2^0}{dx} + \frac{h_3}{2} \frac{dw_3^0}{dx} + \bar{p} \tau_0 + \bar{r} \frac{d^2 \tau_0}{dx^2} \\
 & + q \phi_{x_2} - q^* \phi_{x_3} + s \frac{d^2 \phi_{x_2}}{dx^2} + s^* \frac{d^2 \phi_{x_3}}{dx^2} + \bar{t} \frac{d\sigma_0}{dx} \quad (2.152)
 \end{aligned}$$

where:

$$\begin{aligned}
 \bar{p} = & [- \bar{A}_{13}|_1 \frac{h_2}{8} - \bar{A}_{13}|_{2M+1} \frac{h_3}{8} - (\Delta + \bar{A}_{55})_1 \frac{3h_2}{4} \\
 & - (\Delta + \bar{A}_{55})_{2M+1} \frac{3h_3}{4} + G_1 - G_{2M+1}^*] \quad (2.153)
 \end{aligned}$$

$$\bar{r} = \left[\frac{13}{384} \bar{A}_{33} \Big|_1 h_2^3 + \frac{13}{384} \bar{A}_{33} \Big|_{2M+1} h_3^2 + F_1 - F_{2M+1}^* \right] \quad (2.154)$$

$$q = \left[\bar{A}_{13} \bar{Q}_{55} \Big|_1 \frac{h_2}{6} - (1 + \Delta \bar{Q}_{55}) \Big|_1 \frac{2h_2}{3} + E_1 \right] \quad (2.155)$$

$$q^* = \left[- \bar{A}_{13} \bar{Q}_{55} \Big|_{2M+1} \frac{h_3}{6} + (1 + \Delta \bar{Q}_{55}) \Big|_{2M+1} \frac{2h_3}{3} + E_{2M+1}^* \right] \quad (2.156)$$

$$s = \frac{11}{480} \bar{A}_{33} \bar{Q}_{55} \Big|_1 h_2^3 + D_1 \quad (2.157)$$

$$s^* = \frac{11}{480} \bar{A}_{33} \bar{Q}_{55} \Big|_{2M+1} h_3^3 - D_{2M+1}^* \quad (2.158)$$

$$\bar{t} = \left[- \bar{A}_{33} \Big|_1 \frac{h_2^2}{8} + \bar{A}_{33} \Big|_{2M+1} \frac{h_3^2}{8} + H_1 - H_{2M+1}^* \right] \quad (2.159)$$

(b) Equation (2.148) - Derivation of

Differentiate equation (2.148) with respect to (x)

$$\frac{dw_2}{dx} \left(x, -\frac{h_2}{2} \right) - \frac{dw_3}{dx} \left(x, \frac{h_3}{2} \right) = \frac{1}{C_N} \frac{d\sigma_o}{dx} \quad (2.160)$$

Substituting in equation (2.58) with $K = 1$ and τ_{ou} and its derivatives = 0, a relation for $\frac{dw_2}{dx}$ at $z = -\frac{h_2}{2}$ is obtained.

$$\begin{aligned} \frac{dw_2}{dx} (x, -\frac{h_2}{2}) &= \frac{dw_2^0}{dx} - \bar{A}_{13}|_1 \frac{\tau_0}{2} + \bar{A}_{13} \bar{Q}_{55}|_1 \phi_{x_2} \\ &+ [-\bar{A}_{33}|_1 \frac{h_2^2}{16} - \bar{A}_{33}|_1 \frac{h_2^2}{48} + \bar{A}_{33}|_1 \frac{3h_2^2}{16}] \frac{d^2\tau_0}{dx^2} \\ &+ [-\bar{Q}_{55}|_1 \frac{h_2^2}{8} + \bar{Q}_{55}|_1 \frac{h_2^2}{48} - \cancel{\bar{Q}_{55}|_1 \frac{h_2^2}{8}} - \cancel{\alpha_1 \frac{h_2^2}{2}} \\ &+ \bar{Q}_{55}|_1 \frac{h_2^2}{6}] \bar{A}_{33}|_1 \frac{d^2\phi_{x_2}}{dx^2} - \bar{A}_{33}|_1 \frac{d\sigma_0}{dx} \frac{h_2}{2} \end{aligned}$$

Simplifying this relation one gets

$$\begin{aligned} \frac{dw_2}{dx} (x, -\frac{h_2}{2}) &= \frac{dw_2^0}{dx} - \bar{A}_{13}|_1 \frac{\tau_0}{2} + \bar{A}_{13} \bar{Q}_{55}|_1 \phi_{x_2} \\ &+ \frac{5}{48} \bar{A}_{33}|_1 h_2^2 \frac{d^2\tau_0}{dx^2} + \frac{1}{16} \bar{A}_{33} \bar{Q}_{55}|_1 h_2^2 \frac{d^2\phi_{x_2}}{dx^2} \end{aligned}$$

$$- \bar{A}_{33}|_1 \frac{h_2}{2} \frac{d\sigma_o}{dx} \quad (2.161)$$

A similar relationship for $\frac{dw_3}{dx}$ can be obtained for $z = + \frac{h_3}{2}$ by employing equation (2.147)

$$\begin{aligned} \frac{dw_3}{dx} (x, \frac{h_3}{2}) &= \frac{dw_3^o}{dx} - \bar{A}_{13}|_{2M+1} \frac{\tau_o}{2} + A_{13} Q_{55}|_{2M+1} \phi_{x_3} \\ &+ [- \frac{h_3^2}{16} \bar{A}_{33}|_{2M+1} - \frac{h_3^2}{48} \bar{A}_{33}|_{2M+1} + \frac{3}{16} \bar{A}_{33}|_{2M+1} h_3^2] \frac{d^2 \tau_o}{dx^2} \\ &+ [- \bar{A}_{33} \bar{Q}_{55}|_{2M+1} \frac{h_3^2}{8} + \bar{A}_{33} \bar{Q}_{55}|_{2M+1} \frac{h_3^2}{48} \\ &- \bar{A}_{33} b_{55}|_{2M+1} \frac{h_3^2}{8} + \bar{A}_{33} \alpha^*|_{2M+1} \frac{h_3}{2} + \bar{A}_{33} \bar{Q}_{55}|_{2M+1} \frac{h_3^2}{6}] \frac{d^2 \phi_{x_3}}{dx^2} \\ &+ \bar{A}_{33}|_{2M+1} \frac{h_3}{2} \frac{d\sigma_o}{dx} \end{aligned}$$

Again, simplifying the previous expression yields

$$\begin{aligned}
 \frac{dw_3}{dx} (x, \frac{h_3}{2}) &= \frac{dw_3^0}{dx} - \bar{A}_{13}|_{2M+1} \frac{\tau_0}{2} + \bar{A}_{13} \bar{Q}_{55}|_{2M+1} \phi_{x_3} \\
 &+ \frac{5}{48} \bar{A}_{33}|_{2M+1} h_3^2 \frac{d^2 \tau_0}{dx^2} + \frac{1}{16} \bar{A}_{33} \bar{Q}_{55}|_{2M+1} h_3^2 \frac{d^2 \phi_{x_3}}{dx^2} \\
 &+ \bar{A}_{33}|_{2M+1} \frac{h_3}{2} \frac{d\sigma_0}{dx} \quad (2.162)
 \end{aligned}$$

Substituting equation (2.161) and (2.162) into (2.148) gives

$$\begin{aligned}
 \frac{1}{C_N} \frac{d\sigma_0}{dx} &= \frac{dw_2^0}{dx} - \frac{dw_3^0}{dx} + \left[-\frac{\bar{A}_{13}|_1}{2} + \frac{\bar{A}_{13}|_{2M+1}}{2} \right] \tau_0 \\
 &+ \bar{A}_{13} \bar{Q}_{55}|_1 \phi_{x_2} - \bar{A}_{13} \bar{Q}_{55}|_{2M+1} \phi_{x_3} \\
 &+ \left[\frac{5}{48} \bar{A}_{33}|_1 h_2^2 - \frac{5}{48} \bar{A}_{33}|_{2M+1} h_3^2 \right] \frac{d^2 \tau_0}{dx^2} \\
 &+ \frac{1}{16} \bar{A}_{33} \bar{Q}_{55}|_1 h_2^2 \frac{d^2 \phi_{x_2}}{dx^2} - \frac{1}{16} \bar{A}_{33} \bar{Q}_{55}|_{2M+1} h_3^2 \frac{d^2 \phi_{x_3}}{dx^2}
 \end{aligned}$$

$$+ [- \bar{A}_{33}|_1 \frac{h_2}{2} - \bar{A}_{33}|_{2M+1} \frac{h_3}{2}] \frac{d\sigma_o}{dx}$$

Again rearranging the terms of the above expression and introducing new parameters, the resulting equation is

$$\begin{aligned} \frac{1}{C_N} \frac{d\sigma_o}{dx} = & \frac{dw_o^2}{dx} - \frac{dw_o^3}{dx} + \bar{u} \tau_o + \bar{\beta} \frac{d^2 \tau_o}{dx^2} \\ & + \gamma \frac{d^2 \phi_{x_2}}{dx^2} - \gamma^* \frac{d^2 \phi_{x_3}}{dx^2} + v \phi_{x_2} - v^* \phi_{x_3} - \bar{z} \frac{d\sigma_o}{dx} \quad (2.163) \end{aligned}$$

where:

$$\bar{u} = \frac{\bar{A}_{13}|_{2M+1}}{2} - \frac{\bar{A}_{13}|_1}{2} \quad (2.164)$$

$$\bar{\beta} = \frac{5}{48} \bar{A}_{33}|_1 h_2^2 - \frac{5}{48} \bar{A}_{33}|_{2M+1} h_3^2 \quad (2.165)$$

$$\gamma = \bar{A}_{33} \bar{Q}_{55}|_1 \frac{h_2^2}{16} \quad (2.166)$$

$$\gamma^* = \bar{A}_{33} Q_{55}|_{2M+1} \frac{h_3^2}{16} \quad (2.167)$$

$$v = \bar{A}_{13} \bar{Q}_{55}|_1 \quad (2.168)$$

$$v^* = \bar{A}_{13} \bar{Q}_{55}|_{2M+1} \quad (2.169)$$

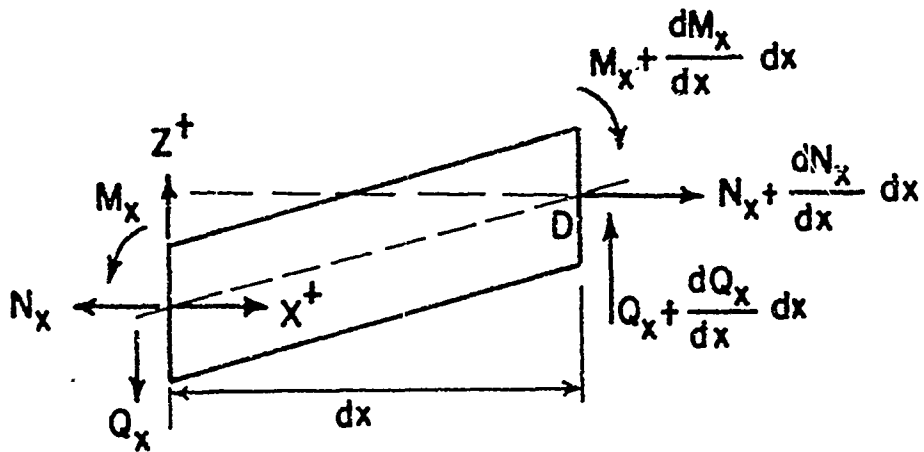
$$\bar{z} = \bar{A}_{33} \frac{h_2}{2} + \bar{A}_{33}|_{2M+1} \frac{h_3}{2} \quad (2.170)$$

Note that the (1) designation implies the lamina of the upper laminate that is adjacent to the adhesive. The (2M+1) designation implies the lamina of the lower laminate (Part 3) that is adjacent to the adhesive.

2. Overall Equilibrium Equations

The equilibrium equations for Parts (1), (2), (3) and (4) will be derived, considering differential moment and axial load effects. Shear and normal stress effects are also considered where applicable.

Parts (1) and (4)



$$\Sigma F_x = 0$$

$$\boxed{\frac{dN_x}{dx} = 0}$$

(2.171)

$$\Sigma F_z = 0$$

$$-Q_x + Q_x + \frac{dQ_x}{dx} dx = 0$$

$$\boxed{\frac{dQ_x}{dx} = 0}$$

(2.172)

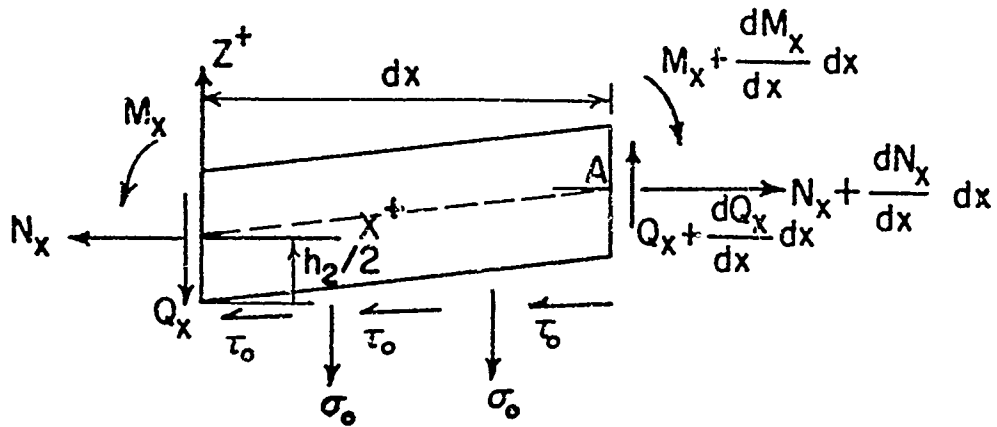
$$\Sigma M_D = 0 \quad \curvearrowright + M$$

$$M_x - M_x - \frac{dM_x}{dx} dx + Q_x dx = 0$$

$$\boxed{\frac{dM_x}{dx} - Q_x = 0}$$

(2.173)

Part (2)



$$\Sigma F_x = 0$$

$$N_x + \frac{dN_x}{dx} dx - N_x - \tau_o dx = 0$$

$$\boxed{\frac{dN_x}{dx} - \tau_o = 0}$$

(2.174)

$$\Sigma F_z = 0$$

$$- Q_x + Q_x + \frac{dQ_x}{dx} - \sigma_o dx = 0$$

$$\boxed{\frac{dQ_x}{dx} - \sigma_o = 0}$$

(2.175)

$$\Sigma M_A = 0 \quad \curvearrowright + M$$

$$M_x - M_x - \frac{dM_x}{dx} dx + Q_x dx + \tau_o dx \frac{dx}{2}$$

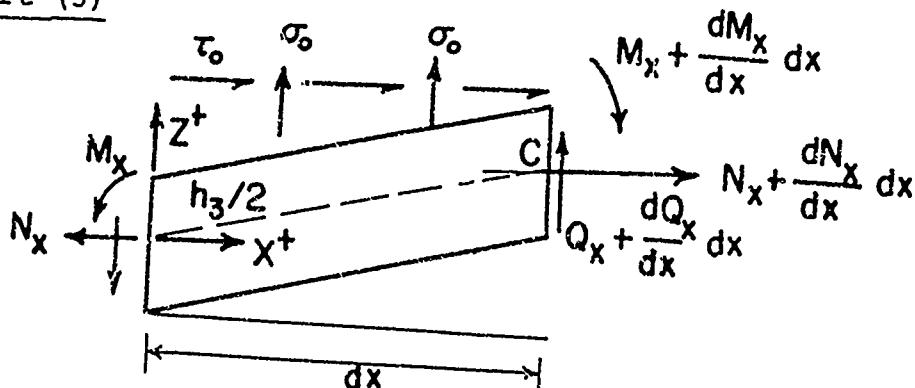
$$- \tau_o dx \left(\frac{h_2}{2}\right) = 0$$

$$- \frac{dM_x}{dx} dx + Q_x dx - \tau_o \frac{h_2}{2} dx = 0$$

$$\boxed{\frac{dM_x}{dx} - Q_x + \tau_o \frac{h_2}{2} = 0}$$

(2.176)

Part (3)



$$\Sigma F_x = 0$$

$$N_x + \frac{dN}{dx} dx - N_x + \tau_o dx = 0$$

$$\boxed{\frac{dN}{dx} + \tau_o = 0}$$

(2.177)

$$\Sigma F_z = 0$$

$$- Q_x + Q_x + \frac{dQ}{dx} dx + \sigma_o dx = 0$$

$$\boxed{\frac{dQ}{dx} + \sigma_o = 0}$$

(2.178)

$$\Sigma M_c = 0 \quad \curvearrowleft + M$$

$$M_x - M_x - \frac{dM}{dx} dx + Q_x dx + \frac{\sigma_o dx^2}{2} - \tau_o dx \left(\frac{h_3}{2}\right) = 0$$

$$- \frac{dM}{dx} dx + Q_x dx - \tau_o \frac{h_3}{2} dx = 0$$

$$\boxed{\frac{dM}{dx} - Q_x + \tau_o \frac{h_3}{2} = 0}$$

(2.179)

3. Summary of Governing Equations and Unknowns

There follows on pages 114-119 a summary of the pertinent equations necessary to effect a solution to the problem at hand. Note that $\tau_{oL} = \tau_{ou} = \tau_o$ and $\sigma_{oL} = \sigma_{ou} = \sigma_o$ where necessary.

Parts (1) and (4)

The governing equations for parts (1) and (4) are summarized below using equations (2.106-2.111) and (2.171-2.173).

$$\frac{dN_x}{dx} = 0 \quad (2.180)$$

$$\frac{dQ_x}{dx} = 0 \quad (2.181)$$

$$\frac{dM_x}{dx} - Q_x = 0 \quad (2.182)$$

$$M_x = - D_{11} \frac{d^2 w_o}{dx^2} + F \frac{d^3 \phi_x}{dx^3} + G \frac{d\phi_x}{dx} \quad (2.183)$$

$$N_x = A \frac{d^3 \phi_x}{dx^3} + B \frac{d\phi_x}{dx} + \bar{A} \frac{du^o}{dx} \quad (2.184)$$

$$Q_x = K_5 \phi_x \quad (2.185)$$

The unknowns are N_x , Q_x , M_x , w^o , ϕ_x , u^o .

Upon inspection one notes that there are six equations in six unknowns and thus parts (1) and (4) possess a determinant solution.

Part (2)

The governing equations relating to part (2) can be summarized employing equations (2.112-2.114) and (2.174-2.176) .

$$\frac{dN_x}{dx} - \tau_o = 0 \quad (2.186)$$

$$\frac{dQ_x}{dx} - \sigma_o = 0 \quad (2.187)$$

$$\frac{dM_x}{dx} - Q_x + \tau_o \frac{h_2}{2} = 0 \quad (2.188)$$

$$M_x = - D_{112} \frac{d^2 w_o}{dx^2} + F \frac{d^3 \phi_{x_2}}{dx^3} + G \frac{d\phi_{x_2}}{dx} + H \frac{d^3 \tau_o}{dx^3} + I \frac{d\tau_o}{dx} \quad (2.189)$$

$$N_x = A \frac{d^3 \phi_{x_2}}{dx^3} + B \frac{d\phi_{x_2}}{dx} + C \frac{d^3 \tau_o}{dx^3} + D \frac{d\tau_o}{dx} + E \frac{d^2 \sigma_o}{dx^2} + \bar{A}_{11} \frac{du_o}{dx} \quad (2.190)$$

$$Q_x = \frac{h_2}{2} \tau_o + K_5 \phi_{x_2} \quad (2.191)$$

Inspection of equations (2.186-2.191) reveals that there are eight unknowns, namely, N_x , Q_x , M_x , τ_o , σ_o , w_o , ϕ_{x_2} , u_o while we presently only have six independent equations.

Part (3)

The governing equations relating to part (3) can be summarized by employing equations (2.116-2.118) and (2.177-2.179).

$$\frac{dN_x}{dx} + \tau_o = 0 \quad (2.192)$$

$$\frac{dQ_x}{dx} + \sigma_o = 0 \quad (2.193)$$

$$\frac{dM_x}{dx} - Q_x + \tau_o \frac{h_3}{2} = 0 \quad (2.194)$$

$$M_x = - D_{113}^* \frac{d^2 w_o^3}{dx^2} + F^* \frac{d^3 \phi_{x_3}}{dx^3} + G^* \frac{d\phi_{x_3}}{dx} + H^* \frac{d^3 \tau_o}{dx^3} + I^* \frac{d\tau_o}{dx} \quad (2.195)$$

$$N_x = A^* \frac{d^3 \phi_{x_3}}{dx^3} + B^* \frac{d\phi_{x_3}}{dx} + C^* \frac{d^3 \tau_o}{dx^3} + D^* \frac{d\tau_o}{dx} + E^* \frac{d^2 \sigma_o}{dx^2} + \bar{A}_{11}^* \frac{du_o^3}{dx} \quad (2.196)$$

$$Q_x = \frac{h_3}{2} \tau_o + K_5^* \phi_{x_3} \quad (2.197)$$

Inspection of equations (2.192-2.197) reveals that there are eight unknowns, namely, N_x , Q_x , M_x , τ_o , σ_o , w_o^3 , ϕ_{x_3} , u_o^3 of which six are nonrepetitive as

τ_o and σ_o were also found in part (2). Again we have six independent equations.

4. Equations Necessary for a Determinant Solution of Parts (2) and (3)

Parts (2) and (3) have twelve equations but fourteen unknowns as τ_o and σ_o are the same for both parts. Thus, two more equations are necessary to make the problem a determinant one. These are provided by the stress-strain relations of the adhesive given by equations (2.152) and (2.163), namely:

$$\begin{aligned} \frac{\tau_o}{C_s} = & \frac{h_2}{2} \frac{dw_o^2}{dx} + \frac{h_3}{2} \frac{dw_o^3}{dx} + \bar{p} \tau_o + \bar{r} \frac{d^2 \tau_o}{dx^2} + q \phi_{x_2} \\ & - q^* \phi_{x_3} + s \frac{d^2 \phi_{x_2}}{dx^2} + s^* \frac{d^2 \phi_{x_3}}{dx^2} + \bar{t} \frac{d\sigma_o}{dx} + u_o^2 - u_o^3 \end{aligned} \quad (2.198)$$

$$\begin{aligned} \frac{1}{C_N} \frac{d\sigma_o}{dx} = & \frac{dw_o^2}{dx} - \frac{dw_o^3}{dx} + \bar{u} \tau_o + \bar{\beta} \frac{d^2 \tau_o}{dx^2} + \gamma \frac{d^2 \phi_{x_2}}{dx^2} \\ & - \gamma^* \frac{d^2 \phi_{x_3}}{dx^2} + v \phi_{x_2} - v^* \phi_{x_3} - \bar{z} \frac{d\sigma_o}{dx} \end{aligned} \quad (2.199)$$

Note that equations (2.180-2.199) reduce down to the more conventional relationships when an isotropic material is considered and transverse shear and normal stresses are neglected.

SOLUTION OF THE GOVERNING DIFFERENTIAL EQUATIONS

The solution of the equations presented on pages 114-119 will now be determined. A solution to parts (1) and (4) will first be attained. Subsequent to this a solution of parts (2) and (3) will collectively be attained by employing the stress-strain relations of the adhesive.

F. SOLUTION OF THE GOVERNING DIFFERENTIAL EQUATIONS
OF PARTS (1) AND (4)

The six governing equations are given by equations (2.180-2.185) on pages 114-115. Substitute the relations for N_x and Q_x , namely equations (2.184-2.185), into equations (2.180) and (2.181), respectively.

$$A \frac{d^4 \phi_x}{dx^4} + B \frac{d^2 \phi_x}{dx^2} + \bar{A} \frac{d^2 u^o}{dx^2} = 0 \quad (2.200)$$

$$K_5 \frac{d \phi_x}{dx} = 0 \quad (2.201)$$

From equation (2.201) it follows that $\frac{d \phi_x}{dx}$ and its

higher derivatives are zero. Thus, at most $\phi_x = \text{constant}$.
Equation (2.200) reduces to

$$\bar{A} \frac{d^2 u^0}{dx^2} = 0$$

Therefore,

$$\frac{d^2 u^0}{dx^2} = 0 \quad (2.202)$$

and its solution is

$$u^0 = a + bx \quad (2.203)$$

Based on the result of equation (2.201), namely that $\frac{d\phi_x}{dx} = 0$ equation (2.183) reduces to

$$M_x = - D_{11} \frac{d^2 w^0}{dx^2} \quad (2.204)$$

Moreover, referring to Figure 1 on page 34 one can discern that

$$M_x = T \cos \theta [\theta X_1 - w_1^0(x)] \quad (2.205)$$

$$0 \leq X_1 \leq L_1$$

where (θ) represents the angle between the X_1 - axis and the line of action AB of the applied force (T) and is approximately equal to

$$\theta \cong \frac{(h_2+h_3)}{2(L_1+L_2+L_4)} \quad (2.206)$$

Thus, equating equations (2.204) and (2.205) one gets

$$- D_{11} \frac{d^2 w_1^0}{dx^2} = T \cos \theta [\theta X_1 - w_1^0(x)]$$

Rearranging terms gives

$$\frac{d^2 w_1^0}{dx^2} - \frac{T \cos \theta}{D_{11}} w_1 = - \frac{T \cos \theta}{D_{11}} \theta X_1 \quad (2.207)$$

The solution to equation (2.207) can be succinctly written as

$$w_1^0(x) = E \sinh KX_1 + F \cosh KX_1 + \theta X_1 \quad (2.208)$$

$$0 \leq X_1 \leq L_1$$

where $K^2 = \frac{T \cos \theta}{D_{11}}$

If the upper and lower adherends are not identical

in geometrical make-up and influenced by exactly the same boundary conditions, then the deflection equations for parts (1) and (4) will be different, therefore, the general solution for $w_4^o(x)$ will be determined.

Again referring to Figure 1 on page 34 one can discern that

$$M_x = - T \cos \theta [\theta(L_4 - X_4) + w_4^o(x)] \quad (2.209)$$

$$0 \leq X_4 \leq L_4$$

Again equating equations (2.204) and (2.209) gives

$$-\bar{D}_{114} \frac{d^2 w_4^o}{dx^2} = - T \cos \theta [\theta(L_4 - X_4) + w_4^o(x)]$$

Rearranging terms gives

$$\frac{d^2 w_4^o}{dx^2} = + \frac{T \cos \theta}{\bar{D}_{114}} [\theta(L_4 - X_4) + w_4^o(x)] \quad (2.210)$$

Again the solution to equation (2.210) can succinctly be written as

$$w_4^o(x) = - \theta (L_4 - X_4) + \bar{E} \sinh \bar{K} X_4 + \bar{F} \cosh \bar{K} X_4 \quad (2.211)$$

$$0 \leq X_4 \leq L_4$$

where

$$\bar{K}^2 = \frac{T \cos \theta}{D_{114}}$$

G. BOUNDARY CONDITIONS

Employing certain boundary conditions one can now get specific solutions for the inplane displacement and lateral deflection in part (1).

1. Boundary Conditions for u_1^o - (2 needed)

Assuming our reference point for inplane displacements to be at $X_1 = 0$ and that continuity of displacements between parts (1) and (2) at their common boundary must exist one can state the two conditions necessary to effect a solution for $u_1^o(x)$, namely:

$$u_1^o(0) = 0 \quad (2.212)$$

$$u_1^o(L_1) = u_2^o(0) \quad (2.213)$$

Employing equations (2.203) and (2.212)

$$u_1^o(0) = 0 = a + 0$$

$$0 = a$$

Thus equation (2.203) becomes

$$u_1^o(x) = bx \quad (2.214)$$

However, by employing equations (2.180) and (2.184) one gets

$$\frac{dN_x}{dx} = \bar{A} \frac{d^2 u^o}{dx^2} = 0 \quad (2.215)$$

Thus, $N_x = \bar{A} \frac{du^o}{dx} = \text{constant at most}$ which in this particular case is the applied load $= T \cos \theta$

Therefore,

$$\frac{du_1^o}{dx} = b = \frac{T \cos \theta}{\bar{A}} \quad (2.216)$$

Thus, in final form the inplane displacement in part (1) is:

$$u_1^o(x) = \frac{T \cos \theta}{\bar{A}} x \quad (2.217)$$

2. Boundary Conditions for $w_1^o(w_4^o)$ - (2 needed)

Since at this time one is considering only adherends of an identical nature, if one solves explicitly

equation (2.208) for $w_1^o(x)$ a solution for $w_4^o(x)$ is also obtained as $w_1^o(x) = -w_4^o(x)$. This is only true when both adherends are identical.

A solution will be rendered assuming that at the end ($x_1 = 0$), the end is supported from moving laterally and at the end ($x_1 = L_1$), the lateral displacements are continuous. Thus, the boundary conditions are:

$$w_1^o(0) = 0 \quad (2.218)$$

$$w_1^o(L_1) = \bar{w}^o(0) \quad (2.219)$$

Employing equations (2.208) and (2.218) will give

$$w_1^o(0) = F = 0$$

Therefore

$$w_1^o(x) = E \sinh Kx_1 + \theta x_1 \quad (2.220)$$

The evaluation of (E) will be determined later in conjunction with the solution to part (2).

3. Boundary Conditions for $u_4^o(x)$ - (2 needed)

One can obtain the necessary boundary conditions by seeking continuity of the inplane displacements at the interface of parts (3) and (4). Also it is obvious that the axial load at the far end ($X_4 = L_4$) must equal $T \cos \theta$. Therefore, the boundary conditions are:

$$N_x(L_4) = T \cos \theta \quad (2.221)$$

$$U_4(X_4 = 0) = U_3(L_3) \quad (2.222)$$

Employing equations (2.203) and (2.216) gives

$$N_x = \bar{A} \frac{du_4^o}{dx} = \bar{A} \bar{b} \quad (2.223)$$

Employing boundary conditions (2.221) gives

$$\bar{A} \bar{b} = T \cos \theta$$

Therefore,

$$\bar{b} = \frac{T \cos \theta}{\bar{A}} \quad (2.224)$$

Thus,

$$U_4^o(x) = \bar{A} + \frac{T \cos \theta}{\bar{A}} X_4 \quad (2.225)$$

Again, the evaluation of the constant \bar{A} will be found at a later time.

H Parts (2) and (3) - Determination of \bar{w}^o

To effect a solution of the constant (E) and in turn $w_1^o(x)$ the following analysis is performed.

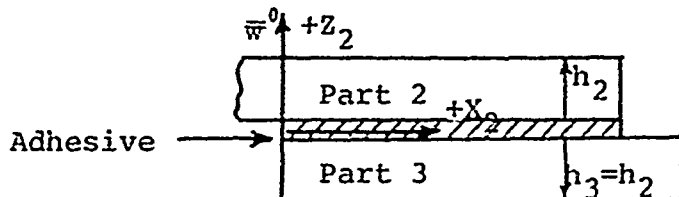


FIGURE (2-6)

Referring to Figure 6, assume the part of the two sheets which overlap parts (2) and (3) is a homogeneous plate with a discontinuous thickness and neutral plane at the ends of the joint section. The resulting deflection of this section will be defined as \bar{w}^o . It is necessary to find \bar{w}^o in order to calculate the moments (M_1 , M_4) and the shears (V_1 and V_4) defined on Figure 2, page 36. These in turn are necessary to solve for $\tau_o(x)$ and $\sigma_o(x)$ later on!

Referring to Figure 1, page 34, one can discern that

$$\bar{M}_x = T \cos \theta \left[\theta (L_1 + x_2) - \bar{w}^o - \frac{h_2}{2} \right] \quad (2.226)$$

$$0 \leq x_2 \leq L_2$$

Alternately the moment M_x should be such that

$$\bar{M}_x = - \bar{D}_{11} \frac{d^2 \bar{w}}{dx^2} \quad (2.227)$$

One should note that this part of the solution is only valid for two equal thickness laminates, as it assumes a thickness of $(\frac{h_2}{2})$ in equation (2.226) to bring the deflection to the neutral plane which is the glue line. Also, \bar{D}_{11} is the bending stiffness of the total thickness (h_2+h_3) referred to the glue line as its neutral plane.

$$\bar{D}_{11} = \sum_{K=1}^{4M+2} \int_{H_{K-1}}^{H_K} \bar{Q}_{11}|_K z^2 dz \quad \begin{matrix} \text{sum over the} \\ \text{\{total thickness\}} \\ \text{of both adherends} \end{matrix} \quad (2.228)$$

Equating equations (2.226) and (2.227) gives

$$\frac{d^2 \bar{w}}{dx^2} = - \frac{\bar{M}_x}{\bar{D}_{11}} = - \frac{T \cos \theta}{\bar{D}_{11}} [6 (L_1 + X_2) - \bar{w} - \frac{h_2}{2}] \quad (2.229)$$

Let
$$\hat{K}^2 = \frac{T \cos \theta}{\bar{D}_{11}}$$

Therefore,

$$\frac{d^2 \bar{w}^o}{dx^2} - \frac{T \cos \theta}{\bar{D}_{11}} \bar{w}^o = - \frac{T \cos \theta}{\bar{D}_{11}} \left[\theta (L_1 + x_2) - \frac{h_2}{2} \right] \quad (2.230)$$

Referring to the form of equation (2.207) and its general solution as given in equation (2.208) one can discern the solution to equation (2.230) to be

$$\bar{w}^o = \hat{A} \cosh \hat{K} x + \hat{B} \sinh \hat{K} x + \theta (L_1 + x_2) - \frac{h_2}{2} \quad (2.231)$$

$$0 \leq x_2 \leq L_2$$

I. Boundary Conditions

Since the analysis is presently restricted to two laminates of equal thickness and material properties, the deflections and slopes of parts (1) and (4) are anti-symmetric about the z -axis. Thus, to get a complete solution of equations (2.220) and (2.231) where E , \hat{A} , and \hat{B} are unknown, one needs three boundary conditions.

In summary we have

$$w_1^o(x) = \theta x_1 + E \sinh K x_1 \quad (2.232)$$

$$\bar{w}^o(x) = \hat{A} \cosh \hat{K} x + \hat{B} \sinh \hat{K} x + \theta (L_1 + x_2) - \frac{h_2}{2} \quad (2.233)$$

From page 127 comes our first boundary condition, namely,

$$w_1^o(L_1) = \bar{w}^o(0) \quad (2.234)$$

Realizing that the slopes at the interface must match, our second boundary condition is

$$\frac{dw_1^o(L_1)}{dx} = \frac{d\bar{w}^o(0)}{dx} \quad (2.235)$$

Finally, because of the restriction of equally thick laminates and parts (1) and (4) giving antisymmetrical deflection equations about the z-axis, the third boundary condition is

$$\bar{w}(\frac{L_2}{2}) = 0 \quad (2.236)$$

Employing equations (2.232-2.234) gives

$$\begin{aligned} \theta L_1 + E \sinh K L_1 &= \hat{A} + \theta L_1 - \frac{h_2}{2} \\ \hat{A} &= E \sinh K L_1 + \frac{h_2}{2} \end{aligned} \quad (2.237)$$

Differentiating equations (2.232-2.333) and making use of equation (2.235) yields

$$\frac{dw_1^0}{dx} = \theta + KE \cosh K X_1 \quad (2.238)$$

$$\frac{d\bar{w}^0}{dx} = \hat{K}(\hat{A} \sinh \hat{K} X + \hat{B} \cosh \hat{K} X) + \theta \quad (2.239)$$

$$0 + K E \cosh K L_1 = \hat{K} \hat{B} + \theta$$

$$\hat{B} = \frac{KE \cosh K L_1}{\hat{K}} \quad (2.240)$$

Substituting equation (2.233) into boundary condition equation (2.236) gives

$$0 = \hat{A} \cosh \hat{K} \frac{L_2}{2} + \hat{B} \sinh \hat{K} \frac{L_2}{2} + \theta (L_1 + \frac{L_2}{2}) - \frac{h_2}{2}$$

solving for \hat{B} and using (2.237)

$$\hat{B} = - \frac{(E \sinh K L_1 + \frac{h_2}{2}) \cosh \hat{K} \frac{L_2}{2} - \theta (L_1 + \frac{L_2}{2}) + \frac{h_2}{2}}{\sinh \hat{K} \frac{L_2}{2}} \quad (2.241)$$

If one now substitutes equation (2.240) into (2.241) a solution for (E) emerges.

$$\frac{KE \cosh \hat{K} L_1}{\hat{K}} (\sinh \hat{K} \frac{L_2}{2}) = - E \sinh K L_1 \cosh \hat{K} \frac{L_2}{2}$$

$$- \frac{h_2}{2} \cosh \hat{K} \frac{L_2}{2} - \theta (L_1 + \frac{L_2}{2}) + \frac{h_2}{2}$$

$$E = - \frac{h_2}{2} \cosh \hat{K} \frac{L_2}{2} - \theta (L_1 + \frac{L_2}{2}) + \frac{h_2}{2}$$

$$+ \frac{K \cosh K L_1 \sinh \hat{K} \frac{L_2}{2}}{\hat{K}} + \sinh K L_1 \cosh \hat{K} \frac{L_2}{2}$$

However,

$$-\theta \left(L_1 + \frac{L_2}{2} \right) = - \frac{h_2}{2(L_1 + \frac{L_2}{2})} \left(L_1 + \frac{L_2}{2} \right) = - \frac{h_2}{2}$$

for two equal laminates. Thus,

$$E = - \frac{h_2}{2} \cosh \hat{K} \frac{L_2}{2} + \frac{K \cosh K L_1 \sinh \hat{K} \frac{L_2}{2}}{\hat{K}} + \sinh K L_1 \cosh \hat{K} \frac{L_2}{2} \quad (2.242)$$

Note that \hat{A} and \hat{B} can be found if desired using equations (2.237) and (2.240), respectively. Also, $w_4^0(x)$ can be found as $w_4^0(x) = -w_1^0(x)$ for two equal laminates.

J. CALCULATION OF M_1 AND V_1 (FOR EQUAL LAMINATES
EQUAL TO $-M_4$, $-V_4$)

It is presently desirable to determine $M_1(L_1)$ and $Q_1(L_1)$ at the interface of parts (1) and (2). In turn, these numerical relations will be used as boundary conditions to obtain a solution for the coupled solution of parts (2) and (3).

Differentiation of equation (2.220) twice with respect to (x) gives

$$\frac{d^2 w_1^o(x)}{dx^2} = K^2 E \sinh K X_1 \quad (2.243)$$

Recalling that

$$M_1(x) = - D_{11} \frac{d^2 w_1^o(x)}{dx^2} \quad (2.244)$$

and the value of the moment is desired at $X_1 = L_1$, one gets

$$M_1(L_1) = - D_{11} \frac{d^2 w_1^o(L_1)}{dx^2} = - D_{11} K^2 E \sinh K L_1$$

but

$$K^2 = \frac{T \cos \theta}{D_{11}}$$

Therefore,

$$M_1(L_1) = T \cos \theta E \sinh K L_1 \quad \begin{array}{l} \text{For equal} \\ \text{laminates only} \end{array} \quad (2.245)$$

and

$$M_4(0) = - M_1(L_1) \quad (2.246)$$

Moreover, if one uses equation (2.182), namely

$$\frac{dM_x}{dx} - Q_x = 0 \quad (2.247)$$

one can find $Q_1(L_1)$. Substituting equation (2.243) into equation (2.244) and differentiating $w/R(x)$ gives

$$\frac{dM_x}{dx} = - D_{11} \frac{d^3 w_1^0}{dx^3} = - D_{11} K^3 E \cosh K X_1 \quad (2.248)$$

Substitute (2.248) into (2.247) one gets an expression for Q_{x_1}

$$- D_{11} K^3 E \cosh K X_1 = Q_{x_1}$$

Simplifying

$$- D_{11} \frac{T \cos \theta}{D_{11}} K E \cosh K X_1 = Q_{x_1}$$

$$Q_{x_1} = K E (T \cos \theta) \cosh K X_1 \quad (2.249)$$

Therefore,

$$V_1(L_1) = KE(T \cos \theta) \cosh K L_1 \begin{cases} \text{for equal} \\ \text{laminates only} \end{cases} \quad (2.250)$$

$$V_4(o) = - V_1(L_1) \quad (2.251)$$

where (E) is defined by equation (2.242)

K GENERAL SOLUTION OF THE GOVERNING EQUATIONS FOR
PARTS (2) AND (3)

The solution of this section will yield the equations necessary to calculate $\tau_o(x)$ and $\sigma_o(x)$. Fundamentally, fourteen equations in fourteen unknowns will be reduced to two coupled linear nonhomogeneous differential equations. These in turn will be uncoupled per certain considerations leading to a solution for the shear stress and normal stress distributions in the adhesive.

The fourteen equations in fourteen unknowns are:

Note that subscript 2 denotes part (2), and subscript 3 denotes part (3).

$$\frac{dT_2}{dx} - \tau_o = 0 \quad (2.252)$$

$$\frac{dQ_2}{dx} - \sigma_o = 0 \quad (2.253)$$

$$\frac{dM_2}{dx} - Q_2 + \tau_o \frac{h_2}{2} = 0 \quad (2.254)$$

$$\frac{d\tau_3}{dx} + \tau_o = 0 \quad (2.255)$$

$$\frac{dQ_3}{dx} + \sigma_o = 0 \quad (2.256)$$

$$\frac{dM_3}{dx} - Q_3 + \tau_o \frac{h_3}{2} = 0 \quad (2.257)$$

$$M_2 = - D_{112} \frac{d^2 w_2^o}{dx^2} + F \frac{d^3 \phi_{x_2}}{dx^3} + G \frac{d\phi_{x_2}}{dx} + H \frac{d^3 \tau_o}{dx^3} + I \frac{d\tau_o}{dx} \quad (2.258)$$

$$T_2 = A \frac{d^3 \phi_{x_2}}{dx^3} + B \frac{d\phi_{x_2}}{dx} + C \frac{d^3 \tau_o}{dx^3} + D \frac{d\tau_o}{dx} + E \frac{d^2 \sigma_o}{dx^2} + \bar{A} \frac{du_2^o}{dx} \quad (2.259)$$

$$Q_2 = \frac{h_2}{2} \tau_o + K_5 \phi_{x_2} \quad (2.260)$$

$$M_3 = - D_{113}^* \frac{d^2 w_3^o}{dx^2} + F^* \frac{d^3 \phi_{x_3}}{dx^3} + G^* \frac{d\phi_{x_3}}{dx} + H^* \frac{d^3 \tau_o}{dx^3} + I^* \frac{d\tau_o}{dx} \quad (2.261)$$

$$T_3 = A^* \frac{d^3 \phi_{x_3}}{dx^3} + B^* \frac{d\phi_{x_3}}{dx} + C^* \frac{d^3 \tau_o}{dx^3} + D^* \frac{d\tau_o}{dx} + E^* \frac{d^2 \sigma_o}{dx^2} + \bar{A}^* \frac{du_3^o}{dx} \quad (2.262)$$

$$Q_3 = \frac{h_3}{2} \tau_o + K_5^* \phi_{x_3} \quad (2.263)$$

$$\begin{aligned} \frac{h_2}{2} \frac{dw_2^o}{dx} + \frac{h_3}{2} \frac{dw_3^o}{dx} + (\bar{p} - \frac{1}{C_s}) \tau_o + \bar{r} \frac{d^2 \tau_o}{dx^2} + q \phi_{x_2} - q^* \phi_{x_3} \\ + s \frac{d^2 \phi_{x_3}}{dx^2} + s^* \frac{d^2 \phi_{x_3}}{dx^2} + \bar{r} \frac{d\sigma_o}{dx} + u_o^o - u_o^o = 0 \end{aligned} \quad (2.264)$$

$$\begin{aligned} \frac{dw_2^o}{dx} - \frac{dw_3^o}{dx} + \bar{u} \tau_o + \bar{\beta} \frac{d^2 \tau_o}{dx^2} + \gamma \frac{d^2 \phi_{x_2}}{dx^2} - \gamma^* \frac{d^2 \phi_{x_3}}{dx^2} + v \phi_{x_2} \\ - v^* \phi_{x_3} - (\bar{z} + \frac{1}{C_N}) \frac{d\sigma_o}{dx} = 0 \end{aligned} \quad (2.265)$$

To reduce these fourteen equations to two coupled equations in two unknowns the following manipulations are performed. Differentiate equation (2.264) w/R(x) twice

$$\begin{aligned} \frac{h_2}{2} \frac{d^3 w_2^o}{dx^3} + \frac{h_3}{2} \frac{d^3 w_3^o}{dx^3} + (\bar{p} - \frac{1}{C_s}) \frac{d^2 \tau_o}{dx^2} + \bar{r} \frac{d^4 \tau_o}{dx^4} + q \frac{d^2 \phi_{x_2}}{dx^2} \\ - q^* \frac{d^2 \phi_{x_3}}{dx^2} + s \frac{d^4 \phi_{x_2}}{dx^4} + s^* \frac{d^4 \phi_{x_3}}{dx^4} + \bar{r} \frac{d^3 \sigma_o}{dx^3} \end{aligned}$$

$$+ \frac{d^2 u_2^o}{dx^2} - \frac{d^2 u_3^o}{dx^2} = 0 \quad (2.266)$$

Also differentiate equations (2.259) and (2.262) w/R(x) $\frac{d^2 u}{dx^2}$ substituting the results into equation (2.266) for $\frac{d^2 u}{dx^2}$. Combining terms and using relation (2.252) and (2.255) yields

$$\begin{aligned} & \frac{h_2}{2} \frac{d^2 w^o}{dx^3} + \frac{h_3}{2} \frac{d^3 w_3^o}{dx^3} + \left(\bar{p} - \frac{1}{C_s} - \frac{D}{\bar{A}} + \frac{D^*}{\bar{A}^*} \right) \frac{d^2 \tau_o}{dx^2} \\ & + \left(\bar{r} - \frac{C}{\bar{A}} + \frac{C^*}{\bar{A}^*} \right) \frac{d^4 \tau_o}{dx^4} + \left(S - \frac{A}{\bar{A}} \right) \frac{d^4 \phi_{x2}}{dx^4} \\ & + \left(S^* + \frac{A^*}{\bar{A}^*} \right) \frac{d^4 \phi_{x3}}{dx^4} + \left(q - \frac{B}{\bar{A}} \right) \frac{d^2 \phi_{x2}}{dx^2} + \left(-q^* + \frac{B^*}{\bar{A}^*} \right) \frac{d^2 \phi_{x3}}{dx^2} \\ & + \left(\bar{t} - \frac{E}{\bar{A}} + \frac{E^*}{\bar{A}^*} \right) \frac{d^3 \sigma_o}{dx^3} + \tau_o \left[\frac{1}{\bar{A}} + \frac{1}{\bar{A}^*} \right] = 0 \end{aligned} \quad (2.267)$$

Rearranging equations (2.260) and (2.263) gives the following general relationships

$$\phi_{x_N} = \frac{Q_N}{K_5} - \frac{h_2 \tau_o}{2K_5} \quad (2.268)$$

Also,

$$\frac{d^2 \phi_{x_N}}{dx_N^2} = \frac{1}{K_5} \frac{d^2 Q_N}{dx^2} - \frac{h_2}{2K_5} \frac{d^2 \tau_o}{dx^2} \quad (2.269)$$

$$\frac{d^M \phi_{x_N}}{dx^M} = \frac{1}{K_5} \frac{d^M Q_N}{dx_M^M} - \frac{h_2}{2K_5} \frac{d^M \tau_o}{dx_M^M} \quad (2.270)$$

Moreover, from equation (2.253)

$$\sigma_o = \frac{dQ_2}{dx} \quad (2.271)$$

$$\frac{d\sigma_o}{dx} = \frac{d^2 Q_2}{dx^2} \quad (2.272)$$

$$\frac{d^{N-1} \sigma_o}{dx^{N-1}} = \frac{d^N Q_2}{dx^N} \quad (2.273)$$

Subtracting equation (2.256) from (2.253) gives

$$\frac{dQ_2}{dx} = - \frac{dQ_3}{dx} \quad (2.274)$$

and in general

$$\frac{d^N Q_2}{dx^N} = - \frac{d^N Q_3}{dx^N} \quad (2.275)$$

If one integrates equation (2.274), there emerges a relation for the shear in the two adherends, namely,

$$Q_2(x) + Q_3(x) = V_1 \quad (2.276)$$

Substituting equation (2.258) into (2.254) a relation for $\frac{d^3 w_3^o}{dx^3}$ can be found. Similarly, substituting equation (2.261) into (2.257) results in an expression for $\frac{d^3 w_3^o}{dx^3}$. Substitute these relations plus equations (2.268-2.275) into equation (2.267).

$$\frac{h_2}{2D_{112}} \left[\frac{F}{K_5} \frac{d^4 Q_2}{dx^4} - \frac{Fh_2}{2K_5} \frac{d^4 \tau_o}{dx^4} + \frac{G}{K_5} \frac{d^2 Q_2}{dx^2} - \frac{Gh_2}{2K_5} \frac{d^2 \tau_o}{dx^2} \right]$$

$$\begin{aligned}
 & + H \frac{d^4 \tau_o}{dx^4} + I \frac{d^2 \tau_o}{dx^2} - Q_2 + \frac{h_2}{2} \tau_o] + \frac{h_3}{2D_{113}} \left[- \frac{F^*}{K_5} \frac{d^4 Q_2}{dx^2} \right. \\
 & - \frac{F^* h_3}{2K_5} \frac{d^4 \tau_o}{dx^4} - \frac{G^*}{K_5} \frac{d^2 Q_2}{dx^2} - \frac{G^* h_3}{2K_5} \frac{d^2 \tau_o}{dx^2} + H^* \frac{d^4 \tau_o}{dx^4} \\
 & + I^* \frac{d^2 \tau_o}{dx^2} - Q_3 + \frac{h_3 \tau_o}{2} \left. \right] + \left(\bar{p} - \frac{1}{C_s} - \frac{D}{\bar{A}} + \frac{D^*}{\bar{A}^*} - \frac{qh_2}{2K_5} \right. \\
 & + \frac{Bh_2}{2K_5 \bar{A}} + \frac{qh_3}{2K_5^*} - \frac{h_3 B^*}{2K_5^* \bar{A}^*} \left. \right) \frac{d^2 \tau_o}{dx^2} + \left(\bar{r} - \frac{C}{\bar{A}} + \frac{C^*}{\bar{A}^*} - \frac{Sh_2}{2K_5} \right. \\
 & + \frac{Ah_2}{2K_5 \bar{A}_{11}} - \frac{S^* h_3}{2K_5^*} - \frac{h_3 A^*}{2K_5^* \bar{A}^*} \left. \right) \frac{d^4 \tau_o}{dx^4} + \left(\frac{S}{K_5} - \frac{A}{K_5 \bar{A}} - \frac{S^*}{K_5^*} \right. \\
 & - \frac{A^*}{\bar{A}^* K_5^*} + \bar{t} - \frac{E}{\bar{A}} + \frac{E^*}{\bar{A}^*} \left. \right) \frac{d^4 Q_2}{dx^4} + \left(\frac{q}{K_5} - \frac{B}{K_5 \bar{A}_{11}} + \frac{q^*}{K_5^*} \right. \\
 & - \frac{B^*}{K_5^* \bar{A}^*} \left. \right) \frac{d^2 Q_2}{dx^2} + \tau_o \left(\frac{1}{\bar{A}} + \frac{1}{\bar{A}^*} \right) = 0 \quad (2.277)
 \end{aligned}$$

Combining terms and employing equation (2.276) gives us the first governing equation:

$$\left[- \frac{1}{4D_{112}} \frac{h_2^2}{K_5} + \frac{h_2 H}{2D_{112}} - \frac{F^* h_3^2}{4D_{113} K_5^*} + \frac{h_3 H^*}{2D_{113}} + \bar{r} - \frac{C}{\bar{A}} + \frac{C^*}{\bar{A}^*} \right.$$

$$\begin{aligned}
 & - \frac{Sh_2}{2K_5} - \frac{S^*h_3}{2K_5^*} + \frac{Ah_2}{2K_5\bar{A}} - \frac{h_3A^*}{2K_5^*\bar{A}^*} \Big] \frac{d^4\tau_o}{dx^4} + \Big[- \frac{Gh_2^2}{4D_{112}K_5} \\
 & + \frac{h_2I}{2D_{112}} - \frac{G^*h_3^2}{4D_{113}K_5^*} + \frac{I^*h_3}{2D_{113}} + \bar{p} - \frac{1}{C_s} - \frac{D}{\bar{A}} + \frac{D^*}{\bar{A}^*} \\
 & - \frac{qh_2}{2K_5} + \frac{Bh_2}{2K_5\bar{A}} + \frac{q^*h_3}{2K_5^*} - \frac{h_3B^*}{2K_5^*\bar{A}^*} \Big] \frac{d^2\tau_o}{dx^2} + \Big[\frac{h_2^2}{4D_{112}} + \frac{h_3^2}{4D_{113}^*} \\
 & + \frac{1}{\bar{A}} + \frac{1}{\bar{A}^*} \Big] \tau_o + \Big[\frac{h_2F}{2K_5D_{112}} - \frac{h_3F^*}{2K_5^*D_{113}} + \frac{S}{K_5} - \frac{A}{K_5\bar{A}} - \frac{S^*}{K_5^*} - \frac{A^*}{\bar{A}^*K_5^*} \\
 & + \bar{t} - \frac{E}{\bar{A}} + \frac{E^*}{\bar{A}^*} \Big] \frac{d^4Q_2}{dx^4} + \Big[\frac{h_2G}{2K_5D_{112}} - \frac{h_3G^*}{2K_5^*D_{113}} + \frac{q}{K_5} - \frac{B}{K_5\bar{A}} \\
 & + \frac{q^*}{K_5^*} - \frac{B^*}{K_5^*\bar{A}^*} \Big] \frac{d^2Q_2}{dx^2} + \Big[- \frac{h_2}{2D_{112}} + \frac{h_3}{2D_{113}} \Big] Q_2 = \frac{h_3V_1}{2D_{113}^*}
 \end{aligned}
 \tag{2.277}$$

In a more compact form this equation can be rewritten as:

$$\begin{aligned}
 & A_1 \frac{d^4\tau_o}{dx^4} + A_2 \frac{d^2\tau_o}{dx^2} + A_3 \tau_o + A_4 \frac{d^4Q_2}{dx^4} + A_5 \frac{d^2Q_2}{dx^2} + A_6 Q_2(x) \\
 & = \frac{h_3V_1}{2D_{113}^*}
 \end{aligned}
 \tag{2.278}$$

Where the constants $A_1 - A_6$ are defined explicitly on page 148. The second governing relation will now be derived. Differentiate equation (2.265) $w/R(x)$ twice.

Substitute equations (2.268-2.276) and the relations for $\frac{d^2 w_2^0}{dx^2}$ and $\frac{d^3 w_3^0}{dx^2}$ into it to give the second governing relations in two unknowns.

$$\begin{aligned}
 & \left[-\frac{F h_2}{2K_5 D_{112}} + \frac{H}{D_{112}} + \frac{F^* h_3}{2K_5^* D_{113}} - \frac{H^*}{D_{113}} + \bar{\beta} - \frac{\gamma h_2}{2K_5} \right. \\
 & \quad \left. + \frac{\gamma^* h_3}{2K_5^*} \right] \frac{d^4 \tau_0}{dx^4} + \left[-\frac{G h_2}{2K_5 D_{112}} + \frac{I}{D_{112}} + \frac{G^* h_3}{2K_5^* D_{113}} \right. \\
 & \quad \left. - \frac{I^*}{D_{113}} + \bar{u} - \frac{v h_2}{2K_5} + \frac{v^* h_3}{2K_5^*} \right] \frac{d^2 \tau_0}{dx^2} + \left[\frac{h_2}{2D_{112}} - \frac{h_3}{2D_{113}} \right] \tau_0 \\
 & \quad + \left[-\frac{F}{K_5 D_{112}} + \frac{F^*}{K_5^* D_{113}} + \frac{\gamma}{K_5} + \frac{\gamma^*}{K_5^*} - \bar{z} - \frac{1}{C_N} \right] \frac{d^4 Q_2}{dx^4} \\
 & \quad + \left[\frac{G}{K_5 D_{112}} + \frac{G^*}{K_5^* D_{113}} + \frac{v}{K_5} + \frac{v^*}{K_5^*} \right] \frac{d^2 Q_2}{dx^2} + \left[-\frac{1}{D_{112}} - \frac{1}{D_{113}} \right] Q_2 \\
 & = -\frac{V_1}{D_{113}^*}
 \end{aligned} \tag{2.279}$$

Rewriting equation (2.279) in a more compact notation gives:

$$B_1 \frac{d^4 \tau_o}{dx^4} + B_2 \frac{d^2 \tau_o}{dx^2} + B_3 \tau_o + B_4 \frac{d^4 Q_2}{dx^4} + B_5 \frac{d^2 Q_2}{dx^2} + B_6 Q_2 = - \frac{V_1}{D_{113}^*} \quad (2.280)$$

The constants $B_1 - B_6$ are defined explicitly on page 149

$$A_1 = \left[- \frac{F h_2^2}{4D_{112} K_5} + \frac{h_2 H}{2D_{112}} - \frac{F^* h_3^2}{4D_{113} K_5^*} + \frac{h_3 H^*}{2D_{113}} + \bar{r} - \frac{C}{\bar{A}} + \frac{C^*}{\bar{A}^*} - \frac{S h_2}{2K_5} - \frac{S^* h_3}{2K_5^*} + \frac{A h_2}{2K_5 \bar{A}} - \frac{h_3 A^*}{2K_5^* \bar{A}^*} \right] \quad (2.281)$$

$$A_2 = \left[- \frac{G h_2^2}{4D_{112} K_5} + \frac{h_2 I}{2D_{112}} - \frac{G^* h_3^2}{4D_{113} K_5^*} + \frac{I^* h_3}{2D_{113}} - \frac{1}{C_s} + \bar{p} - \frac{D}{\bar{A}} + \frac{D^*}{\bar{A}^*} - \frac{q h_2}{2K_5} + \frac{B h_2}{2K_5 \bar{A}} + \frac{q^* h_3}{2K_5^*} - \frac{h_3 B^*}{2K_5^* \bar{A}^*} \right] \quad (2.282)$$

$$A_3 = \left[\frac{h_2^2}{4D_{112}} + \frac{h_3^2}{4D_{113}^*} + \frac{1}{\bar{A}} + \frac{1}{\bar{A}^*} \right] \quad (2.283)$$

$$A_4 = \left[\frac{h_2 F}{2K_5 D_{112}} - \frac{h_3 F^*}{2K_5^* D_{113}} + \frac{S}{K_5} - \frac{A}{K_5 \bar{A}} - \frac{S^*}{K_5^*} - \frac{A^*}{\bar{A}^* K_5^*} + \bar{t} \right. \\ \left. - \frac{E}{\bar{A}} + \frac{E^*}{\bar{A}^*} \right] \quad (2.284)$$

$$A_5 = \left[\frac{h_2 G}{2K_5 D_{112}} - \frac{h_3 G^*}{2K_5^* D_{113}} + \frac{q}{K_5} - \frac{B}{K_5 \bar{A}} + \frac{q^*}{K_5^*} - \frac{B^*}{K_5^* \bar{A}^*} \right] \quad (2.285)$$

$$A_6 = \left[-\frac{h_2}{2D_{112}} + \frac{h_3}{2D_{113}} \right] \quad (2.286)$$

$$B_1 = \left[-\frac{F h_2}{2K_5 D_{112}} + \frac{H}{D_{112}} + \frac{F^* h_3}{2K_5^* D_{113}} - \frac{H^*}{D_{113}} + \bar{\beta} - \frac{\gamma h_2}{2K_5} \right. \\ \left. + \frac{\gamma^* h_3}{2K_5^*} \right] \quad (2.287)$$

$$B_2 = \left[-\frac{G h_2}{2K_5 D_{112}} + \frac{I}{D_{112}} + \frac{G^* h_3}{2K_5^* D_{113}} - \frac{I^*}{D_{113}} + \bar{u} - \frac{v h_2}{2K_5} \right. \\ \left. + \frac{v^* h_3}{2K_5^*} \right] \quad (2.288)$$

$$B_3 = \left[\frac{h_2}{2D_{112}} - \frac{h_3}{2D_{113}} \right] \quad (2.289)$$

$$B_4 = \left[\frac{F}{K_5 D_{112}} + \frac{F^*}{K_5^* D_{113}} + \frac{\gamma}{K_5} + \frac{\gamma^*}{K_5^*} - \bar{z} - \frac{1}{C_N} \right] \quad (2.290)$$

$$B_5 = \left[\frac{G}{K_5 D_{112}} + \frac{G^*}{K_5^* D_{113}} + \frac{v}{K_5} + \frac{v^*}{K_5^*} \right] \quad (2.291)$$

$$B_6 = \left[-\frac{1}{D_{112}} - \frac{1}{D_{113}} \right] \quad (2.292)$$

1. TWO LAMINATES OF EQUAL THICKNESS AND MATERIAL PROPERTIES

In examining equations (2.277) and (2.279) it can be shown that for two adherends of equal lamina properties, orientation and thicknesses the following constants go to zero.

$$A_4 = A_5 = A_6 = B_1 = B_2 = B_3 = 0$$

Thus, the two governing equations are uncoupled and can be rewritten as

$$A_1 \frac{d^4 \tau_o}{dx^4} + A_2 \frac{d^2 \tau_o}{dx^2} + A_3 \tau_o = \frac{h_3 V_1}{2D_{11}} \quad (2.293)$$

$$B_4 \frac{d^4 Q_2}{dx^4} + B_5 \frac{d^2 Q_2}{dx^2} + B_6 Q_2 = - \frac{V_1}{D_{11}} \quad (2.294)$$

A solution whereby τ_o and σ_o are independent of each other can now be rendered.

Solution of $\tau_o(x)$

Assume a homogeneous solution of the form

$$\tau_o(x) = \sum_{i=1}^4 C_i e^{\lambda_i x} \quad (2.295)$$

for the adhesive shear stress. Note that such a solution satisfies equation (2.293). Realizing now that $h_2 = h_3$ and $D_{112} = D_{113}$, the particular solution of equation (2.293) is

$$\tau_o(x) = \frac{h_2 V_1}{2D_{11} A_3} \quad (2.296)$$

Thus the complete solution of equation (2.293) and thus the shear stress distribution in the adhesive is

$$\tau_o(x) = \sum_{i=1}^4 C_i e^{\lambda_i x} + \frac{h_2 V_1}{2D_{11} A_3} \quad (2.297)$$

where (λ_i) are the roots of equation (2.293) and may be complex. Substituting equation (2.297) into (2.293) one can determine the equality, the roots (λ_i) must satisfy, namely,

$$A_1 \lambda_i^4 \sum_{i=1}^4 C_i e^{\lambda_i x} + A_2 \lambda_i^2 \sum_{i=1}^4 C_i e^{\lambda_i x} + A_3 \sum_{i=1}^4 C_i e^{\lambda_i x} + \frac{A_3 h_2 V_1}{2D_{11} A_3} = \frac{h_2 V_1}{2D_{11}}$$

Upon simplifying one gets

$$(A_1 \lambda i^4 + A_2 \lambda i^2 + A_3) \text{Si} e^{\lambda i x} = 0 \quad i = 1 + 4 \quad (2.298)$$

Solution of $\sigma_o(x)$

Recalling the definition of B_6 , namely,

$$B_6 = - \left[\frac{1}{D_{112}} + \frac{1}{D_{113}} \right]$$

Then from equation (2.294)

$$B_6 Q_2 = - \left[\frac{Q_2}{D_{112}} + \frac{Q_2}{D_{113}} \right] \quad (2.299)$$

using expression (2.276) gives

$$B_6 Q_2 = - \left[\frac{Q_2(x)}{D_{112}} - \frac{Q_3(x)}{D_{113}} + \frac{V_1}{D_{113}} \right] \quad (2.300)$$

Substitution of the $B_6 Q_2$ term into equation (2.294) gives

$$B_4 \frac{d^4 Q_2}{dx^4} + B_5 \frac{d^2 Q_2}{dx^2} - \frac{Q_2(x)}{D_{112}} + \frac{Q_3(x)}{D_{113}} = 0 \quad (2.301)$$

Differentiating equation (2.301) w/R (x) and recalling equations (2.253) and (2.256) there results:

$$B_4 \frac{d^4 \sigma_o}{dx^4} + B_5 \frac{d^2 \sigma_o}{dx^2} - \frac{1}{D_{11}} [\sigma_o + \sigma_o] = 0 \quad (2.302)$$

Thus, equation (2.294) can be rewritten as

$$B_4 \frac{d^4 \sigma_o}{dx^4} + B_5 \frac{d^2 \sigma_o}{dx^2} - \frac{2\sigma_o}{D_{11}} = 0 \quad (2.303)$$

Let one assume a solution of the form

$$\sigma_o(x) = F_i e^{\lambda_i x} \quad i = 5 + 8 \quad (2.304)$$

where (λ_i) are the roots of equation (2.303), may be complex, and must satisfy relation (2.305).

$$(B_4 \lambda_i^4 + B_5 \lambda_i^2 - \frac{2}{D_{11}}) F_i e^{\lambda_i x} = 0 \quad i = 5 + 8 \quad (2.305)$$

Thus, summarizing we have two fourth order linear non-homogeneous differential equations whose roots must satisfy equation (2.293) for $i = 1, 4$ and equation (2.294) for $i = 5, 8$. The most efficient way to obtain these roots is employing a numerical method for a particular set of data.

1. Boundary Conditions - Eight Required

Having the roots of the two governing equations, the final step is to find values for the eight unknowns $S_1 \rightarrow S_4$ and $F_1 \rightarrow F_4$.

These will be found by manipulation of the original fourteen governing equations on page 139 to produce the eight boundary condition equations required.

Differentiate equation (2.265) with respect to (x) once.

$$\begin{aligned} \frac{d^2 w_2^o}{dx^2} - \frac{d^2 w_3^o}{dx^2} + \bar{u} \frac{d\tau_o}{dx} + \bar{\beta} \frac{d^3 \tau_o}{dx^3} + \gamma \frac{d^3 \phi_{x_2}}{dx^3} - \gamma^* \frac{d^3 \phi_{x_3}}{dx^3} \\ + v \frac{d\phi_{x_2}}{dx} - v^* \frac{d\phi_{x_3}}{dx} - \left(\bar{z} + \frac{1}{C_N}\right) \frac{d^2 c_o}{dx^2} = 0 \end{aligned} \quad (2.306)$$

Solving equations (2.258) and (2.261) for $\frac{d^2 w_2^o}{dx^2}$ and $\frac{d^2 w_3^o}{dx^2}$ substituting these and relation (2.270) into equation (2.306) gives

$$-\frac{M_2}{D_{11}} + \frac{M_3}{D_{11}} + \left[\frac{F}{K_5 D_{11}} + \frac{\gamma}{K_5} + \frac{F^*}{K_5^* D_{11}} + \frac{\gamma^*}{K_5^*} - \bar{z} \right]$$

$$\begin{aligned}
 & - \frac{1}{C_N} \frac{d^2 \sigma_o}{dx^2} + \left[\frac{G}{K_5 D_{11}} + \frac{v}{K_5} + \frac{G^*}{K_5^* D_{11}} + \frac{v^*}{K_5^*} \right] \sigma_o \\
 & + \left[- \frac{F h_2}{2K_5 D_{11}} - \frac{\gamma h_2}{2K_5} + \frac{F^* h_3}{2D_{11} K_5^*} + \frac{\gamma^* h_3}{2K_5^*} + \frac{H}{D_{11}} - \frac{H^*}{D_{11}} \right. \\
 & \left. + B \right] \frac{d^3 \tau_o}{dx^3} + \left[- \frac{G h_2}{2K_5 D_{11}} - \frac{v h_2}{2K_5} + \frac{G^* h_3}{2K_5^* D_{11}} + \frac{v^* h_3}{2K_5^*} \right. \\
 & \left. + \frac{I}{D_{11}} - \frac{I^*}{D_{11}} + \bar{u} \right] \frac{d\tau_o}{dx} = 0 \quad (2.307)
 \end{aligned}$$

Inspection of equation (2.307) leads one to notice that the

First term in brackets is B_4

Second term in brackets is B_5

Third term in brackets is B_1

Fourth term in brackets is B_2

Thus, the first boundary condition equation is

$$- \frac{M_2}{D_{11}} + \frac{M_3}{D_{11}} + B_4 \frac{d^2 \sigma_o}{dx^2} + B_5 \sigma_o + B_1 \frac{d^3 \tau_o}{dx^3} + B_2 \frac{d\tau_o}{dx} = 0 \quad (2.308)$$

If one proceeds to differentiate equation (2.308) with respect to (x) there results

$$\begin{aligned}
 & - \frac{1}{D_{11}} \frac{dM_2}{dx} + \frac{1}{D_{11}} \frac{dM_3}{dx} + B_4 \frac{d^3 \sigma_o}{dx^3} + B_5 \frac{d\sigma_o}{dx} + B_1 \frac{d^4 \tau_o}{dx^4} \\
 & + B_2 \frac{d^2 \tau_o}{dx^2} = 0
 \end{aligned} \tag{2.309}$$

Rearranging equations (2.254) and (2.257) for $\frac{dM}{dx}$ gives

$$\frac{dM_2}{dx} = Q_2 - \frac{h_2}{2} \tau_o \tag{2.310}$$

$$\frac{dM_3}{dx} = Q_3 - \frac{h_3}{2} \tau_o \tag{2.311}$$

Substitution of these into equation (2.309) yields the second boundary condition equation.

$$\begin{aligned}
 & - \frac{Q_2}{D_{11}} + \frac{Q_3}{D_{11}} + \left[\frac{h_2}{2D_{11}} - \frac{h_3}{2D_{11}} \right] \tau_o + B_4 \frac{d^3 \sigma_o}{dx^3} + B_5 \frac{d\sigma_o}{dx} \\
 & + B_1 \frac{d^4 \tau_o}{dx^4} + B_2 \frac{d^2 \tau_o}{dx^2} = 0
 \end{aligned} \tag{2.312}$$

where the term in brackets is B_3 .

A third and final coupled boundary condition equation can be found, thusly; differentiate equation (2.264) with respect to (x) . There results

$$\begin{aligned} & \frac{h_2}{2} \frac{d^2 w_2^0}{dx^2} + \frac{h_3}{2} \frac{d^2 w_3^0}{dx^2} + \left(\bar{\rho} - \frac{1}{C_s} \right) \frac{d\tau_0}{dx} + \bar{r} \frac{d^3 \tau_0}{dx^3} + q \frac{d\phi_{x_2}}{dx} \\ & - q^* \frac{d\phi_{x_3}}{dx} + s \frac{d^3 \phi_{x_2}}{dx^3} + s^* \frac{d^3 \phi_{x_3}}{dx^3} + \bar{t} \frac{d^2 \sigma_0}{dx^2} + \frac{du_2^0}{dx} \\ & - \frac{du_3^0}{dx} = 0 \end{aligned} \quad (2.313)$$

Solving equations (2.259) and (2.262) for $\frac{du_2^0}{dx}$ and $\frac{du_3^0}{dx}$, respectively, and equations (2.258) and (2.261) for $\frac{d^2 w}{dx^2}$ and employing relation (2.270) and substituting these relations in (2.313) gives, after rearranging, the third boundary condition equation.

$$- \frac{h_2 M_2}{2D_{11}} - \frac{h_3 M_3}{2D_{11}} + \frac{T_2}{\bar{A}} - \frac{T_3}{\bar{A}^*} + \left[\frac{F h_2}{2K_5 D_{11}} - \frac{F^* h_3}{2K_5^* D_{11}} \right]$$

$$\begin{aligned}
 & + \frac{S}{K_5} - \frac{S^*}{K_5^*} - \frac{A}{\bar{A} K_5} - \frac{A^*}{\bar{A}^* K_5^*} - \frac{E}{\bar{A}} + \frac{E^*}{\bar{A}^*} + \bar{\tau} \left] \frac{d^2 \sigma_0}{dx^2} \right. \\
 & + \left[\frac{G h_2}{2D_{11} K_5} - \frac{G^* h_3}{2D_{11} K_5^*} + \frac{q}{K_5} + \frac{q^*}{K_5^*} - \frac{B}{\bar{A} K_5} - \frac{B^*}{K_5^* \bar{A}^*} \right] \sigma_0 \\
 & + \left[- \frac{F h_2^2}{4D_{11} K_5} - \frac{F^* h_3^2}{4K_5^* D_{11}} + \frac{H h_2}{2D_{11}} + \frac{H^* h_3}{2D_{11}} + \bar{r} - \frac{Sh_2}{2K_5} \right. \\
 & \left. - \frac{S^* h_3}{2K_5^*} + \frac{Ah_2}{2\bar{A} K_5} - \frac{C}{\bar{A}} - \frac{A^* h_3}{2K_5^* \bar{A}^*} + \frac{C^*}{\bar{A}^*} \right] \frac{d^3 \tau_0}{dx^3} \\
 & + \left[- \frac{Gh_2^2}{4K_5 D_{11}} + \frac{Ih_2}{2D_{11}} - \frac{G^* h_3^2}{4K_5^* D_{11}} + \frac{I^* h_3}{2D_{11}} + \bar{p} - \frac{1}{C_s} \right. \\
 & \left. - \frac{qh_2}{2K_5} + \frac{q^* h_3}{2K_5^*} + \frac{Bh_2}{2K_5 \bar{A}} - \frac{D}{\bar{A}} - \frac{B^* h_3}{2K_5^* \bar{A}^*} + \frac{D^*}{\bar{A}^*} \right] \frac{d\tau_0}{dx} = 0
 \end{aligned}
 \tag{2.314}$$

Again inspection of equation (2.314) leads one to notice that the

First term in brackets is A_4

Second term in brackets is A_5

Third term in brackets is A_1

Fourth term in brackets is A_2

Thus, the third boundary condition can be written as

$$\begin{aligned}
 & - \frac{h_2 M_2}{2D_{11}} - \frac{h_3 M_3}{2D_{11}} + \frac{T_2}{\bar{A}} - \frac{T_3}{\bar{A}^*} + A_4 \frac{d^2 \sigma_o}{dx^2} + A_5 \sigma_o + A_1 \frac{d^3 \tau_o}{dx^3} \\
 & + A_2 \frac{d \tau_o}{dx} = 0
 \end{aligned} \tag{2.315}$$

Having developed the necessary boundary condition equations one can now write the eight boundary conditions required to solve for the eight unknowns $S_1 \rightarrow S_4$ and $F_1 \rightarrow F_4$. Remembering that for our case

$$A_4 = A_5 = A_6 = B_1 = B_2 = B_3 = 0$$

The boundary condition equations for two equal adherends are now written. Employing equation (2.297) the first two boundary condition equations are

$$\tau_o(o) = 0 = S_1 + \frac{h_2 V_1}{2D_{11} A_3} \tag{2.316}$$

$$\tau_o(L_2) = 0 = Si e^{\lambda i L_2} + \frac{h_2 V_1}{2D_{11} A_3} \quad (2.317)$$

Employing equation (2.308) the third and fourth boundary condition equations are

$$@ x_2 = 0$$

$$M_2(x) = M_1$$

$$M_3(x) = 0$$

Therefore,

$$- \frac{M_1}{D_{11}} + B_4 \frac{d^2 \sigma_o(o)}{dx^2} + B_5 \sigma_o(o) = 0$$

Using equation (2.304) the third equation is

$$- \frac{M_1}{D_{11}} + B_4 \lambda^2 Fi + B_5 Fi = 0 \quad (2.318)$$

Similarly,

$$@ X = L_2$$

$$M_2(x) = 0$$

$$M_3(x) = M_4$$

Therefore equation (2.308) reduces to

$$\frac{M_4}{D_{11}} + B_4 \frac{d^2 \sigma_o(L_2)}{dx^2} + B_5 \sigma_o(L_2) = 0$$

Again substituting for $\sigma_o(x)$ the fourth equation is

$$\frac{M_4}{D_{11}} + B_4 \frac{2}{\lambda i F_i} e^{\lambda i L_2} + B_5 F_i e^{\lambda i L_2} = 0 \quad (2.319)$$

Employing equation (2.312) the fifth and sixth boundary condition equations are

$$@ X = 0$$

$$Q_2(x) = V_1$$

$$Q_3(x) = 0$$

Therefore equation (2.312) reduces to

$$-\frac{V_1}{D_{11}} + B_4 \frac{d^3 \sigma_o(o)}{dx^3} + B_5 \frac{d\sigma_o(o)}{dx}$$

Modifying it for $\sigma_o(x)$ gives the fifth equation, namely,

$$-\frac{V_1}{D_{11}} + B_4 \lambda_i^3 F_i + B_5 \lambda_i F_i \quad (2.320)$$

Similarly,

$$@ X = L_2$$

$$Q_2(x) = 0$$

$$Q_3(x) = V_4$$

Substituting into equation (2.312) and using equation (2.304) for $\sigma_o(x)$ the sixth equation is

$$\frac{V_4}{D_{11}} + B_4 \lambda_i^3 F_i e^{\lambda_i L_2} + B_5 \lambda_i F_i e^{\lambda_i L_2} = 0 \quad (2.321)$$

Finally making use of equation (2.315) the last two equations are determined

$$@ X = 0$$

$$M_2(x) = M_1$$

$$T_2(x) = T \cos \theta$$

$$M_3(x) = 0$$

$$T_3(x) = 0$$

Therefore equation (2.315) reduces to

$$-\frac{h_2 M_1}{2D_{11}} + \frac{T \cos \theta}{\bar{A}} + A_1 \frac{d^3 \tau_0(o)}{dx^3} + A_2 \frac{d\tau_0(o)}{dx} = 0$$

Employing equation (2.297) for $\tau_0(x)$ the seventh equation is

$$-\frac{h_2 M_1}{2D_{11}} + \frac{T \cos \theta}{\bar{A}} + A_1 \lambda^3 \text{Si} + A_2 \lambda \text{Si} = 0 \quad (2.322)$$

Similarly,

$$@ X = L_2$$

$$M_2(x) = 0$$

$$T_2(x) = 0$$

$$M_3(x) = M_4$$

$$T_3(x) = T \cos \theta$$

Again equation (2.315) reduces to

$$-\frac{h_3 M_4}{2D_{11}} - \frac{T \cos \theta}{\bar{A}^*} + A_1 \frac{d^3 \tau_o(L_2)}{dx^3} + A_2 \frac{d\tau_o(L_2)}{dx} = 0$$

Employing equation (2.297) again gives us the final equation, namely,

$$-\frac{h_3 M_4}{2D_{11}} - \frac{T \cos \theta}{\bar{A}^*} + A_1 \lambda^3 \text{Si} e^{\lambda i L_2} + A_2 \lambda \text{Si} e^{\lambda i L_2} = 0 \quad (2.323)$$

SUMMARY

Having determined the roots and the necessary boundary conditions one can now solve for the shear stress distribution $\tau_o(x)$ and the normal stress distribution $\sigma_o(x)$ in the adhesive. Knowing these distributions one can calculate the transverse shear stress $\tau_{xz}|_K$ and normal stress $\sigma_z|_K$ distributions throughout the laminates using equations (2.29), (2.33) and (2.144), respectively. In addition if one wishes to calculate in-plane loads $T_2(x)$, $T_3(x)$, moments $M_2(x)$, $M_3(x)$, inplane and lateral displacements $u_2(x)$, $u_3(x)$, $w_2^o(x)$, $w_3^o(x)$, and the lateral shears $Q_2(x)$, $Q_3(x)$ he may do so using the following procedure.

The transverse shear $Q_2(x)$ in part (2) may be

found by integrating equation (2.253) on page 139 over the length of the overlap. Thus,

$$Q_2(x) = \int_0^x \sigma_o dx + V_1$$

$$Q_2(x) = \int_0^x F_i e^{\lambda i x} dx + V_1$$

$$Q_2(x) = \frac{F_i}{\lambda i} e^{\lambda i x} - \frac{F_i}{\lambda i} + V_1 \quad (2.324)$$

Employing equation (2.276) on page 144 the transverse shear $Q_3(x)$ can be determined. Thus, per equation (2.276)

$$Q_3(x) = -Q_2(x) + V_1$$

Substituting for $Q_2(x)$ one gets

$$Q_3(x) = -\frac{F_i}{\lambda i} e^{\lambda i x} + \frac{F_i}{\lambda i} \quad (2.325)$$

The axial load in part (2) at a particular point along the overlap can be determined by integrating equation (2.252) on page 139. Thus,

$$T_2(x) = \int_0^x \tau_o dx + T_2(o)$$

Substituting for $\tau_o(x)$ and completing the integration gives

$$T_2(x) = \frac{Si}{\lambda i} e^{\lambda i x} - \frac{Si}{\lambda i} + \frac{h_2 V_1 x}{2D_{11} A_3} + T \cos \theta \quad (2.326)$$

The axial load in part (3) at a particular point along the overlap can be found in a similar manner per equation (2.255).

$$T_3(x) = - \int_0^x \tau_o \, dx + T_3(o)$$

Substituting for $\tau_o(x)$ and integrating the result is

$$T_3(x) = - \frac{Si}{\lambda i} e^{\lambda i x} + \frac{Si}{\lambda i} - \frac{h_2 V_1 x}{2D_{11} A_3} \quad (2.327)$$

A similar procedure to those above will generate the moment in parts (2) and (3) at a particular point. Rearranging and integrating equation (2.254) yields

$$M_2(x) = \int_0^x Q_2(x) \, dx - \frac{h_2}{2} \int_0^x \tau_o(x) \, dx + M_2(o)$$

Making the necessary substitutions and integrating one gets

$$M_2(x) = \frac{Fi}{\lambda i^2} e^{\lambda i x} - \frac{Fi}{\lambda i^2} - \frac{Fi}{\lambda i} x + V_1 x - \frac{h_2}{2} \frac{Si}{\lambda i} e^{\lambda i x}$$

$$+ \frac{h_2}{2} \frac{Si}{\lambda i} - \frac{h_2^2 V_1}{4D_{11} A_3} X + M_1 \quad (2.328)$$

Rearranging and integrating equation (2.257) an expression for the moment at a particular point along the overlap in part (3) is obtained.

$$M_3(x) = \int_0^x Q_3 dx - \frac{h_3}{2} \int_0^x \tau_0 dx + M_3(0)$$

Making the necessary substitutions and completing the integration yields

$$M_3(x) = - \frac{Fi}{\lambda i^2} e^{\lambda i X} + \frac{Fi}{\lambda i^2} + \frac{Fi}{\lambda i} X - \frac{h_3}{2} \frac{Si}{\lambda i} e^{\lambda i X} \\ + \frac{h_3}{2} \frac{Si}{\lambda i} - \frac{h_3 h_2 V_1}{4D_{11} A_3} X \quad (2.329)$$

It is now expedient to determine the unknowns ϕ_{x_2} and ϕ_{x_3} as they will be used to determine the inplane and lateral displacements. Per equations (2.260) and (2.263).

$$\phi_{x_2} = \frac{Q_2(x) - \frac{h_2}{2} \tau_o(x)}{K_5} \quad (2.330)$$

and

$$\phi_{x_3} = \frac{Q_3(x) - \frac{h_3}{2} \tau_o(x)}{K_5^*} \quad (2.331)$$

Employing equation (2.259) an expression for the inplane displacement in part (2) is determined. Thus,

$$\begin{aligned} \frac{du_2^o}{dx} = & \frac{1}{A} [T_2(x) - A \frac{d^3 \phi_{x_2}}{dx^3} - B \frac{d\phi_{x_2}}{dx} - C \frac{d^3 \tau_o}{dx^3} - D \frac{d\tau_o}{dx} \\ & - E \frac{d^2 \sigma_o}{dx^2}] \end{aligned} \quad (2.332)$$

Integrating equation (2.332) with respect to (x), using boundary condition equation (2.213) on page 125 and equation (2.217) yields

$$\frac{T}{\bar{A}} L_1 = u_2^o(x) \quad (2.333)$$

and thus the relation for $u_2^o(x)$ can be determined. Employing a similar procedure with equation (2.262) results in

$$\begin{aligned} \frac{du_3^o}{dx} = \frac{1}{\bar{A}^*} [T_3(x) - A^* \frac{d^3\phi_{x3}}{dx^3} - B^* \frac{d\phi_{x3}}{dx} - C^* \frac{d^3\tau_o}{dx^3} \\ - D^* \frac{d\tau_o}{dx} - E^* \frac{d^2\sigma_o}{dx^2}] \end{aligned} \quad (2.334)$$

Once again integrating equation (2.334) with respect to (x) will give a relation for $U_3^o(x)$ with one unknown. This unknown will be determined in conjunction with the lateral displacements $w_2^o(x)$ and $w_3^o(x)$.

Finally, the lateral displacements are determined. Rearranging equation (2.258)

$$\begin{aligned} \frac{d^2w_2^o(x)}{dx^2} = \frac{1}{D_{11}} [-M_2(x) + F \frac{d^3\phi_{x2}}{dx^3} + G \frac{d\phi_{x2}}{dx} + H \frac{d^3\tau_o}{dx^3} \\ + I \frac{d\tau_o}{dx}] \end{aligned} \quad (2.335)$$

Integrating equation (2.335) twice with respect to (x) and using the fact that

$$w_1^o(L_1) = w_2^o(o) \quad (2.336)$$

$$\frac{dw_1^o}{dx}(L_1) = \frac{dw_2^o}{dx}(o) \quad (2.337)$$

one can get the expression for $w_2^o(x)$. Following a similar procedure $w_3^o(x)$ is found. Rearranging equation (2.261)

$$\begin{aligned} \frac{d^2 w_3^o(x)}{dx^2} = \frac{1}{D_{11}} \left[-M_3(x) + F^* \frac{d^3 \phi_{x_3}}{dx^3} + G^* \frac{d\phi_{x_3}}{dx} + H^* \frac{d^3 \tau_o}{dx^3} \right. \\ \left. + I^* \frac{d\tau_o}{dx} \right] \end{aligned} \quad (2.338)$$

Integrating equation (2.338) twice with respect to (x) and using the fact that

$$w_4^o(o) = w_3^o(L_3) \quad (2.339)$$

$$\frac{dw_4^o(o)}{dx} = \frac{dw_3^o(L_3)}{dx} \quad (2.340)$$

one can obtain the desired expression for $w_3^o(x)$. To obtain a complete solution one must yet obtain relations for $u_3^o(0)$ and \bar{A} . Per equation (2.264) on page 141 a relation for u_3^o can be obtained exclusive of any new boundary value constants. Thus, rearranging terms one gets

$$u_3^o = \frac{h_2}{2} \frac{dw_o^2}{dx} + \frac{h_3}{2} \frac{dw_o^3}{dx} + \left(\bar{\rho} - \frac{1}{C_s}\right) \tau_o + \bar{r} \frac{d^2 \tau_o}{dx^2} + q \phi_{x_2} - q^* \phi_{x_3} + S \frac{d^2 \phi_{x_2}}{dx^2} + S^* \frac{d^2 \phi_{x_3}}{dx^2} + \bar{t} \frac{d\sigma_o}{dx} + u_2^o \quad (2.341)$$

Now, the only unknown is \bar{A} in the expression for $u_4^o(x)$. It can be obtained using boundary condition (2.222) on page 128, namely,

$$u_4^o(0) = u_3^o(L_3)$$

where $u_4^o(x)$ is given by equation (2.225). Thus, using equation (2.222), (2.225) and (2.341)

$$\bar{A} = \frac{h_2}{2} \frac{dw_o^2(L_3)}{dx} + \frac{h_3}{2} \frac{dw_o^3(L_3)}{dx} + \left(\bar{\rho} - \frac{1}{C_s}\right) \tau_o(L_3) + \bar{r} \frac{d^2 \tau_o(L_3)}{dx^2}$$

$$\begin{aligned}
 & + q \phi_{x_2}(L_3) - q^* \phi_{x_3}(L_3) + S \frac{d^2 \phi_{x_2}(L_3)}{dx^2} + S^* \frac{d^2 \phi_{x_3}(L_3)}{dx^2} \\
 & + \bar{t} \frac{d\sigma_o(L_3)}{dx} + u_o^o(L_3)
 \end{aligned}
 \tag{2.342}$$

This completes the problem of two adherends bonded in a single lap joint configuration under a static load. Again note that it was assumed the adherend's lamina were in a balanced configuration about their geometrical centerline, were of like material and orientation and of equal thickness.

M. TWO LAMINATES OF UNEQUAL THICKNESS AND/OR UNEQUAL MATERIAL PROPERTIES

To solve the general problem whereby $L_1 \neq L_2 \neq L_4$ and $h_2 \neq h_3$ and while the lamina of the adherends are symmetric about their own geometrical mid-planes they are not necessarily of the same material or orientation, two items are needed: (1) the calculation of M_1 , M_4 , V_1 , V_4 ; (2) the solution of the general eighth order equation of parts (2) and (3) and its associated boundary conditions.

1. Determination of M_1 , M_4 , V_1 and V_4

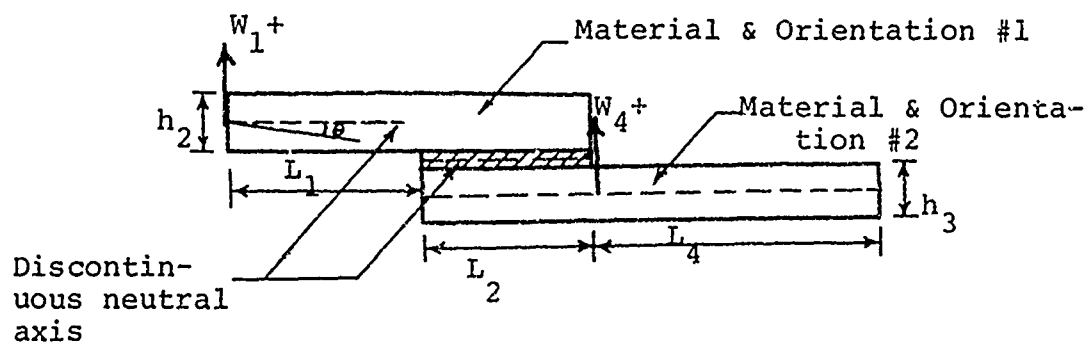


FIGURE (7)

The moment relation for part (1) is given by equation (2.205).

$$M_x = T \cos \theta [\theta X_1 - w_1^o(x)] \quad 0 \leq X_1 \leq L_1 \quad (2.343)$$

Moreover, the moment relations for parts (2) and (4) can be determined using Figure 7. They are

$$M_x = T \cos \theta [\theta(X_4 - L_4) - w_4^o(x)] \quad (2.344)$$

$$0 \leq X_4 \leq L_4$$

$$M_x = T \cos \theta [\theta(L_1 + X_2) - \bar{w}^o(x) - \frac{h_2}{2} - \frac{(h_3 - h_2)}{2}] \quad (2.345)$$

$$0 \leq X \leq L_2$$

Referring back to the case whereby both adherends were identical it was determined that $w_4^o(x) = -w_1^o(x)$. However, for the general case this is not true. Thus, a relation for $w_4^o(x)$ must be derived. From equation (2.211)

$$w_4^o(x) = \theta(X_4 - L_4) + \bar{E} \sinh \bar{K} X_4 + \bar{F} \cosh \bar{K} X_4 \quad (2.346)$$

$$0 \leq X_4 \leq L_4$$

The boundary conditions are

$$w_4^o(L_4) = 0 \quad (2.347)$$

$$w_4^0(0) = w_3^0(L_2) \quad (2.343)$$

Substituting equation (2.211) into (2.347) gives

$$0 = \bar{E} \sinh \bar{K} L_4 + \bar{F} \cosh \bar{K} L_4$$

Thus,

$$\bar{E} = -\bar{F} \coth \bar{K} L_4 \quad (2.349)$$

Moreover,

$$w_4^0(x) = \theta(x_4 - L_4) - \bar{F} (\coth \bar{K} L_4 \sinh \bar{K} x_4 - \cosh \bar{K} x_4) \quad (2.350)$$

$$0 \leq x_4 \leq L_4$$

The constant \bar{F} will be determined later.

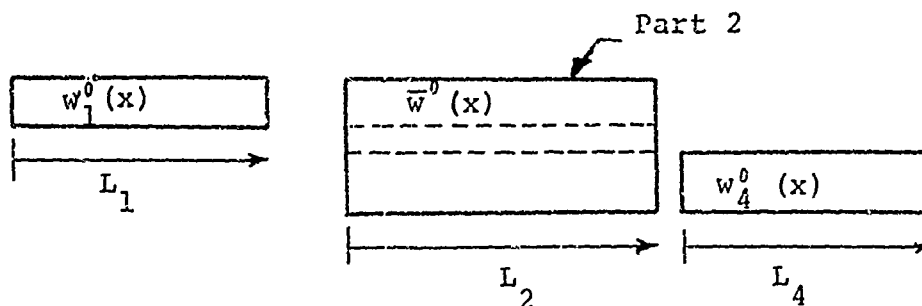


FIGURE (8)

Recalling the deflection equations for parts (1) and (2), namely, from equation (2.220)

$$w_1^o(x) = \theta X_1 + E \sinh KX_1 \quad (2.351)$$

$$0 \leq X_1 \leq L_1$$

and from equation (2.231) with the necessary addition of the last term to satisfy equation (2.345)

$$\bar{w}^o(x) = \hat{A} \cosh \hat{K} X + \hat{B} \sinh \hat{K} X + \theta(L_1 + X_2) - \frac{h_2}{2} - \frac{(h_3 - h_2)}{2} \quad (2.352)$$

$$0 \leq X_2 \leq L_2$$

One can now formulate the necessary boundary conditions and determine $w_1^o(x)$ and $w_4^o(x)$. The boundary conditions are

$$w_1^o(L_1) = \bar{w}^o(0) \quad (2.353)$$

$$\frac{dw_1^o(L_1)}{dx} = \frac{d\bar{w}^o(0)}{dx} \quad (2.354)$$

$$w_4^o(0) = \bar{w}^o(L_2) \quad (2.355)$$

$$\frac{dw_4^o(0)}{dx} = \frac{d\bar{w}^o(L_2)}{dx} \quad (2.356)$$

Note should be made that $\hat{k}^2 = \frac{T \cos \theta}{\bar{D}}$ where \bar{D} is calculated with respect to the geometrical mid-plane of part (2) in Figure 8 which is not necessarily the adhesive centerline!

Employing boundary condition (2.353) one gets an expression for \hat{A} , namely,

$$\hat{A} = E \sinh KL_1 + \frac{h_2}{2} + \frac{(h_3 - h_2)}{2} \quad (2.357)$$

Differentiating equations (2.351) and (2.352) and using boundary condition (2.354) yields an expression for \hat{B} , namely,

$$\hat{B} = \frac{KE \cosh KL_1}{\hat{K}} \quad (2.358)$$

Use of boundary condition (2.355) stipulates an expression for \bar{F} in terms of \hat{A} and \hat{B} , namely,

$$\bar{F} = A \cosh KL_2 + B \sinh KL_2 + \theta (L_1 + L_2 + L_4) - \frac{h_2}{2} - \frac{(h_3 - h_2)}{2} \quad (2.359)$$

Substitution of equations (2.357) and (2.358) into (2.359) gives the desired expression for \bar{F} .

$$\begin{aligned}
 \bar{F} = & E \sinh KL_1 \cosh \hat{KL}_2 + \frac{h_2}{2} \cosh \hat{KL}_2 + \\
 & + \frac{(h_3-h_2)}{2} \cosh \hat{KL}_2 + \frac{KE \cosh KL_1}{\hat{K}} \sinh \hat{KL}_2 \\
 & + \frac{(h_2+h_3)}{2(L_1+L_2+L_4)} (L_1+L_2+L_4) - \frac{h_2}{2} - \frac{(h_3-h_2)}{2} \quad (2.360)
 \end{aligned}$$

Per boundary condition (2.356) an expression for \bar{F} in terms of \hat{A} and \hat{B} emerges, namely,

$$\bar{K}\bar{F} \coth \bar{KL}_4 = - \hat{K}\hat{A} \sinh \hat{KL}_2 - \hat{K}\hat{B} \cosh \hat{KL}_2$$

Substitution of equations (2.357) and (2.358) into this relation gives an expression in terms of unknowns \bar{F} and E .

$$\begin{aligned}
 \bar{K}\bar{F} \coth \bar{KL}_4 = & - \hat{K}L \sinh KL_1 \sinh \hat{KL}_2 - \hat{K} \frac{h_2}{2} \sinh \hat{KL}_2 \\
 & - \hat{K} \frac{(h_3-h_2)}{2} \sinh \hat{KL}_2 - \frac{\hat{K}K}{\hat{K}} E \cosh KL_1 \cosh \hat{KL}_2
 \end{aligned}$$

Finally, substitution of equation (2.360) into this expression gives an explicit expression to determine E in terms of known quantities. The resulting expression is

$$E = - \frac{h_2}{2} \bar{K} \coth \bar{K} L_4 \cosh \hat{K} L_2 - \hat{K} \frac{h_2}{2} \sinh \hat{K} L_2$$

$$\hat{K} \sinh K L_1 \sinh \hat{K} L_2 + K \cosh K L_1 \cosh \hat{K} L_2$$

$$- \hat{K} \frac{(h_3-h_2)}{2} \sinh \hat{K} L_2 - \bar{K} \frac{(h_3-h_2)}{2} \coth \bar{K} L_4 \cosh \hat{K} L_2$$

$$+ \bar{K} \coth \bar{K} L_4 \sinh K L_1 \cosh \hat{K} L_2$$

$$- \bar{K} \coth \bar{K} L_4 \left[\frac{(h_2+h_3)}{2} - \frac{h_2}{2} - \frac{(h_3-h_2)}{2} \right]$$

$$+ \frac{K\bar{K}}{K} \coth \bar{K} L_4 \cosh K L_1 \sinh \hat{K} L_2 \quad (2.361)$$

Substitution of the expression for E into equations (2.357-2.359) will determine the values of \hat{A} , \hat{B} and \bar{F} .

$M_1(L_1)$ can be determined using equation (2.245) while employing equation (2.361) for the determination of E. Thus,

$$M_1(L_1) = T \cos \theta E \sinh K L_1 \quad (2.362)$$

Moreover, $V_1(L_1)$ can be determined using equation (2.250) with the proper value of E thus

$$V_1(L_1) = KE (T \cos \theta) \cosh K L_1 \quad (2.363)$$

$M_4(x)$ and $Q_4(x)$ can be determined as follows:

Differentiate equation (2.346) twice and substitute into

$$M_4 = - D_{114} \frac{d^2 w_4^o(x)}{dx^2} \quad (2.364)$$

Thus for $x_4 = 0$

$$M_4(0) = - D_{114} \bar{F} \bar{K}^2 \quad (2.365)$$

However,

$$\bar{K}^2 = \frac{T \cos \theta}{L_{114}}$$

Thus

$$M_4(0) = - \bar{F} T \cos \theta \quad (2.366)$$

where \bar{F} can be determined using equation (2.360).

A relation can be derived for $Q_4(X_4)$ by employing equation (2.182) and equation (2.346). Thus,

$$\frac{dM_x}{dx} = Q_4(x) \quad (2.367)$$

$$\frac{d^3 w_4^0}{dx^3} = - \bar{F} \bar{K}^3 (\coth h \bar{K} L_4 \cosh h K X_4 - \sinh h \bar{K} X_4) \quad (2.368)$$

Also,

$$\frac{dM_x}{dx} = - D_{114} \frac{d^3 w_4^0}{dx^3} \quad (2.369)$$

Substitution of equations (2.367) and (2.368) into (2.369) and realizing that $\bar{K}^2 = \frac{T \cos \theta}{D_{114}}$ yields the desired result.

$$Q_4(x) = \bar{F} \bar{K} (T \cos \theta) (\coth h \bar{K} L_4 \cosh h \bar{K} X_4 - \sinh h \bar{K} X_4) \quad (2.370)$$

Thus,

$$V_4(0) = - \bar{F} \bar{K} T \cos \theta \coth \bar{K} L_4 \quad (2.371)$$

2 Solution of the General Linear Ordinary Differential Equations

Having obtained the necessary boundary value constants, namely, M_1 , V_1 , M_4 and V_4 one can obtain the general solution to the two fourth order linear ordinary differential equations in two unknowns $\tau_0(x)$ and $Q_2(x)$, namely, equations (2.278) and (2.280). These two equations will now be reduced to one equation in one unknown $\tau_0(x)$ by algebraic manipulation.

Given:

$$\begin{aligned} & A_1 \frac{d^4 \tau_0}{dx^4} + A_2 \frac{d^2 \tau_0}{dx^2} + A_3 \tau_0 + A_4 \frac{d^4 Q_2}{dx^4} + A_5 \frac{d^2 Q_2}{dx^2} + A_6 Q_2 \\ & = \frac{h_3 V_1}{2D_{113}} \end{aligned} \quad (2.372)$$

$$B_1 \frac{d^4 \tau_0}{dx^4} + B_2 \frac{d^2 \tau_0}{dx^2} + B_3 \tau_0 + B_4 \frac{d^4 Q_2}{dx^4} + B_5 \frac{d^2 Q_2}{dx^2}$$

$$+ B_6 v_2 = - \frac{V_1}{D_{113}} \quad (2.373)$$

Let $D = \frac{d}{dx}$

Equations (2.372-2.373) can be rewritten as

$$\begin{aligned} & (A_1 D^4 + A_2 D^2 + A_3) \tau_0 + (A_4 D^4 + A_5 D^2 + A_6) Q_2 \\ & = \frac{h_3 V_1}{2D_{11}} \end{aligned} \quad (2.374)$$

$$\begin{aligned} & (B_1 D^4 + B_2 D^2 + B_3) \tau_0 + (B_4 D^4 + B_5 D^2 + B_6) Q_2 \\ & = - \frac{V_1}{D_{11}} \end{aligned} \quad (2.375)$$

Multiply equation (2.374) by $(B_4 D^4 + B_5 D^2 + B_6)$ and equation (2.375) by $(A_4 D^4 + A_5 D^2 + A_6)$ and subtract the two resulting relations.

Moreover, realizing that certain terms on the right-hand side are zero as $V_1 = \text{constant}$ the resulting equa-

tion in condensed notation is:

$$\begin{aligned}
 & c_9 \frac{d^8 \tau_o}{dx^8} + c_7 \frac{d^6 \tau_o}{dx^6} + c_5 \frac{d^4 \tau_o}{dx^4} + c_3 \frac{d^2 \tau_o}{dx^2} + c_1 \tau_o \\
 & = \left[\frac{h_3}{2} B_6 + A_6 \right] \frac{V}{D_{113}} \quad (2.376)
 \end{aligned}$$

where:

$$c_1 = [B_6 A_3 - A_6 B_3] \quad (2.377)$$

$$c_3 = [B_5 A_3 + B_6 A_2 - A_5 B_3 - A_6 B_2] \quad (2.378)$$

$$c_5 = [B_5 A_2 + B_6 A_1 + B_4 A_3 - A_4 B_3 - A_5 B_2 - A_6 B_1] \quad (2.379)$$

$$c_7 = [B_4 A_2 + B_5 A_1 - A_4 B_2 - A_5 B_1] \quad (2.380)$$

$$c_9 = [B_4 A_1 - A_4 B_1] \quad (2.381)$$

Assuming a homogeneous solution for $\tau_o(x) = \sum e^{\lambda_i x}$ the

homogeneous equation is

$$[C_9 \lambda i^8 + C_7 \lambda i^6 + C_5 \lambda i^4 + C_3 \lambda i^2 + C_1] \text{Si } e^{\lambda i X} = 0 \quad (2.382)$$

Use of a numerical routine can get one the roots

$(\lambda i) \ i = 1 \rightarrow 8$ that satisfy equation (2.382). Inspection of equation (2.376) stipulates that the particular solution for $\tau_o(x)$ is

$$\tau_o(x) = \left[\frac{h_3 B_6}{2C_1} + \frac{A_6}{C_1} \right] \frac{V_1}{D_{113}} \quad (2.383)$$

Thus the complete solution for $\tau_o(x)$ is

$$\tau_o(x) = \text{Si } e^{\lambda i X} + \left[\frac{h_3 B_6}{2C_1} + \frac{A_6}{C_1} \right] \frac{V_1}{D_{113}} \quad (2.384)$$

$i = 1 \rightarrow 8$

To find $Q_2(x)$ assume a solution of the form

$$Q_2(x) = F i e^{\lambda i X} + z \quad i = 1 \rightarrow 8 \quad (2.385)$$

where z = the particular solution. Substitute equation (2.385) into either equation (2.374) or (2.375) to determine the dependent constants F_i in terms of the independent constants S_i . In addition the particular solution for $Q_2(x)$ can be found. Upon substituting into equation (2.374) and equating the homogeneous parts, one gets a relation for F_i in terms of S_i , namely,

$$F_i = - S_i \left[\frac{A_1 \lambda i^4 + A_2 \lambda i^2 + A_3}{A_4 \lambda i^4 + A_5 \lambda i^2 + A_6} \right] \quad i = 1 \rightarrow 8 \quad (2.386)$$

If one uses equation (2.375) the relation for F_i is

$$F_i = - S_i \left[\frac{B_1 \lambda i^4 + B_2 \lambda i^2 + B_3}{B_4 \lambda i^4 + B_5 \lambda i^2 + B_6} \right] \quad i = 1 \rightarrow 8 \quad (2.387)$$

whereby the terms in brackets must be equivalent.

Similarly, equating the particular solutions one gets

$$\frac{h_3 V_1}{2A_6 D_{113}} - \frac{A_3}{A_6} \left[\frac{h_3 B_5}{2C_1} + \frac{A_6}{C_1} \right] \frac{V_1}{D_{113}} = z \quad (2.388)$$

Summarizing, the total solution for $Q_2(x)$ is

$$Q_2(x) = F_i e^{\lambda i x} + \frac{h_3 V_1}{2A_6 D_{113}} - \frac{A_3}{A_6} \left[\frac{h_3 B_6}{2C_1} + \frac{A_6}{C_1} \right] \frac{V_1}{D_{113}}$$

$i = 1 + 8 \quad (2.389)$

Solution for $\sigma_0(x)$ Expression

Finally, through the use of equation (2.253) on page 139 and equation (2.386) the expression for $\sigma_0(x)$ is

$$\sigma_0(x) = \frac{dQ_2}{dx} = \lambda i F_i e^{\lambda i x}$$

$$= - S_i \lambda i e^{\lambda i x} \left[\frac{A_1 \lambda i^4 + A_2 \lambda i^2 + A_3}{A_4 \lambda i^4 + A_5 \lambda i^2 + A_6} \right] \quad (2.390)$$

Letting

$$\beta i = \frac{A_1 \lambda i^4 + A_2 \lambda i^2 + A_3}{A_4 \lambda i^4 + A_5 \lambda i^2 + A_6}$$

The final expression for $\sigma_o(x)$ is

$$\sigma_o(x) = - \sum_{i=1}^8 \beta_i \lambda_i S_i e^{\lambda_i x} \quad i = 1 \rightarrow 8 \quad (2.391)$$

3. Formulation of the Boundary Conditions

Having derived the general solution for the shear and normal stresses in the adhesive layer, one must determine the eight unknowns S_i . The unknowns S_i can be determined using equations (2.308), (2.312), (2.315) and the fact that the shear stress $\tau_o(x)$ at the joint ends must be zero. The resulting boundary conditions are:
(Using equation (2.384) the first two conditions are:)

$$\tau_o(0) = 0 = S_i + \left[\frac{h_3 B_6}{2C_1} + \frac{A_6}{C_1} \right] \frac{V_1}{D_{113}} \quad i = 1 \rightarrow 8 \quad (2.392)$$

$$\tau_o(L_2) = 0 = S_i e^{\lambda_i L_2} + \left[\frac{h_3 B_6}{2C_1} + \frac{A_6}{C_1} \right] \frac{V_1}{D_{113}} \quad i = 1 \rightarrow 8 \quad (2.393)$$

Substitution into equation (2.308) and using relations

(2.384) and (2.391) the third and fourth conditions are determined, namely,

$$@ X = 0$$

$$M_2(o) = M_1$$

$$M_3(o) = 0$$

Thus,

$$\begin{aligned}
 & - \frac{M_1}{D_{112}} - B_4 \beta i \lambda i^3 Si - B_5 \beta i \lambda i Si + B_1 \lambda i^3 Si \\
 & + B_2 \lambda i Si = 0
 \end{aligned}
 \tag{2.394}$$

Similarly,

$$@X = L_2$$

$$M_2(L_2) = 0$$

$$M_3(L_2) = M_4$$

Thus,

$$\begin{aligned} \frac{M_4}{D_{113}} - B_4 \lambda i^3 \text{Si} e^{\lambda i L_2} - B_5 \lambda i \text{Si} e^{\lambda i L_2} \\ + B_1 \lambda i^3 \text{Si} e^{\lambda i L_2} + B_2 \lambda i \text{Si} e^{\lambda i L_2} = 0 \end{aligned} \quad (2.395)$$

Per equation (2.312) and employing expressions (2.384) and (2.391) the fifth and sixth boundary conditions are determined, namely,

$$Q_X = 0$$

$$Q_2(0) = V_1$$

$$Q_3(0) = 0$$

Thus,

$$-\frac{V_1}{D_{112}} + B_1 \lambda i^4 \text{Si} + B_2 \lambda i^2 \text{Si} + B_3 \text{Si}$$

$$+ B_3 \left[\frac{h_3 B_6}{2C_1} + \frac{A_6}{C_1} \right] \frac{V_1}{D_{113}} - B_4 \beta i \lambda i^4 \text{Si} - B_5 \beta i \lambda i^2 \text{Si} = 0 \quad (2.396)$$

Similarly,

$$\phi X = L_2$$

$$Q_2(L_2) = 0$$

$$Q_3(L_2) = v_4$$

Thus,

$$\frac{V_4}{D_{113}} + B_1 \lambda i^4 \text{Si} e^{\lambda i L_2} + B_2 \lambda i^2 \text{Si} e^{\lambda i L_2} + B_3 \text{Si} e^{\lambda i L_2}$$

$$+ B_3 \left[\frac{h_3 B_6}{2C_1} + \frac{A_6}{C_1} \right] \frac{V_1}{D_{113}} - B_4 \beta i \lambda i^4 \text{Si} e^{\lambda i L_2}$$

$$- B_5 \beta i \lambda i^2 \text{Si} e^{\lambda i L_2} = 0 \quad (2.397)$$

The last two boundary conditions are obtained by using equation (2.315) in conjunction with equations (2.384)

and (2.391).

$$\theta_X = 0$$

$$M_2(0) = M_1$$

$$T_2(0) = T \cos \theta$$

$$M_3(0) = 0$$

$$T_3(0) = 0$$

Thus, the resulting expression is

$$- \frac{h_2 M_1}{2D_{112}} + \frac{T \cos \theta}{\bar{A}} + A_1 \lambda i^3 Si + A_2 \lambda i Si - A_4 \beta i \lambda i^3 Si$$

$$- A_5 \beta i \lambda i Si = 0 \quad (2.398)$$

Finally,

$$\theta_X = L_2$$

$$M_2(L_2) = 0$$

$$T_2(L_2) = 0$$

$$M_3(L_2) = M_4$$

$$T_3(L_2) = T \cos \theta$$

Substituting into equation (2.315) the final expression is

$$\begin{aligned}
 & - \frac{h_3 M_4}{2D_{113}} - \frac{T \cos \theta}{\bar{A}} + A_1 \lambda i^3 \text{Si} e^{\lambda i L_2} + A_2 \lambda i \text{Si} e^{\lambda i L_2} \\
 & - A_4 \beta i \lambda i^3 \text{Si} e^{\lambda i L_2} - A_5 \beta i \lambda i \text{Si} e^{\lambda i L_2} = 0 \quad (2.399)
 \end{aligned}$$

SUMMARY

Having determined the roots and the necessary boundary conditions one can now solve for the shear stress distribution $\tau_o(x)$ and the normal stress distribution $\sigma_o(x)$ in the adhesive. Knowing these distributions one can calculate the transverse shear stress $\tau_{xz}|_K$ and normal stress $\sigma_{z|K}$ distributions throughout the laminates using equations (2.29), (2.33) and (2.144). In addition, if one wishes to calculate inplane loads $T_2(x)$, $T_3(x)$, moments $M_2(x)$, $M_3(x)$, inplane and lateral displacements $u_2(x)$, $u_3(x)$, $w_2^o(x)$, $w_3^o(x)$, and the lateral shears $Q_2(x)$, $Q_3(x)$ he may do so using the procedure outlined previously.

CHAPTER III

A STUDY OF CERTAIN PARAMETERS INVOLVING JOINTS WITH IDENTICAL ADHERENDS

The objectives of this chapter are twofold. Initially, it provides one the opportunity to check the methods of analysis with the assumptions it includes and to ascertain whether the programming has been performed correctly. Secondly, upon learning the influence of certain important variables on the output, one can determine how to minimize adhesive stresses. This would enable one to design a joint for maximum loads, less weight and/or longer life if fatigue is a consideration. However, although the analysis is valid throughout the elastic range of the materials being used one should recognize that in certain instances the adherend is the critical component and that it's failure will pre-empt failure of the adhesive.

The following discussion will detail results assuming the adhesive is first to fail. This is normally a valid assumption when the length of overlap to adherend thickness is ten or less.

The baseline geometry, material properties and

loading are given below in Figure 3-1. It is from these initial values that all parameters are altered. Moreover only the equal adherend case is studied herein. The analysis procedure referred to is entitled Bond 3.

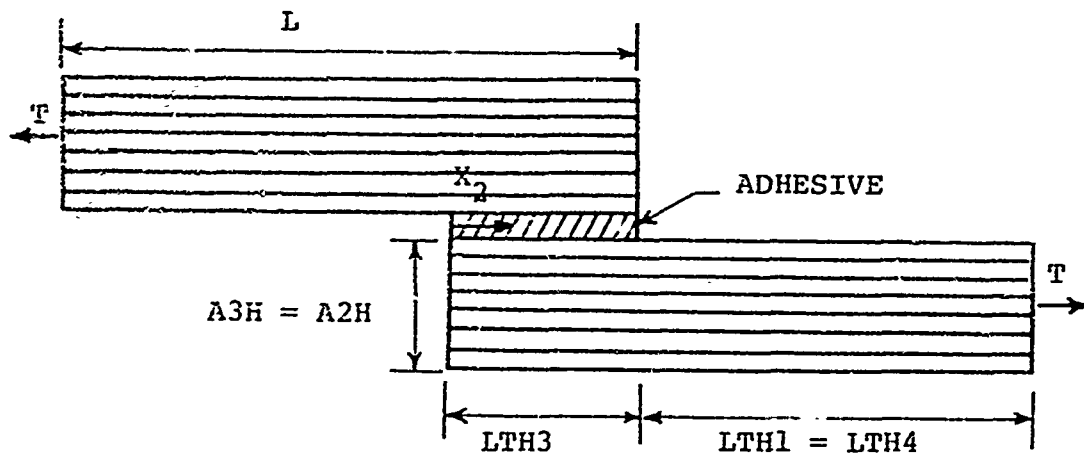


FIGURE 3-1 BASELINE CONFIGURATION:

BASELINE INPUT INTO THE BOND3 PROGRAM IS:

$$T = 1000\#$$

$$LTH1 = LTH4 = 4.21"$$

$$LTH3 = .31"$$

$$A2H = A3H = .063"$$

ADHESIVE PROPERTIES:

$$\text{EFFECTIVE SHEAR MODULUS} = 4.5 \times 10^6 \text{ PSI}$$

$$\text{EFFECTIVE TENSION MODULUS} = 7.0 \times 10^6 \text{ PSI}$$

ADHEREND PROPERTIES (IDENTICAL ADHERENDS):

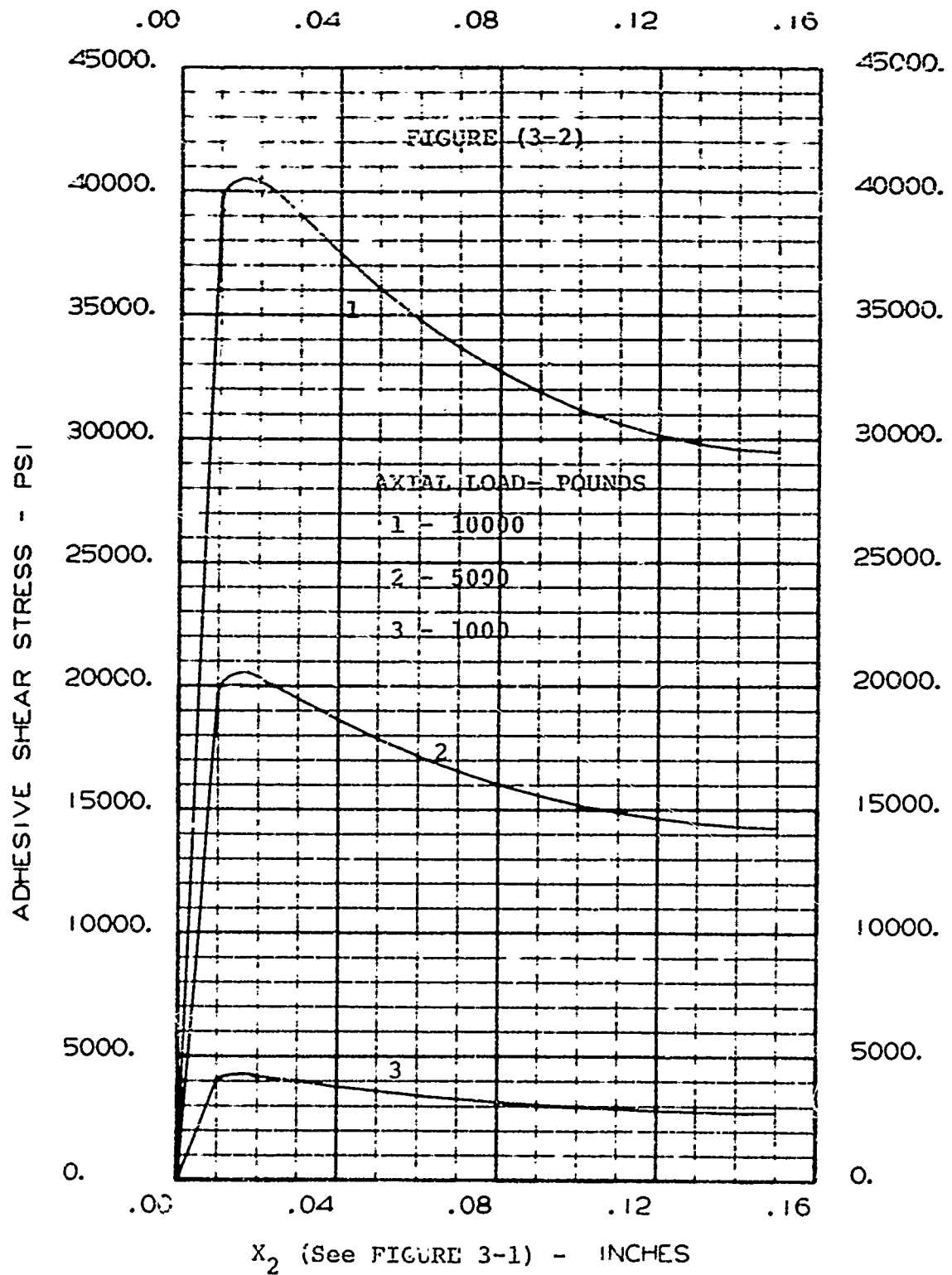
$$Q_{11} = 6.8 \times 10^6 \text{ PSI}$$

$$Q_{55} = 1.0 \times 10^6 \text{ PSI}$$

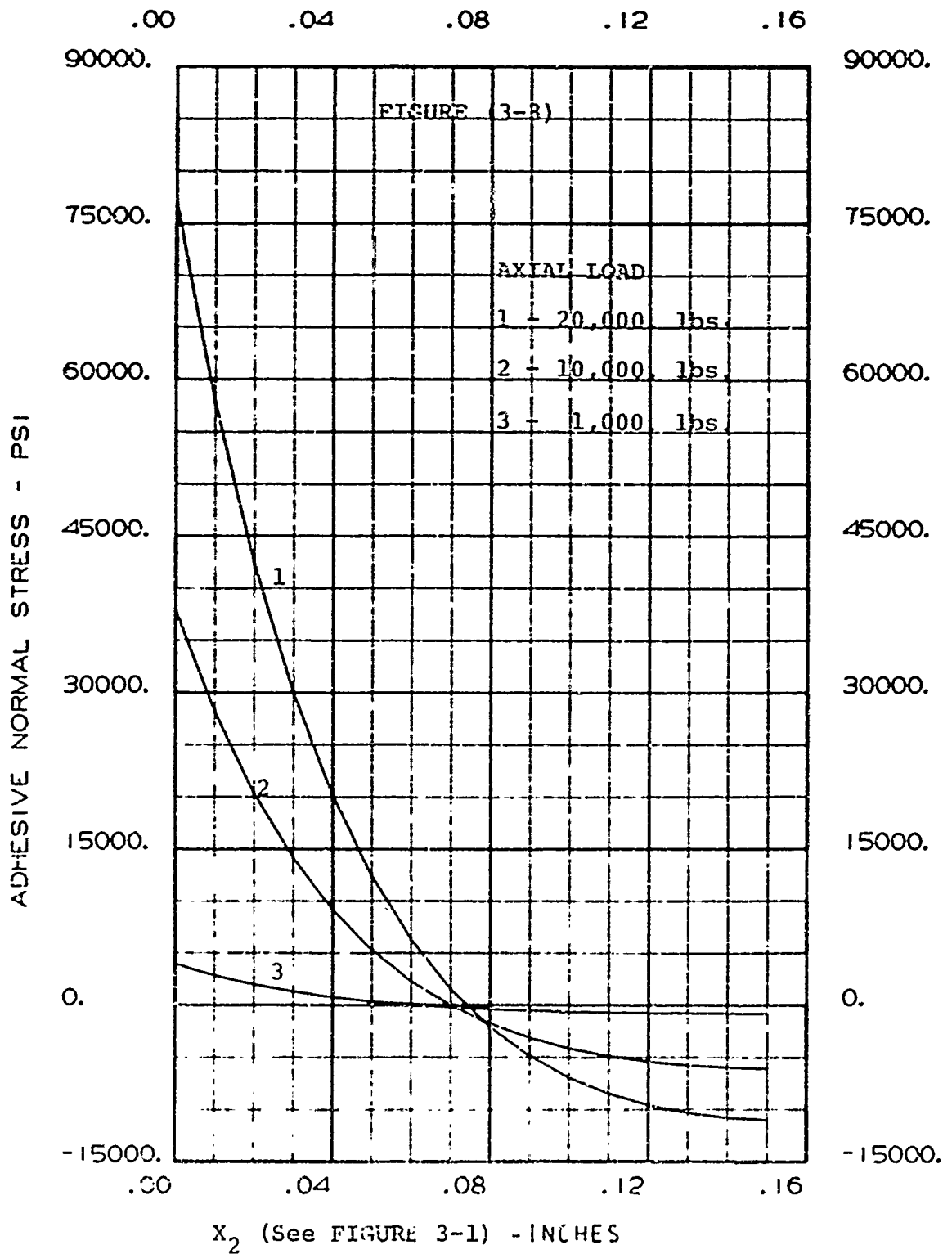
ALL PLYS ARE OF EQUAL THICKNESS AND 0 DEGREE ORIENTATION

The baseline parameters were chosen in order to represent a homogeneous isotropic adherend material as closely as possible. This will enable one to compare this closed form analysis to the best existing theory later in this chapter.

The initial variable investigated is axial load. Figure (3-2) and (3-3) show the effect of increasing the axial load on the adhesive shear and normal stresses respectively. Figure (3-2) shows that the shear stress increased linearly with load. Thus a tenfold increase in load nets a tenfold increase in shear stress. This seems totally plausible because, for equilibrium to be maintained, the integral of the stress over the adhesive area must equal the applied load. Thus, one would expect a 1:1 relationship between load and shear stress. Figure (3-3) invites one to observe two distinct phenomena. First, the normal stress does not increase in a linear manner vs. axial load as does the shear stress. This is due to the non-linear increase in moment at the end of



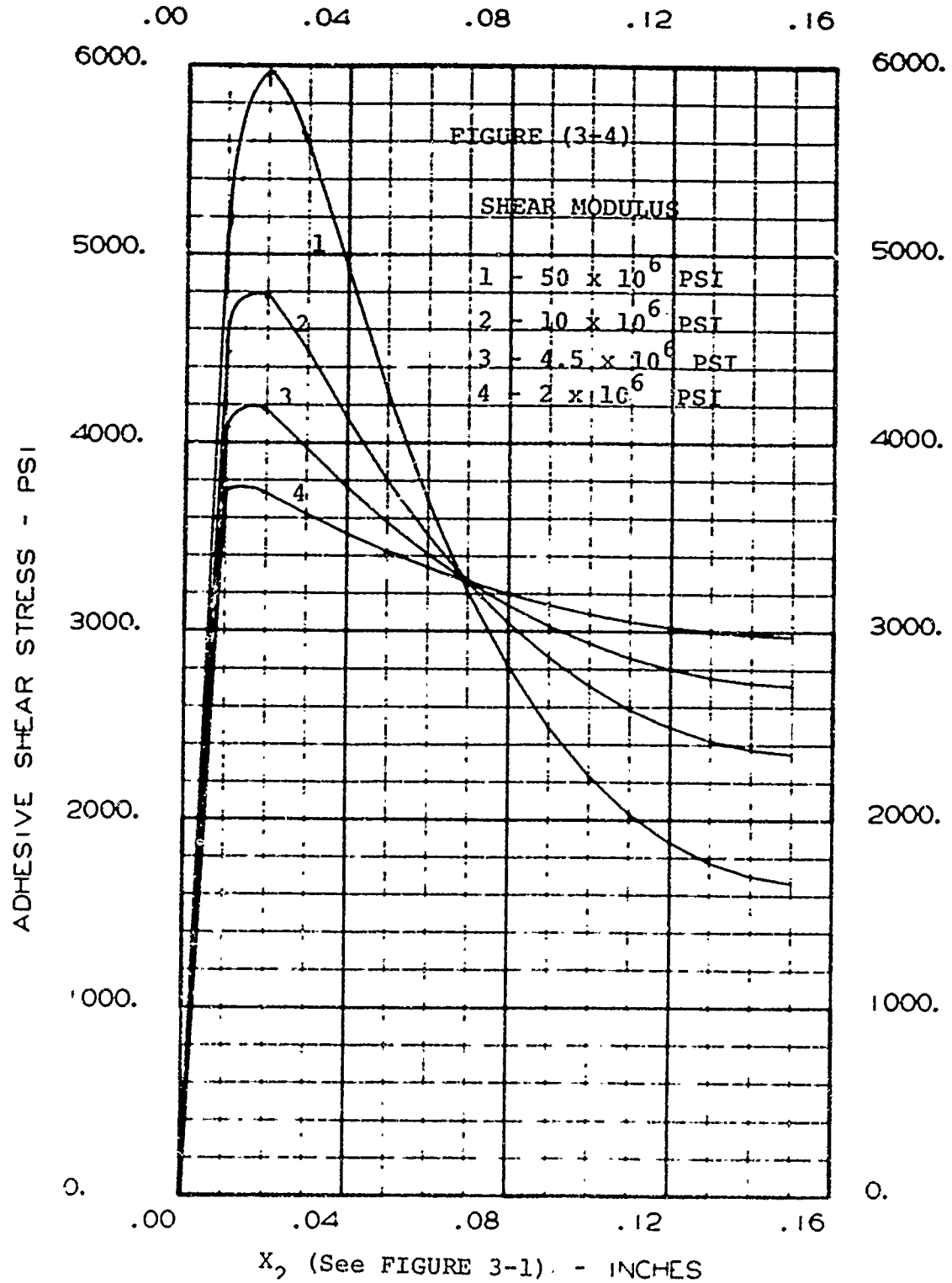
THE EFFECT OF AXIAL LOAD ON SHEAR STRESS



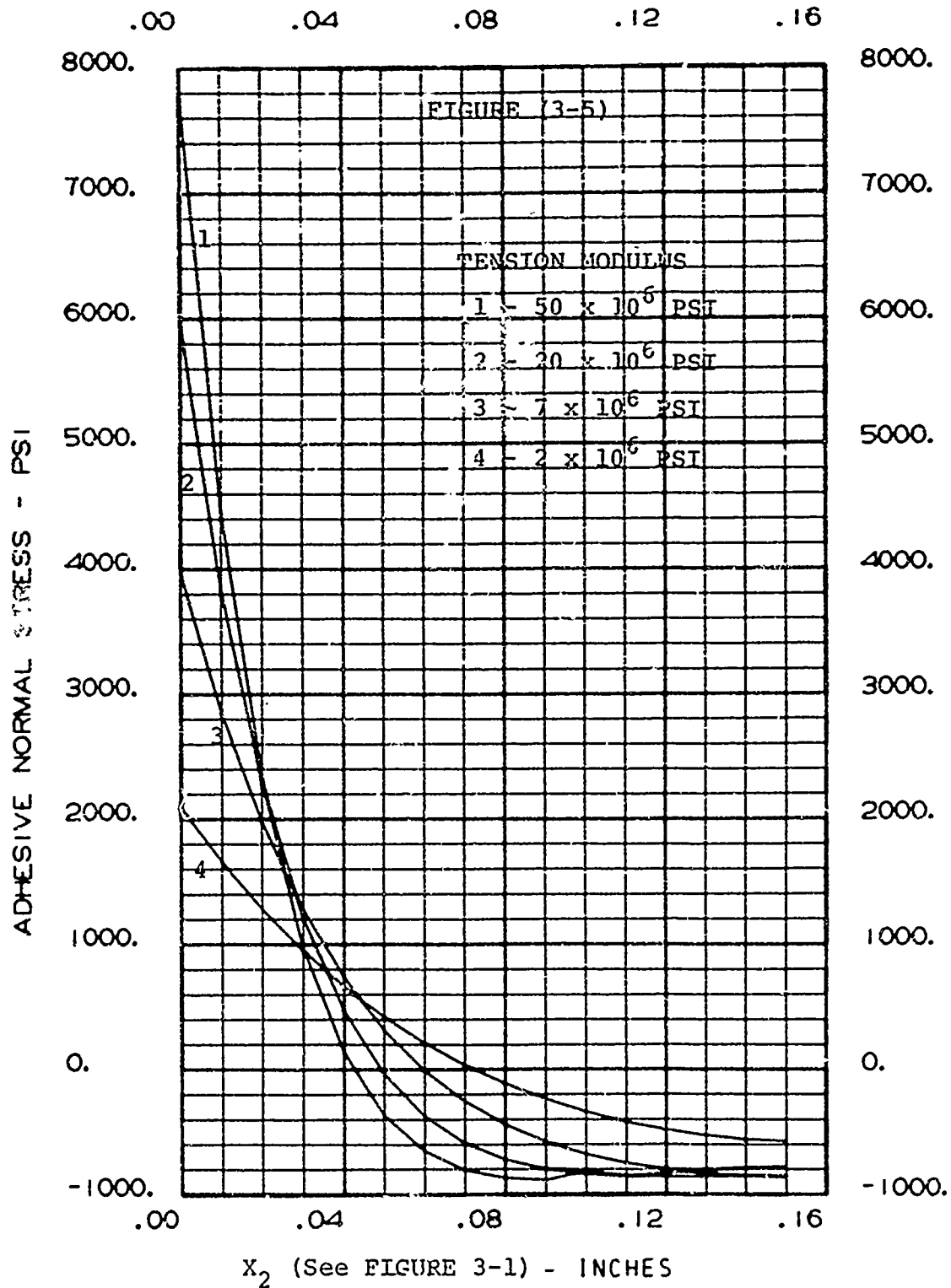
THE EFFECT OF AXIAL LOAD ON NORMAL STRESS

the overlap which in turn is a function of the non-linearly increasing lateral displacement of the two adherends. Secondly, and of possible significance, is the fact that the normal stresses go to zero at approximately the same point along the overlap. This is further emphasized in Figure (3-12) which plots overlap length vs. normal stress. The significance of this is not obvious. However, it is believed by the author to perhaps provide a significant clue as to the reason distinct bands on failed fatigue specimens appear. This item is pursued in more detail in Chapter (V).

For equal adherends the analysis is such that the shear modulus and tension modulus effects are uncoupled (i.e. the shear modulus does not influence the normal stresses and vice versa). Figure (3-4) relates the influence of shear modulus on the shear stress distribution. Again, because of equilibrium consideration the area under each curve in Figure (3-4) must equal the applied load (since the specimen is of unit width). As is to be expected for any spring system the stiffer the spring (i.e. shear) modulus the greater the peak stress. However, like many systems the shear modulus vs. load effect is not linear. At low modulus values the peak stress is quite sensitive, whereas at a high modulus



EFFECT OF SHEAR MODULUS ON ADHESIVE SHEAR STRESS

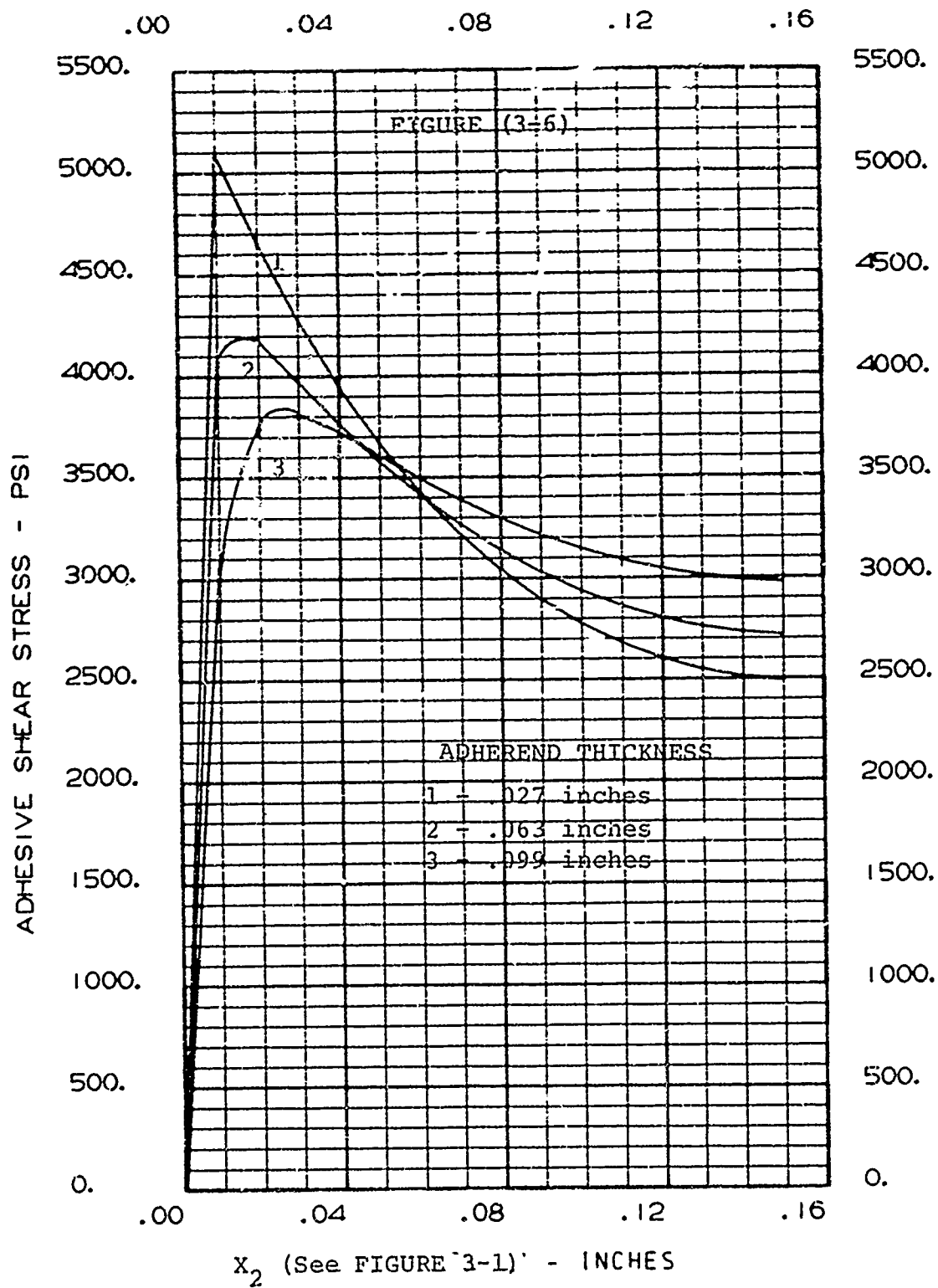


EFFECT OF TENSION MODULUS ON ADHESIVE NORMAL STRESS

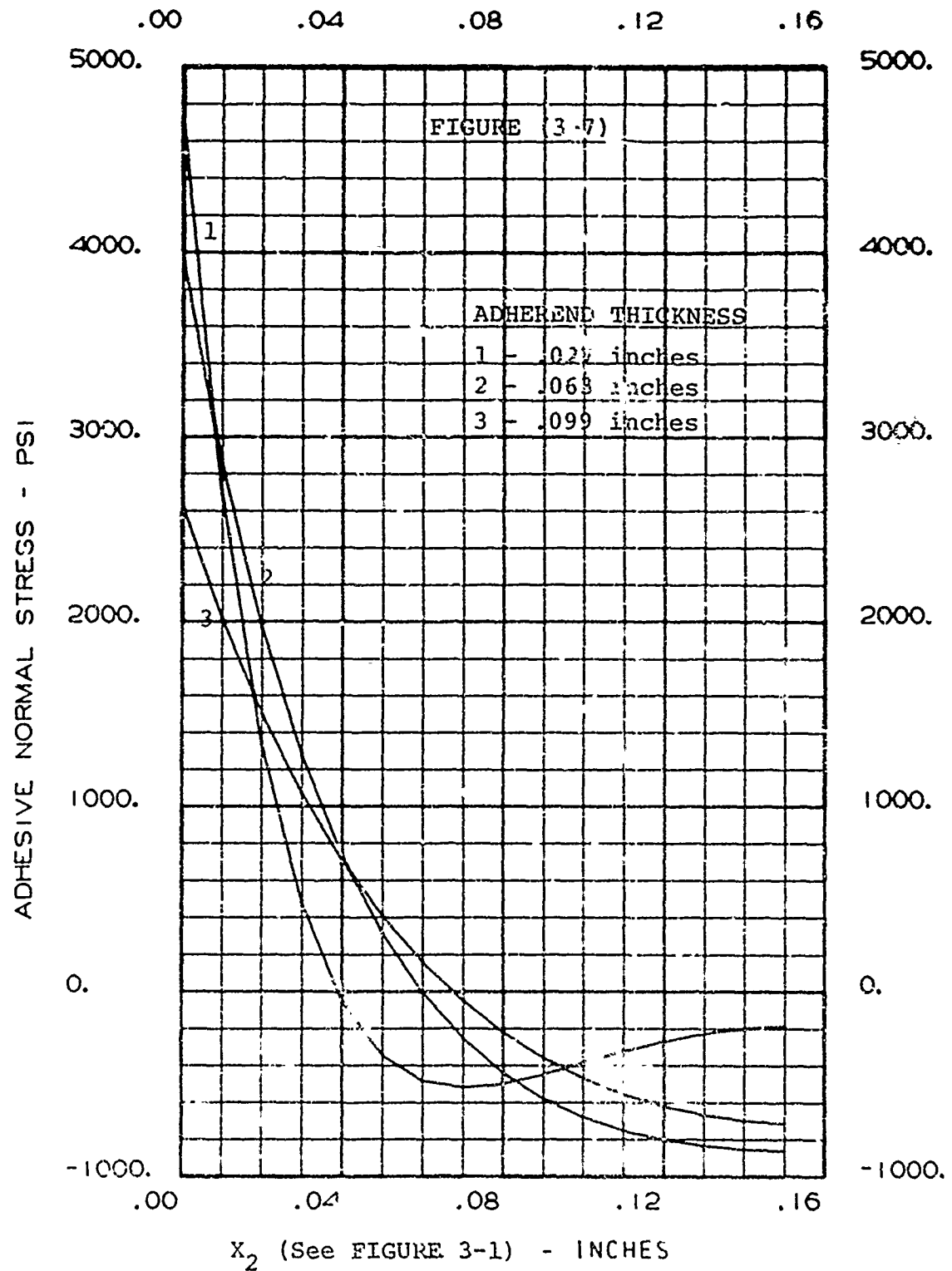
value, analogous to an almost rigid body, the variation of peak shear stress becomes insensitive. Such a trend is obvious in Figure (3-4).

Figure (3-5) displays an effect similar to that of Figure (3-4). Namely, the tension modulus has a non-linear effect on peak tensile stresses for the same reason outlined above. Thus, if one wished to minimize peak shear and tensile stresses in the adhesive, one very effective way would be to use a "soft" adhesive. This would increase the load capacity of the joint. Moreover, many times such adhesives exhibit a ductile behavior which increases the fatigue life of a lap joint for a certain load level.

The effect of adherend thickness on the adhesive shear and normal stresses is displayed in Figures (3-6) and (3-7). Again, in Figure (3-6) the area under each shear curve must be equal from equilibrium considerations. Moreover, one should note that both the adhesive shear and normal stresses increase as the adherend becomes thinner. The normal stress results are primarily due to the "softening" laterally of the adherends as they decrease in thickness. This effect is much more significant than the reduction of edge moment due to decreased eccentricity



EFFECT OF ADHEREND THICKNESS ON ADHES. SHEAR STRESS

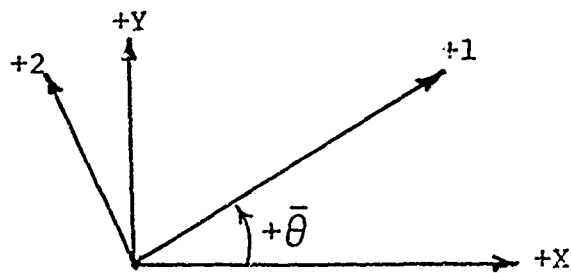
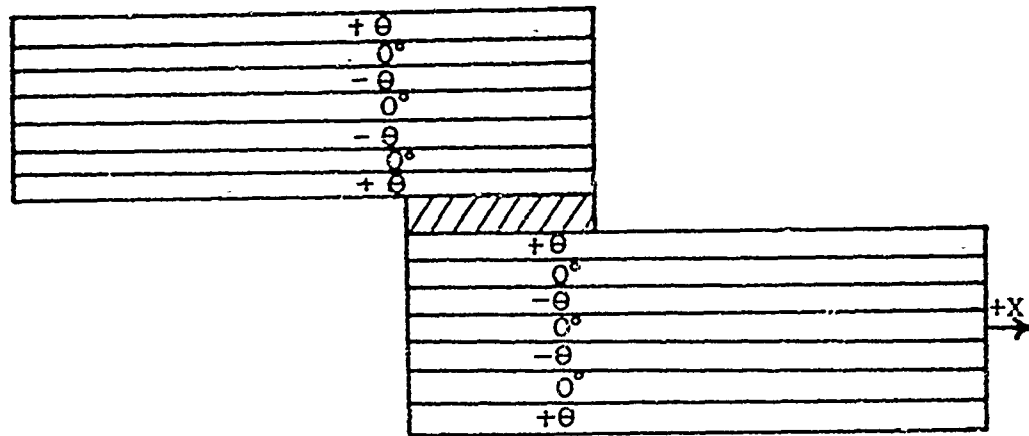


EFFECT OF ADHEREND THICKNESS ON ADHES NORMAL STR.

of the lap joint, the net result being an increase in peak normal stress. In addition, the peak shear stress increases for thinner adherends because the axial load has less distance laterally to travel to get to the adhesive, each ply being more highly loaded. Thus, the "shear lag" effect is effectively shortened from the outermost ply to the adhesive-adherend interface resulting in a greater amount of the axial load being sheared out over a shorter segment of the interface.

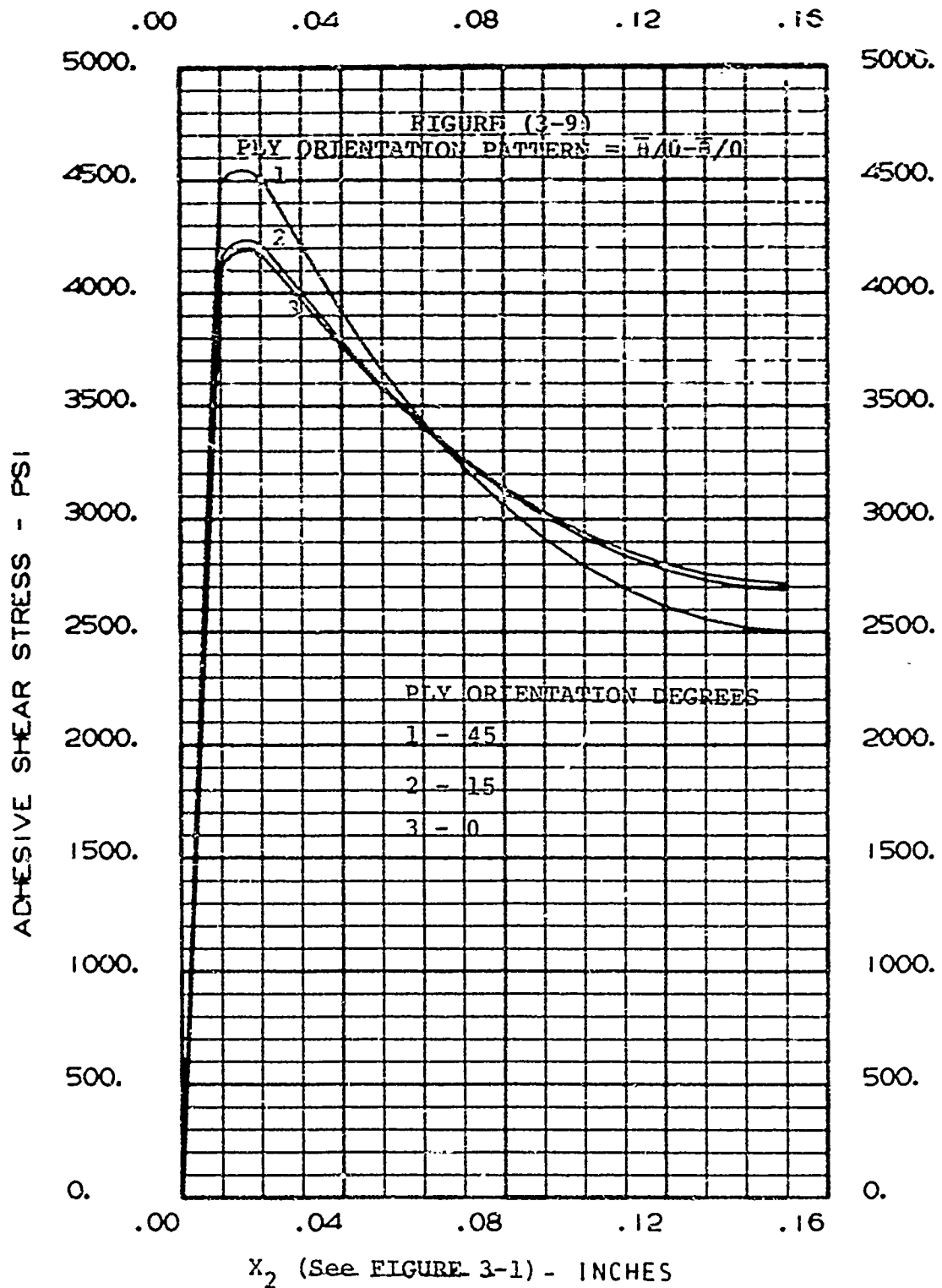
One of the unique characteristics of laminated composites is that each ply can assume any orientation one wishes it to. Thus, the make-up of a certain adherend can be whatever one wishes it to be. However, nothing being free, the complexity of the analysis is significantly increased. To study the influence of this new freedom (i.e. ply orientation) on the adhesive stresses Figures (3-9) and (3-10) are presented.

To avoid any bending-stretching coupling effects and to employ a realistic lamina orientation pattern, the laminae were layed-up per Figure (3-8). Moreover, it is assumed the 1-2 axes are the principle material axes, while the x-y axes are the geometrical axes of the part.

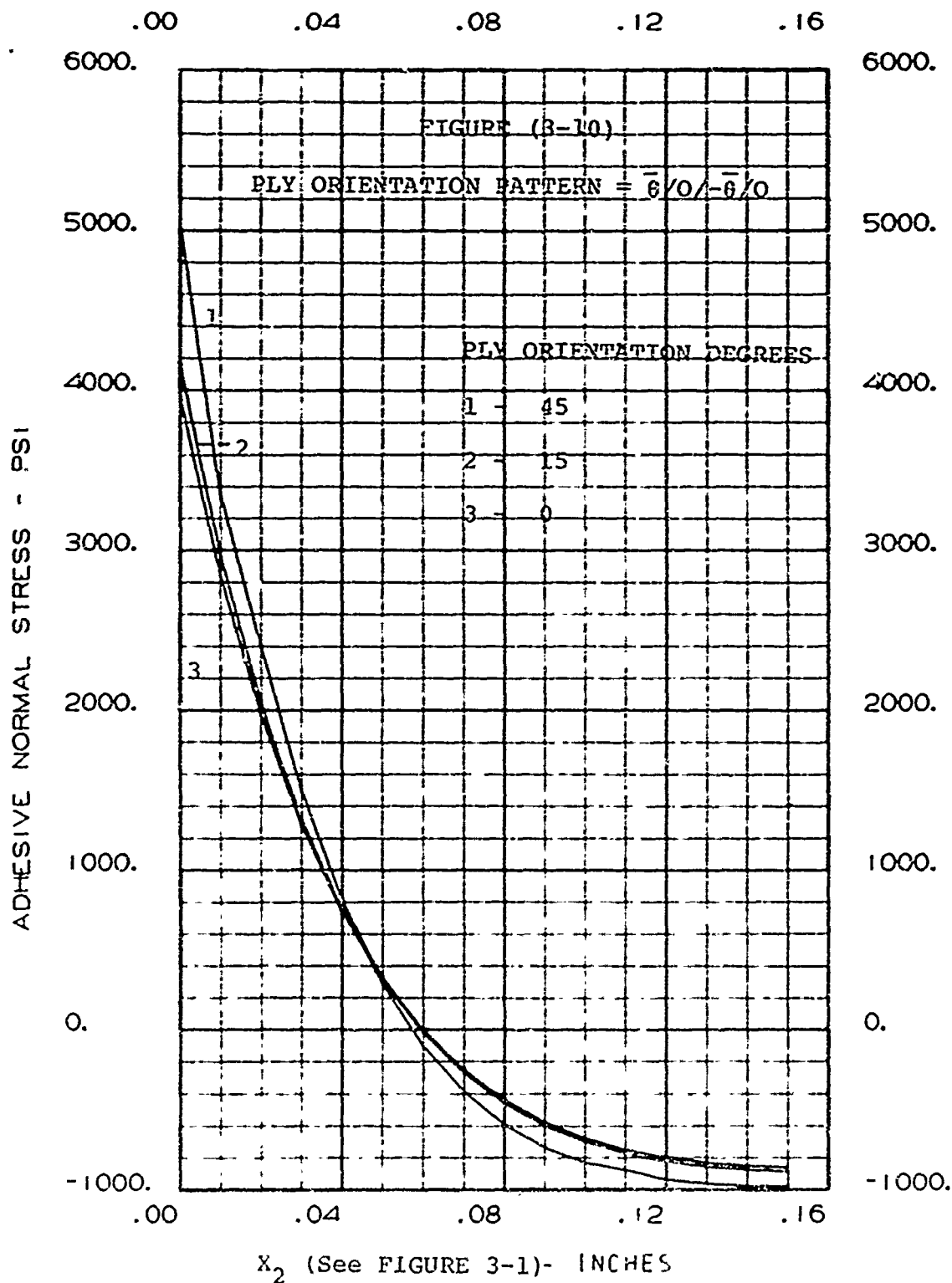


DEFINITION OF POSITIVE ANGLE

FIGURE (3-8) PLY ORIENTATION PATTERN IN ADHERENDS



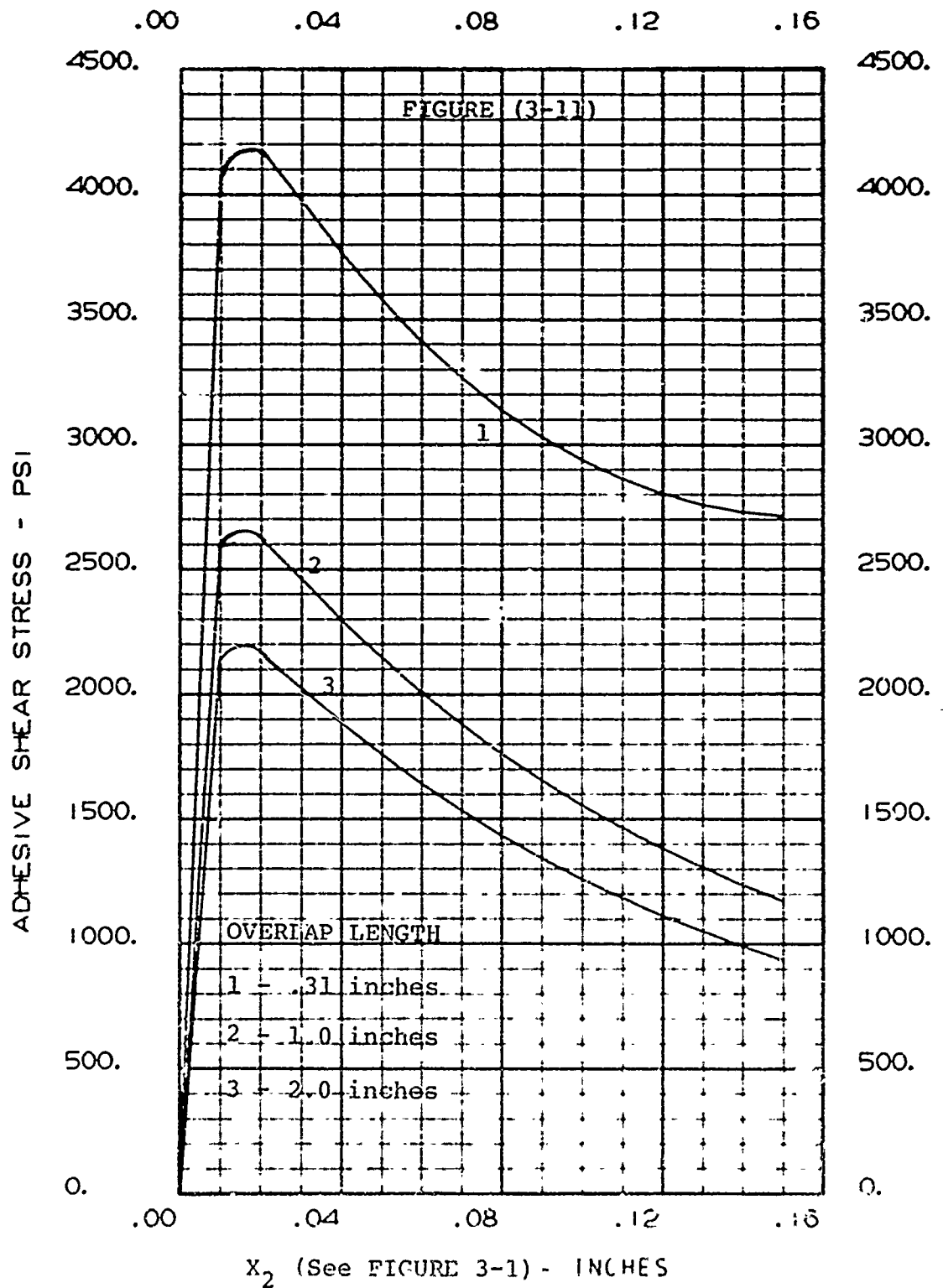
PLY ORIENTATION VS. ADHESIVE SHEAR STRESS



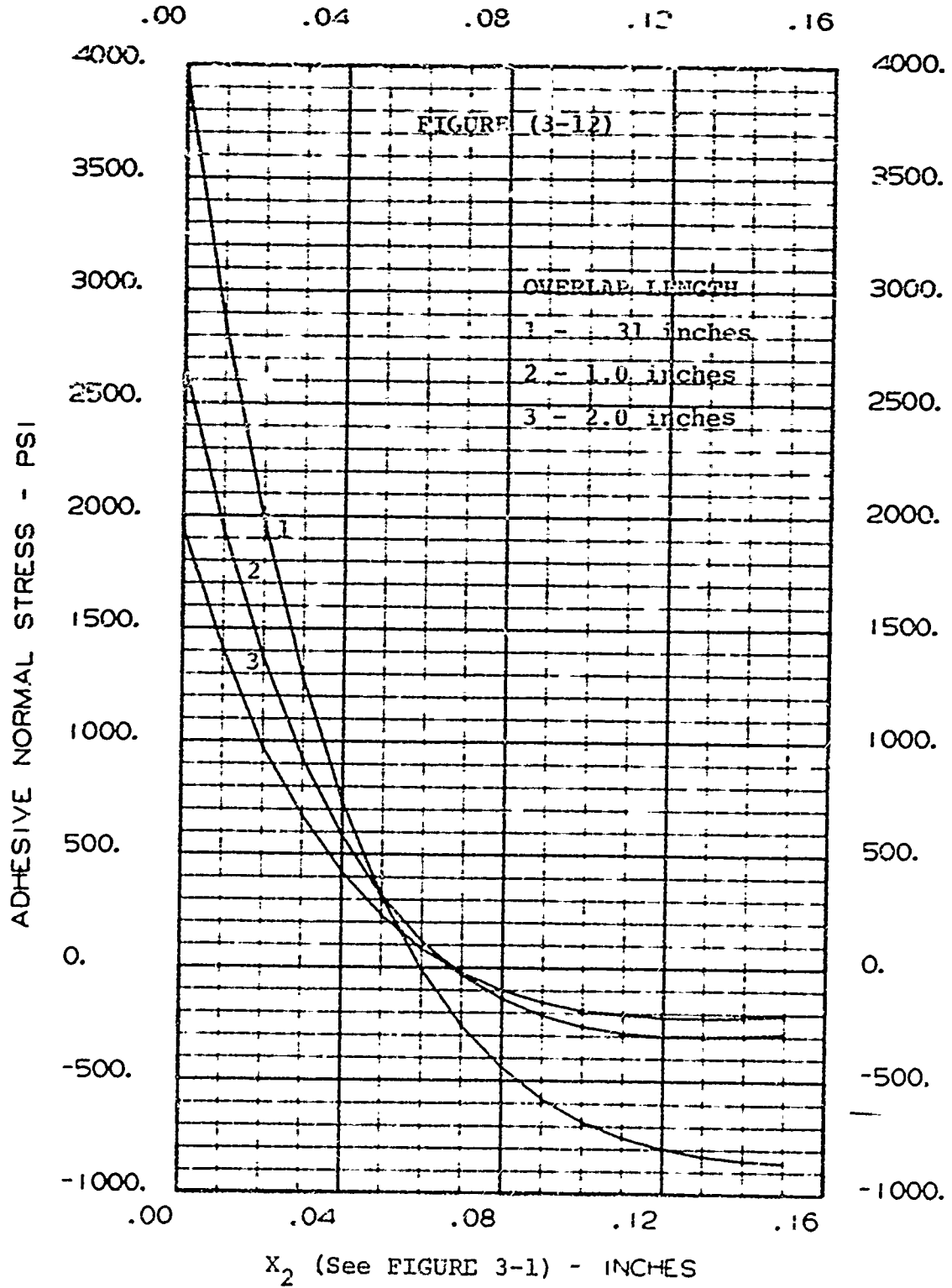
PLY ORIENTATION VS. ADHESIVE NORMAL STRESS

A cursory review of Figures (3-9) and (3-10) would lead to the conclusion that ply orientation has a modest effect on the adhesive stresses for the lamina pattern used. The peak shear stress is increased only 7 per cent for the $45^{\circ}/0^{\circ}/-45^{\circ}/0^{\circ}$ degree case vs. the all 0 degree case. However, the normal stress is increased 25 per cent. This is much more significant as the tensile strength of an adhesive is often times sensitive to such increases, exhibiting low tensile allowables vs. their shear allowable stress. Thus, for a given load and adhesive one can possibly precipitate an adhesive failure merely by orienting the plies of the adherend in an adverse manner. Moreover, it is quite probably that other lamina orientation patterns could cause a more severe redistribution effect of the peak adhesive stresses and should be checked thoroughly.

The influence of altering the overlap length (LTH3 in Figure (3-1)) is often considered a convenient means to lowering an adverse adhesive stress situation. The results of changing this parameter are detailed in Figures (3-11) and (3-12). The overall effect is obvious. As one increases the overlap length (the overall length of the part remaining constant) both the adhesive shear and normal stresses are reduced. However, as is evident



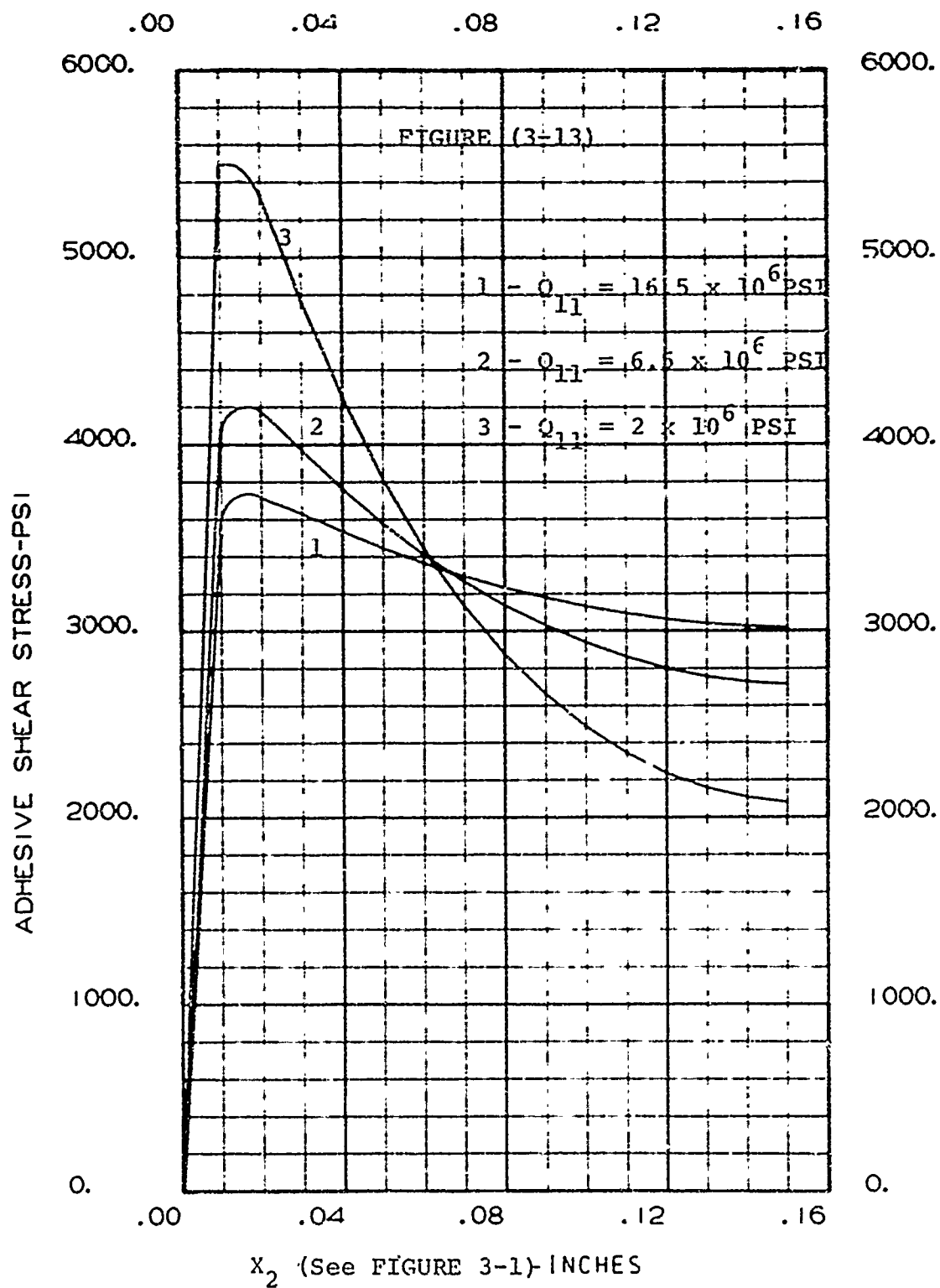
OVERLAP LENGTH VS. ADHESIVE SHEAR STRESS



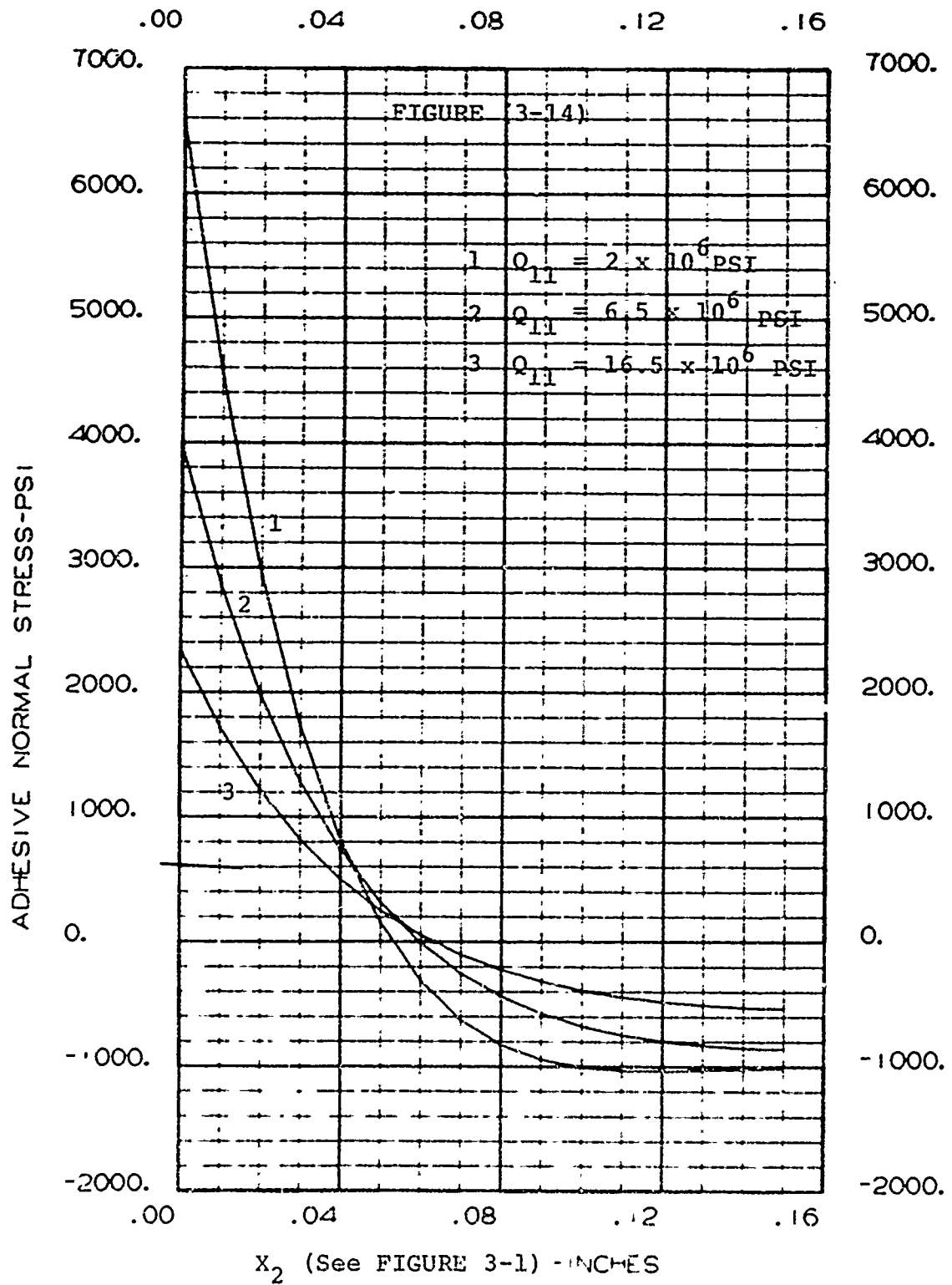
OVERLAP LENGTH VS. ADHESIVE NORMAL STRESS

in Figures (3-11) and (3-12) beyond a certain overlap length one reaches a point of diminishing returns. For example in Figure (3-11) a much greater reduction in peak shear stress occurs for an overlap change of from .31 inches to 1.0 inches than from 1.0 inches to 2.0 inches. A similar effect is observed in Figure (3-12) for the peak normal stresses. Moreover, beyond a length of overlap to adherend thickness ratio of approximately 10-12, depending on ply orientation, failure in interlaminar shear within the adherend or a direct tensile failure of the adherend itself is often encountered first (References 22 and 46). For this study the adherend thickness was constant and equal to .063 inches. Thus, for an overlap length greater than .60 inches a failure in the adherend is most likely to occur first. This would negate the advantages beyond certain limits of reducing the peak stresses in the adhesive.

The influence of certain constitutive constants, namely Q_{11} and Q_{55} , were studied to verify the influence they had on the adhesive shear and normal stresses. Figures (3-13) and (3-14) verify that the primary elastic modulus E_{11} has a significant effect on the shear and normal adhesive stresses, especially as E_{11} becomes numerically small, analogous to a soft spring. Both



EFFECT OF Q_{11} ON ADHESIVE SHEAR STRESS



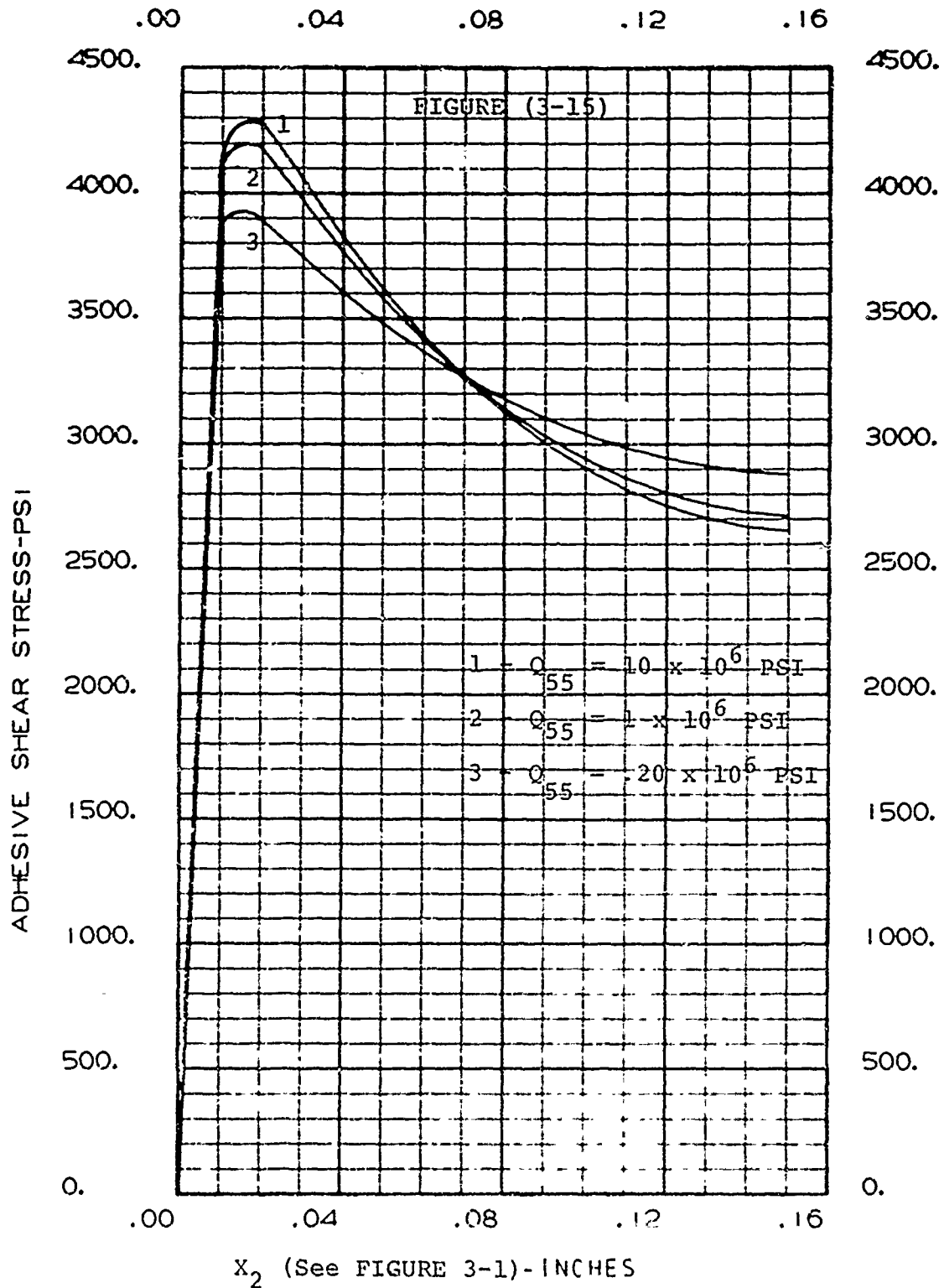
EFFECT OF Q_{11} ON ADHESIVE NORMAL STRESS

plots show a significant reduction in adhesive stress as the value of Q_{11} increases. This is understandable as a stiffer adherend will reduce lateral deflections which will reduce the end shear and moment values which induce the stress concentrations at the overlap ends. Moreover, Figure (3-13) is very convincing in displaying that the shear stress becomes more uniform as the adherends become more rigid. This is highly desirable and is essentially a pure shear result (i.e. $\tau = P/A$).

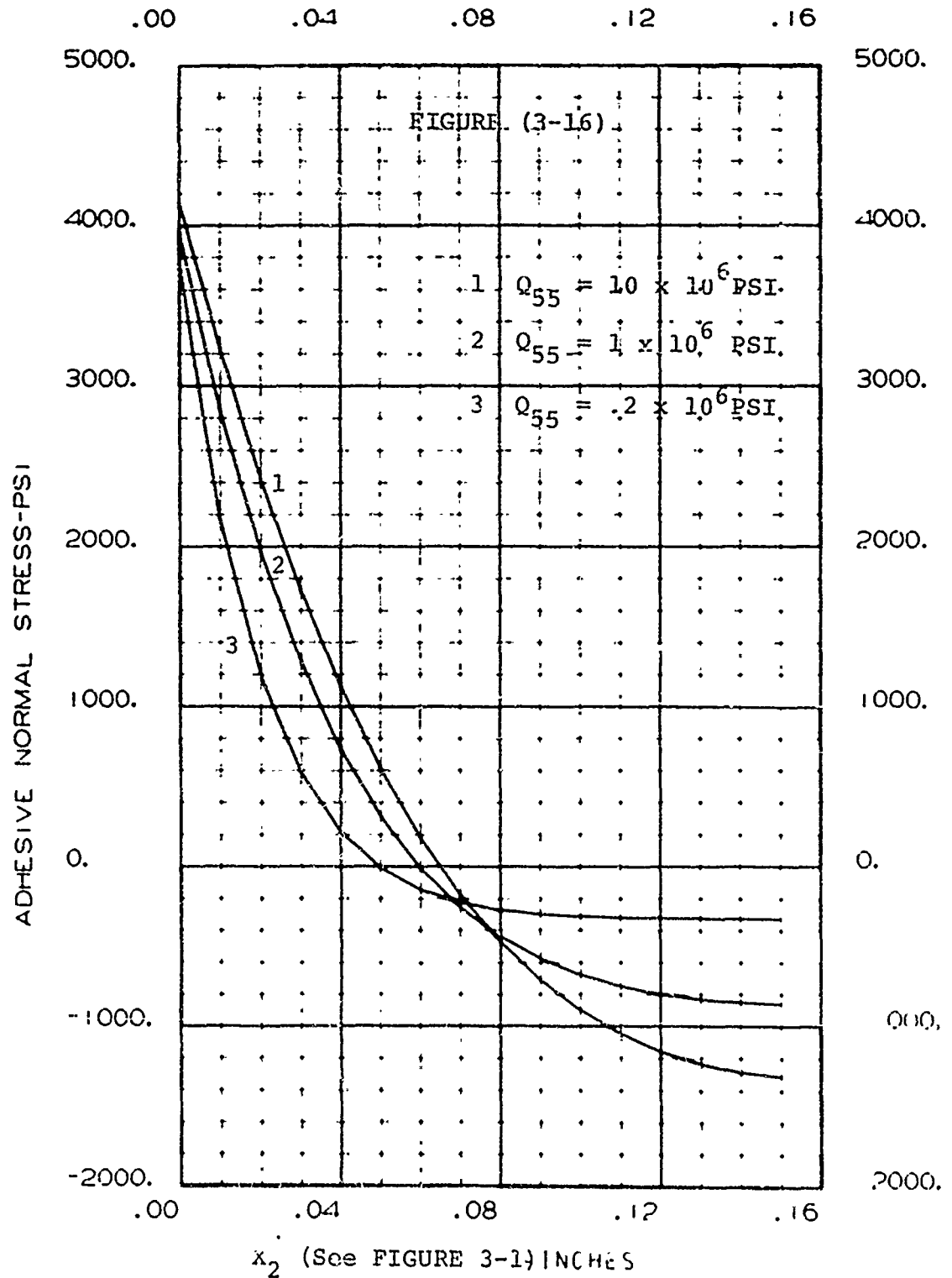
The influence of Q_{55} which is introduced into the analysis by the transverse shear stress term, τ_{xz} as seen in Figures (3-15) and (3-16) is seen to have a minimal influence on the adhesive shear and normal stresses, at least for thin adherends. This too is understandable, for the influence of transverse shear stresses would be minimal for adherends of small thickness (i.e. $h = .063$ ") increasing in influence, especially for anisotropic materials, as the thickness of the adherend increases.

An added flexibility of the analytical technique developed herein is that the stresses through the thickness of the adherend are readily calculated.

Typical distributions of axial stress, transverse



EFFECT OF Q55 ON ADHESIVE SHEAR STRESS

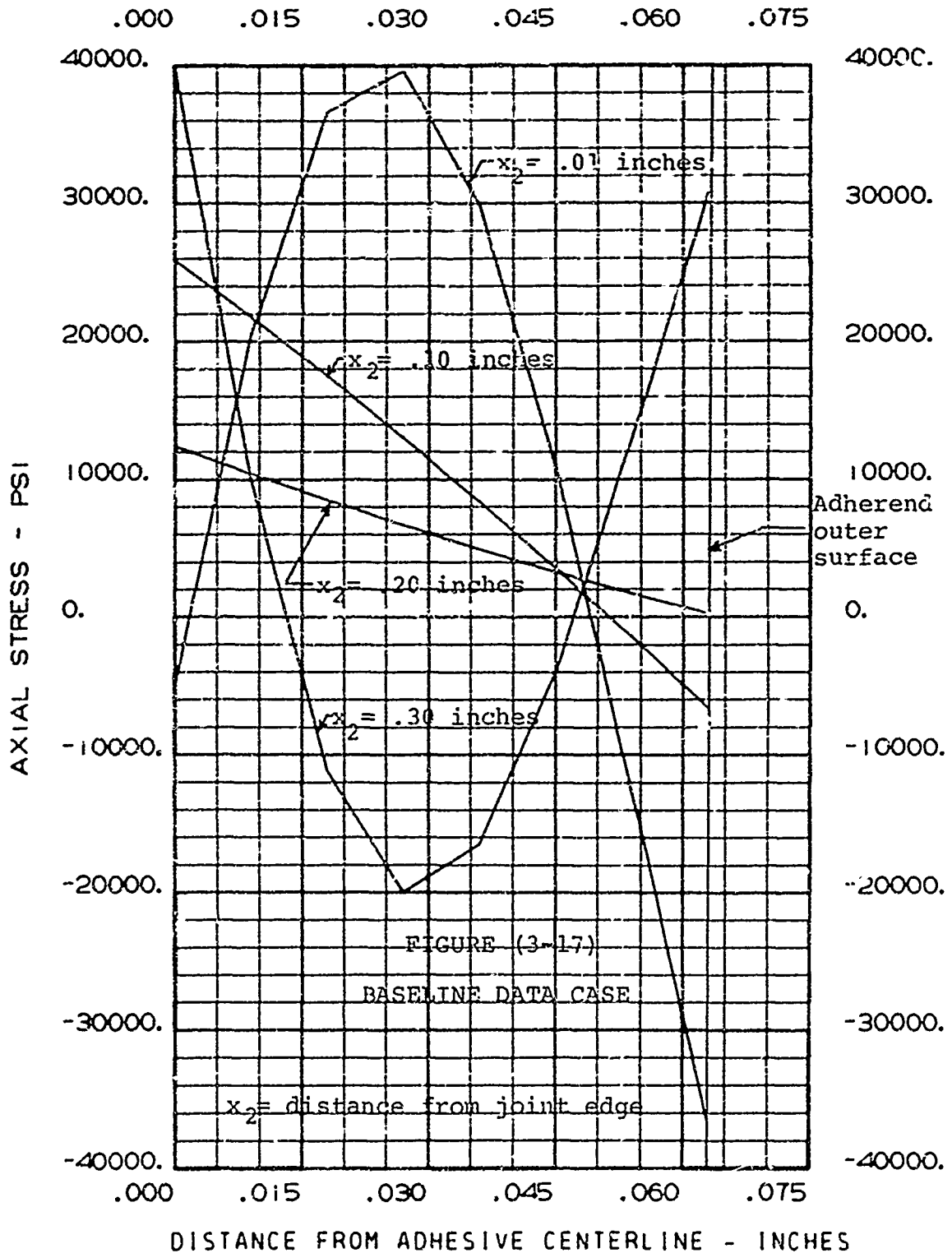


EFFECT OF Q_{55} ON ADHESIVE NORMAL STRESS

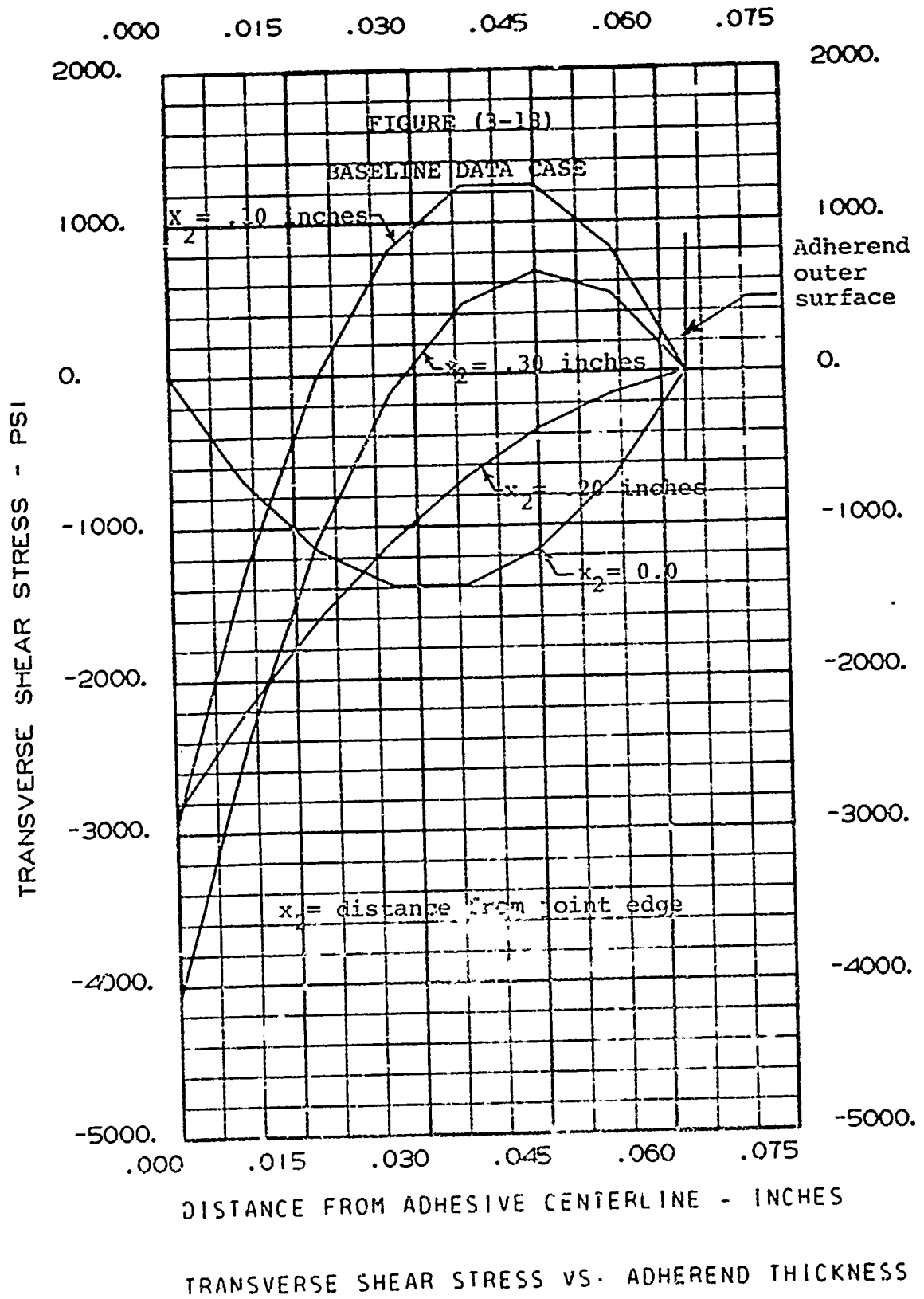
shear stress, normal stress and longitudinal stress through the adherend thickness for the baseline case are shown in Figures (3-17 - 3-20) respectively. The plots also show how these stresses vary along the overlap length.

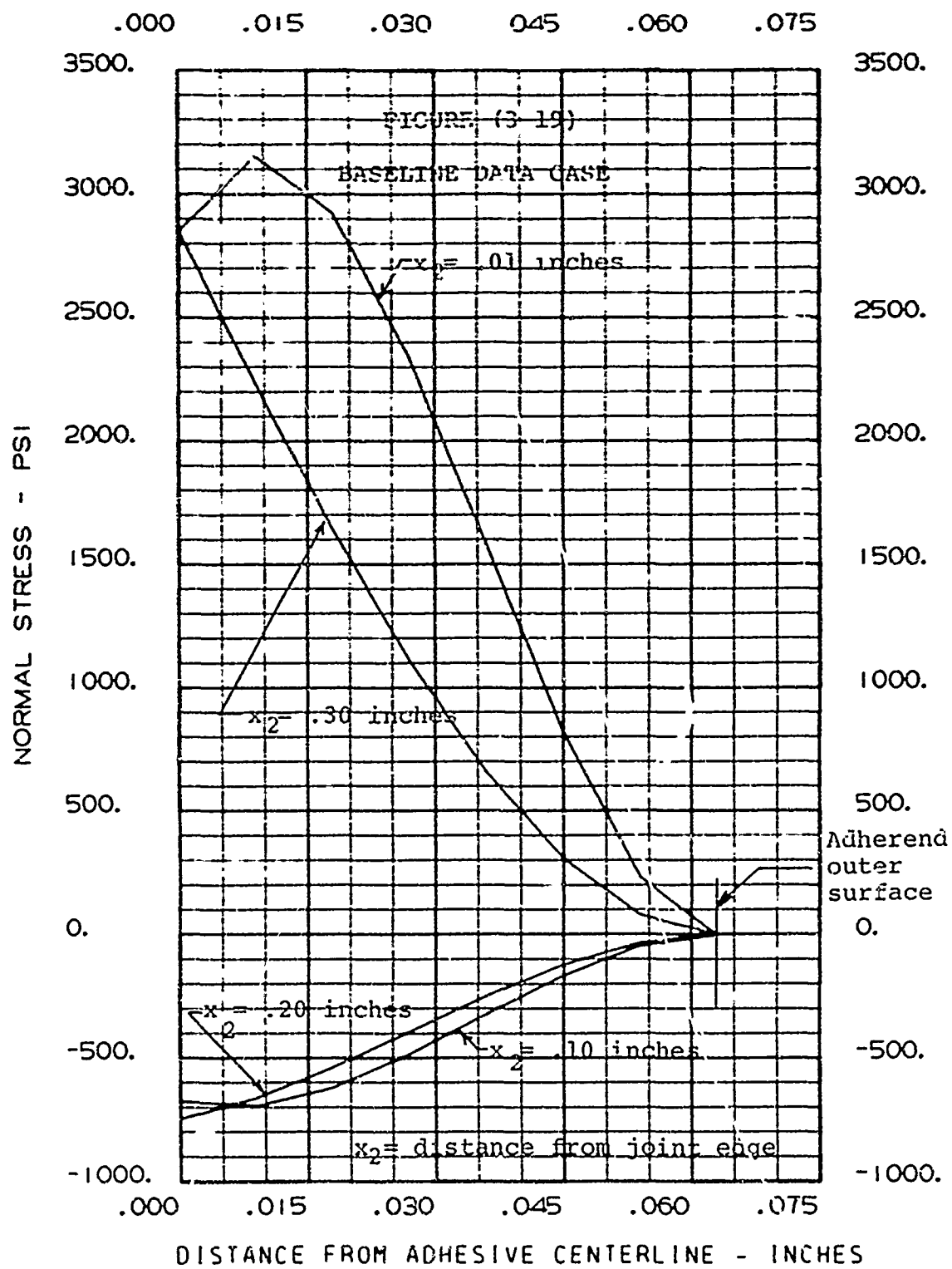
Recalling the baseline data, inspection of Figures (3-17 - 3-20) readily acquaints one with the fact that near the ends of the overlap ($x = .01$ and $x = .30$) where the moments, axial load and shears are largest the peak stresses occur. Moreover, they all vary quite rapidly through the thickness of the adherend. In the central part of the overlap ($x = .10$ and $x = .20$) one sees that the peak stress levels, and range of stresses are of a much less severe nature. Moreover, variation of these stresses through the adherend thickness is much less severe than at the ends of the overlap.

While the longitudinal stresses are relatively small, it is believed that for certain geometries the large tensile and compressive axial stresses near the ends of the overlap in combination with the peak transverse shear and normal stresses are responsible for the lamina and or resin adjacent to the adhesive failing before the adhesive itself. A more thorough discussion of this point will be presented in the static and fatigue test

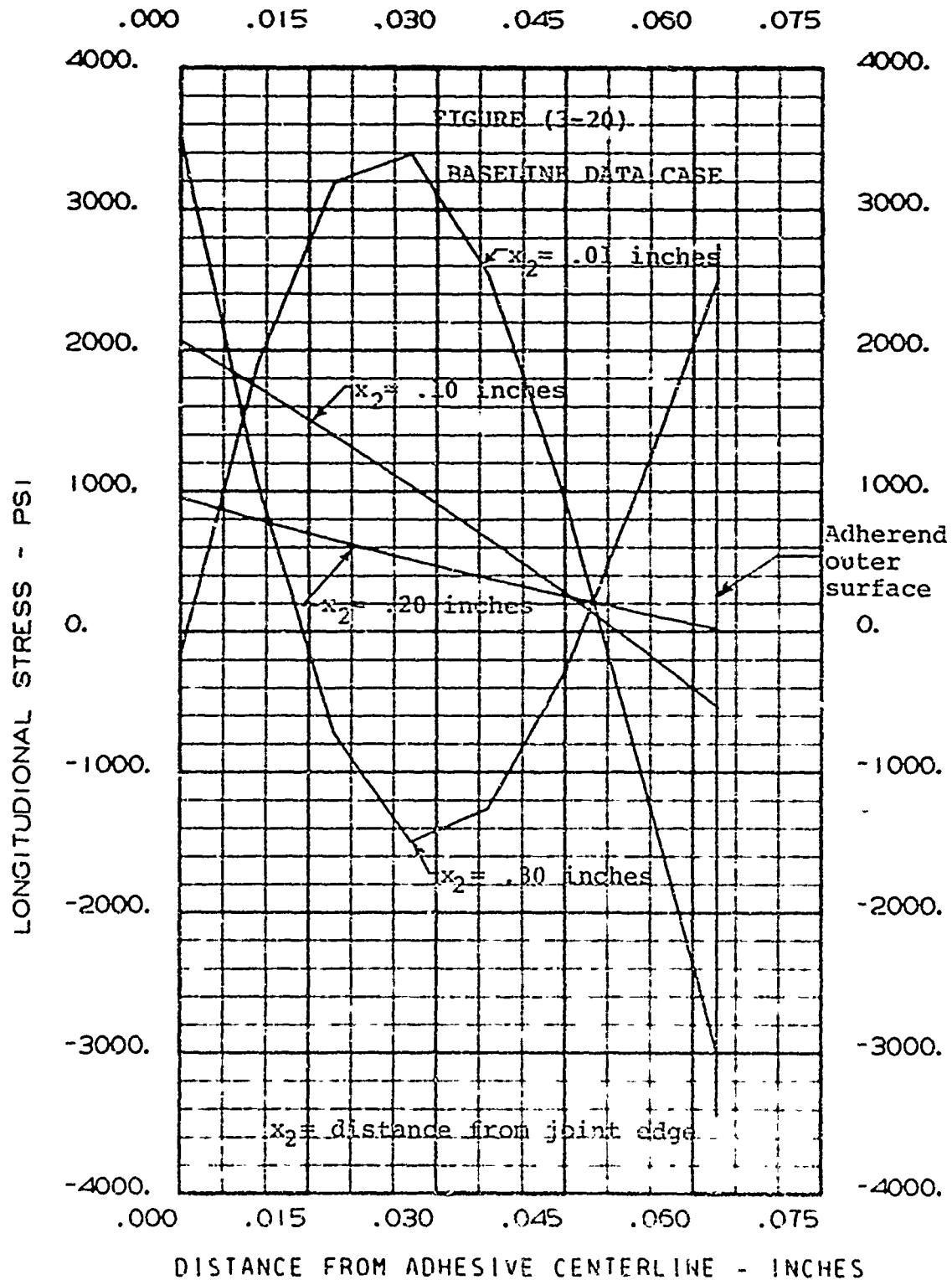


AXIAL STRESS VS. ADHEREND THICKNESS

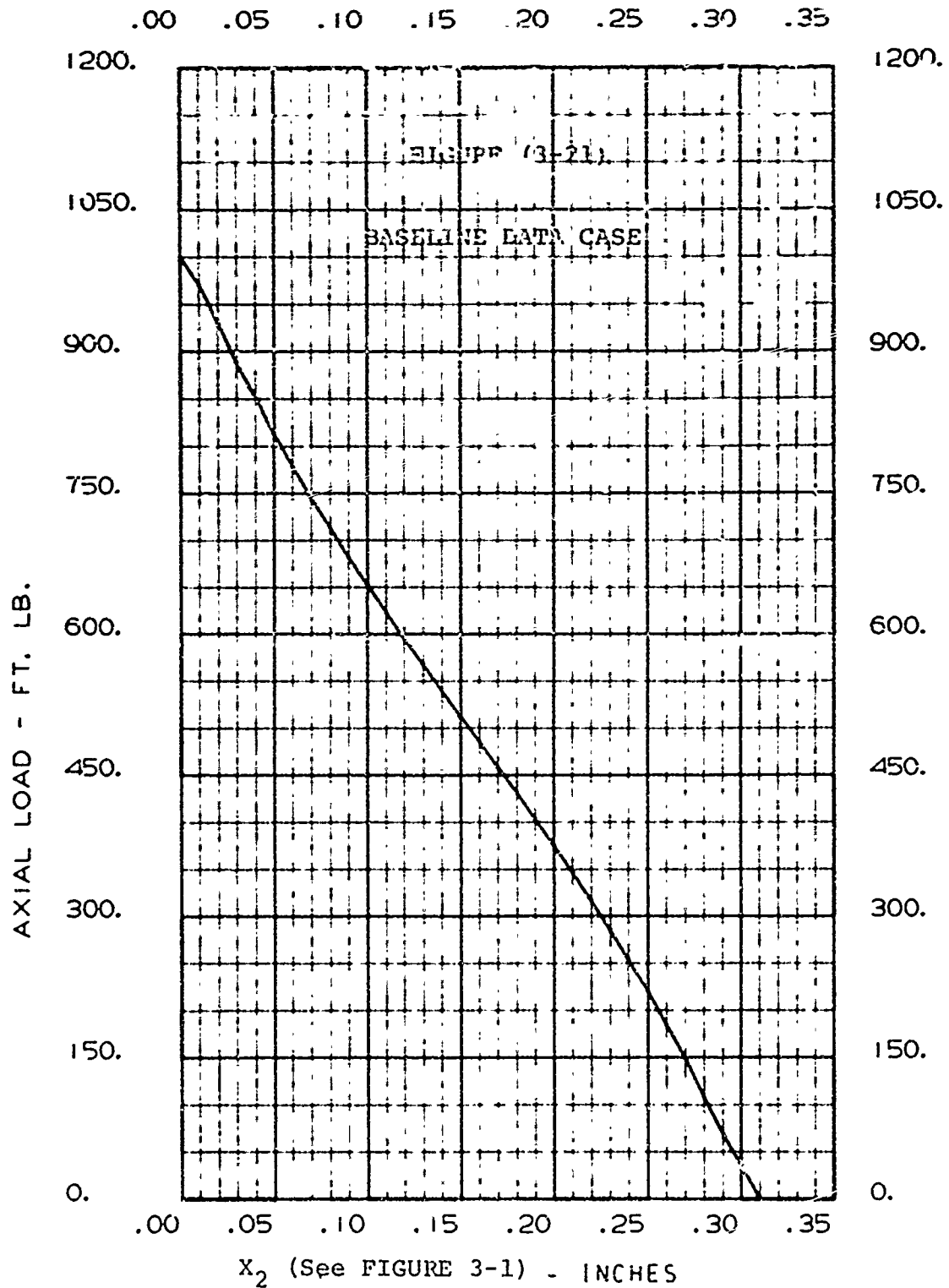




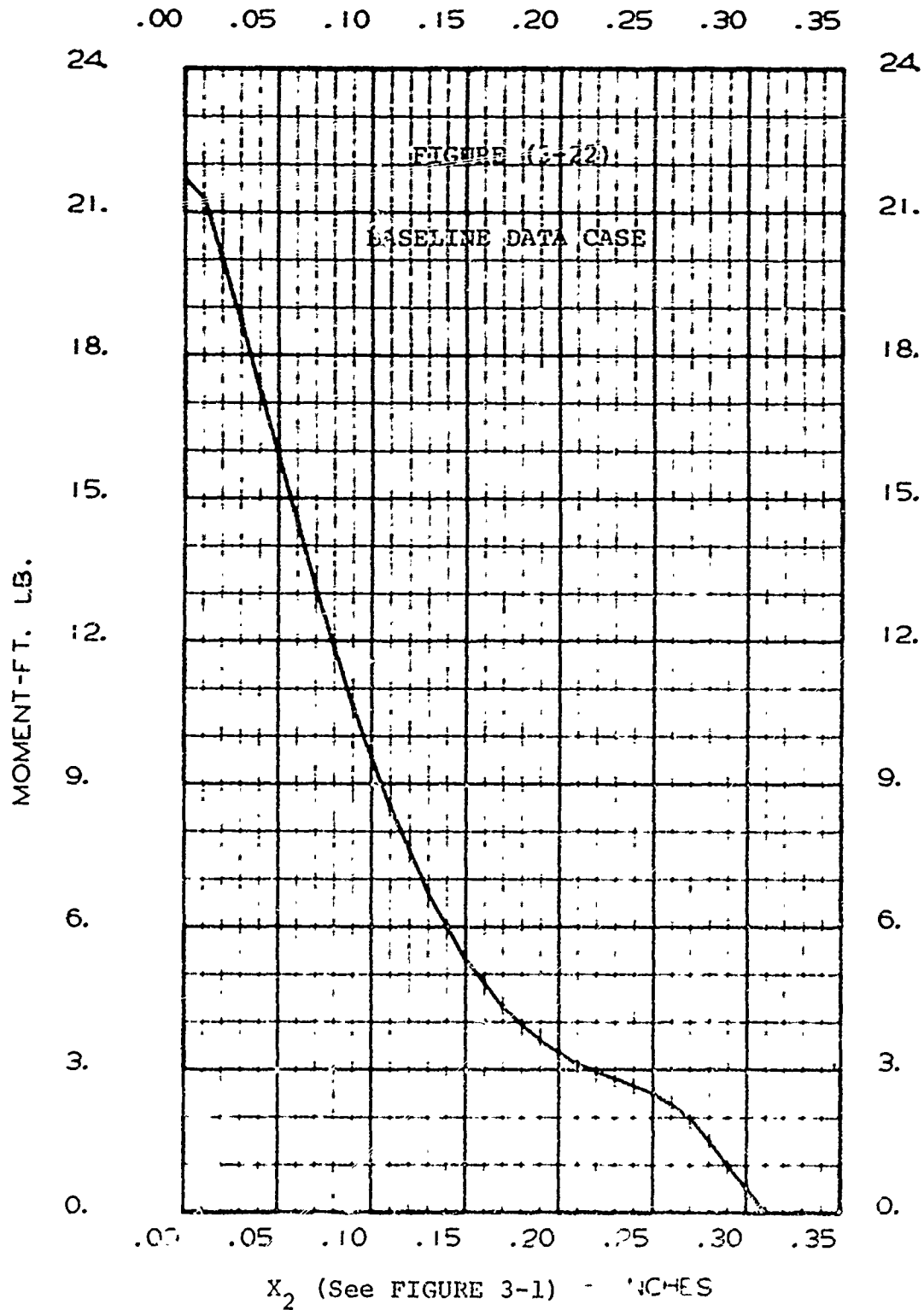
NORMAL STRESS VS. ADHEREND THICKNESS



LONGITUDINAL STRESS VS. ADHEREND THICKNESS



AXIAL LOAD DISTRIBUTION IN ADHEREND.



MOMENT DISTRIBUTION IN ADHEREND

section.

Finally, typical distributions of moment and axial load in the upper adherend over the overlap length are shown in Figures (3-21) and (3-22) respectively. The moment and axial load both go to zero at the free end of the adherend as the boundary conditions require.

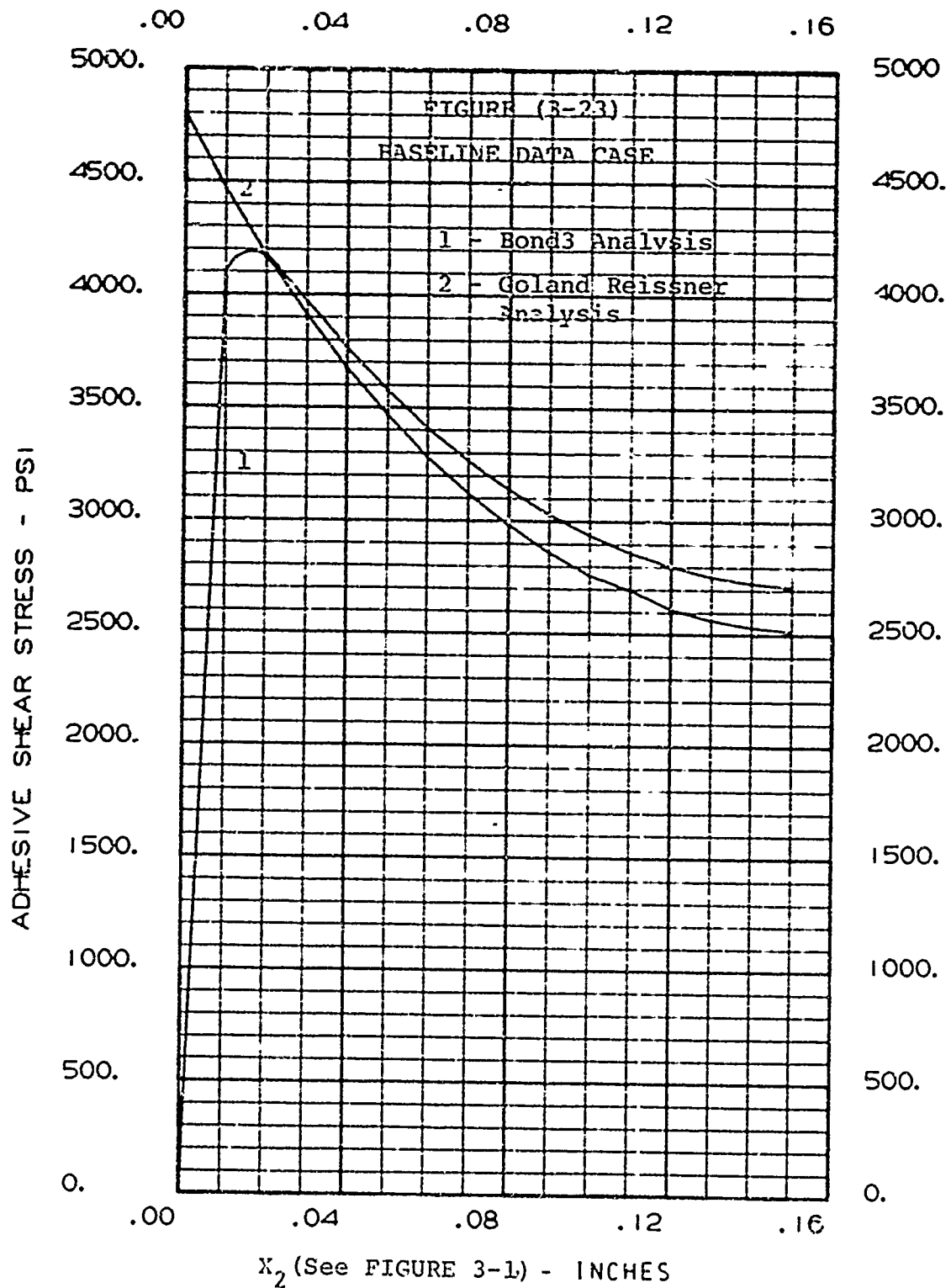
If one were to summarize the results of Figures (3-2) to (3-16), certain significant design recommendations can be given for the case of two equal adherends joined together in such a manner that the adhesive will fail initially (length of overlap to adherend thickness ≤ 10). Primarily, one is interested in maximizing the axial load a given joint can transfer. To do this one wishes to minimize the shear and normal adhesive stresses. This could best be achieved by:

- A. Using an adhesive which maximizes the ratio of shear strength to shear modulus and the ratio of tensile strength to tension modulus.
- B. Maximize the value of Q_{11} or increase adherend thickness. This lowers both shear and normal adhesive stresses.
- C. Minimize Q_{55} . This has a modest effect reducing peak shear and normal stresses.

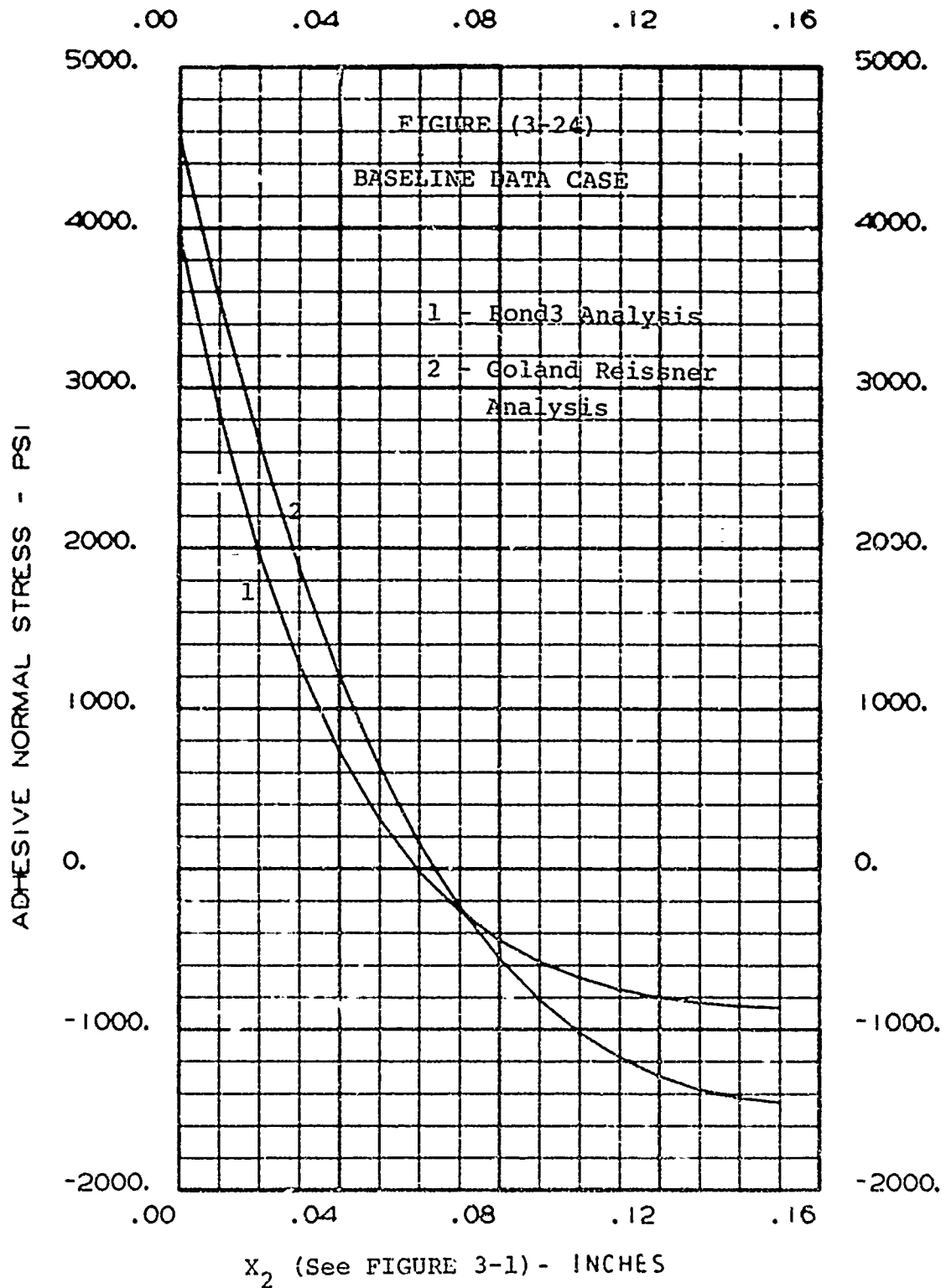
- D. Keep a balanced adherend ($B_{ij} = 0$) while limiting the orientation of the plies to small angles with respect to the load axis of the part.
- E. Keep the length of overlap to thickness of adherend ratio around 10. Above this, the adherends usually fail initially.
- F. Keep the adherends as similar in in-plane stiffness (Et) as practicable. This minimizes the peaking of adhesive shear and tensile stresses due to the lack of symmetry of the lap joint (Reference 22).

To conclude this study it is believed to be of interest to compare the adhesive shear and normal stress distributions of the Bond3 analysis vs. that of Golan and Reissner (Reference 23). To accomplish this, the baseline data case of Figure (3-1) was analyzed by both techniques. Moreover, certain variables were altered and the net results were again compared by analyzing the new joint by both analytical techniques where possible. The results are self-explanatory and are presented in Figures (3-23) to (3-34).

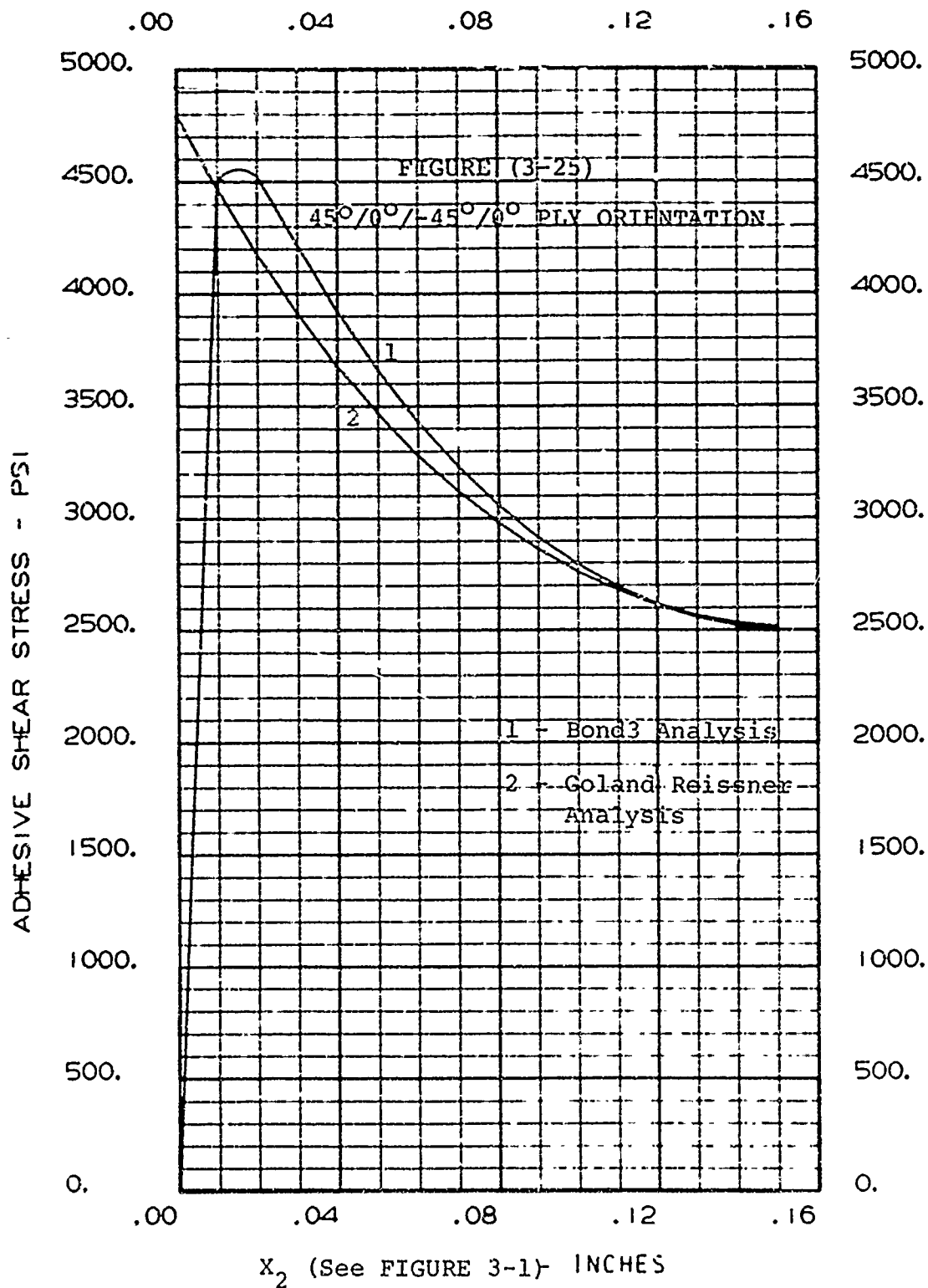
The variables considered were:



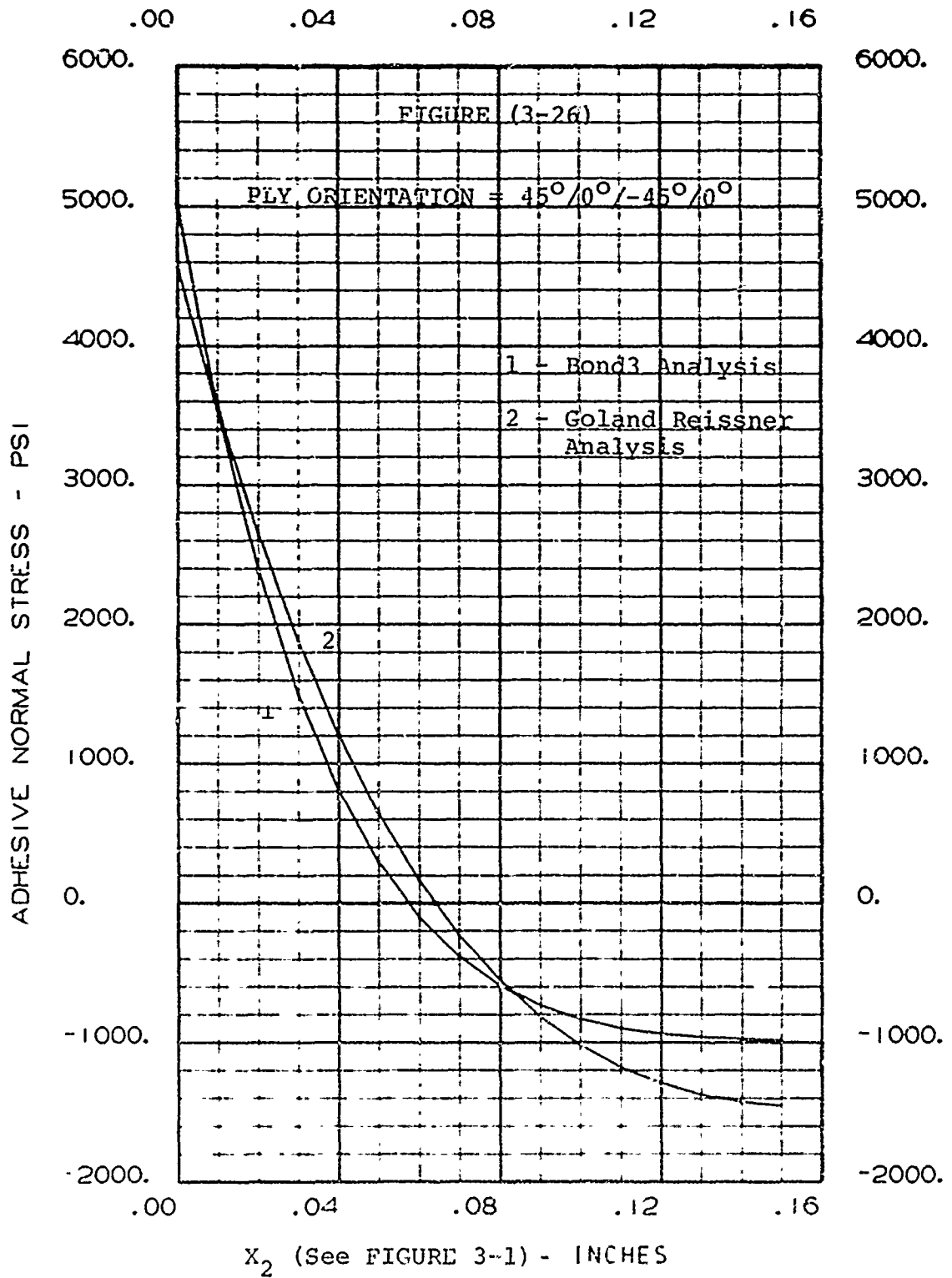
COMPARISON OF REISSNER AND BOND3 SHEAR STRESS



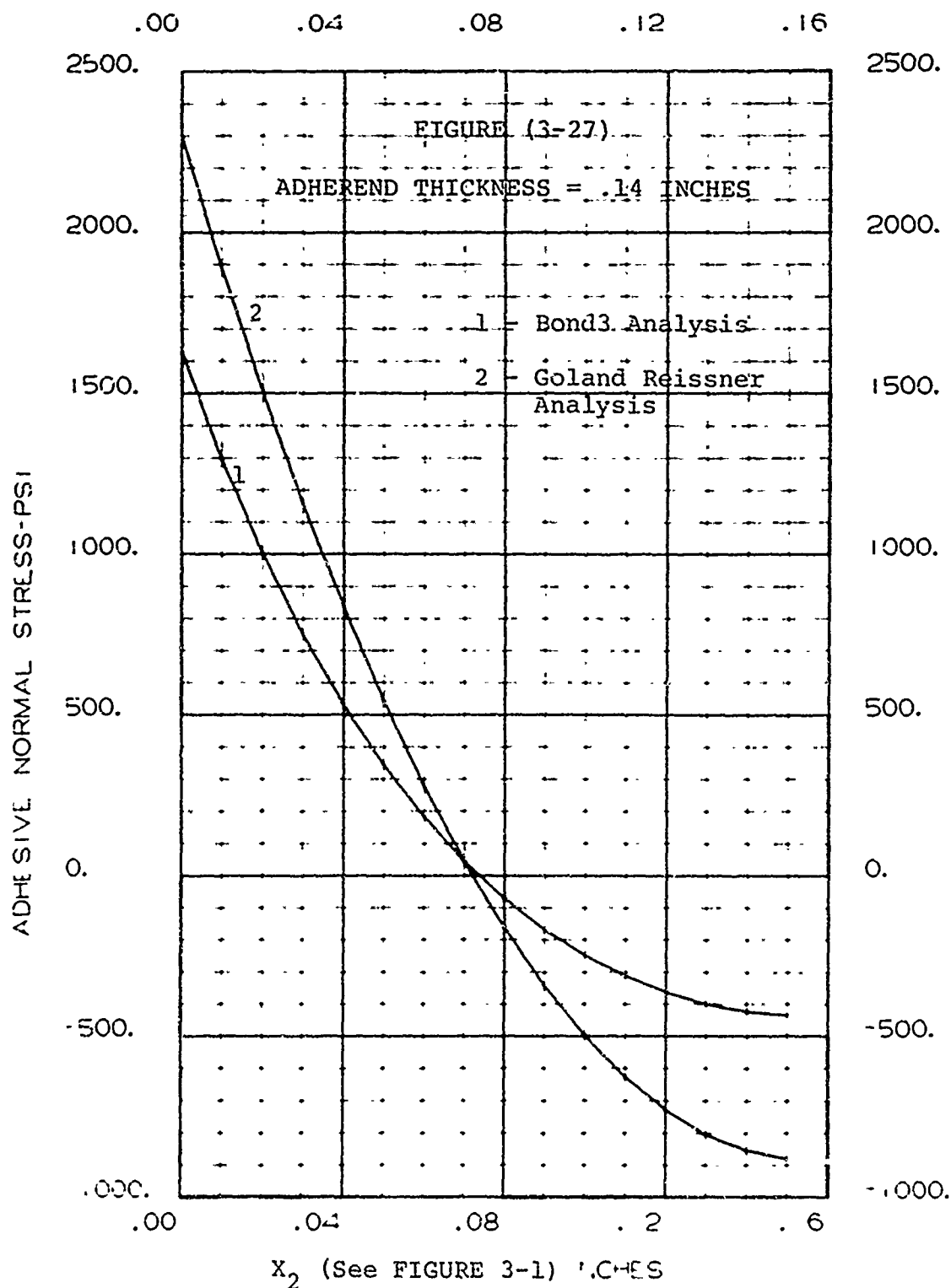
COMPARISON OF REISSNER AND BOND3 NORMAL STRESS



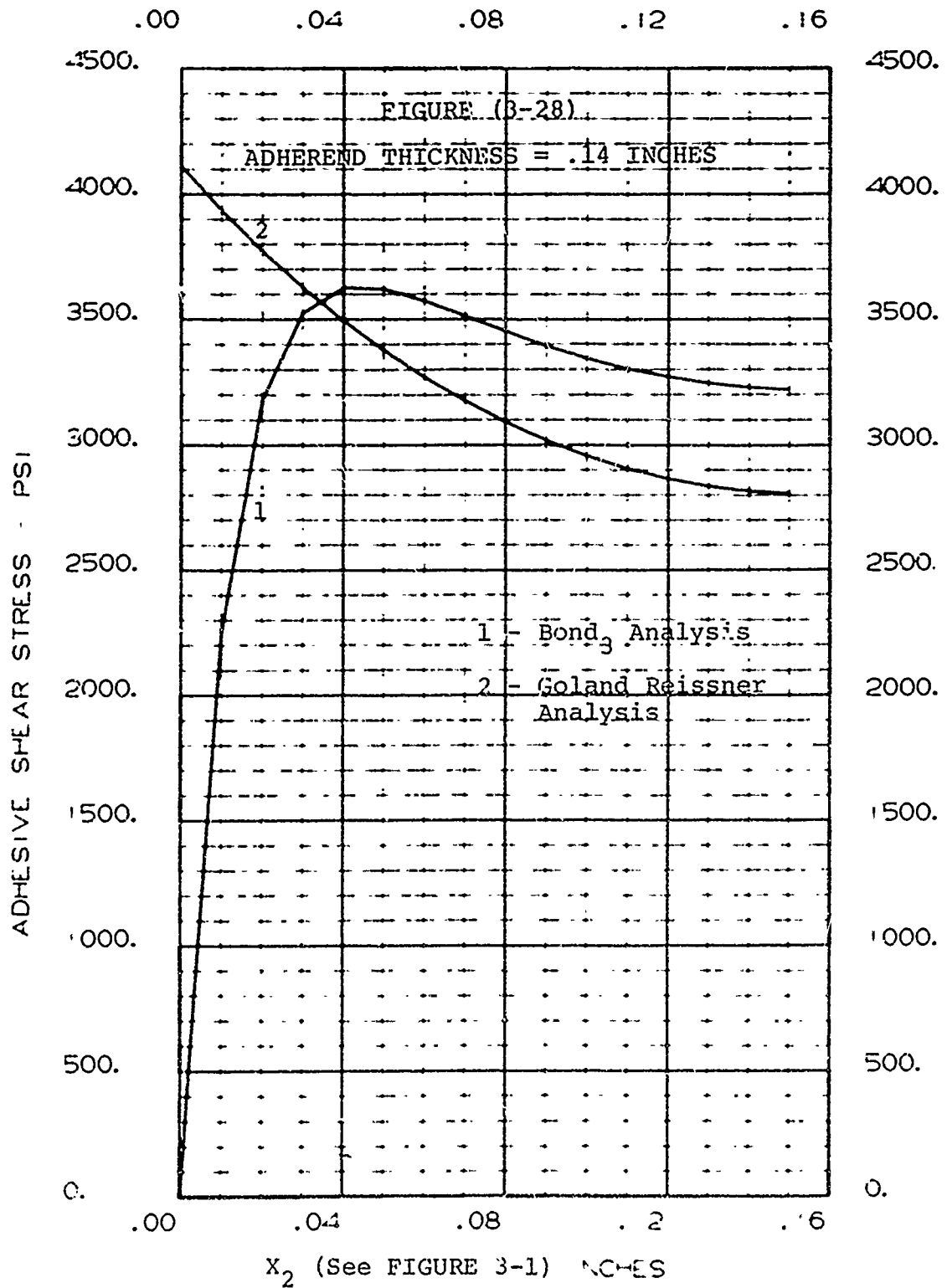
COMPARISON OF REISSNER AND BOND3 SHEAR STRESS



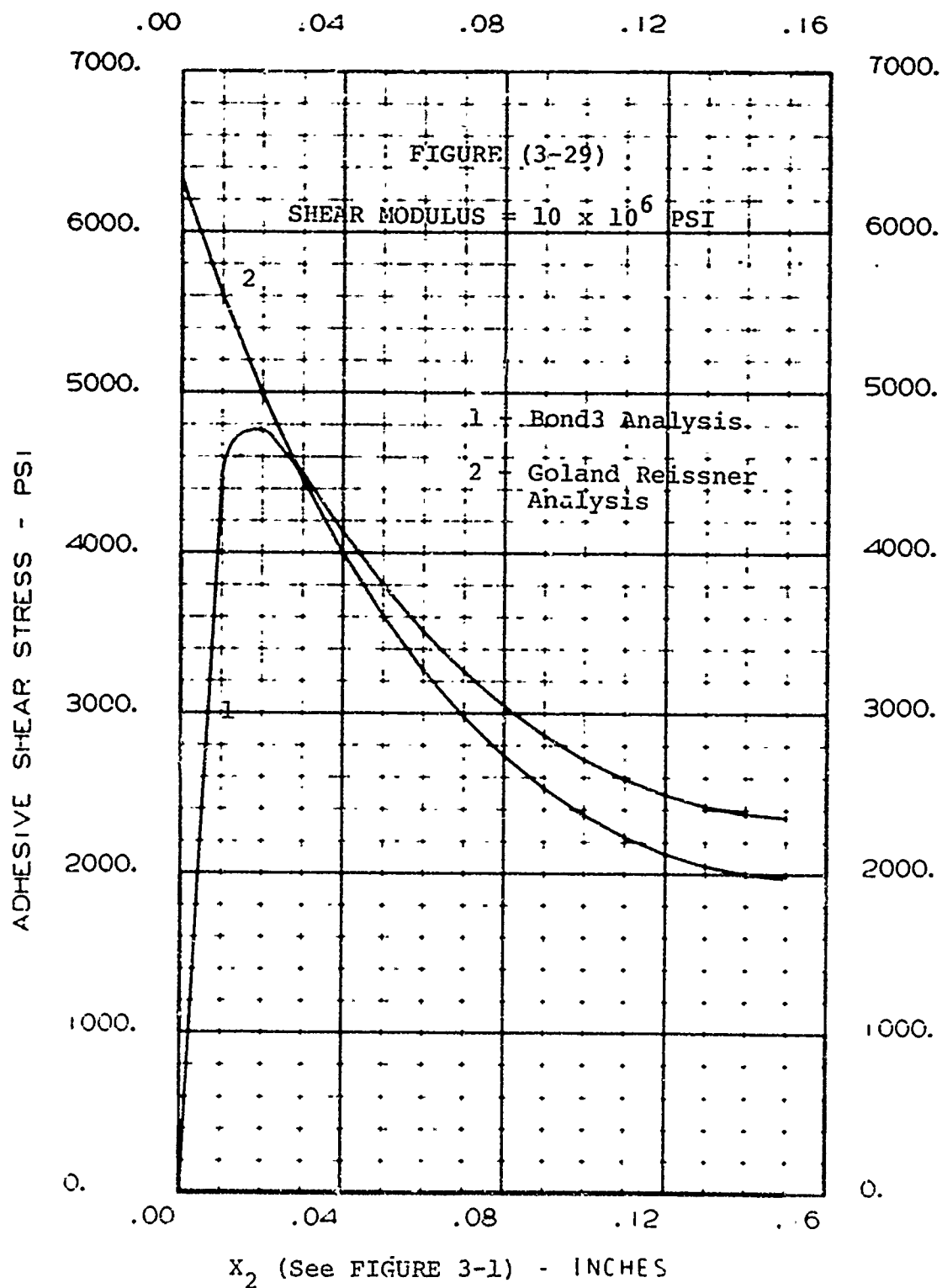
COMPARISON OF REISSNER AND BOND3 NORMAL STRESS



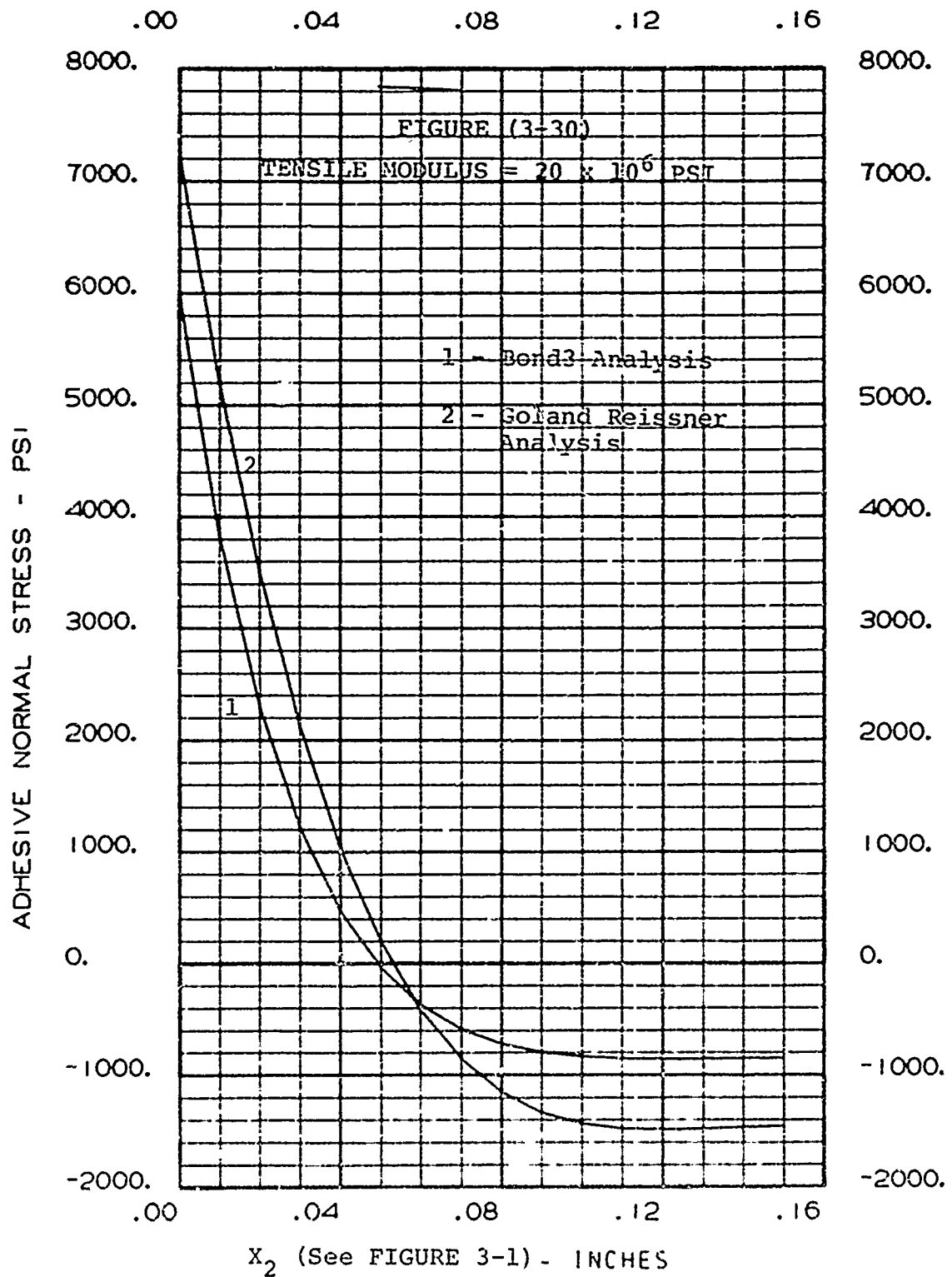
COMPARISON OF REISSNER AND BOND3 NORMAL STRESS



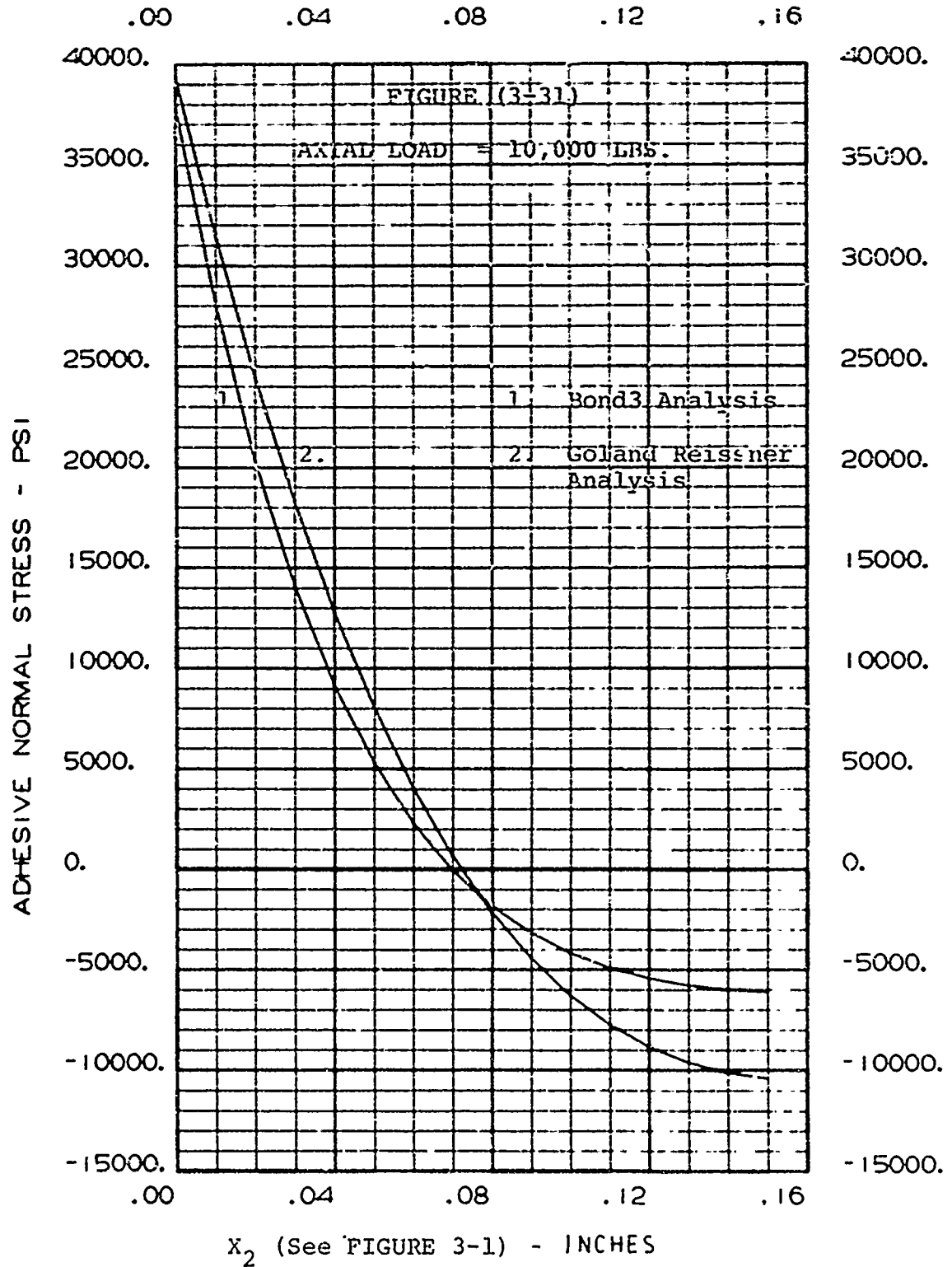
COMPARISON OF REISSNER AND BOND SHEAR STRESS



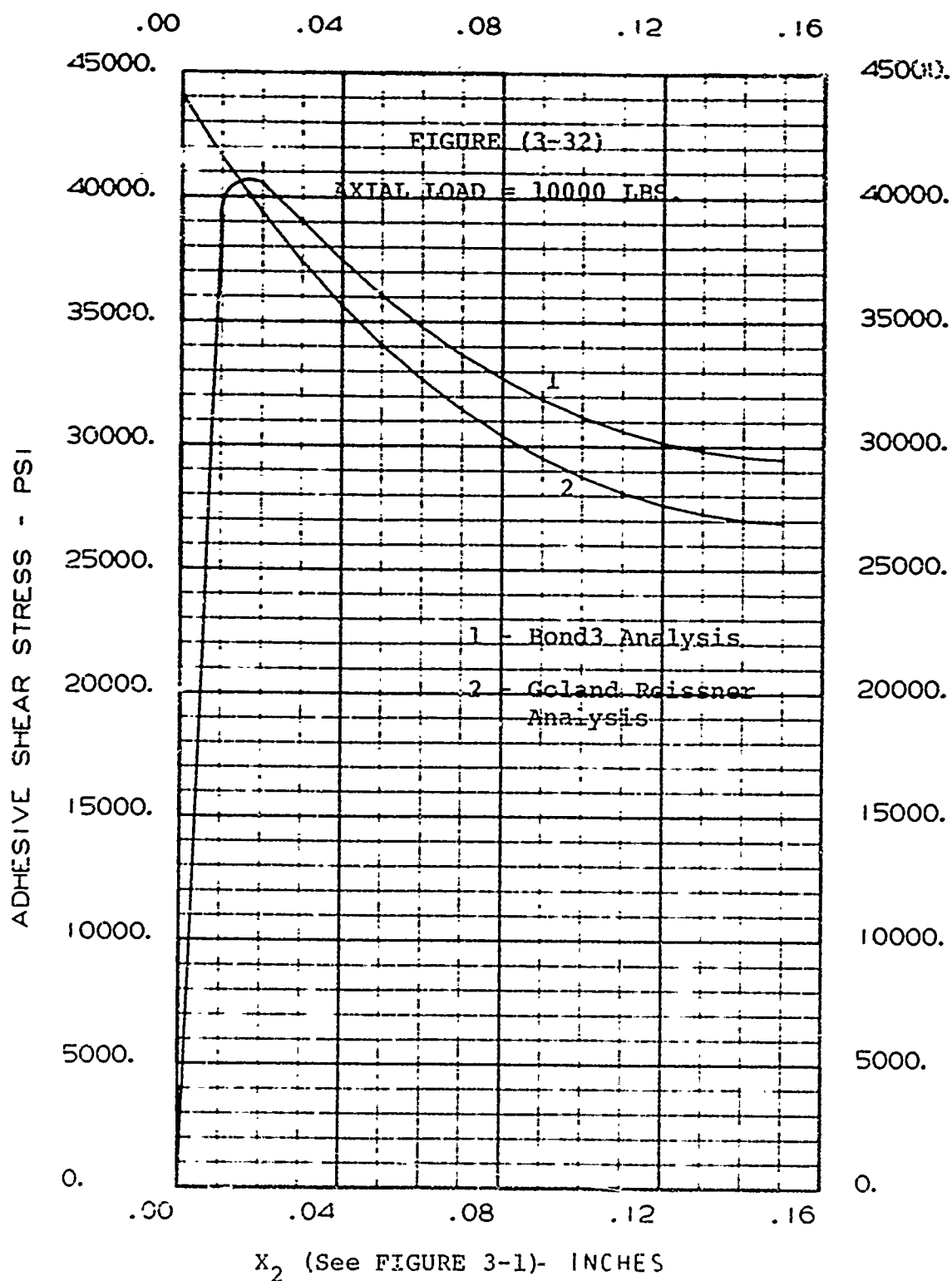
COMPARISON OF REISSNER AND BOND3 SHEAR STRESS



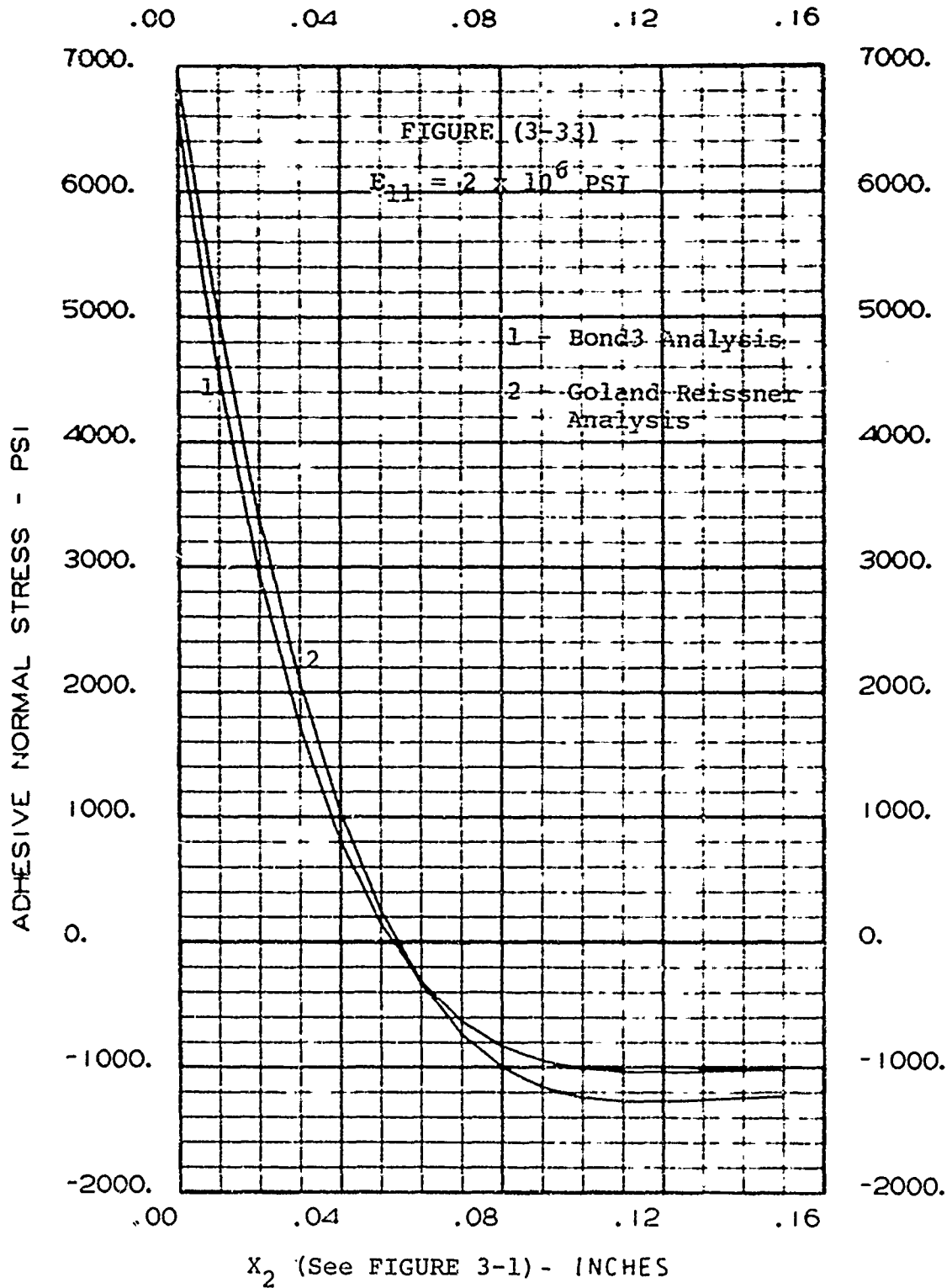
COMPARISON OF REISSNER AND BOND3 NORMAL STRESS



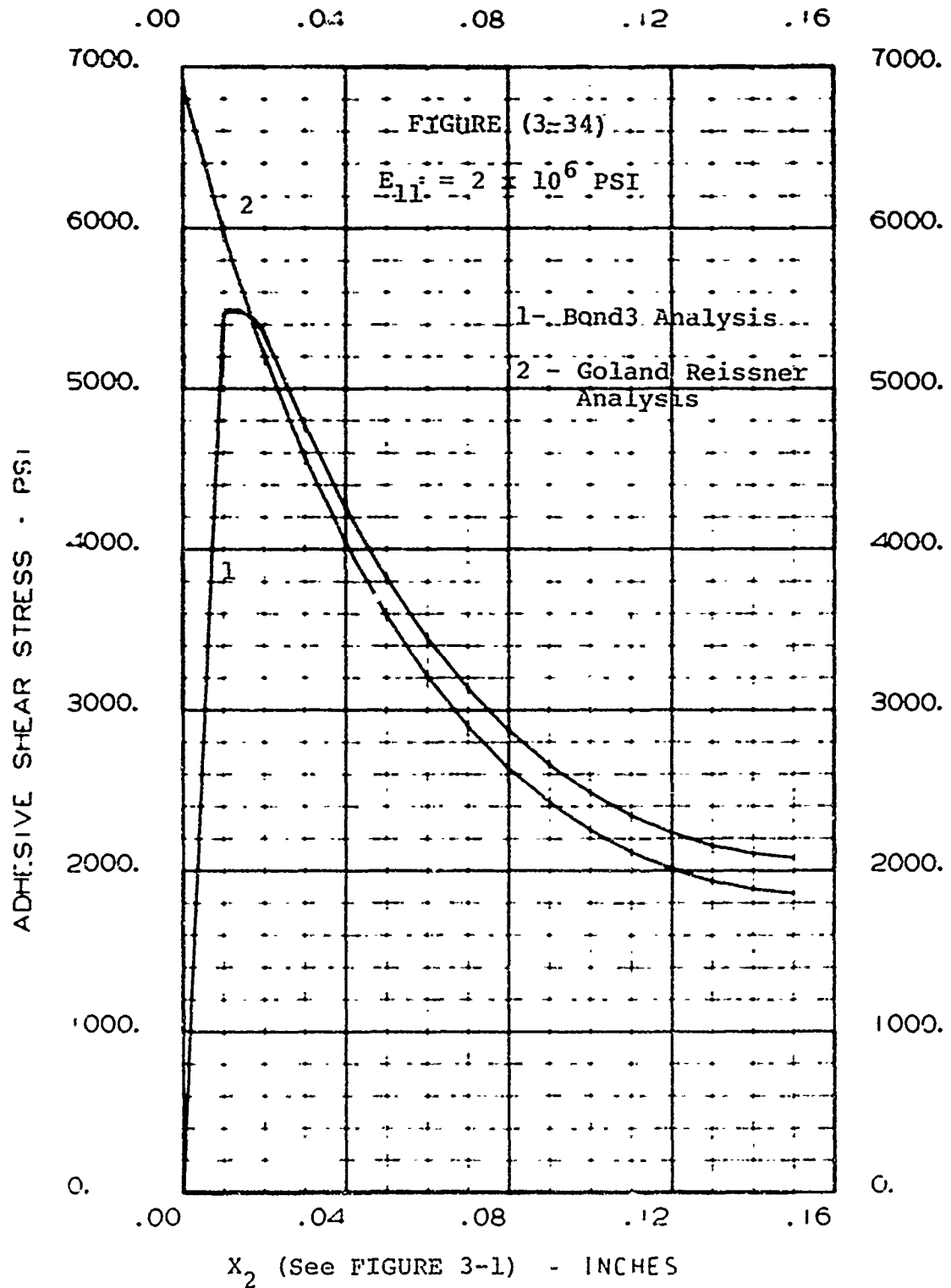
COMPARISON OF REISSNER AND BOND3 NORMAL STRESS



COMPARISON OF REISSNER AND BOND3 SHEAR STRESS



COMPARISON OF REISSNER AND BOND3 NORMAL STRESS



COMPARISON OF REISSNER AND BOND3 SHEAR STRESS

- A. Ply orientation - See Figure (3-8) on page 207 for the lamina orientation pattern.
- B. Thickness of adherends.
- C. Shear and tensile modulus.
- D. Axial load.
- E. Primary elastic modulus of adherend material - E_{11} .

A cursory examination of the results shows excellent agreement between the two analytical techniques for the variation of the selected input variables at the end regions of the overlap. It is within this region that the more elaborate Bond3 analysis is justified. Its inclusion of transverse shear and normal strain effects enables one to satisfy the boundary condition that the shear stress is zero at the end of the overlap. Moreover, it is the inclusion of these secondary effects that accounts for the difference in numerical values at $x = 0.0$. Further advantages of the Bond3 analysis are that:

1. It has the capability to handle anisotropic material systems of various ply orientation.
2. Bond3 can analyze unsymmetric lap - joint configurations.

3. Bond3 can calculate the stresses throughout the thickness of the adherend. This is very useful in predicting adherend initial failures.
4. Per Figures (3-27) and (3-28) it is obvious that the two analyses diverge for thicker adherends. This is because the transverse sheer and normal strain effects become more significant in thicker adherends.

In conclusion, it has been shown that an elaborate analysis for a single-lap joint in the most general configuration has been developed and has been shown to be accurate in all respects.

CHAPTER IV

A. ELASTIC MODULUS MEASUREMENTS ON 1002 S FIBERGLASS MATERIAL

The objective of this section is to substantiate that the material elastic constants as used by the Boeing-Vertol Company are in fact those possessed by the 1002 S fiberglass material used in this test program. To substantiate the Boeing data, a two phase program was conducted.

1. Ultrasonic measurement of E_{11} , E_{22} , E_{33} , and Poisson's ratio were made.
2. The primary tensile modulus (E_{11}) of 0° ply test pieces was determined using the conventional static load test procedure.

These test methods, together with the test specimens and the results are described within this chapter.

The ultrasonic test program was conducted gratis by Mr. John Zurbrick of the General Electric Company, Cincinnati, Ohio. The tests were made using specimens 3" x 3" x .28" thick. They are shown in Figure (4-1). The

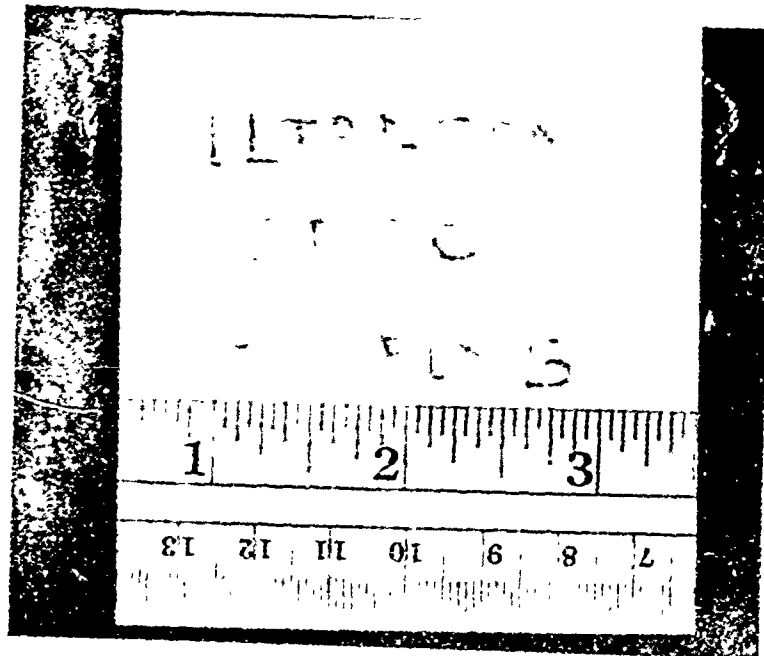


FIGURE (4-1) TYPICAL ULTRASONIC MODULUS SPECIMEN

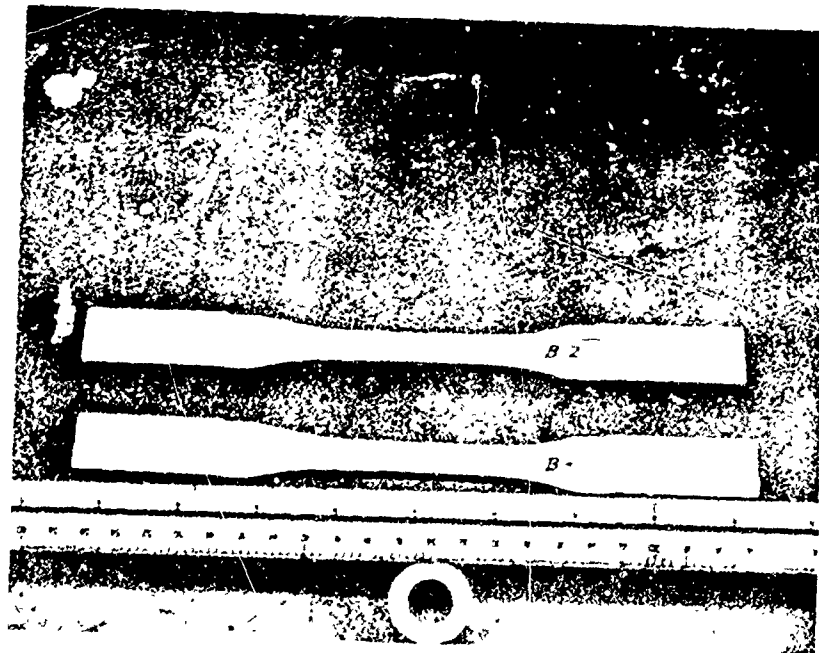


FIGURE (4-3) AND (4-7) MODULUS AND ULTIMATE STRENGTH
DESTRUCTIVE TEST SPECIMEN

test technique is thoroughly described in reference (62) but will be briefly reviewed here.

It has been shown that a correlation exists between non-destructive measurements and destructive measurements in obtaining numerous physical properties of a given material system. One such property is the tensile modulus of composite material systems. The basis for this correlation lies in the observation that the non-destructive test quantity $K\rho V_L^2$ is related to the initial elastic modulus of the material. K is a conversion constant to give one the elastic modulus in PSI units. V_L is the non-destructive bulk wave ultrasonic longitudinal velocity while ρ is the nondestructively determined density of the material being tested. The idea is to measure the ultrasonic velocity and the density at the same point relating the resulting product (i.e. ρV_L^2) to the mechanical properties in question. Such measurements are accomplished by the system displayed in Figure (4-2). The frequency used for such tests is one MHz. Moreover, the accuracy in determining the modulus values is generally no worse than ± 10 per cent to a mean $\pm 2 \sigma$ confidence level with respect to destructively determined modulus measurement. However, one must recognize when comparing ultrasonic modulus values with destructively determined

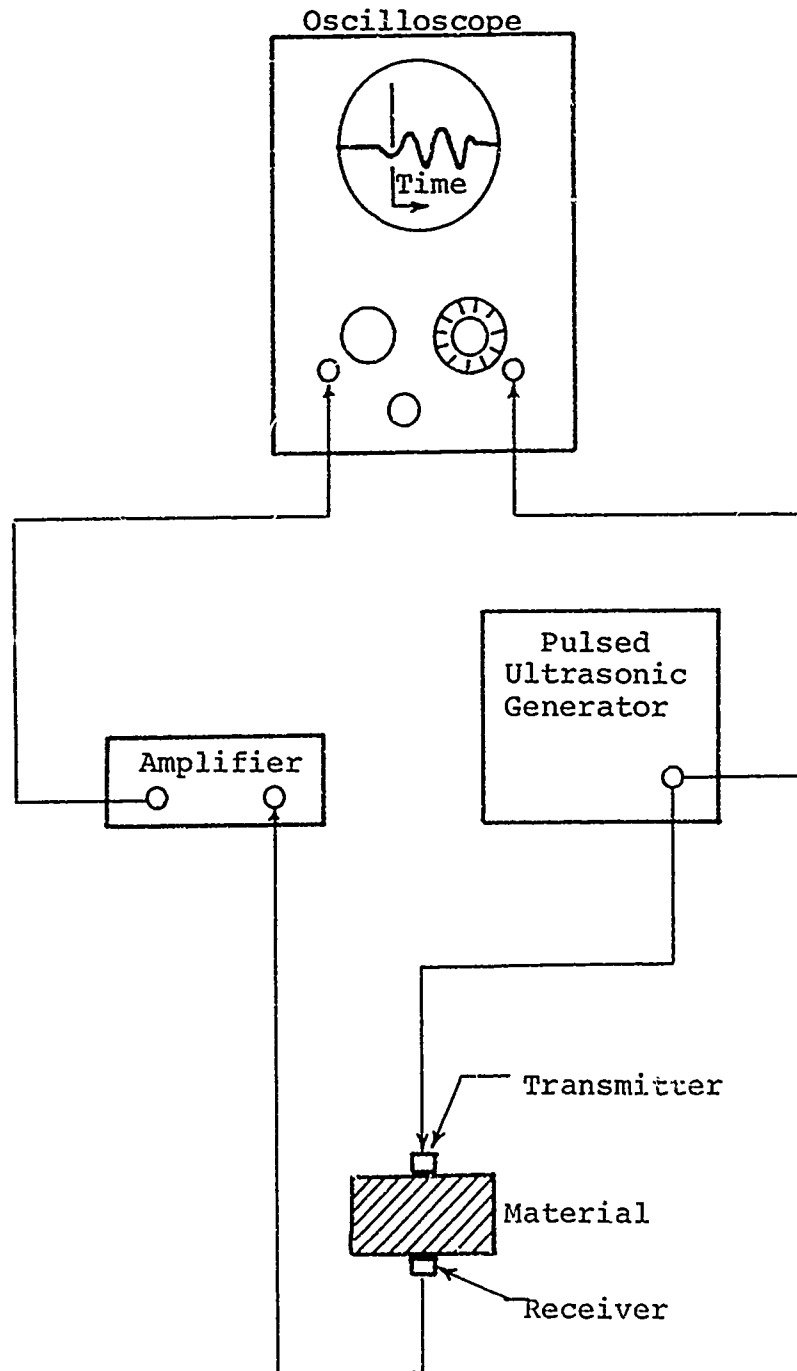


FIGURE (4-2) ULTRASONIC THROUGH-TRANSMISSION TECHNIQUE
FOR LONGITUDINAL WAVE VELOCITY

modulus values that one really does not know which is the absolute right answer from which to measure error. One can only state that the true modulus should be within this narrow band.

The results of the ultrasonic measurements of elastic modulus in the three primary directions and of Poisson's ratio for 1002 S material is given in Table (4-1). The elastic modulus is calculated in PSI units per the equation

$$E = \frac{V_L^2 \rho}{0.0124} \quad (4.1)$$

where

$$K = \frac{1}{0.0124}$$

The results show that the primary elastic modulus is approximately 6.35×10^6 PSI. Moreover, the elastic moduli in the 90 degree and transverse direction are equal and approximately 2.4×10^6 PSI. Poisson's ratios were measured to be .23 inches in all directions. This is a slightly erroneous assumption for if one employs the relation

$$E_i \nu_{ji} = E_j \nu_{ij} \quad (i, j = 1, 2, 3) \quad (4.2)$$

he will see that Poisson's ratios cannot be equal in all

TABLE (4-1)
ULTRASONIC MEASUREMENT OF ELASTIC PROPERTIES AT 1.0 MHz

Identification	Scotchply 1002 S Specimens					
	1		2		3	
	Thk	0°	90°	Thk	0°	90°
Direction						
Dimension, inch	.282	3.000	3.000	.279	3.020	3.000
Transit Time, μ sec	2.215	14.70	-	2.20	14.50	-
Velocity in/ μ sec	.1273	.2041	-	.1267	.2083	-
Weight grams		76.3509			75.6209	
Density gm/cm ³ ρ		1.8357			1.8256	
Directional	2.40	6.17	-	2.36	6.39	-
Modulus, 10 ⁶ psi						

$$E = \frac{V^2 \rho}{0.0124}$$

Poisson's Ratio = 0.23 (All Directions)

NOTE: For a unidirectional system thickness direction and 90° (transverse) direction moduli will compare closely.

76.2535
1.8267

2.42 6.35 2.43

TABLE (4-2)
INSTRON STATIC TEST RESULTS FOR PRIMARY MODULUS - E_{11}
1002 S MATERIAL

SPEC. NO.	LAMINATE THICKNESS (INCH)	LAMINATE WIDTH (INCH)	PLY ORIENTATION	$E_{11} \times 10^6$ (PSI)
B1	.066	.386	All 0°	6.07
				6.07
				6.07
B2	.067	.386	All 0°	5.98
				5.98
				6.09
B3	.071	.386	All 0°	5.74
				5.74
				5.74

AVERAGE = 5.97

directions and satisfy this relation in all cases.

In a further effort to substantiate the values of the elastic constants to be used throughout this program and to correlate destructive and non-destructive test results, a static test program to determine the primary elastic modulus was initiated. Typical test pieces used are shown in Figure (4-3). They were seven ply unidirectional layers with bonded cross-ply doublers on the ends. Pertinent dimensions along with the elastic modulus (E_{11}) results are given in table (4-2).

The testing was performed using an Instron Model TT-DM testing machine. Deformations were recorded using a Tinius-Olsen S-1 2 inch gage length extensometer. The test set-up is shown in Figure (4-4).

Upon loading the specimens, load vs. deformation curves shown in Figures (4-5) and (4-6) were recorded using a Moseley Model 7001A x-y recorder. The test was performed three times on each specimen. The primary modulus was determined using the relation

$$E_{11} = \frac{(\text{Load}) (\text{Gage Length})}{(\text{X-section Area}) (\text{deformation})} \quad (4-3)$$

These results are given in table (4-2).



Figure (4-4) and (4-8) Extensometer-specimen
Modulus and Strength Test Set-up

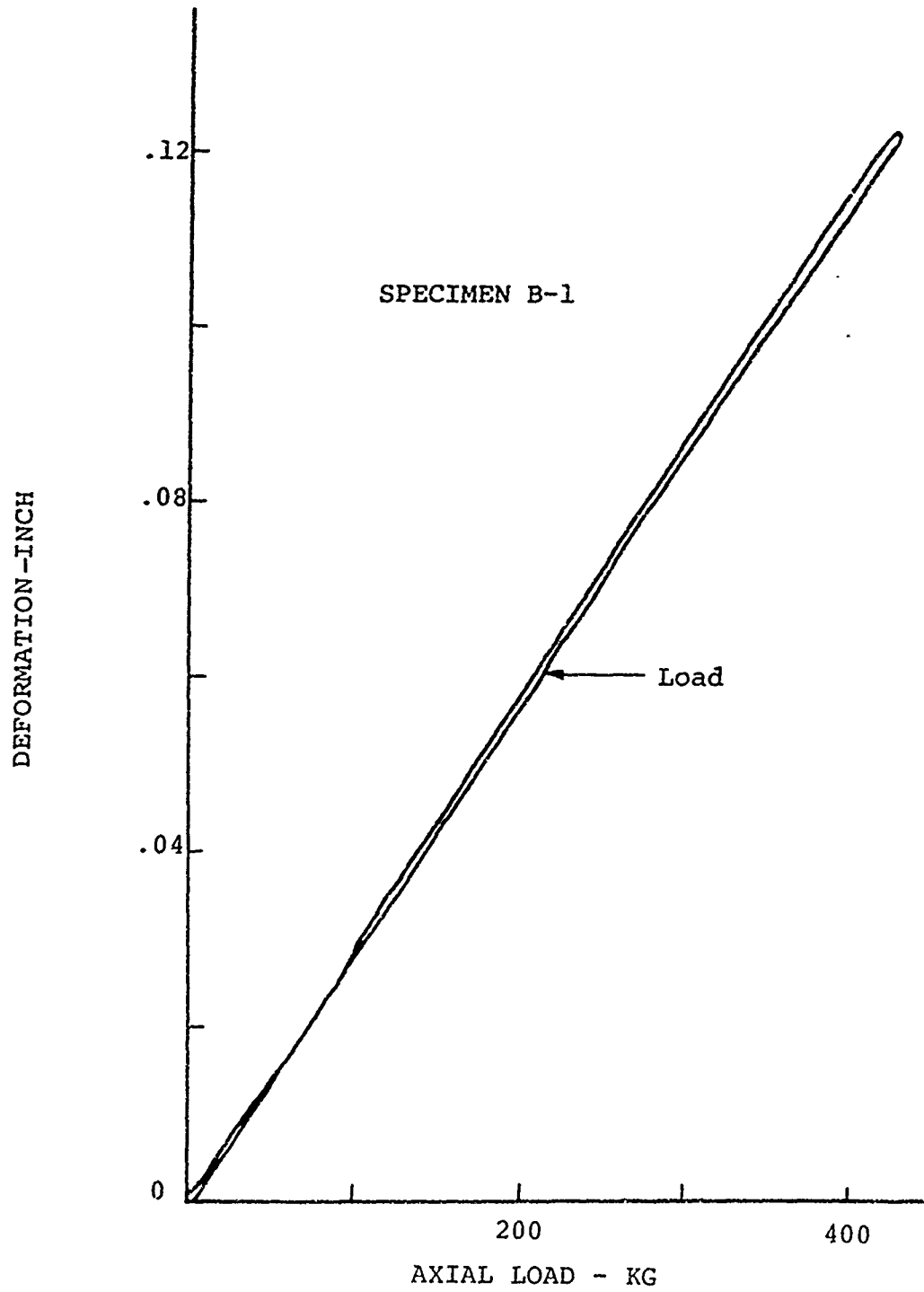


FIGURE (4-5) 1002-S PRE-PREG TAPE PRIMARY ELASTIC MODULUS DATA

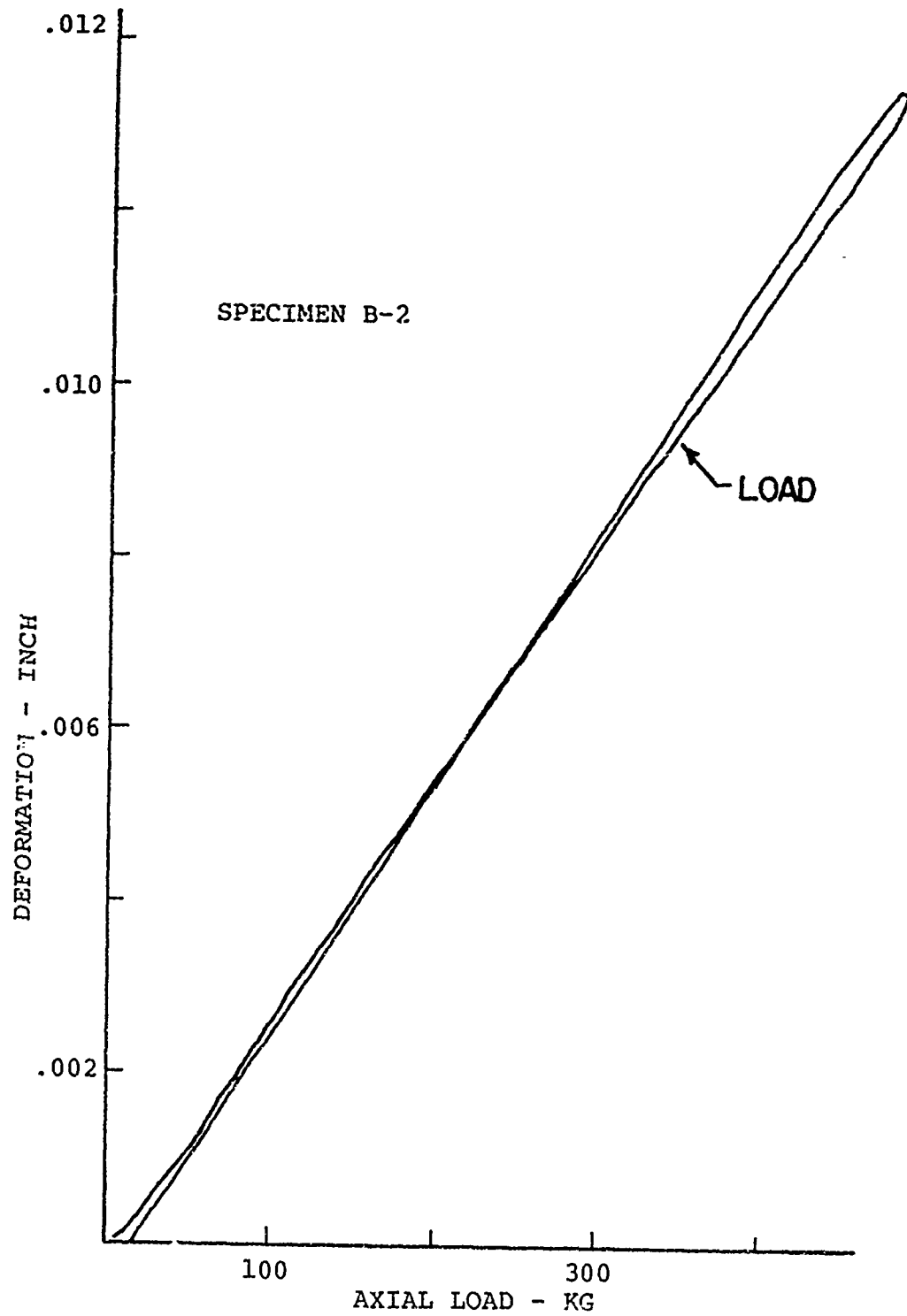


FIGURE (4-6) TYPICAL PRIMARY ELASTIC MODULUS LOAD VS. DEFORMATION DATA

TABLE (4-3)
SUMMARY OF MODULUS MEASUREMENTS
1002 S MATERIAL

ELASTIC PROPERTY $\times 10^6$ (PSI)	BOEING VERTOL DATA		ULTRASONIC MEASUREMENT DATA		INSTRON STATIC TEST DATA	
	(AVERAGE VALUE)		(AVERAGE VALUE)		(AVERAGE VALUE)	
E ₁₁	6.5		6.35		5.97	
E ₂₂	2.1		2.4		-	
E ₃₃	2.1 (Assumed)		2.4		-	
G ₁₂	.50		-		-	
G ₁₃	.50 (Assumed)		-		-	
G ₂₃	.50 (Assumed)		-		-	
ν	.25		.23		-	

A summary of the ultrasonic static and Boeing-Vertol accepted moduli values are stated in table (4-3). The ultrasonic measurements of E_{11} are seen to be larger than the static measurements of E_{11} by about $.35 \times 10^6$, yet all ultrasonically measured properties are very close to the accepted Boeing-Vertol data. No obvious reason for this slight discrepancy is known other than normal experimental scatter. Moreover, it was decided that the Boeing-Vertol data was excellent for the 1002 S material being used in this test program. As a result all calculations employ the numerical values of the elastic constants supplied by the Boeing-Vertol Company.

B. ULTIMATE STRENGTH AND STRESS STRAIN DATA
OF THE ADHEREND MATERIAL.

The objective of this phase of the test program was to determine the ultimate strength of 1002 S prepreg material in an all 0° and a $45^{\circ}/0^{\circ}/-45^{\circ}/0^{\circ}$ lay-up pattern. Also the load-deformation curves of the material were desired.

The tests were performed using the Instron Model TT-DM test machine. Test loads were introduced through cross-ply tabs bonded to the specimen ends. A typical specimen configuration is shown in Figure (4-7). Specimens B1 - B3 are the all 0° items while specimens F21 - F24 are the $45^{\circ}/0^{\circ}/-45^{\circ}/0^{\circ}$ items.

All loading was applied at a crosshead rate of .05 cm/min. and at room temperature. Axial displacements were recorded using a Tinius-Olsen S1 extensometer. The test set up is shown in Figure (4-8). Load vs. displacement plots were recorded using a Moseley Model 7001 A x-y recorder. Figures (4-9), (4-10), (4-11) and (4-12) show the load-deformation plots. They are essentially linear until failure. The jagged marks on the uni-ply

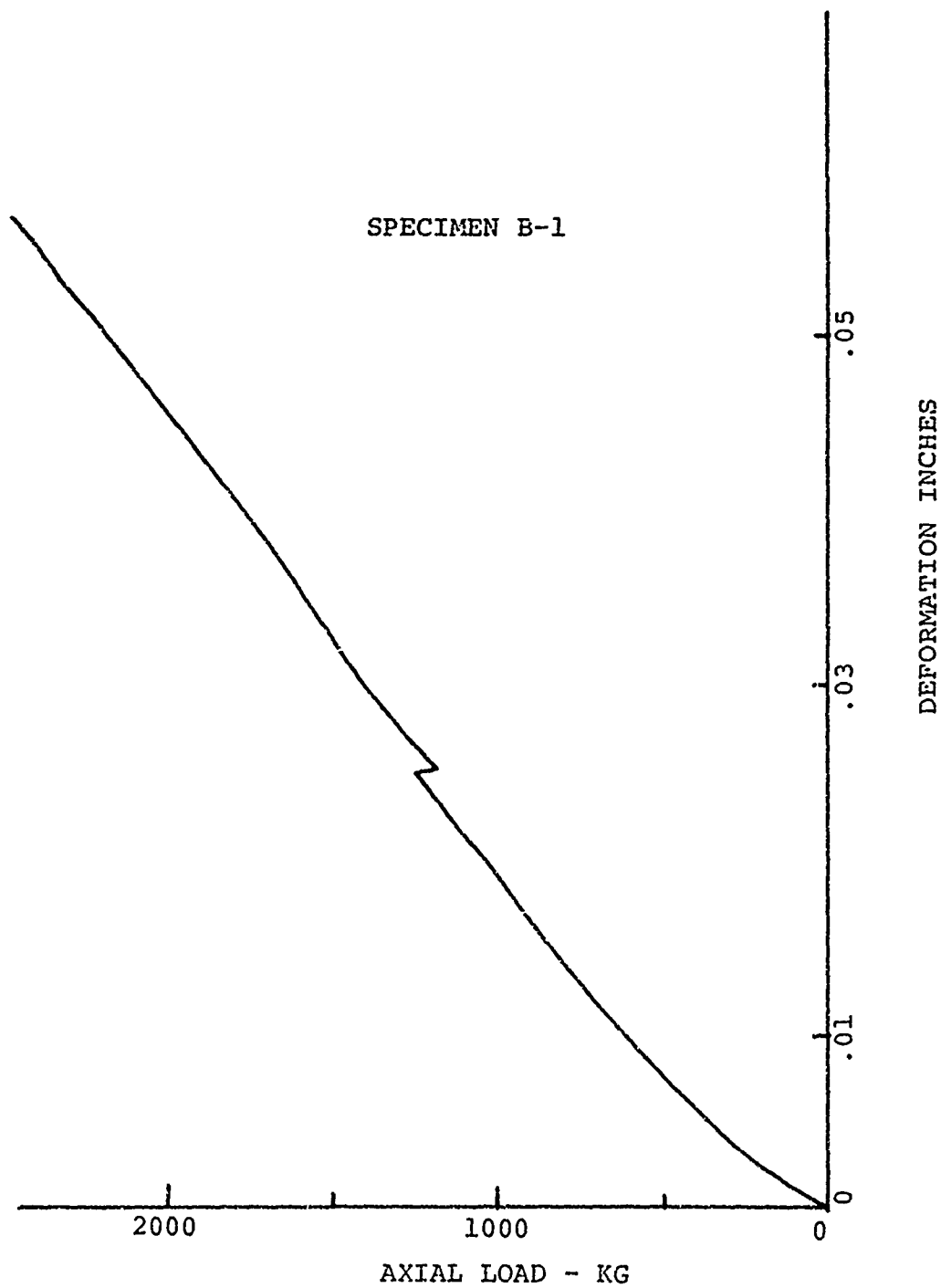


FIGURE (4-9) 1002-S PRE-PREG TAPE LOAD-DEFORMATION DATA

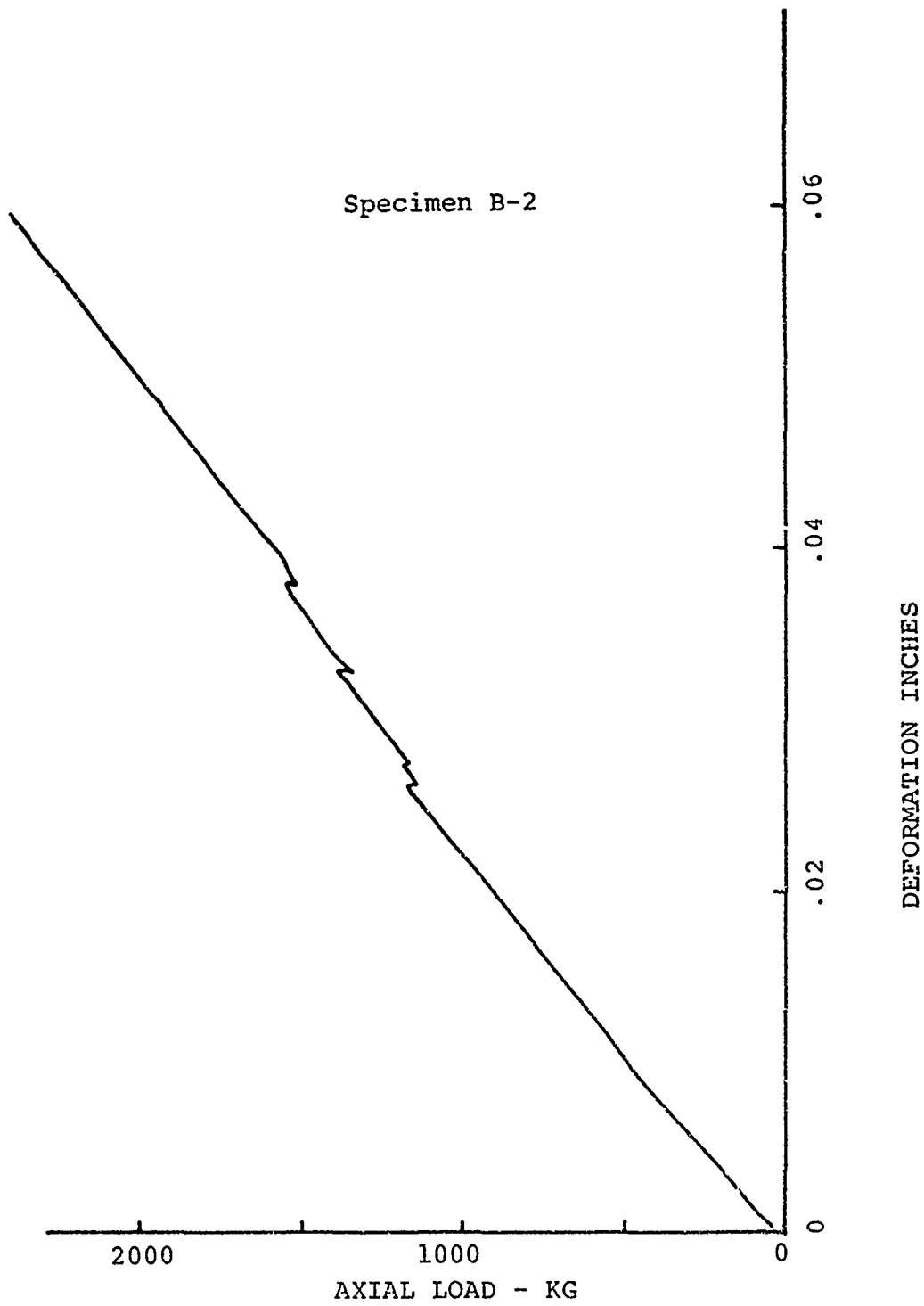


FIGURE (4-10) 1002-S PRE-PREG TAPE LOAD-DEFORMATION DATA

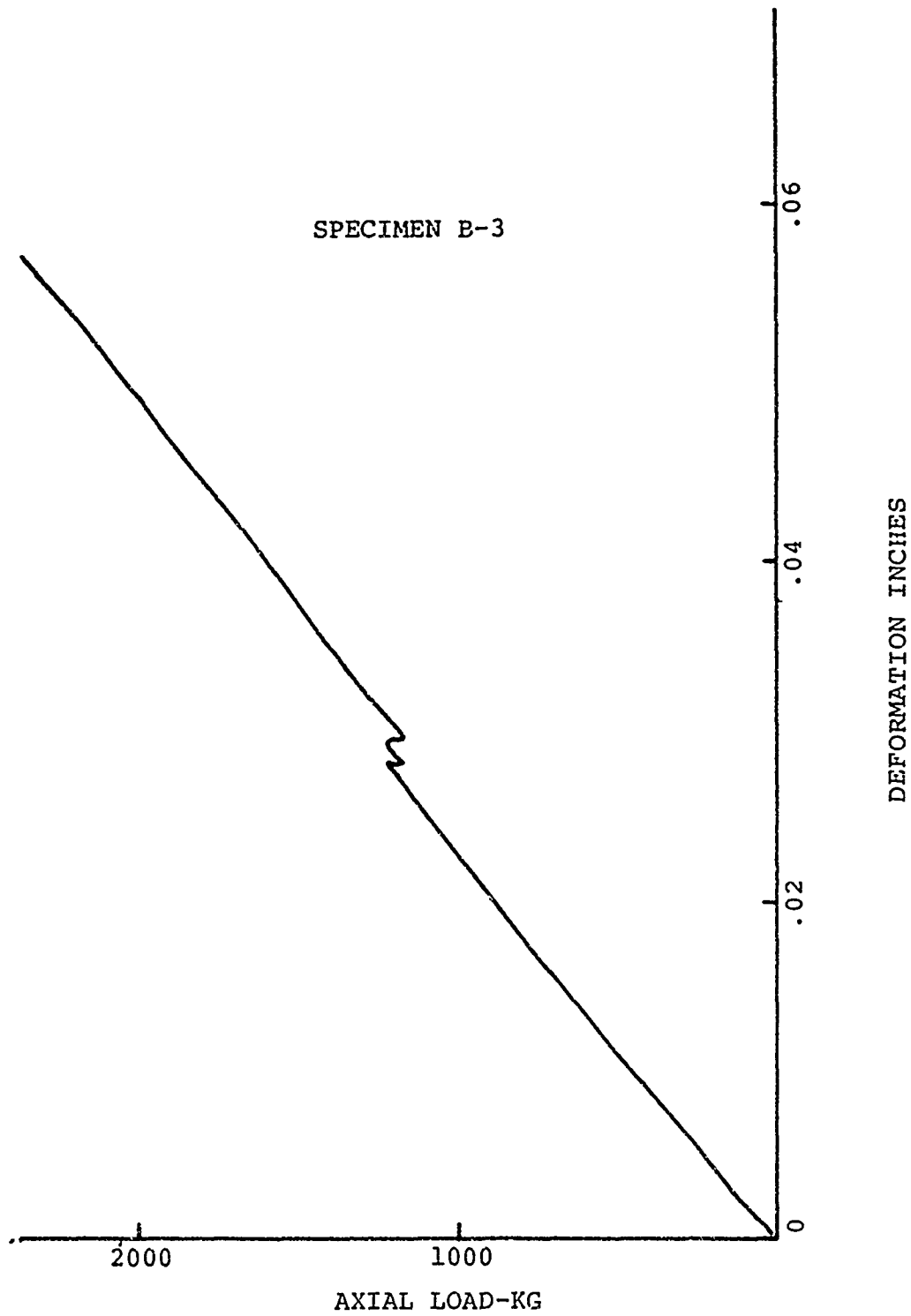
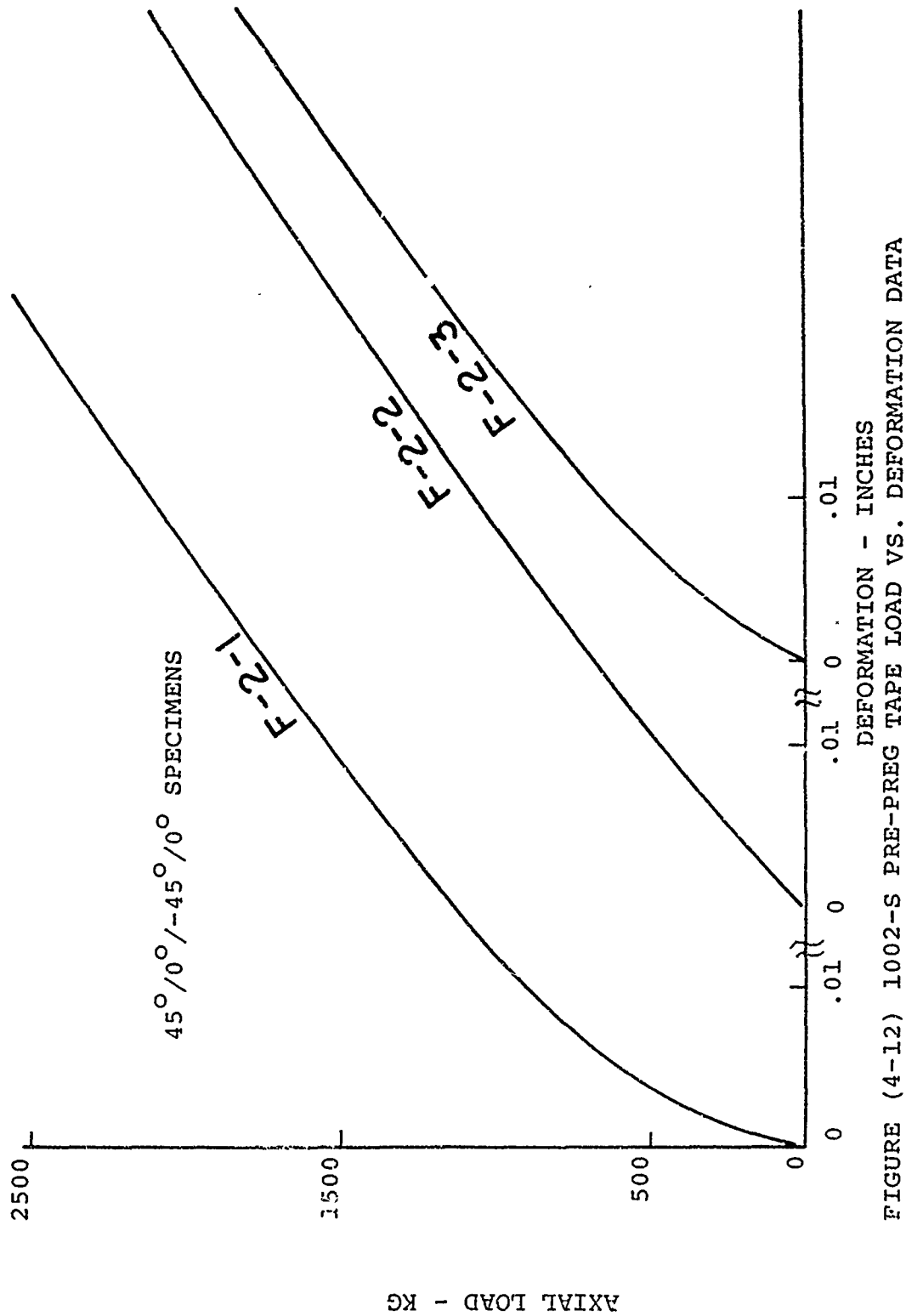


FIGURE (4-11) 1002-S PRE-PREG TAPE LOAD-DEFORMATION DATA



specimens are due to poor specimen design. They point out where the tapered area of the specimen marked (A) in Figure (4-7) broke away from the main specimen.

The ultimate load results are summarized in table (4-4). Pictures of the ultimately failed specimens are displayed in Figures (4-13) and (4-14). The failures were sudden, made a loud banging sound and were generally catastrophic. From table (4-4) one can see that the cross-ply specimens attained an ultimate load of 50 per cent of the all 0° specimens. This is attributed to loading the cross-ply specimens in an adverse manner which results in premature failure of the resin in shear and tension.

In conclusion, the ultimate stress levels attained in these tests are in good agreement with accepted design values for the 1002 S pre-preg material system.

TABLE (4-4)

SUMMARY OF ULTIMATE TEST RESULTS
1002 S PRE-PREG TAPE

SPEC. NO.	LAMINATE PATTERN	LAMINATE Thickness Width		AREA (In)	ULT. LOAD		ULT. STRESS	REMARKS
		(In)	(In)		(kg)	(kg)		
B1	All 0°	.066	.386	.0254	2740		237754.	
B2	All 0°	.067	.386	.0258	2700.		230651.	
B3	All 0°	.071	.386	.0274	2770.		222813.	
					AVG. =		230406.	
F21	45/0/-45/0	.069	1.014	.0699	3690.		116348.	
F22	45/0/-45/0	.069	1.025	.0707	3590.		111914.	
F24	45/0/-45/0	.069	1.004	.0692	3700.		117843.	
					AVG. =		115368.	



Figure (4-13) All 0° Adherend Ultimate Failure Specimen

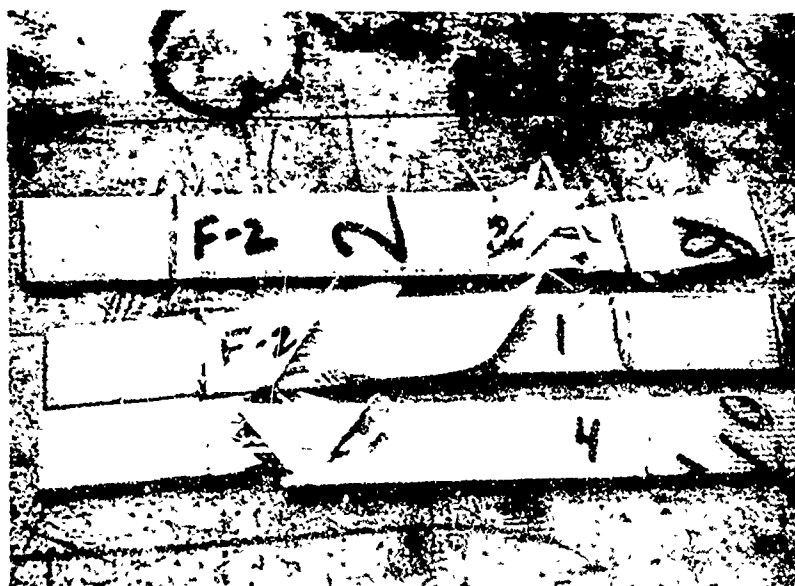


Figure (4-14) $45^{\circ}/0^{\circ}/-45^{\circ}/0^{\circ}$ Adherend Ultimate Failure Specimen

C. SHEAR MODULUS TESTS

Based on the assumptions of the analysis outlined earlier it is necessary to obtain accurate values of the proportional limit and the shear modulus of the adhesive as they exist within the constrained environment of the joint. Also, the general shape of the shear stress-strain curve of EA951 adhesive is needed. These data are presented in this section. Furthermore, the results presented herein reflect the effects of varying the adhesive thickness and varying the overlap length of the joint. The effect of the orientation of the lamina adjacent to the adhesive will also be investigated for both $\theta = 45^\circ$ and 0° .

The test piece selected to determine the desired adhesive properties is shown in Figure (4-15). Basically it is two 0.25 inch thick laminates bonded together with the EA951 adhesive. After curing the material is cut as specified in Figure (4-16) to provide a theoretically ideal adhesive lap shear test piece. The assumption in using this test piece, to acquire the adhesive properties in the constrained environment, is that the two adherends are essentially rigid bodies compared to the soft,

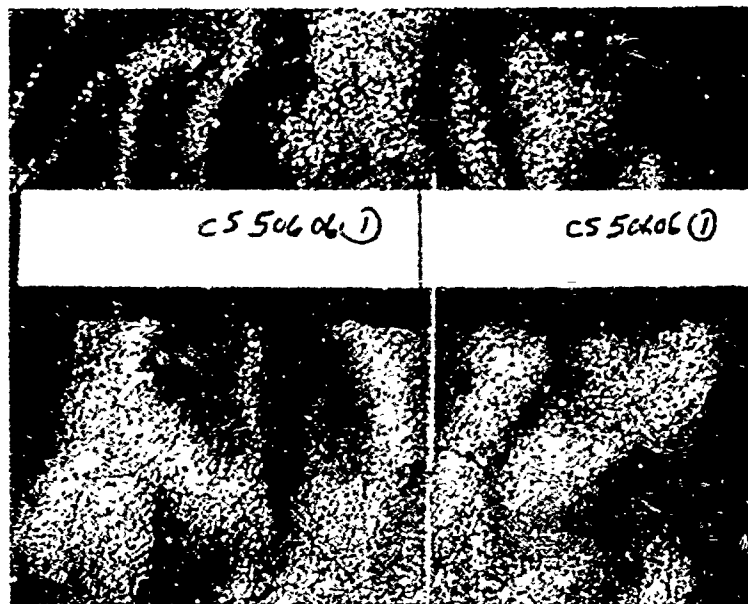


Figure (4-15) Adhesive Shear Modulus Test Specimens

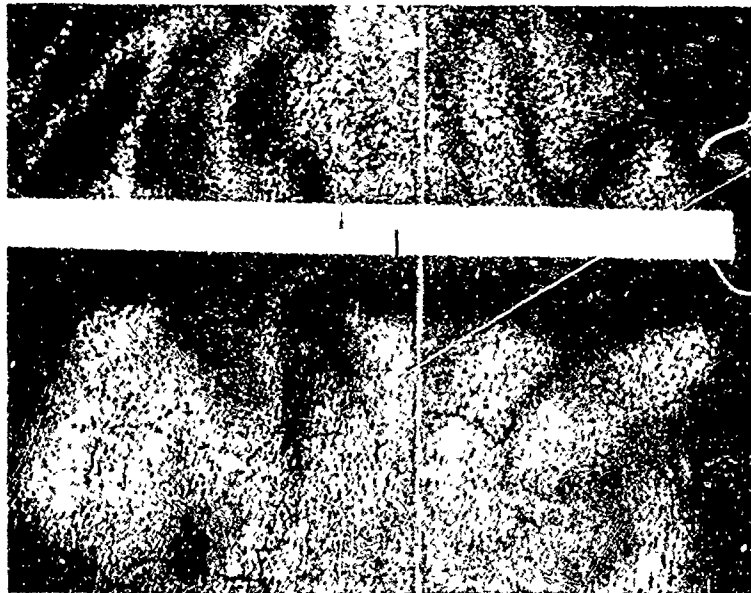


Figure (4-16) Ideal Adhesive Lap Shear Joint

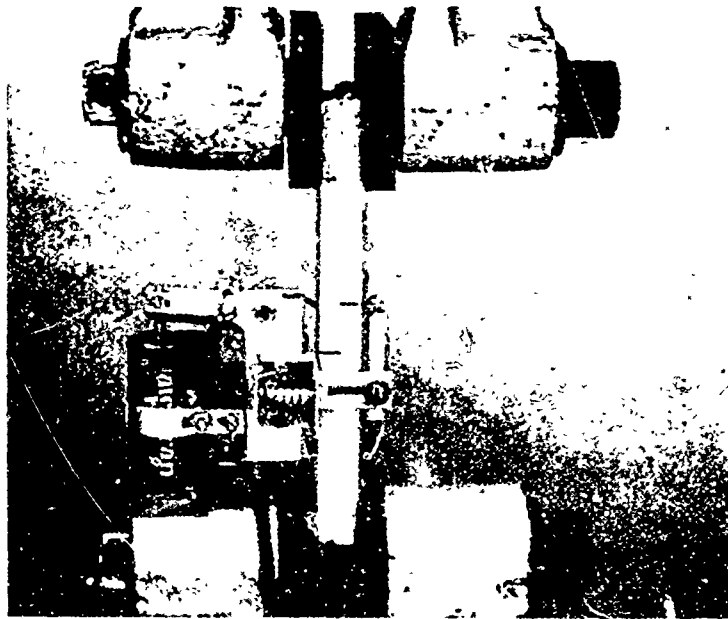


Figure (4-17) Adhesive Modulus Test Set-Up

elastomeric nature of the adhesive. Thus if in the joint area one mounts a zero length extensometer as shown in Figure (4-17) one can measure quite accurately the deformation of the adhesive, especially in the lower load range, to determine adhesive shear modulus and proportional limit.

The test pieces were fabricated at the Boeing-Vertol Company in two steps. First, the thick adherends, approximately .25 inches thick x 24" x 12" were layed up in a mold using 1002 S pre-preg tape. The adherends were then cured in an autoclave at 320 Fahrenheit. Next, the two parcels were bonded together using EA951 film in two basic thicknesses of 2.5 mils and 10 mils. The film was layed on one adherend and then the other adherend was layed on top of the film. The adhesive was cured at 50 psi and 350° Fahrenheit. After this final cure the test pieces were cut from the panel approximately one inch wide each. Finally, a precision cut was made through the thickness of the adherends to give the concentric lap shear specimen shown in Figure (4-15).

Fertinent data of each test piece were measured and are tabulated in Tables (4-5) and (4-6). All dimensions except the adhesive thickness were measured by

TABLE (4-5) SUMMARY OF SHEAR SPECIMEN TEST RESULTS

SPEC.NO.	ADHESIVE THICKNESS (In)	OVERLAP (In)	WIDTH (In)	EFFECTIVE SHEAR MODU- LUS (PSI)	PROPERT. LIMIT LOAD(KG)	ULT. LOAD STRAIN (KG) (In/In)	TYPE FAILURE
XCS50310-1	.0111	.297	.996				Broke
-2	.0108	.290	.998	7990	120	590	Adhesive
-3	.0096	.278	1.010	9110	120	528	Adhesive
XCS50610-1	.0093	.602	1.005	10053	140	1060	Primarily Adh.
-2	.0130	.604	.995	7443	110 (4th load)	1110	Primarily Adh.
-3	.0127	.604	1.005	9200	120	1140	Primarily Adh.
XCS50302-1	.0034	.300	1.004	3110	170	542	Cohesive
-2	.0031	.280	.991	3927	160	528	Cohesive
-3	.0040	.302	1.006	3850	120 (6th load)	568	Cohesive
XCS50602-1	.0034	.600	1.016	1586	140	918	Resin
-2	.0031	.615	1.000	1453	-	950	Resin
-3	.0034	.615	1.001	1769	130	835	Resin

45°/0°/-45°/0° Adherends
EA951 Film

TABLE (4-6) SUMMARY OF SHEAR SPECIMEN TEST RESULTS

SPEC.NC.	ADHESIVE THICKNESS (In)	OVERLAP (In)	WIDTH (In)	EFFECTIVE SHEAR MODU- LUS (PSI)	PROPT. LIMIT LOAD(KG)	ULT. LOAD (KG)	ULT. STRAIN (In/In)	TYPE FAILURE
CS50304-1	.0034	.31	.998	5659.	140	490	1.49	Cohesive
-2	.0034	.325	1.000	6156	-	690	-	Cohesive
-3	.0037	.295	1.005	4236	145	630	-	Cohesive
CS50306-1	.0093	.283	.994	17107	150	608	3.875	Adhesive
-2	.0136	.290	1.000	20187	145	600	-	Adhesive
-3	.0087	.296	1.015	12800	160	662	-	Adhesive
CS50606-1	.0087	.600	1.012	2700	165	1265	3.2	Adhesive
-2	.0077	.594	.992	6036	140	1080	-	Adhesive
-3	.0080	.596	1.005	5119	180	1320	-	Adhesive
CS50604-1	.0034	.600	1.005	2485	160	1070	-	Cohesive
-2	.0031	.600	.997	3311	150	1080	-	Cohesive
-3	.0031	.602	1.000	2270	150	1080	-	Cohesive

All 0° Adherends
EA951 Film

means of a micrometer. The adhesive thickness was determined using a Zeiss optical microscope with a magnification of 80 x. The measurements represent an average adhesive thickness as the interface between the adherend and glue line undulated smoothly as shown in Figure (4-18). In numerous instances the adhesive thickness in the undulated area was thicker than the nominal dimensions of the film. The overall test set-up includes a Tinius-Olsen Model S1 LVDT to measure deformation, an amplifier to amplify the signal from the LVDT, an Instron Model TT-DM testing machine to apply the load, and a Moseley Model 7001A x-y recorder to record the load-deformation information.

The test procedure was:

1. Calibrate the Instron testing machine and the x-y recorder.
2. Place the specimen in the top grip, making sure the specimen hangs in a true vertical position. Put on the lower grip and tighten, being sure that the specimen is not pre-loaded. This is accomplished using the load release lever on the Instron control panel.

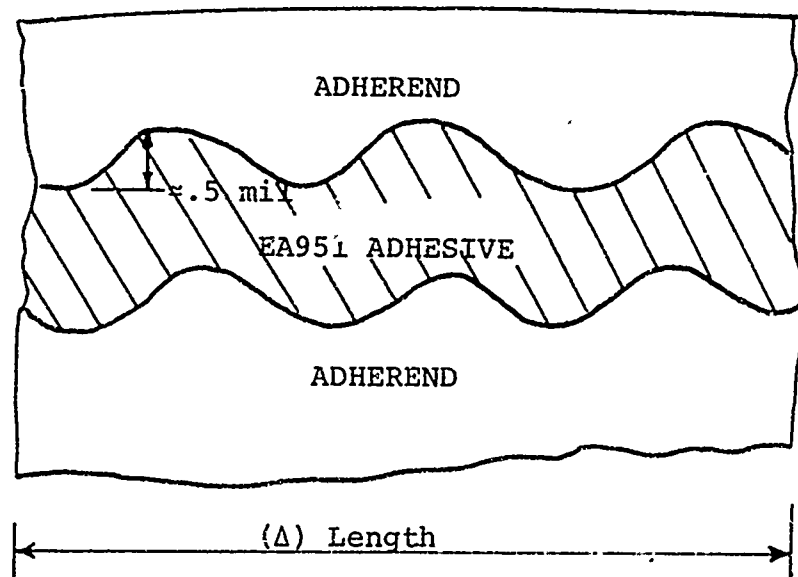


FIGURE (4-18) ENLARGEMENT OF ADHESIVE - ADHEREND
INTERFACE

3. Strike a horizontal line on the specimen where you wish to put the knife edges.
Put the LVDT on the specimen and line up knife edges with this horizontal line.
4. Select the load and deformation scales desired. For most of this test data a 20 kilogram load scale was used with a deformation magnification accurate to 25×10^{-6} inches.
5. Set the load rate to .05 centimeters per minute and set the specimen by preloading it to ten kilograms. This improved the initial segment of the load vs. deformation curve. Load the specimen, recording load vs. deformation data.

In analyzing the test procedure for possible errors, several items are worthy of discussion. As mentioned earlier, the interface between the adhesive and the adherend undulates evenly over the length of the bond. However, this variation was no more than 5 per cent of the overall adhesive thickness and at this time is thought to be insignificant in determining an accurate gage length for the modulus measurements.

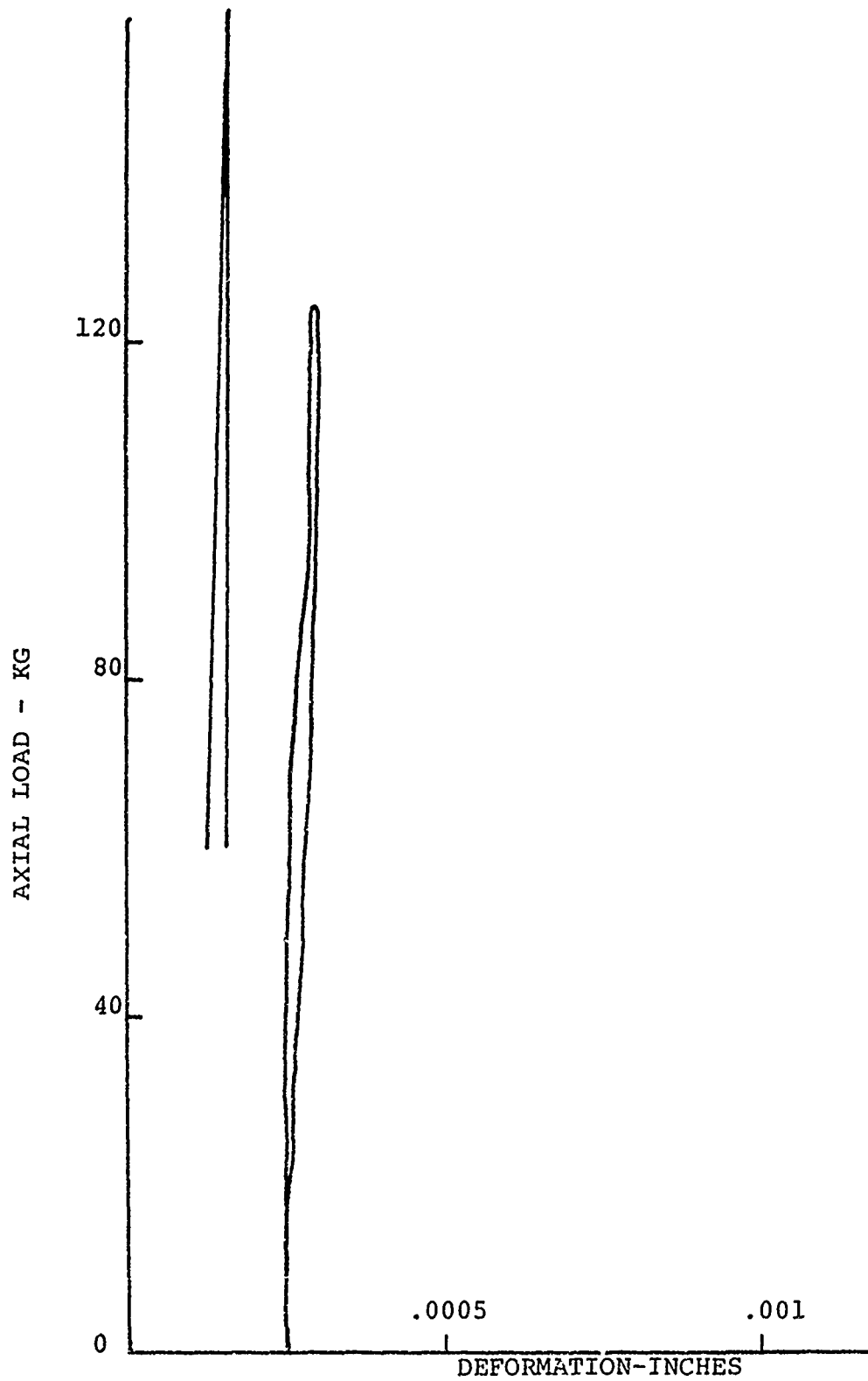


FIGURE (4-19) TYPICAL PROOF TEST OF ZERO LENGTH EXTENSOMETER

Another source of error is the alignment of the knife edges on the specimen such that one has a true zero length extensometer. To check out the LVDT used, the knife edges were lined up visually on regular tensile specimens and load-deformation plots were recorded for the lower load range within which the data for shear modulus and proportional limit load were determined. Figure (4-19) shows the results of a typical proof test on a fiberglass specimen. While the plot would show an error of 10 per cent in some cases, the precision of the LVDT is such that half this error can be attributed to the accuracy limits of the system. Thus overall a maximum error of 5 per cent can be attributed to the positioning of the knife edges.

Finally, it was noted that the LVDT exhibited a nonlinear response over part of its range. The tests were conducted with an eye to staying within the linear range of the extensometer. However, an error up to 5 per cent, could have been introduced due to this factor. Thus, in summary it is felt the data in this section pertaining to shear modulus and the proportional limit of the adhesive are in error by at most ten per cent, as it is believed highly unlikely that the worst case of all probably errors would occur simultaneously.

Before evaluating the test results, one must realize that in most instances of statistical evaluation of the test data one has at best a small sample with which to project the trends of an assumed normal population distribution. This is especially true in determining the effective shear modulus. Therefore, while certain data points look out of line from the general trend and statistically speaking could be discarded (i.e. Chauvenet's criterion), it is believed by the author to be in the best interest of all who interpret these results to view the total picture. Therefore, all data points are included in the evaluation of the test data.

The statistical data given in Figures (4-29) to (4-37) assumes a linear regression analysis to be valid as one only has two distinct data points to study. From these one can get the best fit line through the data plus a measure of the interdependence of the x-axis variable on the y-axis variable. This is given by the correlation coefficient whereby a value of ± 1 means perfect correlation. The mean \pm two standard deviations from the mean give one a 95 per cent confidence that the mean falls within the band (I) specified.

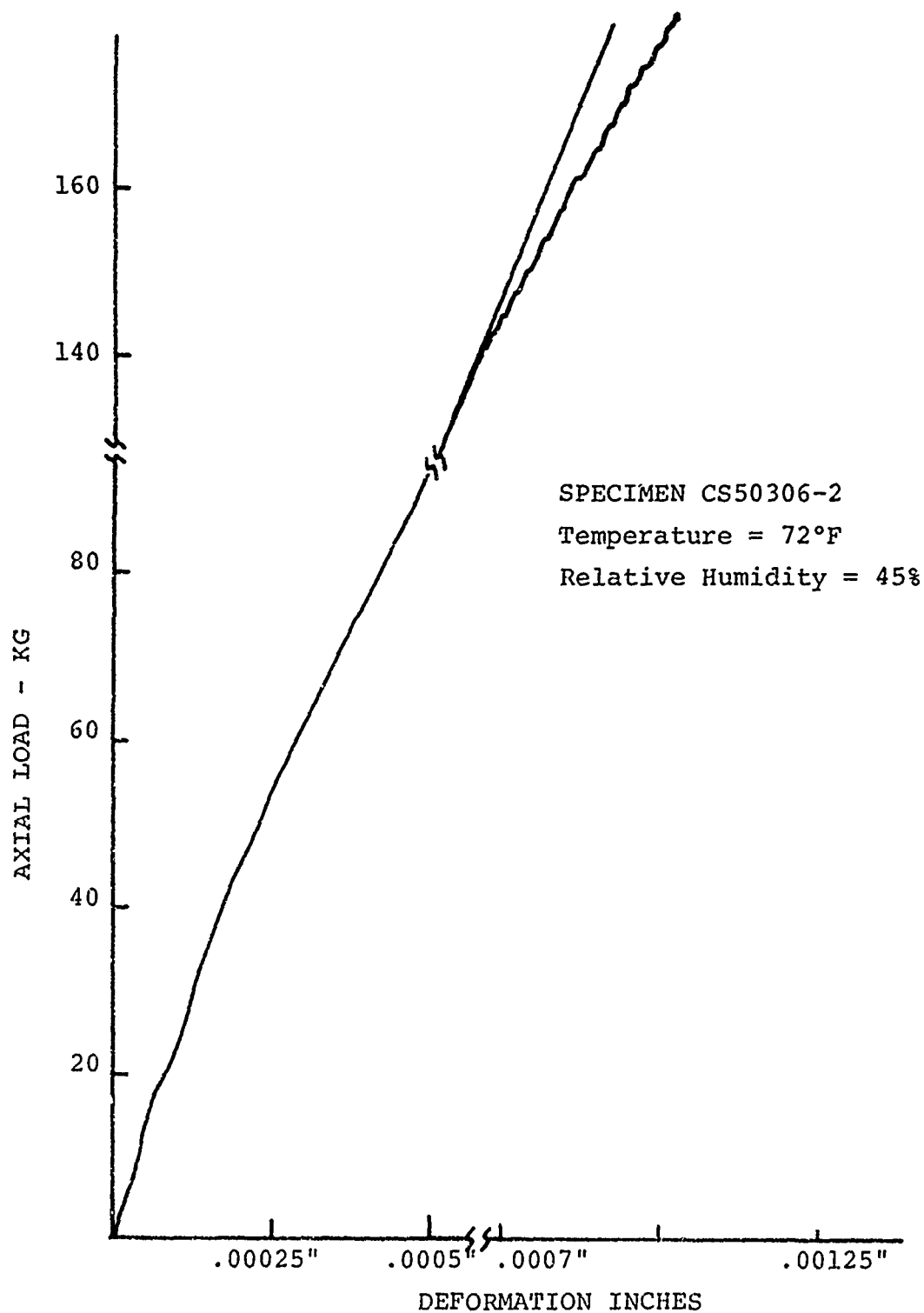


FIGURE (4-20) ADHESIVE SHEAR LOAD DEFORMATION DATA

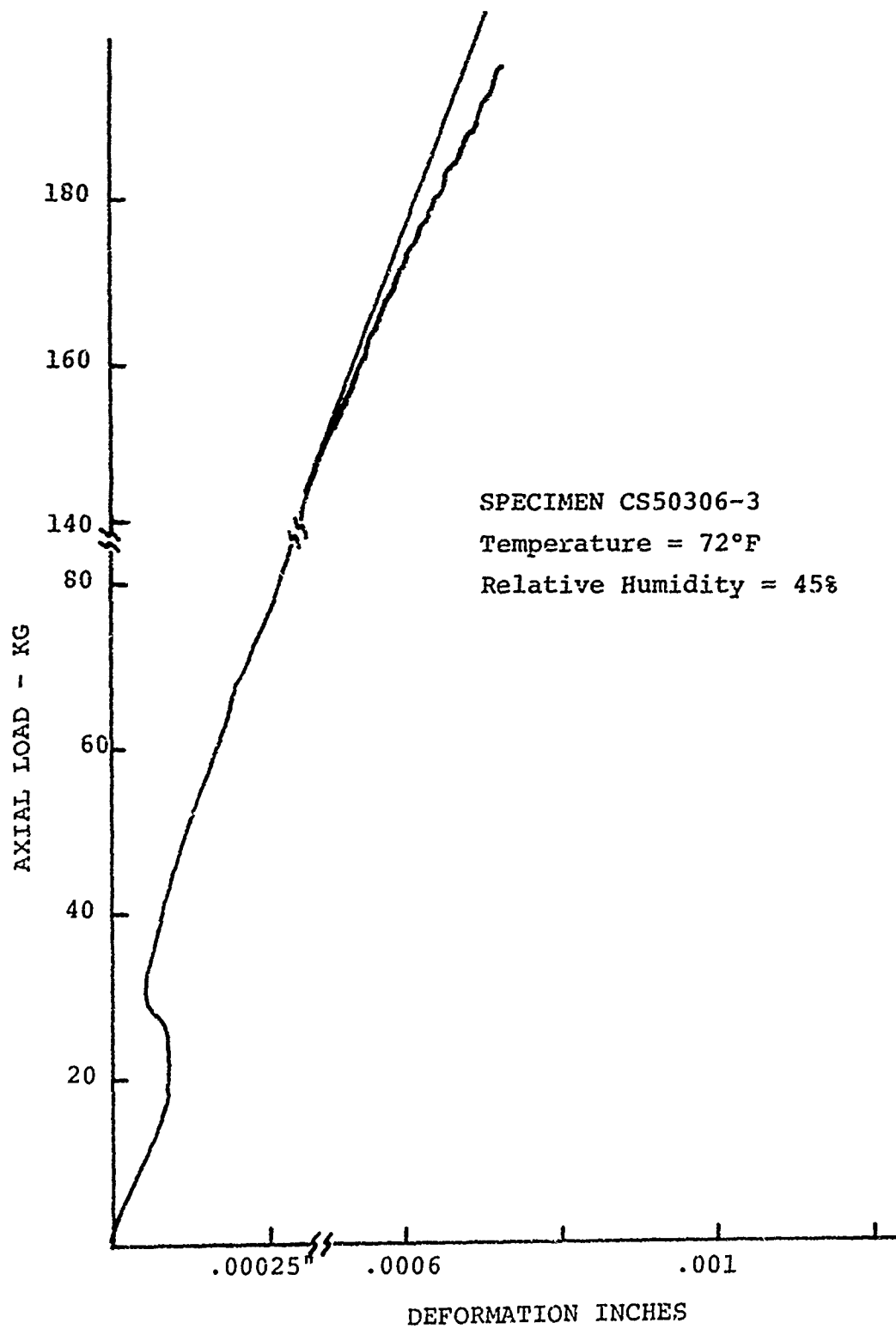


FIGURE (4-21) ADHESIVE SHEAR LOAD DEFORMATION DATA

The effective shear modulus was calculated from the typical load-deformation curves of Figures (4-20) and (4-21). All the data were recorded at a strain rate of .05 cm/min, a temperature of 72° F. and a relative humidity range of from 30-45 per cent. The effective shear modulus (G) was calculated by determining the slope of the load deformation curve over its first 100 kilograms of loading. Therefore the effective shear modulus can be found by

$$G_{(psi)} = \frac{(100KG) (2.204\#/KG)}{\frac{\text{Deformation (Overlap) (Width)}}{\text{Adhesive}}} \quad (4-4)$$

Pertinent dimensions and a summary of the range of (G) values are given in Tables (4-5) and (4-6). One should note that the range of effective shear moduli is from 1500 psi to 20,000 psi accounting for the parametric variables studied. These were (1) orientation of plys in adherends. The two configurations looked at were (a) an all uni-ply adherend, (b) a +45°/0°/-45°/0° adherend with the 45° layer always adjacent to the adhesive. (2) The length of overlap -0.30" and 0.60" were used. (3) The adhesive thickness. Again two nominal thicknesses were used, a 2.5 mil and a 10 mil film. However, on numerous occasions the measured ad-

Reproduced from
best available copy.

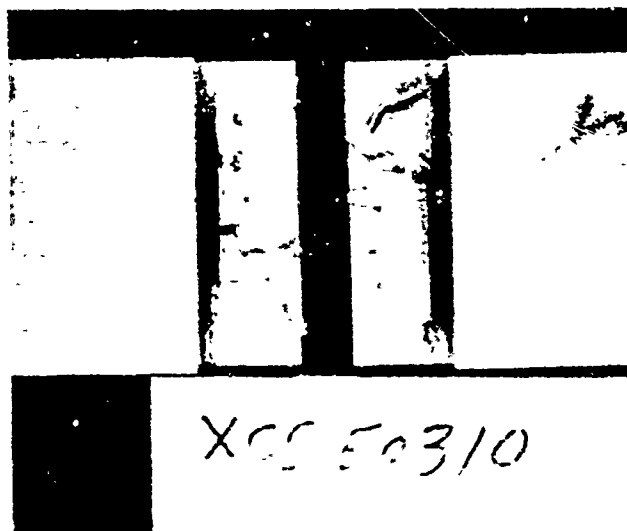


FIGURE (4-22) TYPICAL ADHESIVE SHEAR TEST FAILURE

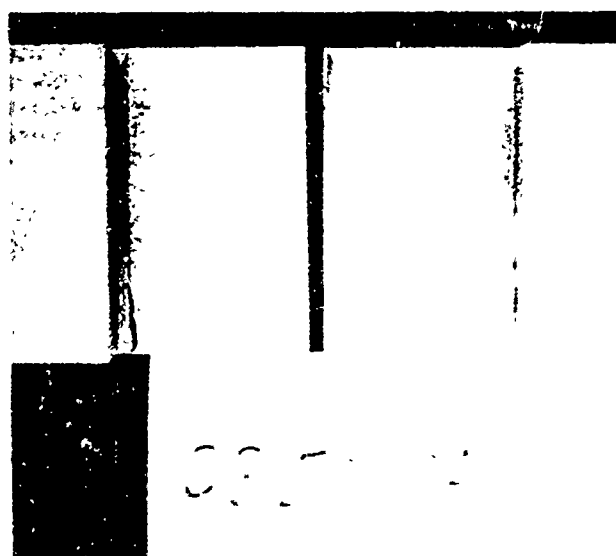


FIGURE (4-23) TYPICAL ADHESIVE SHEAR TEST FAILURE

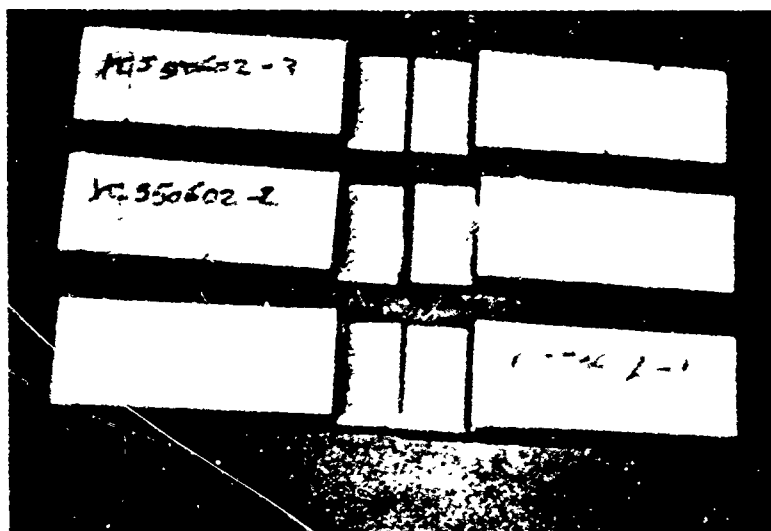


FIGURE (4-24) TYPICAL ADHESIVE SHEAR TEST
RESIN FAILURE

hesive thickness was somewhat larger than the baseline dimension.

The type of failures experienced were primarily adhesive and cohesive. These are shown in Figures (4-22) and (4-23) respectively. However, one set of three specimens (.60 inch overlap, .003 inch adhesive) did fail in the resin and this failure is shown in Figure (4-24). Moreover, the .60 inch overlap and 10 mil adhesive appeared to have a secondary failure initiating in the resin

One final point should be made before evaluating the data. Concern has been expressed that the test was not the idealized pure shear test one hoped it to be. Possibly the adherends did deform appreciably and influence the results and/or the shear strain was not uniform over the length of the overlap. To prove or disprove these fears a grid was marked on a test piece as shown in Figure (4-25). This specimen was then loaded and filmed. The results are shown in Figures (4-26) and (4-27) and (4-28). Summarily they show that over all except the open end of the joint the shear strain is uniform. Moreover, the grid lines on the adherends remained vertical even to the ultimate load

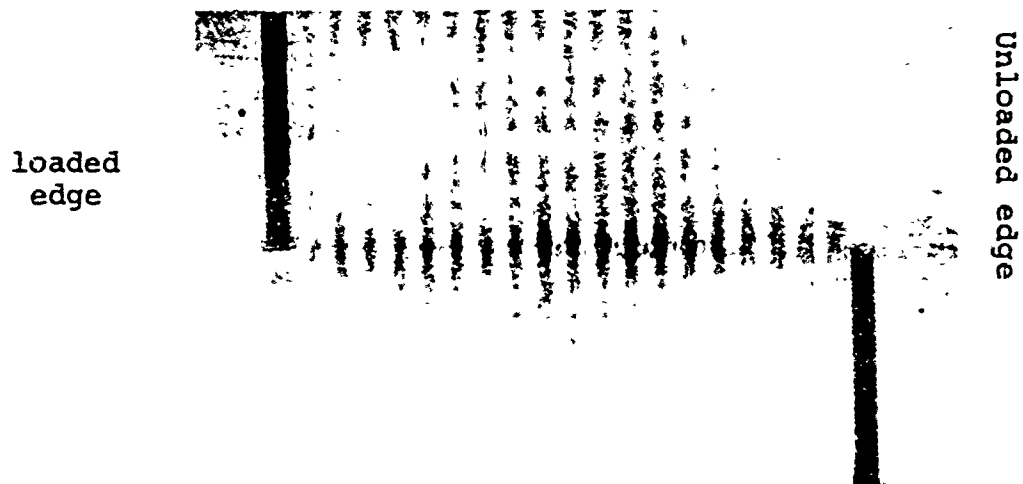


Figure (4-25) Grid Marked Test Specimen

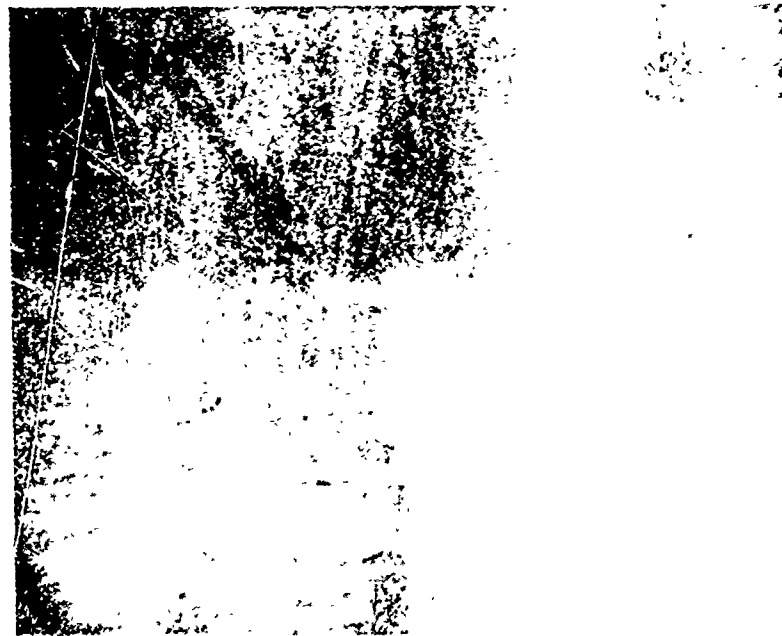


Figure (4-26) Grid Slope in Middle of Joint Under Load



Figure (4-27) Grid Marks in Open End Area Under Load



Figure (4-28) Grid Marks in Closed End Area Under Load

of the adhesive. Therefore, the test is considered to be a legitimate test for calculating the properties of adhesives as they exist within the constrained environment of the joint.

The first parametric variable studied was the effect of the adhesive thickness vs. the effective shear modulus. Figures (4-29) and (4-30) show these results for an overlap of 0.30" and 0.60" respectively. The results consistently show a trend that the shear modulus increases as the adhesive thickness increases. Moreover, for three of the four plots the correlation factor is sufficiently high enough that the element of chance causing this is rather small. One possible explanation is that the flaws, always within a material, are much more critical for the thinner adhesives, thus effectively reducing its modulus.

Moreover, two examples of related research are known by the author. The first is a McDonald-Douglas report on bonded and bolted joints, (Reference 22) They too observed a significant scatter of modulus data using a conventional thin cylindrical torsion shear test. Their results suggested that the shear modulus decreased as the adhesive thickness increased. Moreover,

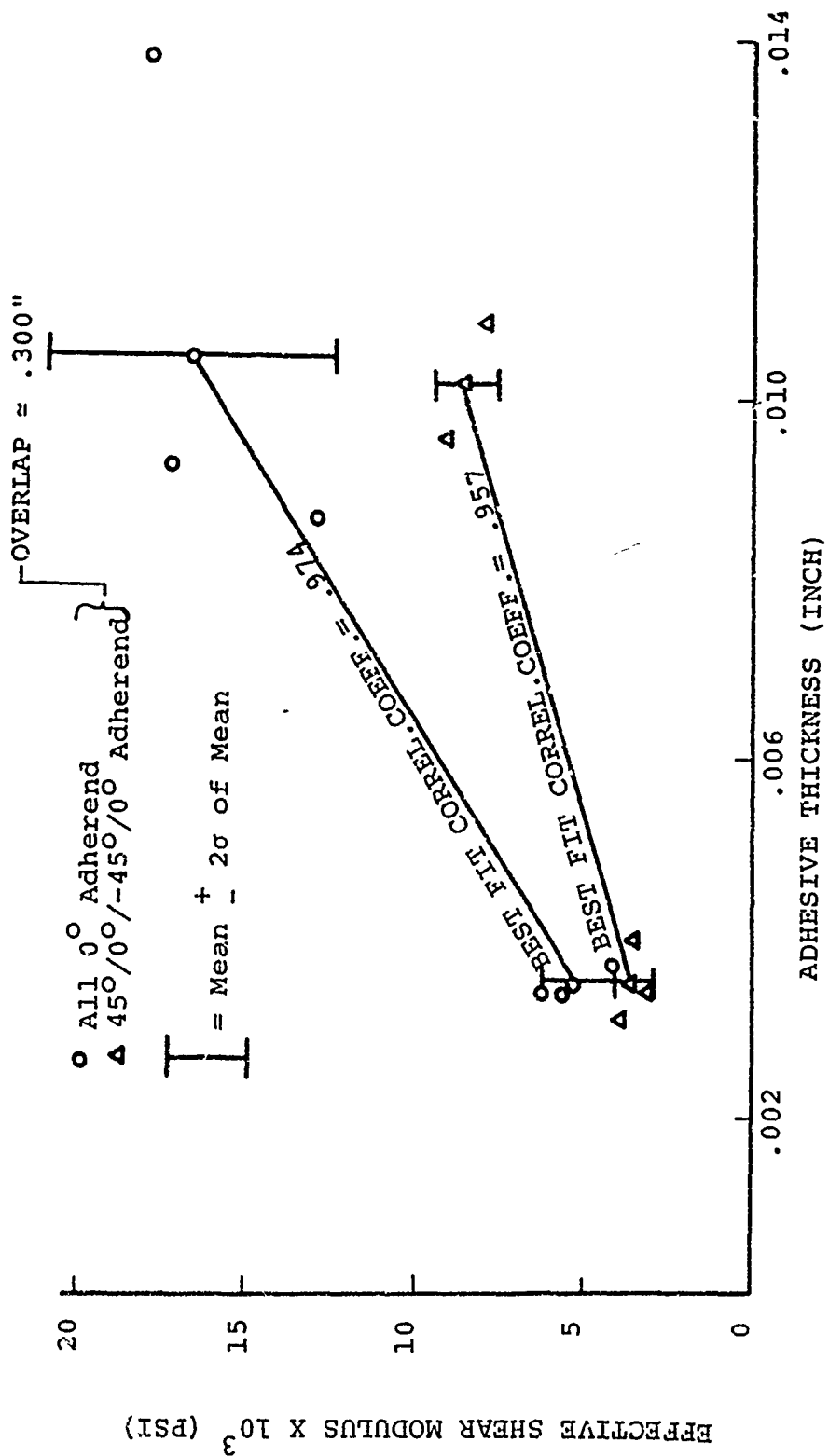


FIGURE (4-29) ADHESIVE EFFECTIVE SHEAR MODULUS VS. ADHESIVE THICKNESS

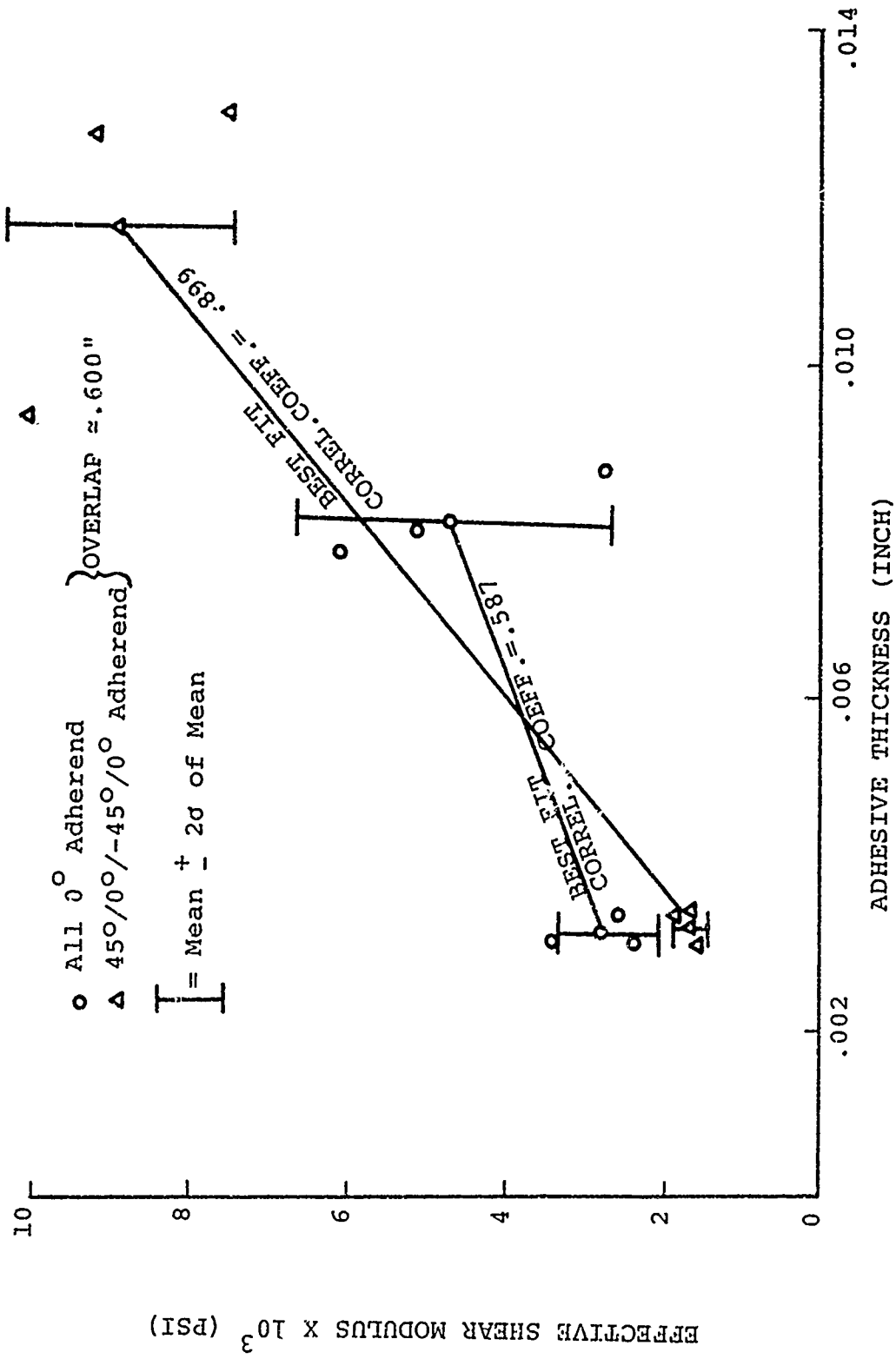


FIGURE (4-30) ADHESIVE EFFECTIVE SHEAR MODULUS VS. ADHESIVE THICKNESS

they generated their results for adhesive thicknesses of primarily from 10 to 16 mils. This contradiction could possibly be explained by the difference in test specimens (ring vs. lap joint) and/or test procedure (torsion vs. axial load). Moreover, the fact that the author's adhesive thickness range of 3 mils to 12 mils was significantly removed from the 10 to 16 mil tests run by McDonald-Douglas, may be nothing more than the generation of legitimate data in the very thin film range. Finally, the discrepancy could have been attributed partly or in whole to the significant differences in adherend stiffnesses between stainless steel and fiberglass material systems. This fact is modestly substantiated by the work of Hughes and Rutherford (59) who used a similar torsion ring test to calculate the shear modulus of more rigid resin systems. Their results, which again showed considerable scatter, indicate that aluminum vs. stainless steel adherends did give different modulus measurements with the aluminum's measurements being slightly lower. Their results were for the 8 to 35 mil range, for several resin systems. They found no dependence of thickness vs. shear modulus over this range of adhesive thicknesses.

The effect of Poisson's ratio may also be

considered. One realizes that for the difference of Poisson's ratio between the adherend and adhesive material systems to have an effect one must investigate a dimensional change in the adhesive under load. In the shear test this is not the case. In a pure shear test one only changes the orientation of the material. Thus the effect of Poisson's ratio on the results is believed to be negligible.

Finally, in observing Figures (4-29) and (4-30) the effect of ply orientation would seem to be minimal at best. This could imply that the angle of the ply next to the adhesive has no effect and/or the modest change in adherend stiffness for the two adherends tested was insignificant.

The influence of overlap length vs. effective shear modulus is shown in Figures (4-31) and (4-32) for a thickness of the adhesive from 8 to 13 mils and 3 mils respectively.

While the influence of ply orientation is readily seen to be modest at best, the decrease of the effective shear modulus vs. overlap length would seem to be very clearly defined by three of the four curves. Any attempt

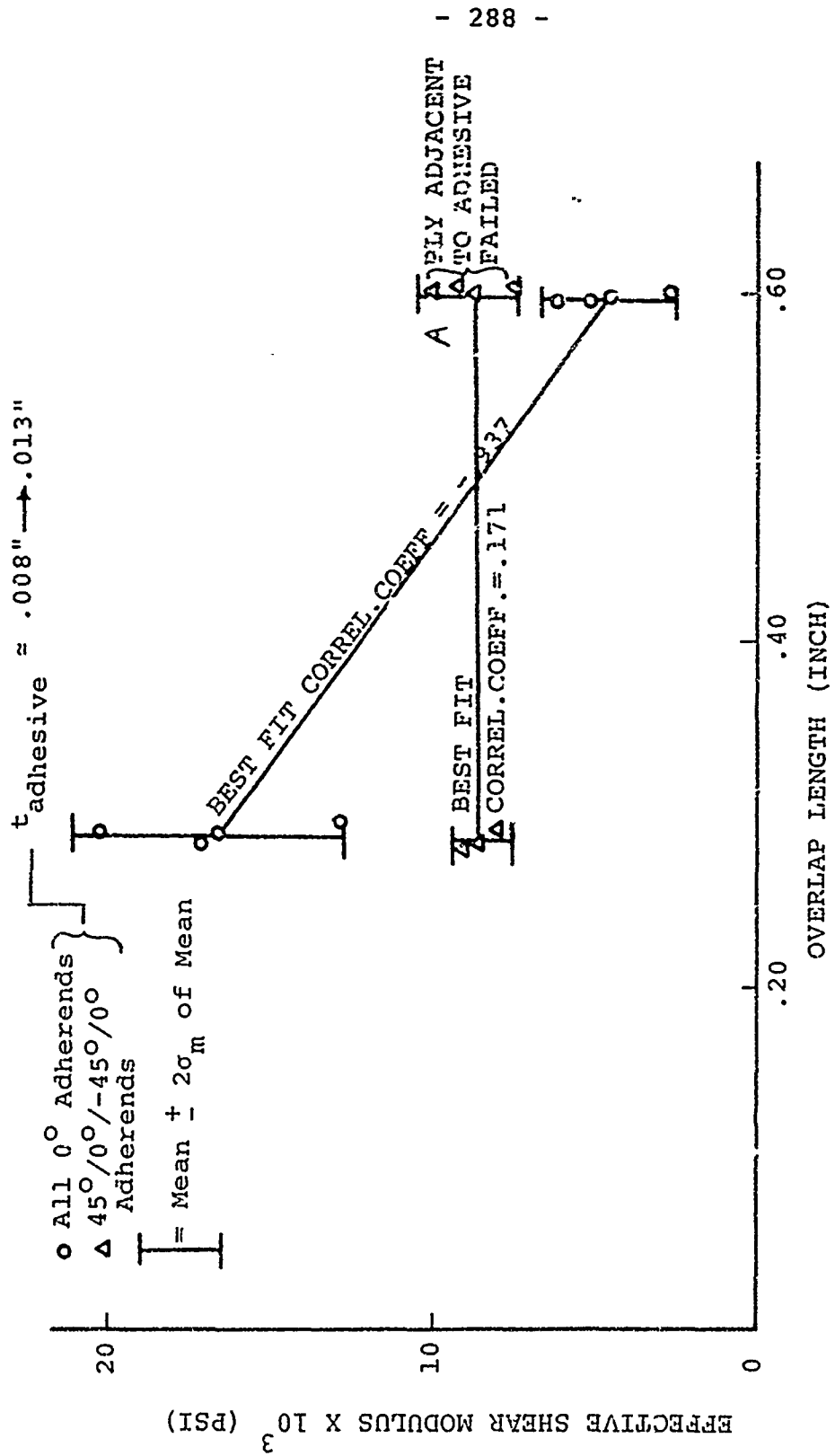


FIGURE (4-31) ADHESIVE EFFECTIVE SHEAR MODULUS VS. OVERLAP LENGTH

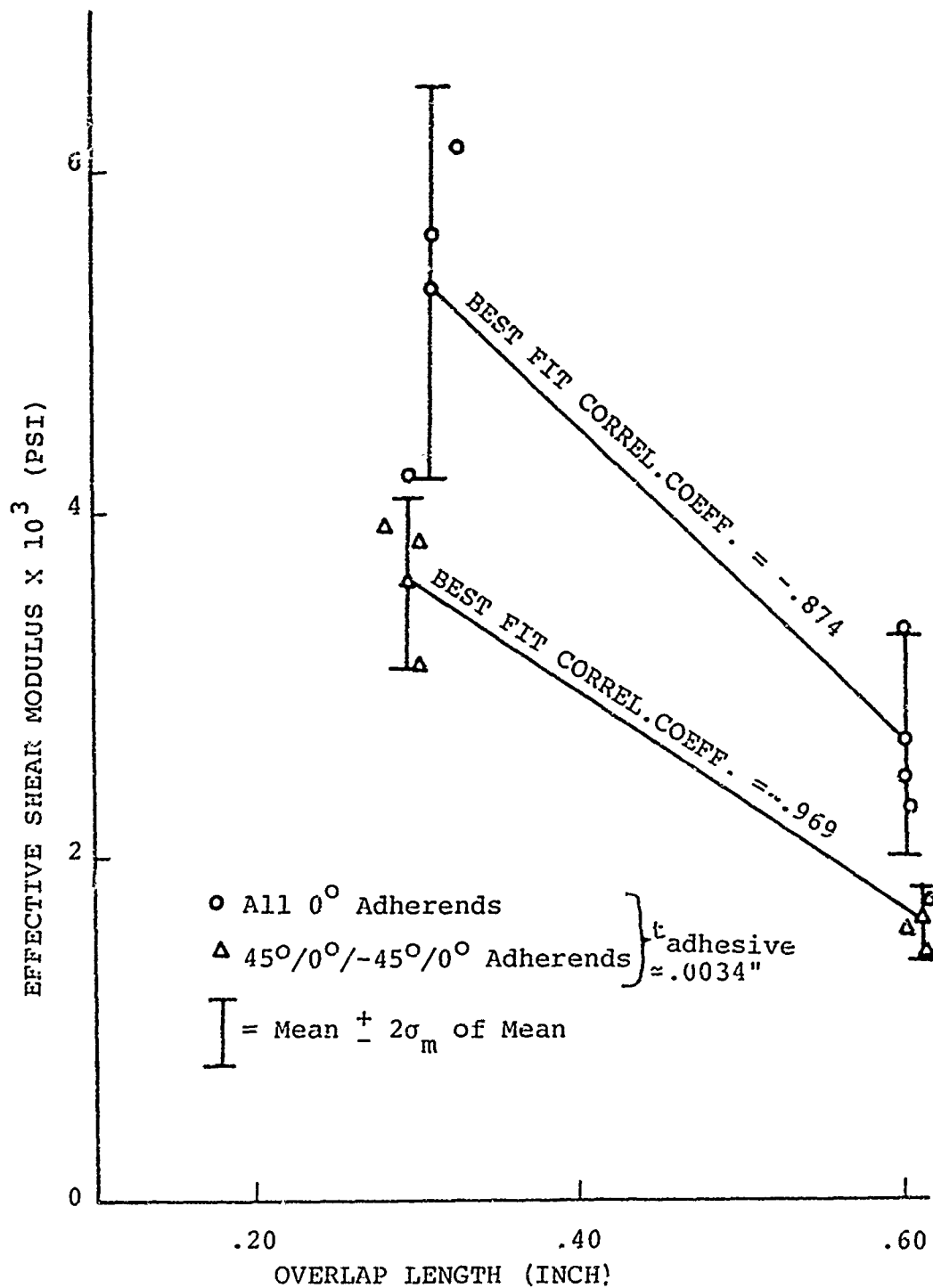


FIGURE (4-32) ADHESIVE EFFECTIVE SHEAR MODULUS VS. OVERLAP LENGTH

to explain why the one curve deviates from a trend based on so few data points is at best conjecture. However, the group of data marked (A) in Figure (4-31) did fail in a mixed mode. While the resin failed in the fibers adjacent to the adhesive, the primary mode of failure was thought to be in the adhesive itself. Possibly this had some unexplained effect.

In concluding this discussion on shear modulus several comments as to the relatively low values of the modulus are felt necessary.

First, the EA951 adhesive is an epoxy-nylon film whose granular make-up is felt to put it in a category with elastomers. Thus, one would expect low modulus values. Second, the overall scatter of data is not unusual as in Reference (22), modulus values of from 13 KSI to 26 KSI for EA951 film were observed using the torsion ring shear test.

It was very desirable to determine the proportional limit of the adhesive during these tests. This was accomplished employing the graphs in Figures (4-20) and (4-21) to determine where the curve broke from its linearity. Moreover, another indicator of the proportional limit was thought to be the emergence of the saw tooth effect on

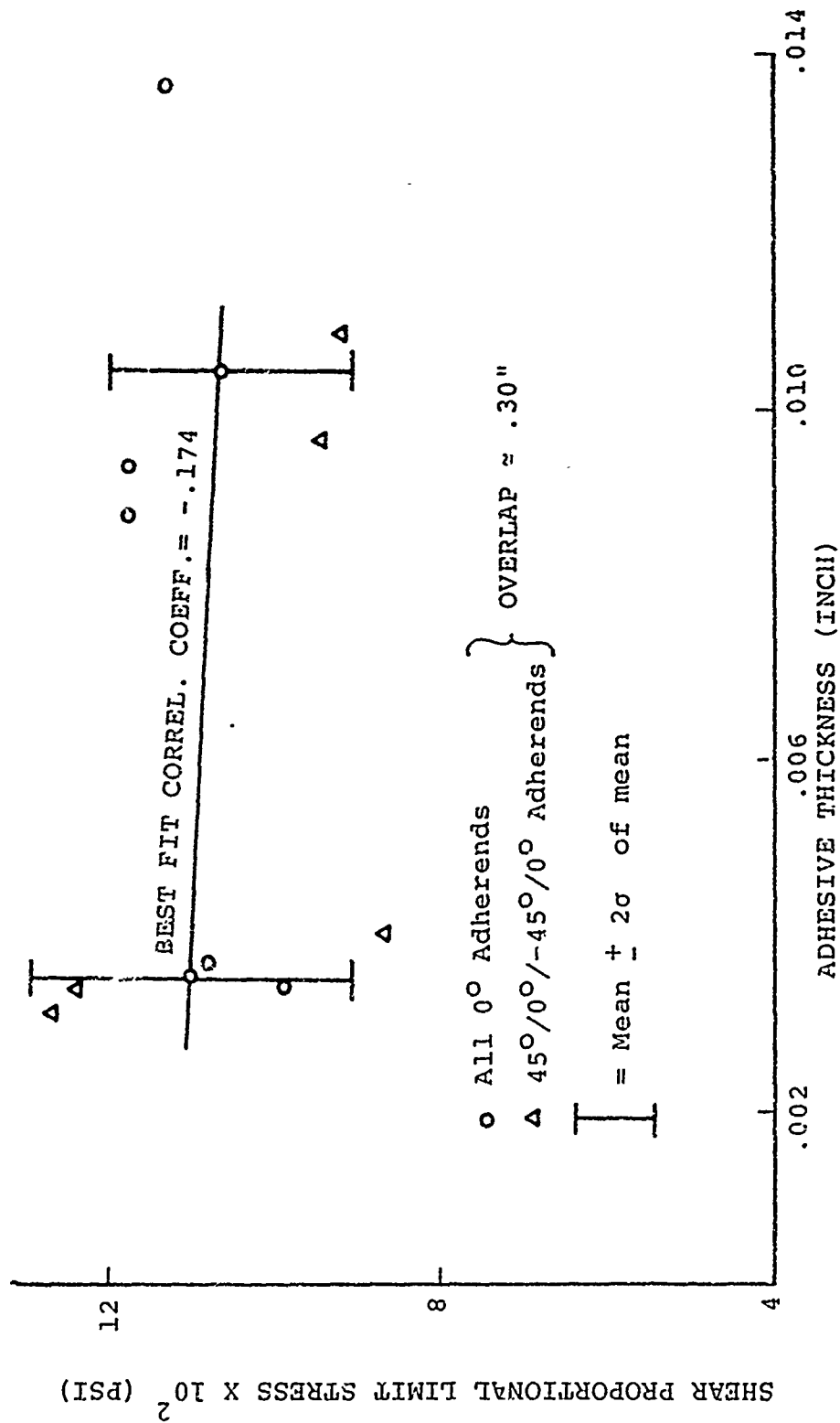


FIGURE (4-33) ADHESIVE THICKNESS VS. PROPORTIONAL LIMIT STRESS

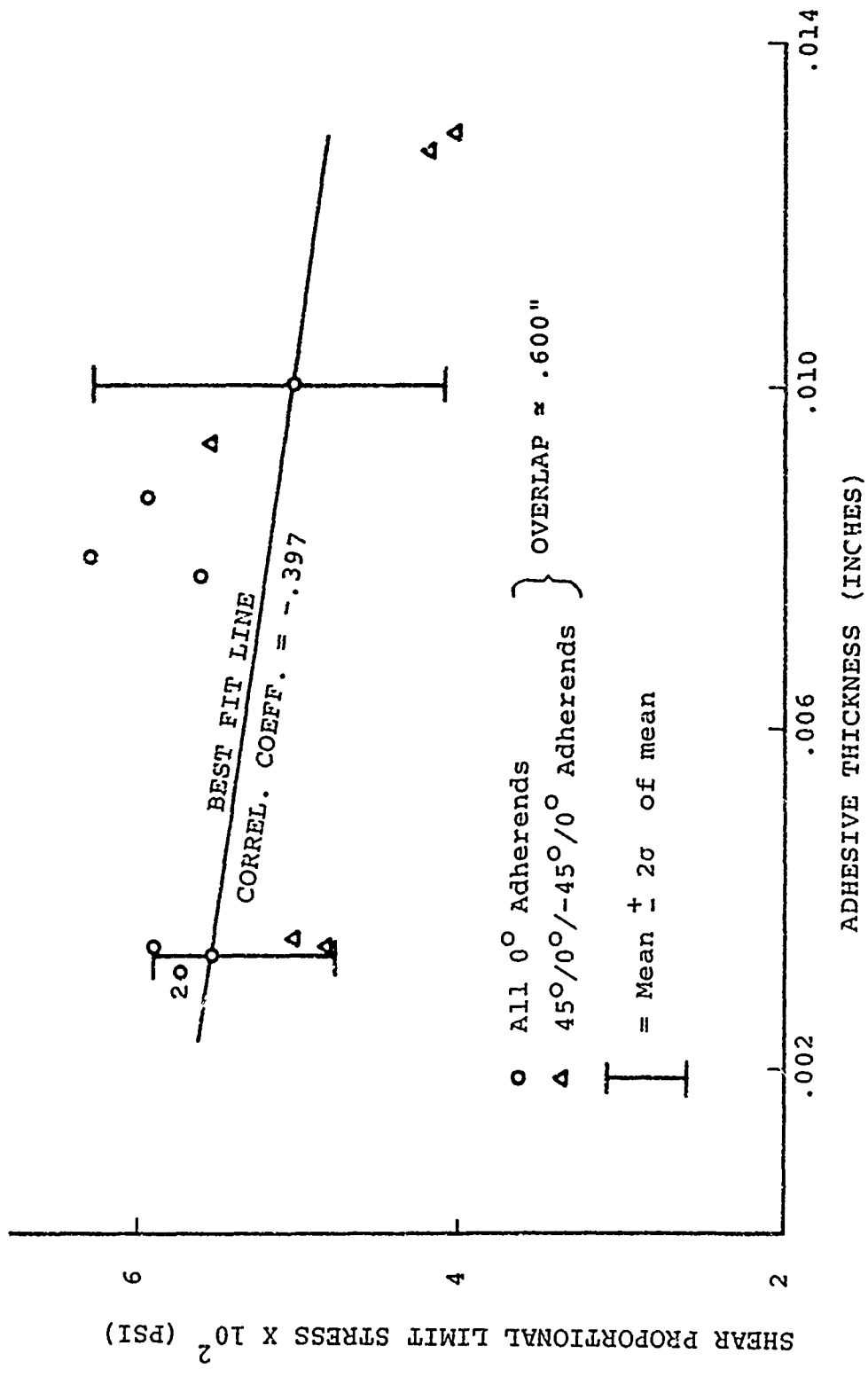


FIGURE (4-34) ADHESIVE THICKNESS VS. SHEAR PROPORTIONAL LIMIT

the upper part of the curves in Figures (4-20) and (4-21). It is theorized that the saw-tooth is really the material creeping rather rapidly. Moreover, it is known that the adhesive is very ductile displaying ultimate strains up to 380 per cent per table (4-6).

Figures (4-33) and (4-34) show in a straight forward manner that adhesive thickness has no effect on the proportional limit over the range of adhesive thicknesses tested. Moreover, the effect of ply orientation seems insignificant. In addition the effect of overlap on the proportional limit is presented in Figures (4-35) and (4-36). Results of Figure (4-35) would suggest that the proportional limit is a function of overlap. However, a further inspection Figure (4-36) reveals that if one looks at the proportional limit load the effect of overlap is minor. This would seem to be a true reading of the influence of geometrical variations on the proportional limit of the adhesive.

Figure (4-37) reveals the ultimate shear stress of the adhesive for all samples. The results seemed to be independent of any geometric variations. The average ultimate shear stress of the adhesive is found to be ≈ 4300 PSI for a .05 cm/min strain rate.

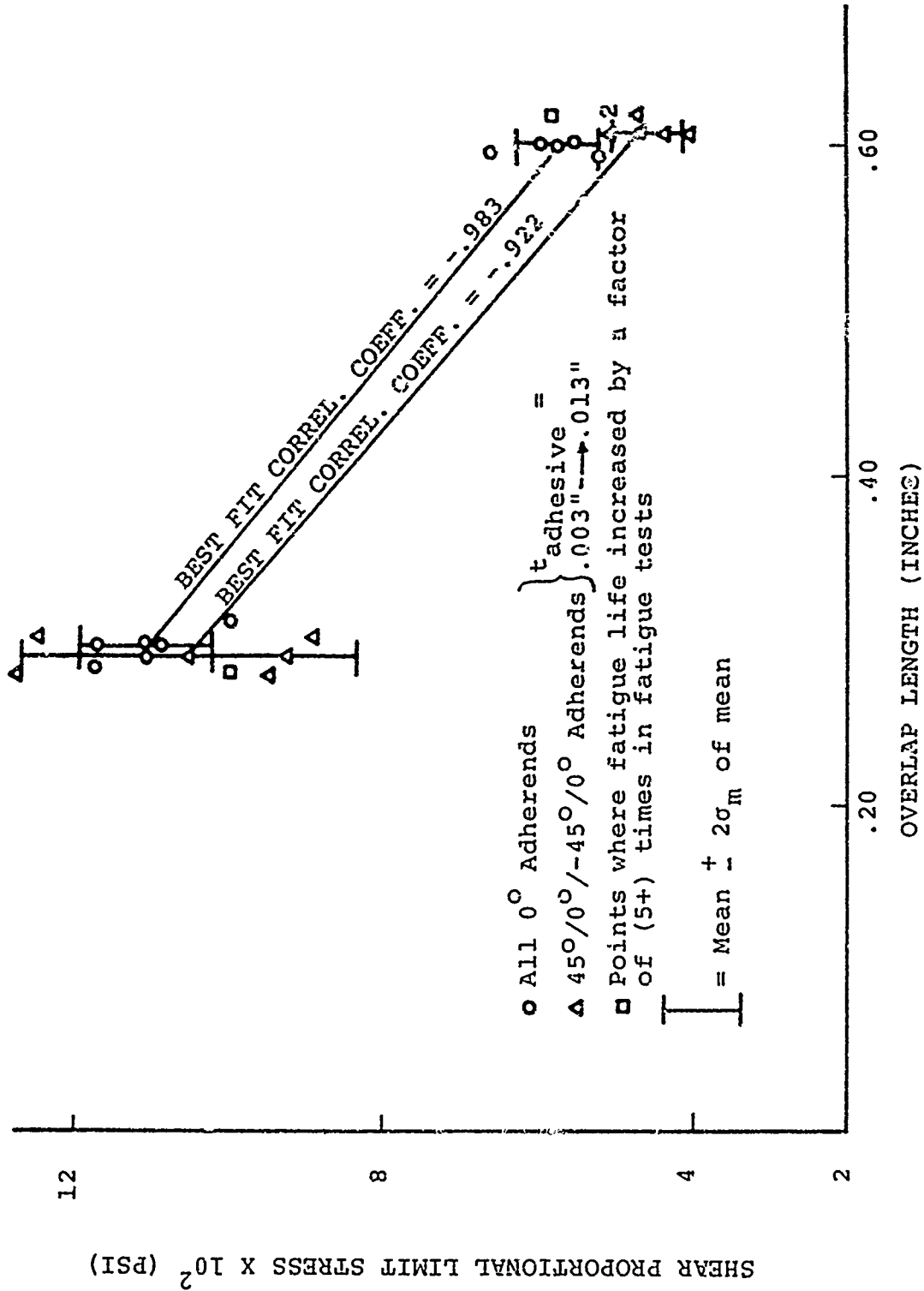


FIGURE (4-35) OVERLAP LENGTH VS. SHEAR PROPORTIONAL LIMIT

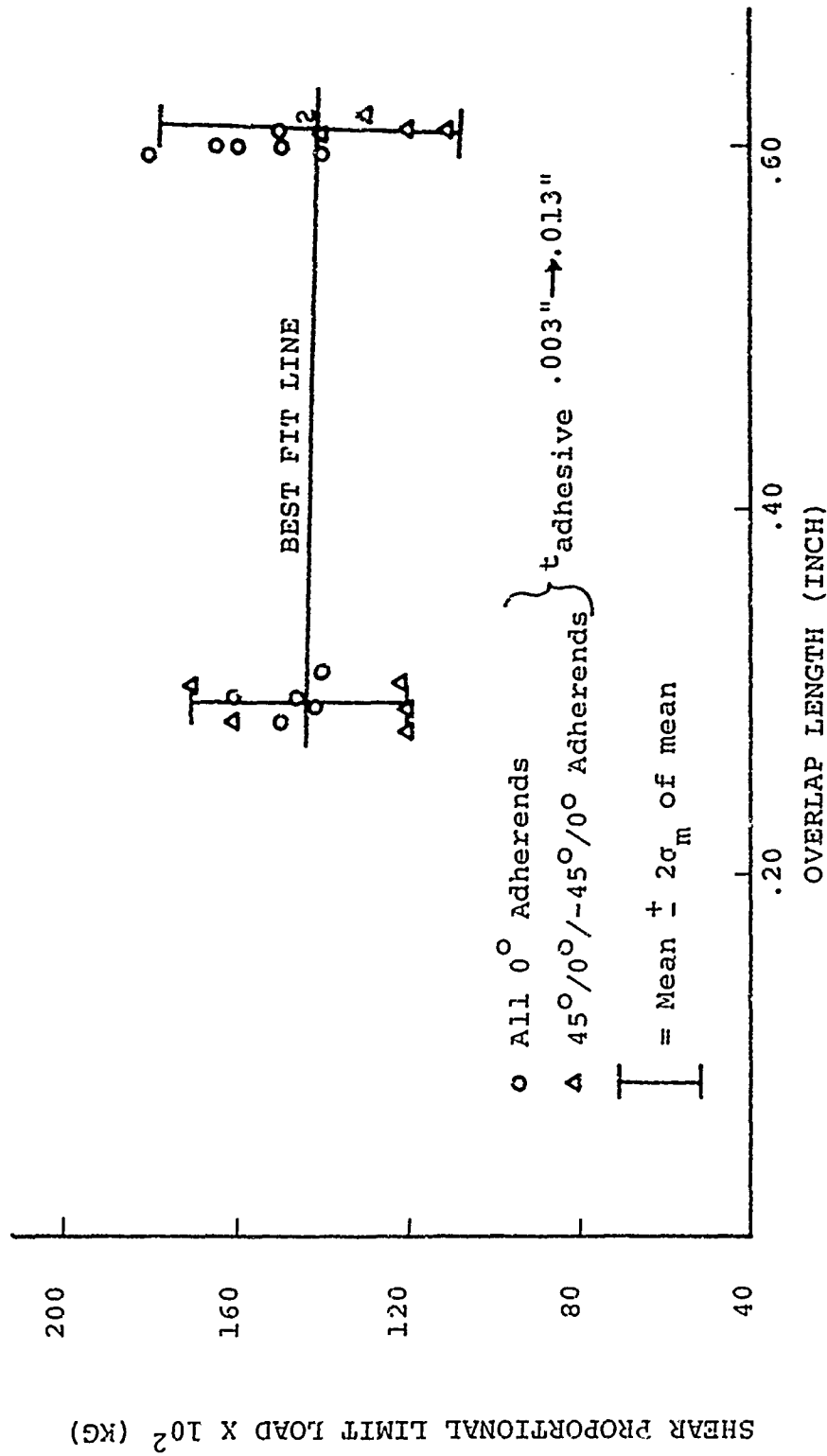


FIGURE (4-36) EFFECT OF OVERLAP LENGTH ON SHEAR PROPORTIONAL LIMIT LOAD

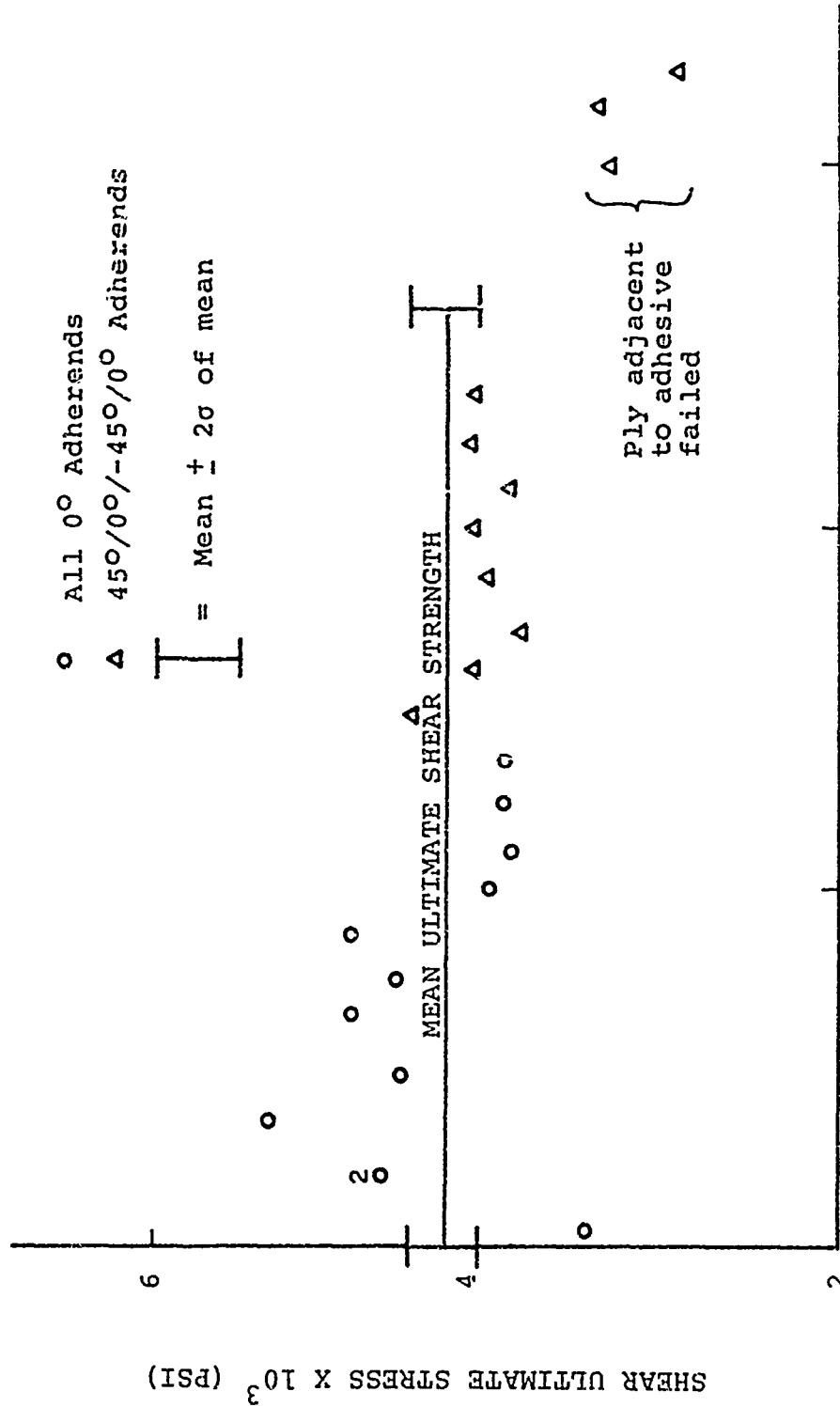


FIGURE (4-3.7) DISTRIBUTION OF SHEAR ULTIMATE STRENGTH
 FOR ALL SHEAR TEST SPECIMENS

Note is made of the three specimens (.60" overlap and a 3 mil adhesive thickness) which failed in the resin. These values were not included in determining the ultimate shear stress of the adhesive.

During the test program two angle-ply adherend specimens were loaded and unloaded as in Figure (4-38) to determine the elastic limit of the adhesives. The two tests while far from being conclusive, consistently showed the elastic limit to be around 80 kilograms. Note is made of the hysteresis loops in Figure (4-38). Most of this is due to the inertia of the Instron machine as one changes load direction.

Again employing two of the uni-ply specimens the characteristic load - deformation curve of the adhesive was determined. Figure (4-39) shows this. One should readily note the ductile nature of this adhesive and that its behavior seems to approach that of an elastic-perfectly plastic material. This information is of value in suggesting a plastic analysis approach of the single lap joint which will be elaborated on in a later report.

Conclusions

1. The test described herein is a satisfactory

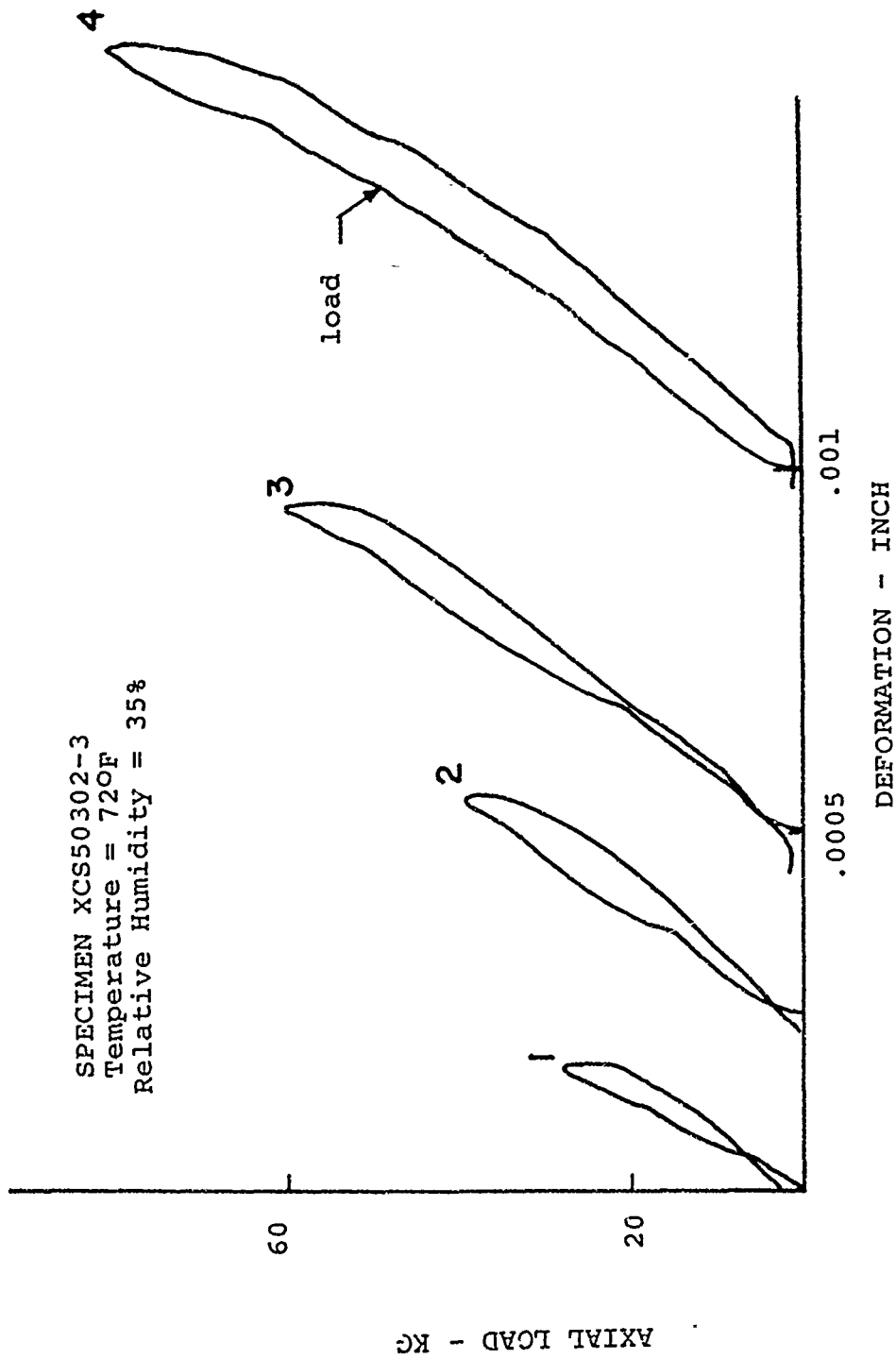


FIGURE (4-38) TYPICAL ELASTIC LIMIT TEST

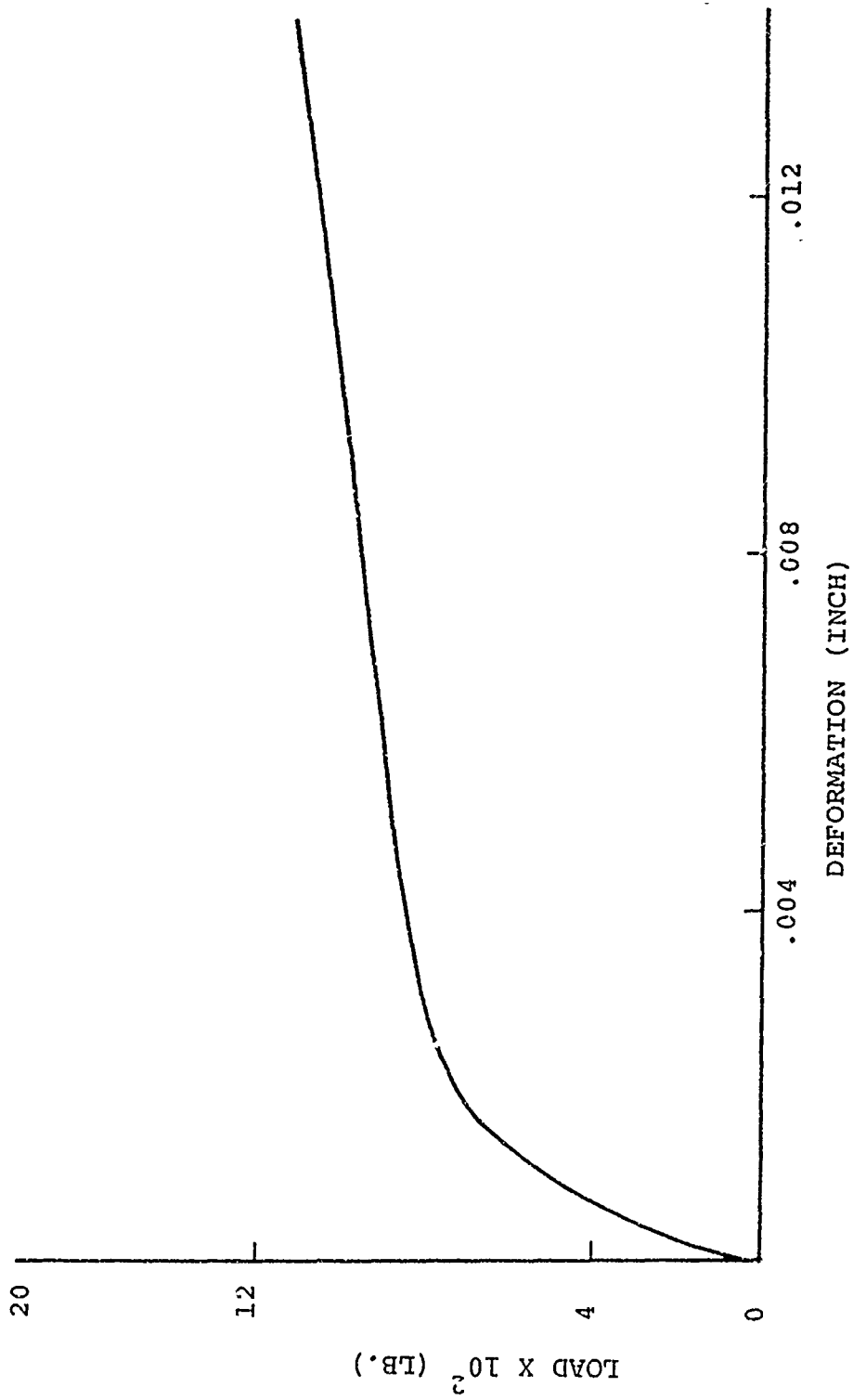


FIGURE (4-39) EA951 ADHESIVE SHEAR LOAD - DEFORMATION CURVE

test to determine the shear modulus within the constrained region of the joint.

2. An error of 10 per cent in the results is possible.
3. Three sets of data by independent researchers resulted in three different results concerning the effect adhesive thickness has on the effective shear modulus.
4. The effect of altering the ply orientation within the adherend has a modest effect.
5. The overlap length of the joint is inversely proportional to the effective shear modulus.
6. Neither overlap, ply-orientation or adhesive film thickness had an effect on the proportional limit .
7. The elastic limit of the EA951 film was found to be approximately 80 kilograms.
8. The ductility of EA951 film makes it desirable for fatigue applications in shear.

Recommended Research

1. The influence of adhesive thickness on the effective shear modulus should be studied in much more detail employing isotropic adherend materials.

2. The influence of overlap length on the effective shear modulus should also be studied in detail employing isotropic adherend materials.
3. Further studies of the influence of adhesive thickness and overlap length, over a wider range of variance, on the shear modulus of EA951 film should be made using fiberglass adherends.
4. The effects of strain rate, pre-strain, and fatigue loading on the shear properties of EA951 film should be studied.

D. ADHESIVE TENSILE TESTS

The behavior of adhesive bonded joints under various loading conditions depends to a great degree on the mechanical properties of the adhesive in the joint. Moreover, these mechanical properties are generally quite different for the adhesive in bulk form vs. its characteristics when restrained by the adherends. Therefore, one needs to know the true tensile modulus and ultimate tensile strength of the adhesive in the joint configuration. It is the intent of these tests to supply an initial evaluation of these properties.

The tests of this section employ EA951 nylon-epoxy adhesive. The results include values for the true Poisson's ratio, tension modulus and ultimate strength. In addition comments on the elastic limit, proportional limit and tensile load-deformation curve for EA951 will be presented.

While it has been shown (Reference 59) that adhesive thickness, pre-strain, strain-rate, type of adherend material and time between loads can influence these results, only two variables will be studied at this

time. They are adhesive thickness and surface area of bond. These two variables were selected, to provide maximum correlation with the shear tests as their results influence the final values of the true tensile modulus and the Poisson's ratio of the adhesive (Reference 61). Moreover, the adhesive thicknesses and surface area values selected are based on duplicating those quantities used in the lap joint specimens.

The test pieces are standard butt joint specimens Figure (4-40). The adherend material is 1002 S fiberglass pre-preg tape. The adherends were fabricated at the Boeing-Vertol Company. The fiberglass plys were layed up to the desired thickness in molds 24 inches x 12 inches. After curing at 320° F the part was cut in two. EA951 adhesive film in 2.5 and 10 mil thicknesses was put in place between the ends of the two cut panels and cured in an autoclave at 50 psi pressure and 350° F. After this cure cycle, one inch wide specimens were cut from the panel and .25 inch diameter pin holes were drilled near each end. Dimensional restrictions specified that the adherend parts interfacing with the adhesive were parallel to each other within \pm .001 inches and had a surface roughness of 5 mils or more as shown in Figure (4-41).

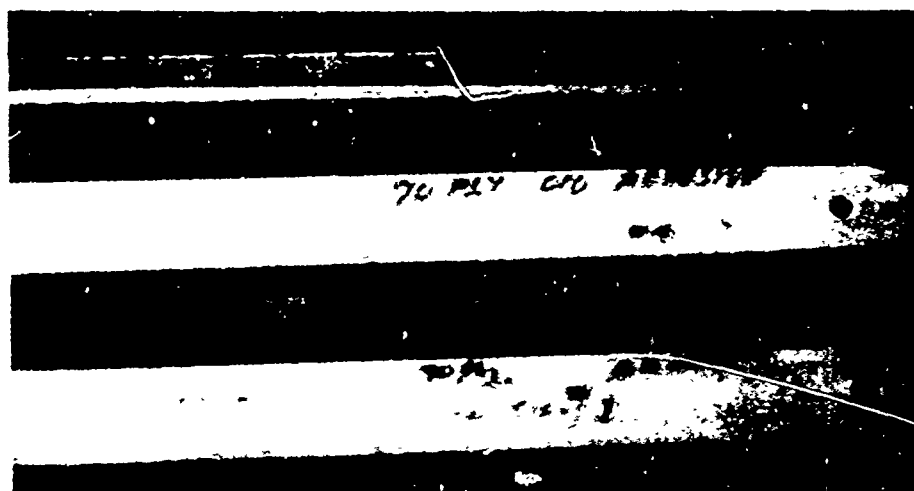


FIGURE (4-40) TYPICAL ADHESIVE TENSILE MODULUS TEST SPECIMENS

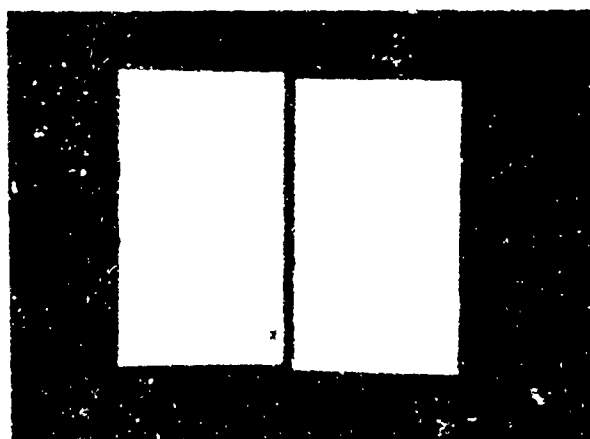


FIGURE (4-42) A TYPICAL POOR BONDED ADHESIVE TENSILE TEST SPECIMEN

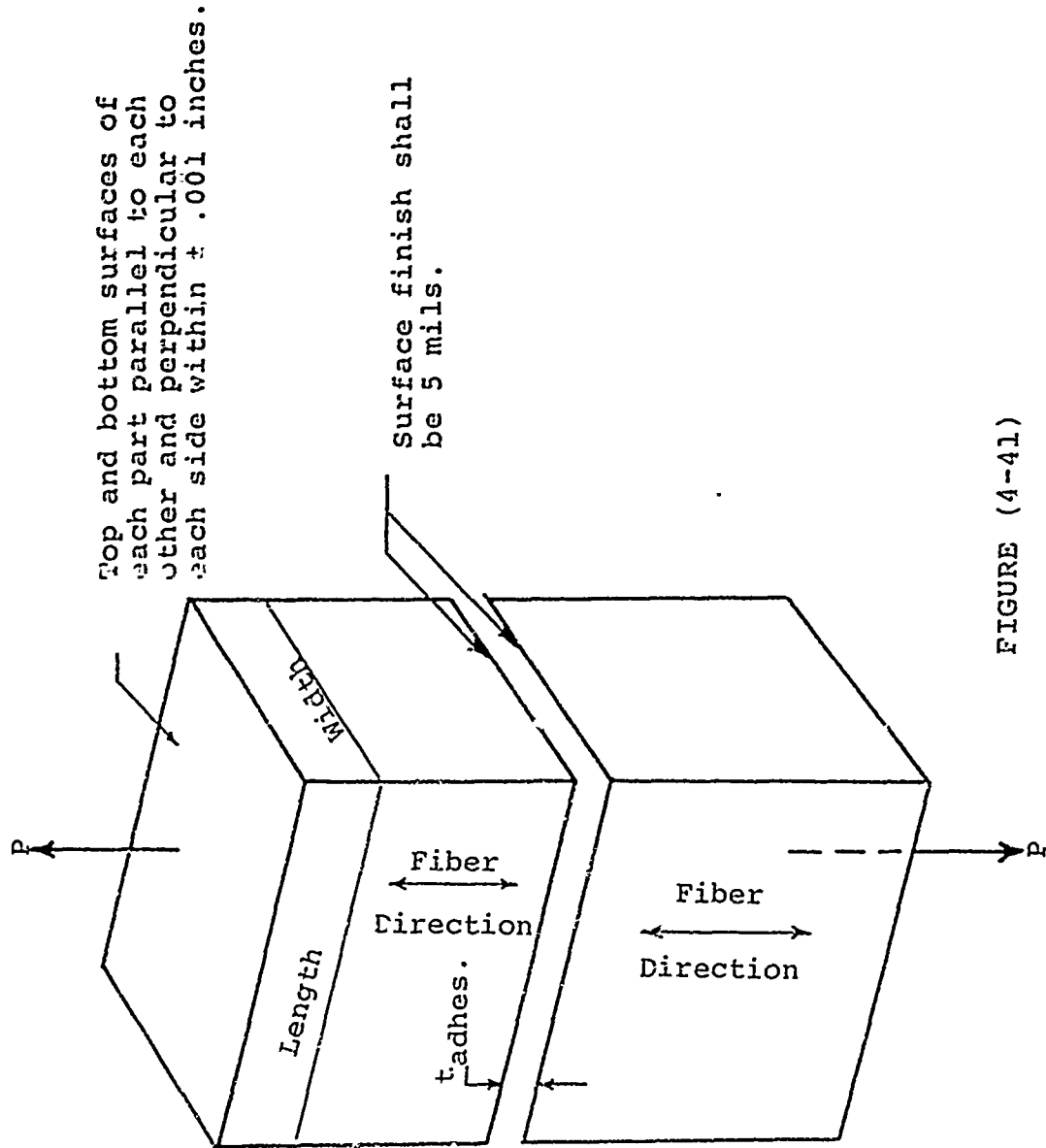


FIGURE (4-41)

The adhesive thicknesses selected were those in use on the fatigue specimens while the surface dimensions of the butt joint were those of the two lap joint configurations, namely 0.60" x 1.0" and 0.30" x 1.0".

Pertinent dimensional data of each test piece are given in Table (4-7). A dial micrometer was used to measure the cross-sectional dimensions while a Zeiss optical microscope was used to measure the adhesive thickness. It was difficult to measure the adhesive thickness as the adhesive seemed to have squeezed out of the joint, making an accurate measurement of adhesive thickness in certain instances difficult. Moreover, several specimens showed a different adhesive thickness depending on the side viewed introducing a slight eccentricity in the joint. This problem was further emphasized by the premature fracture of three test specimens at low loads. All three displayed uneven bonding thicknesses and/or dry spots over the bonding surface (Figure 4-42). Needless to say, dimensional control of the adhesive thickness must be improved for subsequent series of tests.

The test pieces were held in the fixture of the Instron Model TT-DM test machine using 0.25 inch diam.

TABLE (4-7) EA951 FILM TENSILE TEST RESULTS

SPEC NO.	t _{adh} (in)	LENGTH* (in)	WIDTH (in)	SURF. AREA	E _{test} =		ELASTIC LIMIT LOAD (KG)	ULT LOAD (KG)	ULT STRESS (PSI)	ULT STRAIN (in/in)	TYPE FAILURE
					Paxial (2.204) Surf.Area (PSI)	($\frac{DISP}{t_{adh}}$)					
CN2502-1											
-2	.0012	.271	.987	.2675		13182		1040	8568	1.04	Broke- Bad Bond
-3	.0012	.274	1.020	.2795		18925		1195	9423	1.29	Cohesive
-4	.0012	.273	.983	.2583		10600		950	<u>7803</u>	-	Cohesive
AVG=8598											
CN6002-1	.0028	.585	.978	.5721		51777		1625	6260	.630	Cohesive
-2	.0037	.587	.986	.5788		-		-	-	-	Bad Bond
-3	.0037	.580	.578	.3352		58387		1430	9402	.405	Uneven Thickness Cohesive
-4	.00246	.586	.672	.3937		47216		1450	8117	-	Cohesive

307

Table (4-7) Continued

SPEC NO.	t _{adh} (in)	LENGTH* (in)	WIDTH (in)	SURF. AREA	E _{test} =		ELASTIC LIMIT LOAD (KG)	ULT ¹ LOAD (KG)	ULT STRESS (PSI)	ULT STRAIN (in/in)	TYPE FAILURE
					Paxial (2.204) Surf. Area (PSI)	DISP t _{adh} /					
-5	.0034	.583	.992	.5783	-	-	-	-	-	-	Bad Bond
-6	.0031	.587	1.003	.5887	39791			1960	<u>7337</u>	-	Cohesive
AVG=7779											
CN2510-1	.0046	.270	1.004	.2711	42739						
-2	.0031	.275	1.017	.2796	39098						
-3	.0028	.272	.998	.2714	34102			1075	8729	.453	Cohesive
-4	.0034	.274	1.006	.2756	39549			1180	9436	.412	Cohesive
-5	.0031	.271	1.005	.2723	75274		Not Evident	1150	<u>9308</u>	.482	Elastic Limit Test
AVG=9158											
CN6010-1	.0111	.653	1.005	.6562	99418			2350	7893	.126	Cohesive
-2	.0108	.653	1.022	.6673	107012			2300	7596	.177	Cohesive
-3	.0111	.653	1.011	.6602	105874			2250	7515	-	Cohesive
-4	.0111	.654	1.012	.6618	147865		=425KG.	-	-	-	Elastic Limit
-5	.0111	.655	1.001	.6556	149264			2750	<u>9244</u>	.112	Cohesive
AVG=8062											

*See Figure (4-41)



FIGURE (4-13) ADHESIVE TENSILE
TEST PIECE IN PINNED JOINT FIXTURE

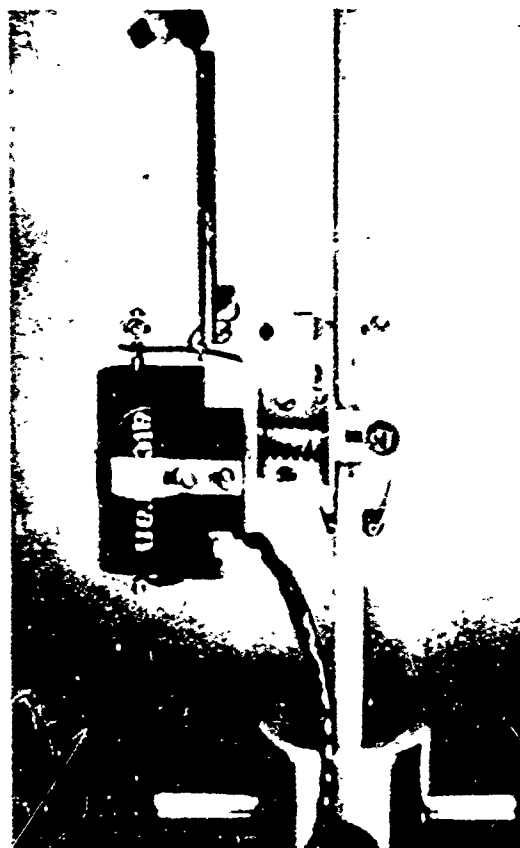


FIGURE (4-44) BUTT JOINT
TEST SET-UP



FIGURE (4-47) ADHESIVE FAILURE SURFACE OF BUTT JOINT
SPECIMENS

hardened steel pins as shown in Figure (4-43). The upper fixture of the test machine was a universal joint assembly. This allowed alignment of the specimen between fixtures without inducing unwanted bending stresses. Next the Tinius-Olsen Model S1 LVDT modified for an almost zero gage length was attached to the specimen such that the knife edges just gapped across the adhesive. A magnifying glass was used to check this. The test piece ready for loading is shown in Figure (4-44). The recording set-up was such that the LVDT signal was amplified by a demodulator which fed the signal into a Moseley Model 7001A x-y recorder. The load signal was fed directly into the recorder from the Instron where load-deformation plots were drawn.

The test procedure to determine the tensile modulus, elastic limit and proportional limit was as follows:

1. Calibrate the Instron test machine and x-y recorder.
2. Run a proof test on an aluminum specimen to check the accuracy of the system.
3. Place the butt joint specimen firmly in fixtures and attach the LVDT so that the knife edges span the adhesive joint.

4. Select the load and deformation scales.

5. Load the specimen @ .05 cm/min to 450 kilograms recording the load-deformation curve, then unload.

The specimen gripping procedure for the ultimate tests was different by necessity as the pins could not withstand loads in excess of 600 kilograms without bending. Therefore, regular grips were used to hold the butt joint specimens in place. The specimen was aligned in the grips vertically using a level. The specimens were then pulled to ultimate load.

Before discussing the test results, a brief summary of possible errors or deficiencies in the test procedure should be mentioned. Initially, the uneven adhesive thickness creates two problems. It leads to eccentricity in the joint causing possible secondary bending stresses across the bond surface. Also an uneven adhesive thickness makes it difficult for one to decide on a true gage length with which to calculate an initial tensile modulus. The error introduced, while thought small, is impossible to evaluate at this time. However, a readily available solution is better adhesive thickness control which will be accomplished on subsequent series of tests, eliminating this problem.

A possible deficiency in this first series of tests was that the measurement of deformation was accurate only to 25×10^{-6} inches. While this may be accurate enough for most modulus measurements it proved to be not sensitive enough to determine elastic or proportional limit load points. As one is aware, minute discontinuities of the order of 1.0×10^{-8} inches from a normal displacement reading may signal the elastic and/or proportional limit load of a material. Moreover, the periodic noise disturbances from the surrounding community often introduced small jogs in the load-displacement curves. These compounded the problem of trying to determine elastic and/or proportional limit loads. Overall, however, it is believed measurement of the tensile moduli and load-deformation data to ultimate load are quite reliable.

Typical tensile load vs. deformation plots from which the test tensile moduli values of Table (1) were calculated are shown in Figures (4-45) and (4-46). The data was generated at room temperature and 37 per cent relative humidity. The noise interference spoken of earlier, is evident in Figure (4-46). Using these plots one can calculate the test tensile modulus per:

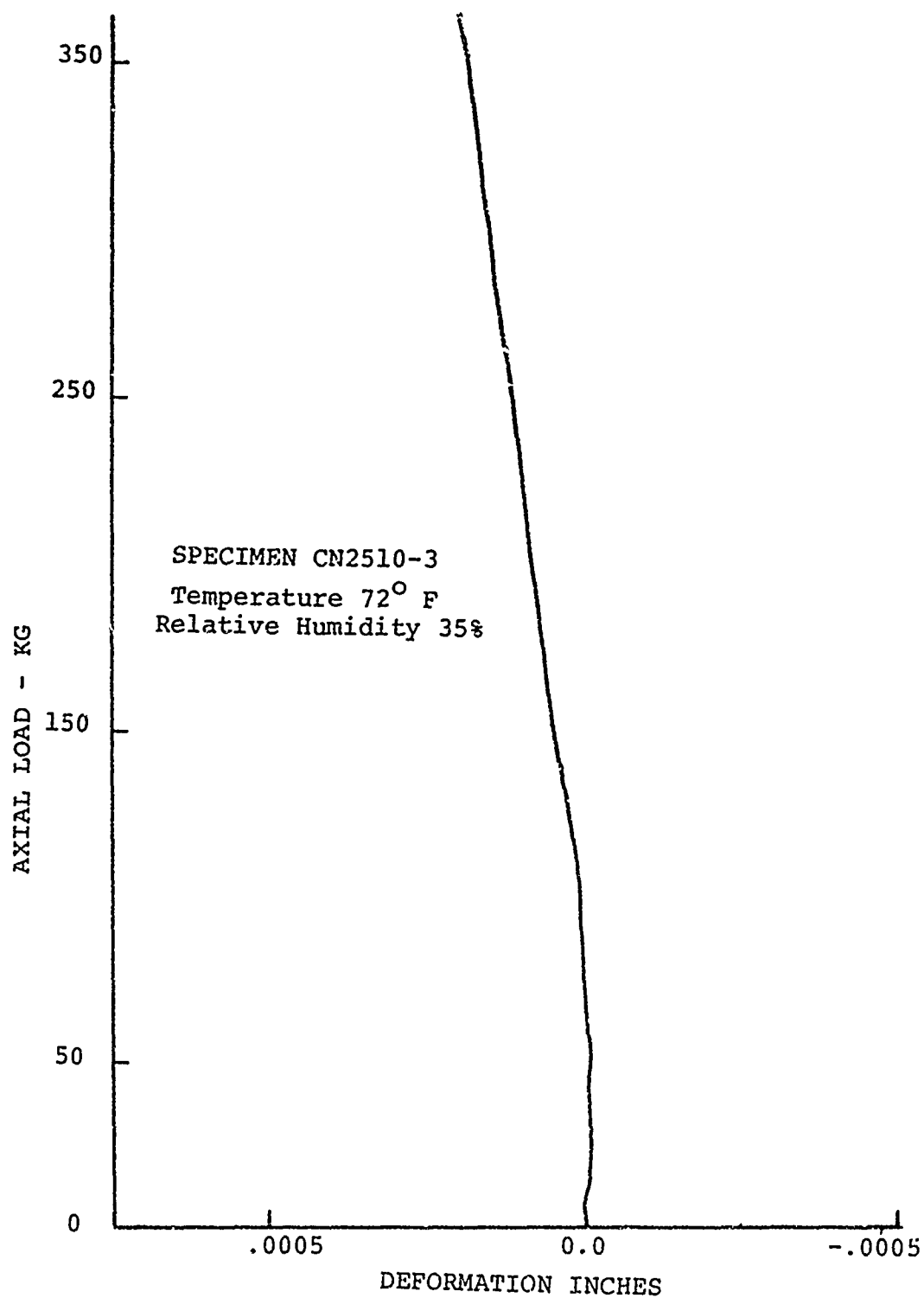


FIGURE (4-45) ADHESIVE TENSILE MODULUS LOAD-DEFORMATION DATA

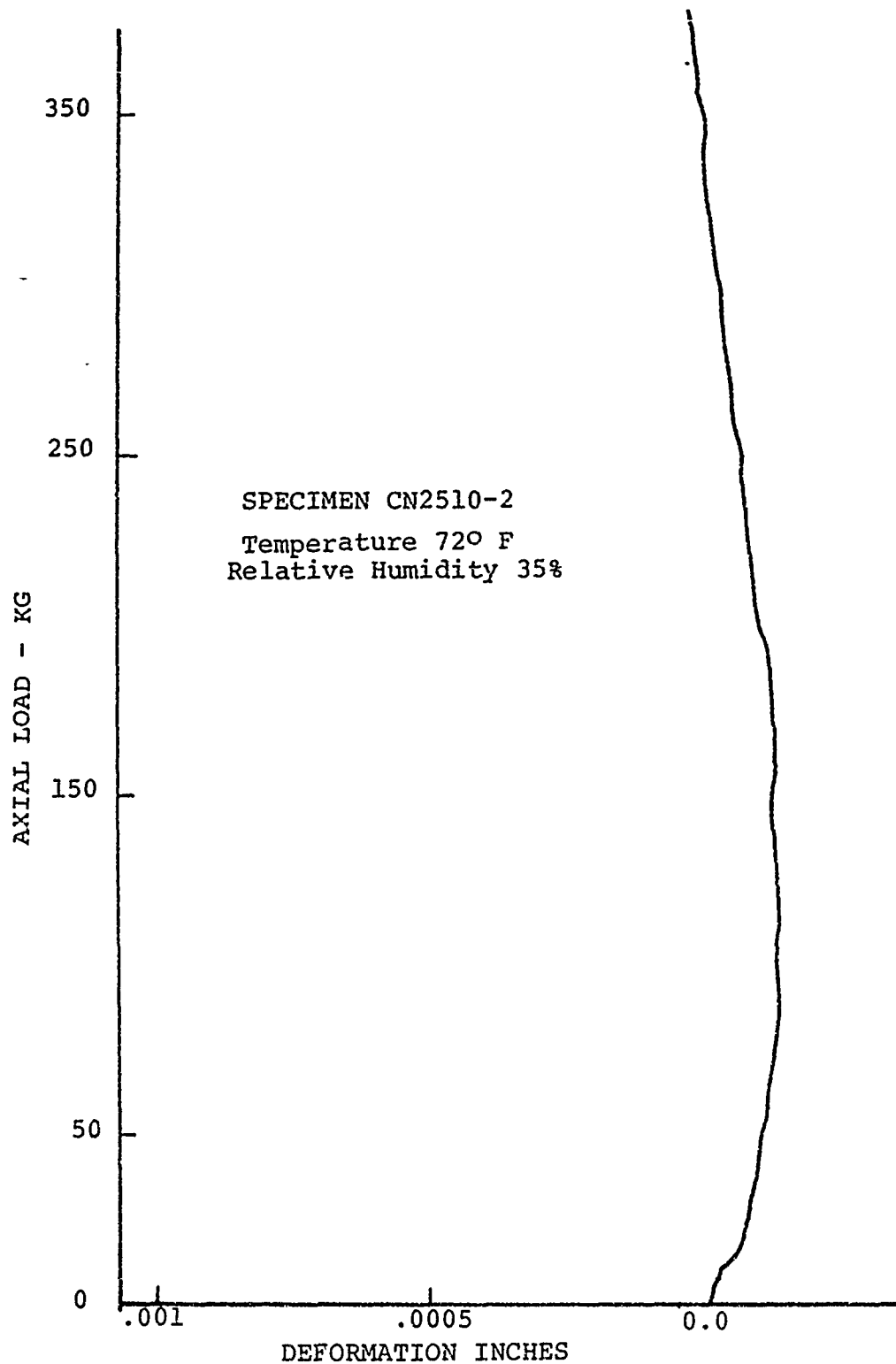


FIGURE (4-46) ADHESIVE TENSILE MODULUS LOAD-DEFORMATION DATA

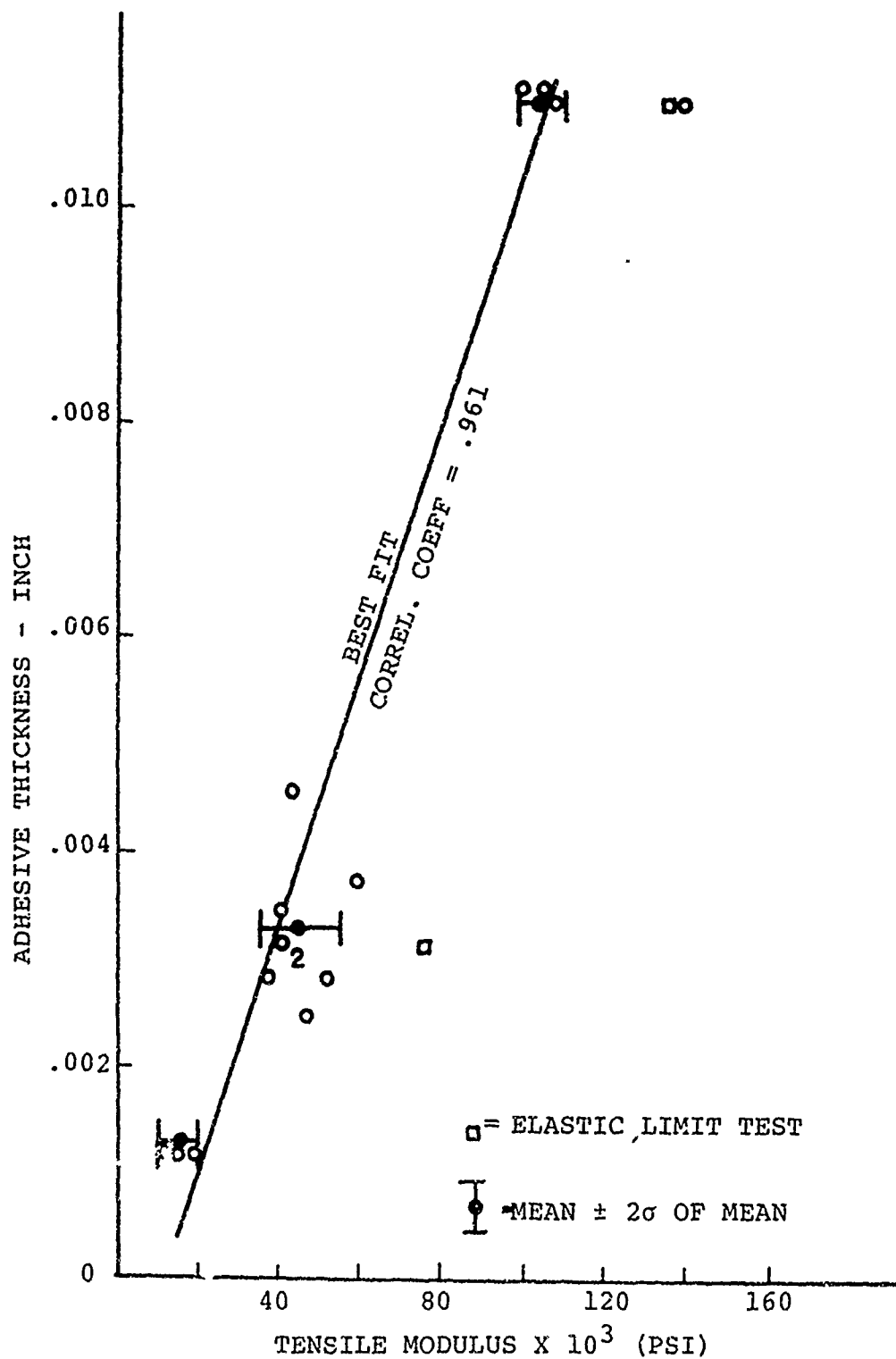


FIGURE (4-48) ADHESIVE TENSILE TEST MODULUS VS. ADHESIVE THICKNESS

$$E_{\text{test}} = \frac{\text{Paxial (2.204 \#/IN)}}{(\text{Surf.Area}) \frac{\text{Displacement}}{\text{Adhesive thickness}}} \quad (4.5)$$

It is these values that are recorded in Table (4-7).

The range of test tensile moduli was from 10600 PSI for an adhesive thickness of 1.2 mils to 107,000 PSI for a 11.1 mil adhesive thickness. The failures were cohesive in nature and examples are shown in Figure (4-47)

As previously mentioned the variables of adhesive thickness and surface area were to be studied. Figure (4-48) shows the effects of adhesive thickness on E_{test} . A linear regression analysis was performed on the data as was a mean $\pm 2\sigma$ standard deviations of the mean. These results are also shown. Moreover, the high correlation coefficient leads one to believe the trend that the test tensile modulus increases as the adhesive thickness increases. The two elastic limit test points were not included in the regression analysis. As mentioned earlier, part of the data scatter can be attributed to bond line thickness control and outside noise problems.

Figure (4-49) is a plot of surface area vs. test tensile modulus. The test data is scattered. This

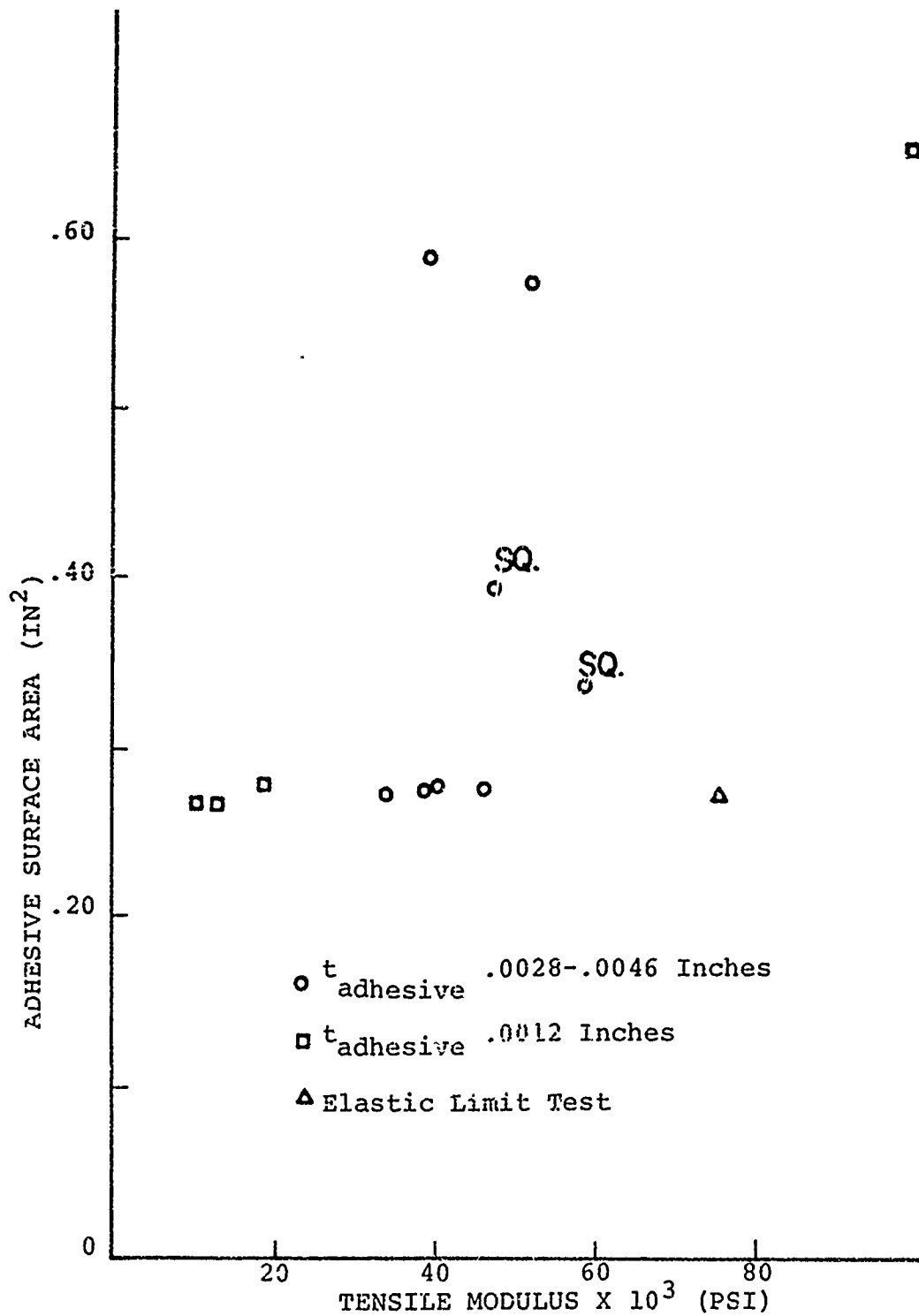


FIGURE (4-49) ADHESIVE TENSILE TEST MODULUS VS. SURFACE AREA

is probably the result of the difficulty in getting consistently good bonds. Little can be said of the results. However, a trend of an increase of tensile test moduli for increased surface area seems possible for the above mentioned specimens. Again, the bondline control problem prevented better correlation between surface area and tensile test modulus for a constant adhesive thickness.

Up until this juncture the term "tensile test modulus" has been used. The reason for this is that when an adhesive deforms in a joint, under a tensile load, the adhesive is restrained by the more rigid adherend material, deforming according to the adherends' Poisson's ratio. Therefore, the simple

$$E = \frac{\text{Stress}}{\text{Strain}} \quad (4.6)$$

relation will not give the correct tensile modulus. In general the adherend restraint has a stiffening effect on the adhesive as its Poisson's ratio is numerically less than the adhesives.

To account for this Poisson effect on the tensile modulus, assuming that EA951 film is an isotropic material, one can employ the basic equations of elasticity. More-

over, if one assumes continuity of displacements at the adherend-adhesive interface the resulting relations for the true tensile modulus and Poisson's ratio of the adhesive can be written as (Reference 61).

$$E_{adh} = 2(1 + \nu_{adh.}) G_{adh} \quad (4.7)$$

where:

$$\nu_{adh} = \frac{2 G_{adh} - E_{test}}{2 (G_{adh} - E_{test} + 2 G_{adh} \nu \frac{E_{test}}{E_{11}})} \quad (4.8)$$

E_{11} = Axial modulus of 1002 S uni-ply material

ν = Poisson's ratio of 1002 S

G_{adh} = Shear modulus for similar adhesive thickness and surface area from shear test results

The numerical values of the adhesives Poisson's ratio and true tensile modulus are tabulated in Table (4-8). In general the influence of the adherend properties ν , E_{11} is minor because they appear as a small part of the denominator in equation (4.8)

Effort was now put forth to determine what trends the true tensile modulus exhibited vs. its surface area and adhesive thickness. These results are shown in Figure (4-50). Two trends seem quite obvious. (1) Over the range of adhesive thicknesses covered, namely 1.2 mils

TABLE (4-8) EA951 FILM TRUE TENSILE MODULUS RESULTS

SPEC NO.	t _{adh} (in)	LENGTH** (in)	E _{test} (PSI)	G* (PSI)	1002-S MAT'L		$\nu_{adh} = \frac{2G - E_{test}}{2(G - E_{test} + 2G\nu_{E_{test}})}$	E _{ll}	E _{adh} = 2(1 + ν_{adh})G
					E _{ll} x 10 ⁶ (PSI)	ν (PSI)			
CN2502-2	.0012	.271	13182	1500.	.25	6.5			
-3	.0012	.274	18925	1500.			.436		4308.
-4	.0012	.273	10600	1500.			.457		4371.
							<u>.417</u>		<u>4251.</u>
							AVG=.436		AVG=4310
CN6002-1	.0028	.585	51777	2500			.475		7375
-3	.0037	.580	58387	2900			.473		8543
-4	.0025	.586	47216	2400			.473		7070
-6	.0031	.587	39791	2600			<u>.465</u>		<u>7618</u>
							AVG=.471		AVG=7651

Table (4-8) Continued

Table (4-8) Continued									
SPEC NO.	t _{adh} (in)	LENGTH** (in)	E _{test} (PSI)	G* (PSI)	1002-S MAT'L		$\nu_{adh} = 2G - E_{test}$		E _{adh} = 2 (1 + ν_{adh}) G
					ν	E ₁₁ x 10 ⁶ (PSI)	$\frac{2(G - E_{test} + 2G\nu E_{test})}{E_{11}}$		
CN2510-1	.0046	.270	42739	7000	.25	6.5	.402		19628
-2	.0031	.275	39098	4500			.435		12915
-3	.0028	.272	34107	4000			.434		11474
-4	.0034	.274	39549	5000			<u>.428</u>		<u>14280</u>
							AVG = .425		AVG = 14573
CN6010-1	.0111	.653	99418	5900			.468		17322
-2	.0108	.653	107012	5900			.471		17358
-3	.0111	.653	105874	5900			.471		17358
-5	.0111	.655	149264	5900			<u>.479</u>		<u>17452</u>
							AVG = .472		AVG = 17372

*Values taken from All 0° Best Fit Curves in Figures (4-22) and (4-23)
of Chapter 4

**See Figure (4-41)

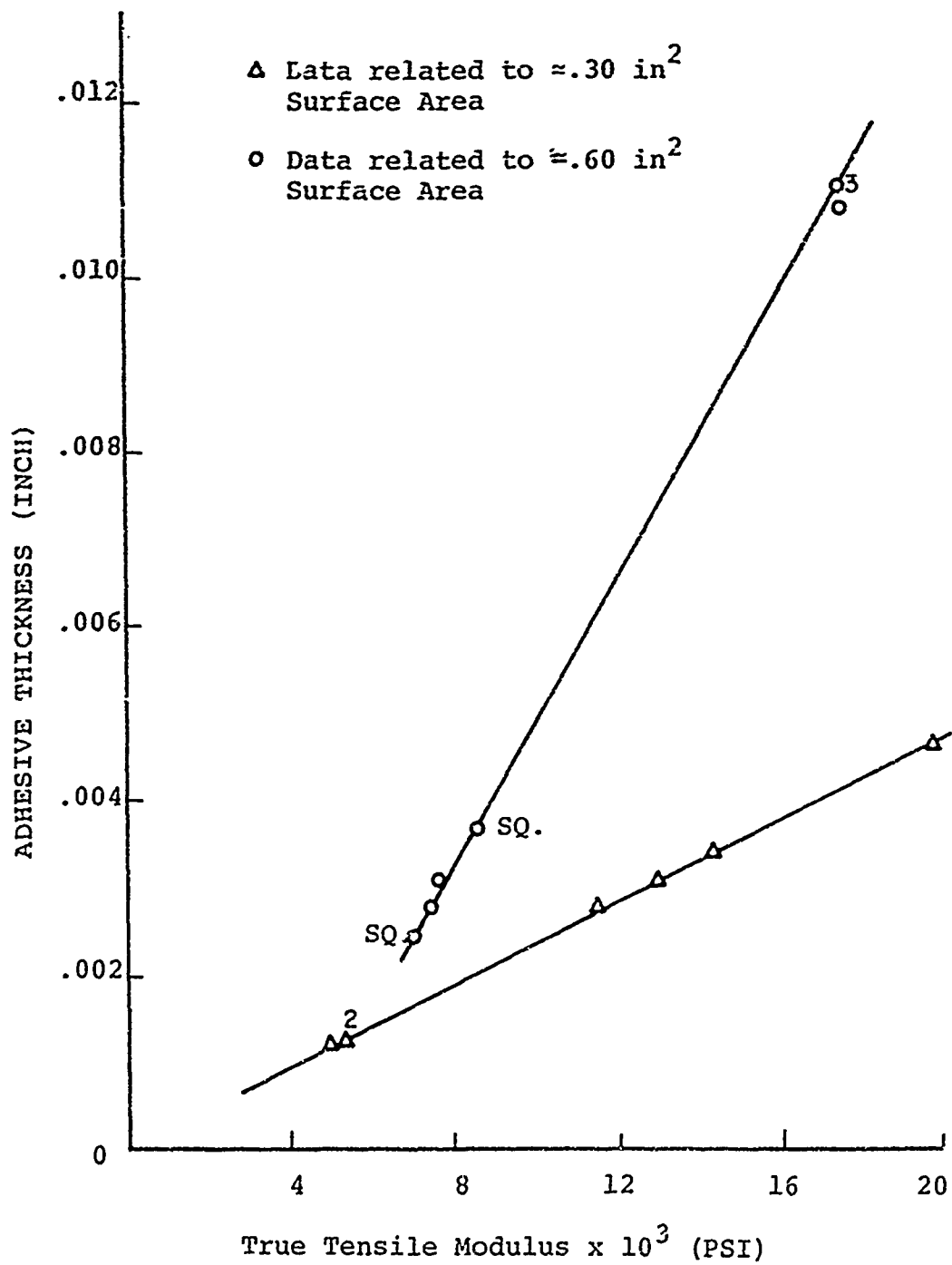


FIGURE (4-50) TRUE ADHESIVE TENSILE MODULUS VS. ADHESIVE THICKNESS

to 11.1 mils , the true tensile modulus increased with adhesive thickness. (2) The true tensile modulus decreased as surface area increased, for a constant adhesive thickness. In both instances however, one should note that there is a coupling of the shear test results with the tension test results per equation (4.8). This makes discerning the cause for a particular result rather difficult.

Basically, two trends have been observed. Are these supported by other works? Are these trends believable? Is the magnitude of the tensile modulus and Poisson's ratio believable? These are all proper questions to ask. Therefore, after an extensive literature search several comments can be made.

In no instance did the author find that such tests had been performed previously with composite material adherends. However, similar butt joint tests of adhesives using thin steel and aluminum cylinders has been performed by Hughes and Rutherford (Reference 59) and by Kuenzi and Stevens (Reference 61).

Rutherford found for epoxies, Epon 9601 and Epon 828/V40 that the true tensile modulus increased as the thickness decreased for thicknesses of 8 to 40 mils.

Moreover, he found that the tensile modulus was generally lower for the softer aluminum adherends vs. stainless steel adherends. Contrary to this Kuenzi and Stevens tested a wide range of adhesives and for Epon 422J tape where the adhesive thickness varied appreciably from 8 to 50 mils the tension modulus increased with increasing adhesive thickness. None of the adhesives mentioned are similar in chemical makeup to EA951 which is a nylon epoxy. However, the conflicting results of these two independent investigations suggest that the trends observed may be a function of chemical makeup of the adhesive and/or the chemical interaction between adherend and adhesive during cure as mentioned by Cuthrell in Reference (60).

One of the adhesives tested by Kuenzi and Stevens, metalbond MN3C, is a nylon tape which seemed quite ductile. Therefore, a general comparison of its moduli and strengths with EA951 film was thought plausible. The results are presented in Table (4-9). Examination of the results shows that the shear and tensile moduli are of the same magnitude. However, the ultimate shear and tensile strengths of EA951 film are far superior.

Finally, no information could be found relating

TABLE (4-9)

SUMMARY OF ADHESIVE PROPERTIES

ADHESIVE	TENSILE MODULUS (PSI)	SHEAR MODULUS (PSI)	POISSON'S RATIO	ULT. SHEAR STR. (PSI)	ULT. TENSILE STR. (PSI)
Metalbond Mn3C ($t_{adh} \approx .07$ in)	5200	1530	.498	2489	1220
EA951 Film ($t_{adh} = .0111$ in)	17372	5900	.472	4300	8500

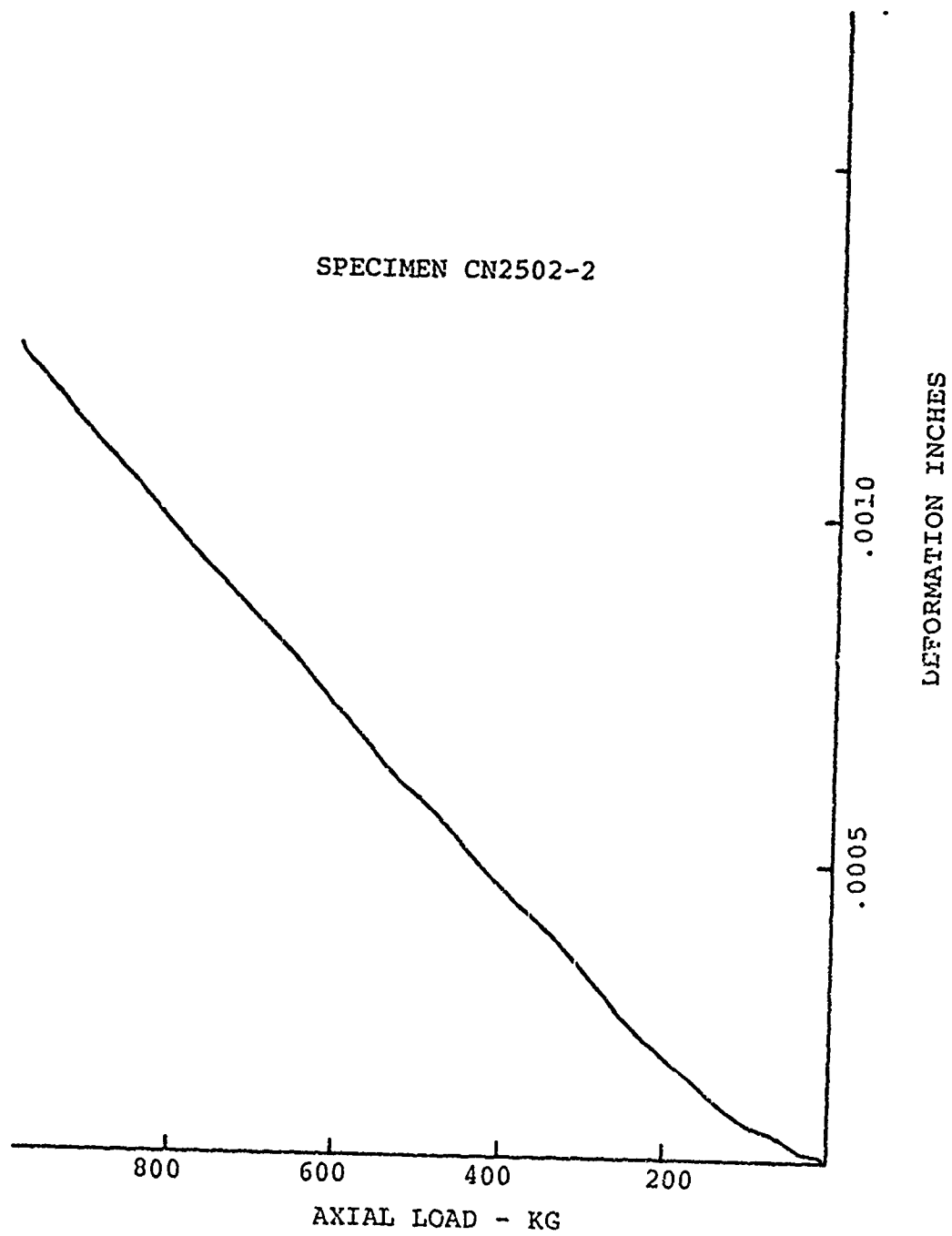


FIGURE (4-51) EA951 ADHESIVE TENSILE LOAD DEFORMATION DATA

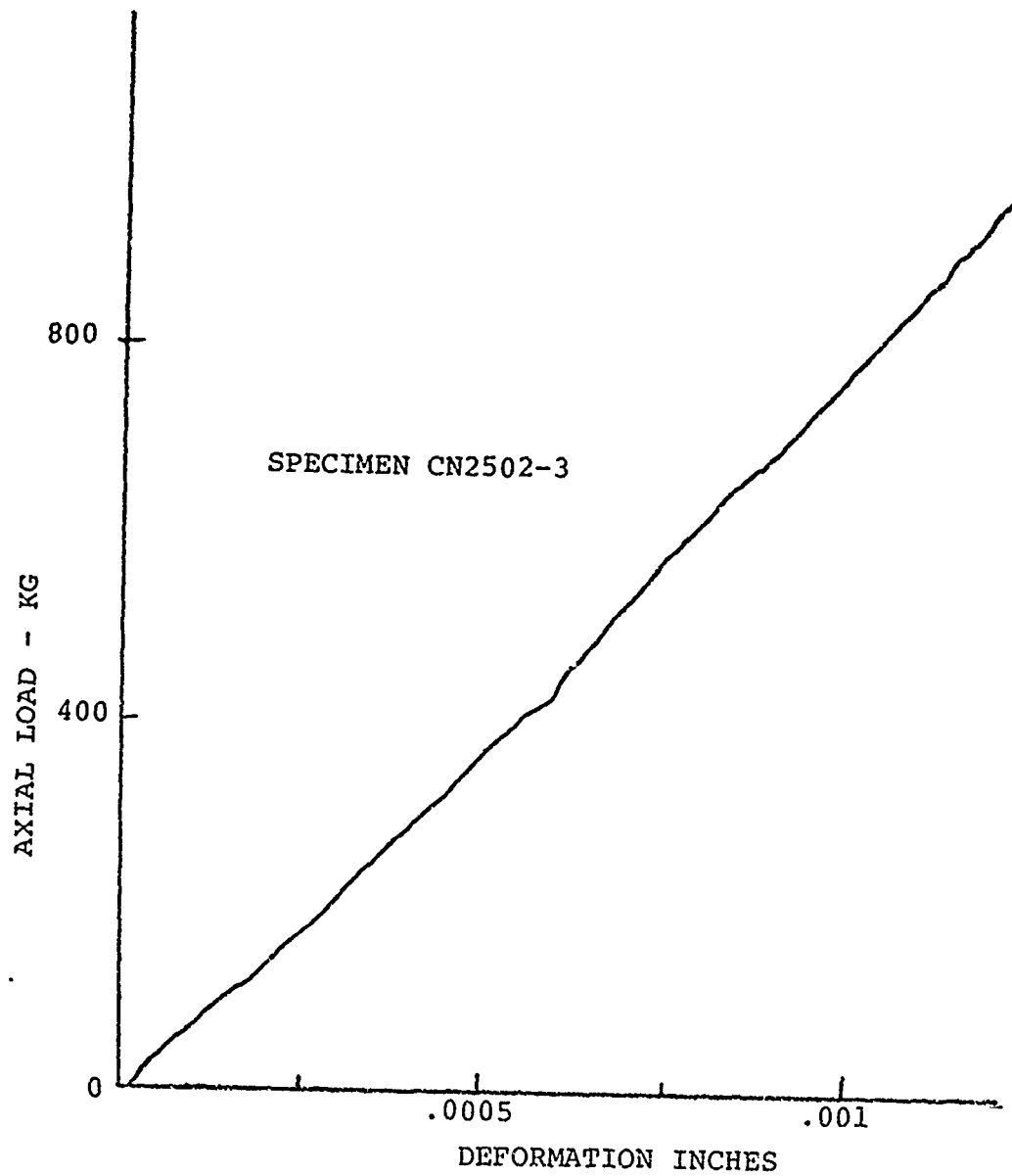


FIGURE (4-52) EA951 ADHESIVE TENSILE LOAD-DEFORMATION DATA

the tensile modulus to the bonded surface area. Moreover, no plausible reason for the surface area effect is available at this time.

Typical load-deformation curves were determined for several of the specimens. Figures (4-51) and (4-52) show that they are essentially linear to failure, becoming non-linear just before ultimate load is reached. Exactly where the elastic limit is cannot be said as two attempts to determine this value proved inconclusive.

Ultimate stress and strain values were also determined and are given in Table (4-7). Readily discernable in Table (4-7) is the fact that EA951 film is significantly less ductile in tension than in shear where its ultimate strain was several hundred per cent. Moreover, the ultimate strain tends to increase with decreasing thickness.

The ultimate tensile strength of this adhesive is quite high. While the data in Table(4-7)shows significant scatter, EA951 film has an average ultimate tensile strength of 8500 PSI. This is an extremely desirable characteristic for an adhesive to possess especially in a lap joint configuration. Moreover, the scatter is felt to be somewhat a function of the adhesive thickness control problem and will be improved upon in future tests.

Attempts were made to discern the proportional limit load of the adhesive in tension. Due to problems mentioned earlier results proved inconclusive. However, it does seem that the proportional limit load is somewhere above 80 per cent of ultimate load. In the next series of tests we will attempt to clarify this item.

Conclusions:

1. The test is a legitimate means of determining the true Poisson's ratio and tensile modulus of the adhesive. Moreover, the adherends, being loaded only to small levels of their capacity can be reused as test pieces saving considerable time and money.
2. The problems of thickness control and extraneous noise and measurement sensitivity tended to introduce small errors into the results, especially in determining an accurate elastic and proportional limit value.
3. The true tensile modulus increased with increasing adhesive thickness for a constant surface area.
4. The true tensile modulus decreased with increasing surface area for a constant adhesive

thickness.

5. EA951 film is significantly less ductile in tension vs. a shear application, yet still ductile by normal standards.
6. The ultimate strain in tension increased with decreasing adhesive thickness for constant surface area.
7. Previous tests of this nature are few and present conflicting results which may be related to the chemical make-up of the adhesive, the adherends used and the interaction during curing of the adhesive at the adhesive-adherend interface.
8. Studies of these failed surfaces using a scanning electron microscope may provide insight into the failures of adhesives in lap joints under ultimate and fatigue loadings.

Recommended Research

1. Further studies of the influence of adhesive thickness, surface area and surface shape over a wider range of variance, on the tensile properties of EA951 film should be made under more uniform thickness control specifications.

2. A study should be conducted to relate the effects of strain rate, type of adherend material, pre-strain, time between loadings and fatigue loading on the tensile properties of EA951 film.
3. A study should be conducted to discern if the chemical make-up of various adhesives and/or their interaction with the adherend at their interface during cure is responsible for the completely opposite trends observed by independent researchers concerning their shear and tensile properties.
4. A determination of the bulk properties of EA951 film should be made.

Summary

Shear and tensile test results of EA951 film have been conducted. The overall results are believed to be reliable as are the trends they unveiled. In addition, EA951 film appears to possess, to a greater degree than other more commonly used adhesives, the qualities most desirable in sustaining the integrity of a structural item more in line with the life expectancy of the item itself. The qualities are:

1. Low moduli in tension and shear precipitating a more forgiving ductile behavior and the ability to reduce peak stress levels at stress concentrations.
2. An adequate ultimate shear strength coupled with a superior ultimate tensile strength.

It is strongly recommended that this adhesive system be considered for all high strength bonding applications where ductility and/or tensile stresses over and above a normal shear application are a problem.

Finally the true test of these results is their usefulness in accurately predicting the ultimate and fatigue failures of the single lap joints. This will now be attempted.

CHAPTER V

A. ULTIMATE LOAD TESTS

An ultimate load test program was conducted encompassing certain parametric variations in an effort to reveal ways to improve the ultimate load capacity of single lap bonded joints. The parameters studied were (1) overlap length-thickness of adherends was a constant, (2) adhesive thickness, (3) orientation of the lamina adjacent to the adhesive layer. These parameters were chosen for this study as various reference articles have shown them to have a definite effect on the strength of the joint. Moreover, the range of variables selected were chosen to ensure that failure will occur in the adhesive rather than in one of the adherends.

The specimens Figure (5-1), were composed of 1002-S glass pre-preg. tape adherends, seven plys thick and one inch wide. The overall specimen length was approximately nine inches in length. The adhesive selected was Hysol EA951 film. It was selected for its low moduli, ductile nature and relatively high ultimate strength in shear and tension. This selection is verified by the shear and



FIGURE (5-1) TYPICAL BONDED LAP JOINT ULTIMATE
AND FATIGUE TEST SPECIMEN

tensile test results of sections C and D of Chapter IV. The extremely low moduli tend to reduce the peak values of the shear stresses in the joint near the ends and should result in a higher ultimate load capacity for the joint.

The adherends were of identical size so that a balanced extensional stiffness (E_t) would exist. Reference (22) has shown that such a configuration maximizes joint strength by balancing the peak stresses at each end of the overlap. The maximum laminate allowable load was 15,000 pounds based on the ultimate strength of 1002-S glass in its primary direction being 230,000 PSI per section B of Chapter IV. The adherend cross sectional area is 0.065 square inches. However, non-uniform bending stresses and the stress concentrations along the joint length would be expected to cause a premature failure of the adherend if it were highly loaded. For these tests the average adherend stress was 46,000 PSI or less.

The ultimate test pieces were fabricated at Boeing-Vertol, being picked at random from the same lot as the fatigue test specimens.

The adherends were fabricated in 24 inch x 48 inch panels. They were then bonded using Hysol EA951 film per

the manufacturer's recommended specification. After this cure cycle, one inch wide specimens were cut out for these static tests.

The lap lengths fabricated were 0.30 and 0.60 inches. The nominal adhesive thicknesses were 2.5 and 10 mil while the ply orientation in the adherends was either an all 0° orientation or a $45^{\circ}/0^{\circ}/-45^{\circ}/0^{\circ}$ orientation.

The all 0° adherend static tests were inadvertently conducted at Boeing-Vertol on an Instron Model TT-D test machine at a loading rate of .05 inches/minute. The $45^{\circ}/0^{\circ}/-45^{\circ}/0^{\circ}$ specimens were tested at the University of Delaware on an Instron Model TT-DM test machine at a loading rate of .05 centimeters/minute. The specimens were gripped using the standard serrated grips without doublers on the ends of the specimens. The specimen in the Instron machine jaws ready to be tested is shown in Figure (5-2). The bending of the joint under load is evident in Figure (5-3).

The all 0° adherend specimens failed in a combination adhesion-cohesion manner. Figure (5-4) and (5-5) show typical failed surfaces. The angle ply adherend specimens also failed in an adhesive or cohesive manner Figure (5-6) except for the 0.60 inch overlap specimens



FIGURE (5-2) ULTIMATE TEST SET-UP

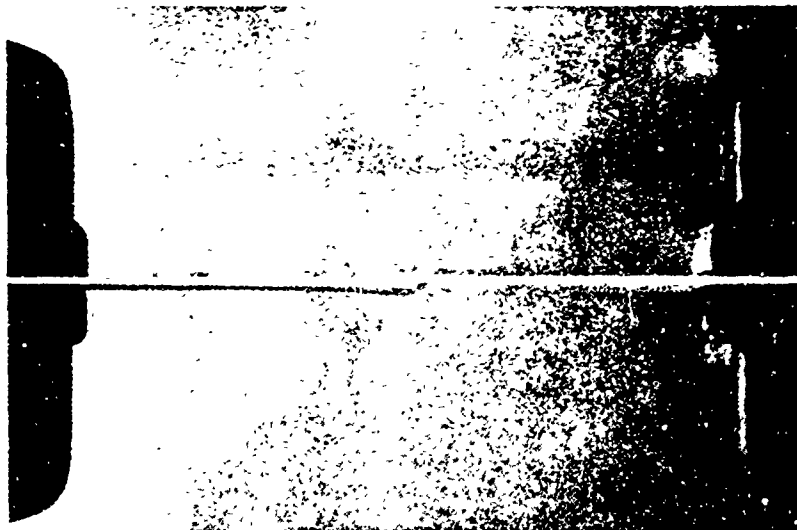


FIGURE (5-3) SINGLE LAP JOINT IN A LOADED CONDITION



FIGURE (5-4) TYPICAL .30 INCH OVERLAP ULTIMATE ADHESIVE FAILURE

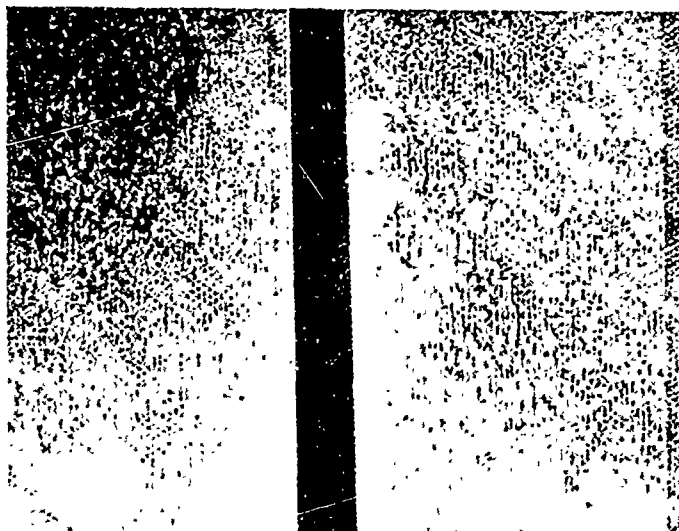


FIGURE (5-5) TYPICAL .60 INCH OVERLAP ULTIMATE ADHESIVE FAILURE

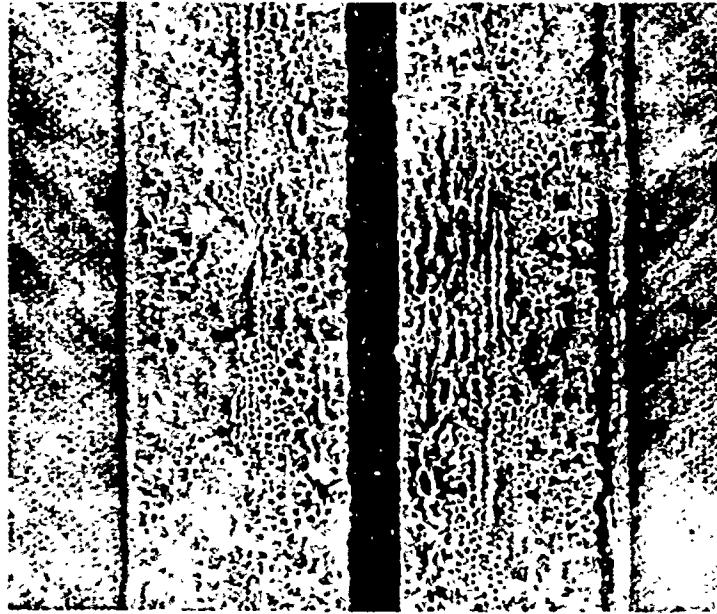


FIGURE (5-6) TYPICAL ANGLE PLY ADHEREND ULTIMATE ADHESIVE FAILURE



FIGURE (5-7) TYPICAL ULTIMATE FAILURE IN THE PLY ADJACENT TO THE ADHESIVE

with a 2 mil adhesive thickness. This group Figure (5-7) appeared to be approximately fifty per cent stronger than its counterparts, failing primarily in the resin of the 45° ply adjacent to the adhesive. Since these test pieces didn't fail in the adhesive, their ultimate shear strength must have exceeded 5200 PSI (See Table 5-1). Since the adhesive thickness shows a negligible effect on the ultimate strength of the joint, it is hypothesized that this group of test pieces were run at a strain rate greater than 0.05 centimeters/minute by mistake, as an increase in strain rate increases the ultimate shear strength of EA951 adhesive (Reference 22). This strain rate is unknown.

The length of overlap to thickness of adherend ratio was from 4.3 to 8.7 for all specimens. Based on the literature an adhesive failure was expected.

The results of all tests are summarized in Table (5-1). The results within each subgroup are closely spaced displaying excellent consistency.

Note is made of the fact that the average ultimate shear stresses are significantly higher than the results of the shear test section would indicate (average ultimate shear stress = 4300 PSI) for all the 0° adherend

TABLE (5-1) SUMMARY OF SINGLE LAP JOINT ULTIMATE TEST RESULTS

SPEC. NO.	FLY ORIENT.	t _{adh} (IN)	OVER- LAP (IN)	WIDTH (IN)	ULT. LOAD (LB)	AVG. ADH. SHEAR STRESS (PSI)	TYPE FAILURE	L/ t	REMARKS
063025-2	All 0°	.002	.310	1.002	1750	5630	Adhesive	4.5	Strain Rate = .05 In/Min
-9	All 0°	.001	.310	1.002	1750 AVG. 1750	5630 AVG. 5630	"	4.5	Strain Rate = .05 In/Min
063045-2	"	.004	.360	1.000	1760	4890	"	5.3	Strain Rate = .05 In/Min
-9	"	.002	.340	1.000	1910 AVG. 1835	5620 AVG. 5442	"	5.1	Strain Rate = .05 In/Min
066029-2	"	.001	.610	1.000	3000	4920	"	8.7	Strain Rate = .05 In/Min
-9	"	.001	.610	1.004	2900 AVG. 2950	4740 AVG. 4830	"	8.7	Strain Rate = .05 In/Min
066049-2	"	.004	.610	1.003	2675	4370	"	9.0	Strain Rate = .05 In/Min
-9	"	.003	.600	1.002	3250 AVG. 2956	5410 AVG. 4860	"	8.8	Strain Rate = .05 In/Min

Table (5-1) - Continued

SPEC. NO.	PLY ORIENT.	t _{adh} (IN)	OVER- LAP (IN)	WIDTH (IN)	ULT. LOAD (LB)	AVG. ADH. SHEAR		L/ t	REMARKS
						STRESS (PSI)	TYPE FAILURE		
063025-4	45°/0°/-45°/0°	.0005	.300	1.007	1275	4231	Primarily Adhesive	4.3	Strain Rate = .05 Cm/Min
-7	"	.001	.315	1.012	1185	3940	Primarily Adhesive	4.6	Strain Rate = .05 Cm/Min
-15	"	.001	.315	.992	1115	3740	Primarily Adhesive	4.6	Strain Rate = .05 Cm/Min
					AVG. 1193	AVG. 3970	Adhesive		
0630105-3	"	.005	.301	.995	1042	3480	Primarily Adhesive	4.3	Strain Rate = .05 Cm/Min
-8	"	.004	.300	1.004	996	3310	Primarily Adhesive	4.3	Strain Rate = .05 Cm/Min
-16	"	.003	.298	1.000	1047	3520	Primarily Adhesive	4.3	Strain Rate = .05 Cm/Min
					AVG. 1110	AVG. 3703	Adhesive		
066029-4	"	.0005	.604	1.007	2061	3390	Primarily Cohesive	8.6	Strain Rate = .05 Cm/Min
-8	"	.0005	.600	1.007	2204	3640	Primarily Cohesive	8.7	Strain Rate = .05 Cm/Min
-11	"	.0005	.600	1.018	2076	3410	Primarily Cohesive	8.7	Strain Rate = .05 Cm/Min
					AVG. 2114	AVG. 3480	Cohesive		

Table (5-1) - Continued

SPEC. NO.	PLY ORIENT.	t _{adh} (IN)	OVER- LAP (IN)	WIDTH (IN)	ULT. LOAD (LB)	AVG. ADH.			REMARKS
						SHEAR STRESS (PSI)	TYPE FAILURE	L/t	
0660109-7	45/0/-45/0	.002	.601	1.010	3152	5190	Cross-Ply Adjacent to Adhes.	8.4	Strain Rate Greater Than .05 Centimeters Per Minute
-10	"	.002	.600	1.005	3085	5100	Cross-Ply Adjacent to Adhes.	8.4	Strain Rate Greater than .05 Centimeters Per Minute
-13	"	.003	.601	.950	2942	5150	Cross-Ply Adjacent to Adhes.	8.4	Strain Rate Greater Than .05 Centimeters Per Minute
					AVG. 3053	AVG. 5150			

specimens. It is felt this reflects a dependence of the ultimate shear strength on strain rate. This is substantiated by Reference 22 which found the ultimate shear strength of Hysol EA951 adhesive to increase with the strain rate. The average ultimate shear stress was 6100 PSI for a strain rate of .05 inches/minute. The shear test results of Section C of Chapter IV were run at .05 centimeters/minute while the all 0° ultimate lap specimens were run at .05 inches/minute. This is a difference in loading rate of 2.54.

Based on the results summarized in Table (5-1) the influence of adhesive thickness, overlap length (L/t ratio) and of ply orientation on the ultimate load capacity of the joint can be discerned. The effect of strain rate can only be surmised as various strain rates for a similar specimen configuration were not tested.

The effect of joint strength vs. overlap length is presented in Figure (5-8). In general the joint strength increased with the length of overlap (L/t ratio) up to the upper overlap length tested of 0.60 inches. It is felt that for larger overlaps this trend would continue, possibly at a reduced rate, until the adherends began to fail. The influence of ply orientation within

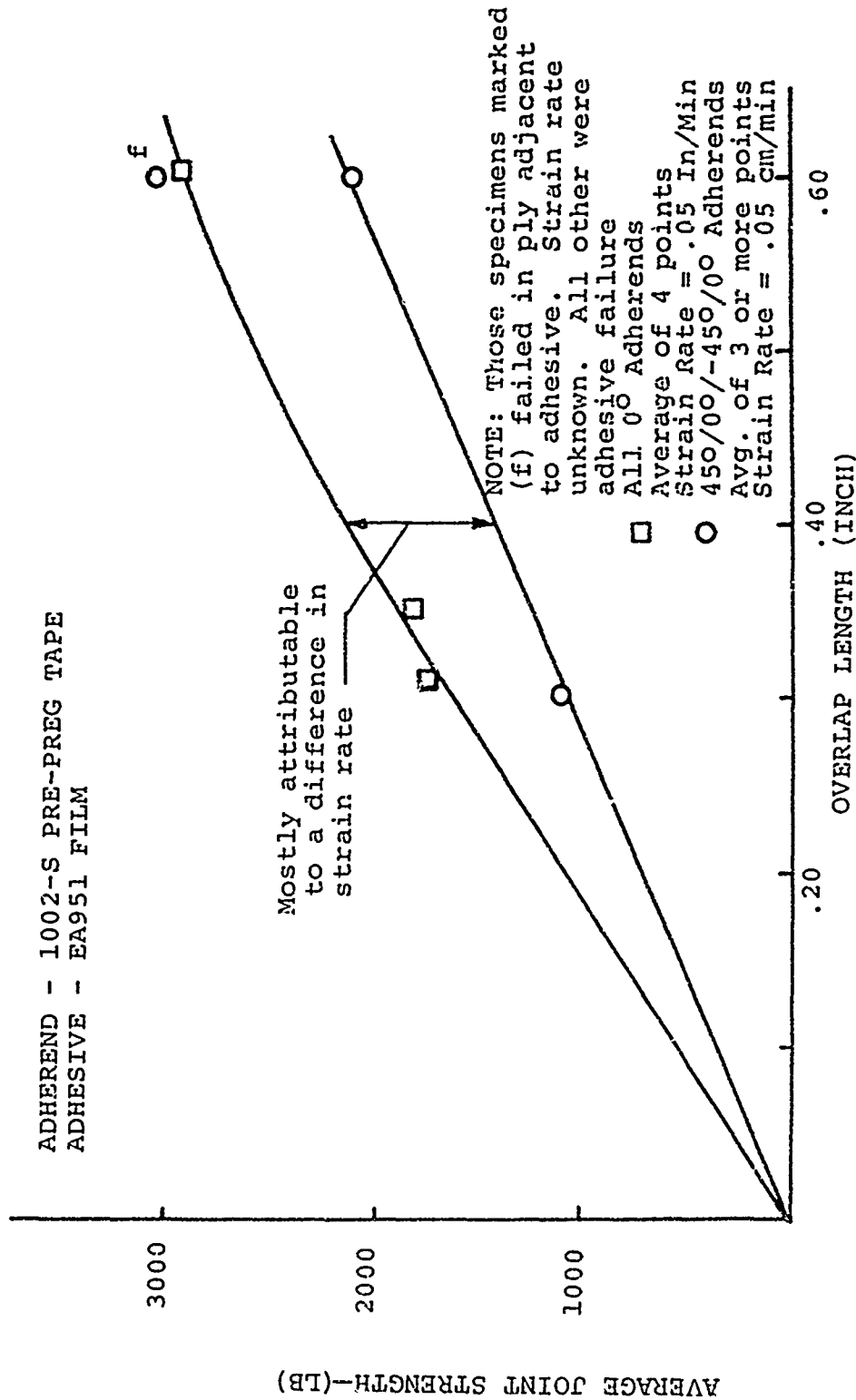


FIGURE (5-8) BONDED JOINT STRENGTH VS. OVERLAP LENGTH

the adherend and/or the orientation of the ply adjacent to the adhesive is not readily discernable. Its effect on joint strength is felt to be minor over the range of overlap lengths tested. The discrepancy observed must be attributed to the difference in strain rates at which the all 0° and $45^{\circ}/0^{\circ}/-45^{\circ}/0^{\circ}$ adherends were run. As previously mentioned this would give much higher ultimate joint loads. The effect of adhesive thickness was not discernable.

Summarizing, the strongest joint is one of large overlap with all 0° adherends and of equal extensional stiffness, loaded at an as yet undetermined optimum strain rate. Such a configuration is similar to one with isotropic adherends. Moreover, the weakest joint is one of short overlap with adherends of other than an all 0° ply orientation, loaded at a lower strain rate.

To discover why and if the results observed, excluding strain rate effects, are realistic, one must return to the parametric and shear test results discussed previously. Upon inspection of these sections the ultimate joint strength results are readily believable.

The parametric study, Figures (3-9) to (3-12) of Chapter III showed us several things.

1. To a minor degree the influence of the $45^{\circ}/0^{\circ}/-45^{\circ}/0^{\circ}$ ply orientation pattern was to increase the peak shear and normal stresses vs. an all 0° adherend pattern. This as is evidenced in Figure (5-8) would cause the ultimate shear stress to be reached at a lower load, yielding reduced joint strength.
2. The length of overlap has a much more severe effect on the peak shear and tensile stresses as evidenced in the parametric study, Figures (3-11) and (3-12). The longer lap length significantly reduced the peak stresses thus leading one to expect an increase in joint capacity as long as the adhesive stress is the critical failure item.

In addition, the shear test results of Chapter IV, Figures (4-31) and (4-50) state that the effective shear and tensile moduli are reduced with increasing overlap length, decreasing the peak stresses and increasing the joint strength even more. To discern how much of an effect these variables had on the results (i.e. the influence of the effective moduli vs. the overlap length itself) is not discernable at this time. However, the length of overlap is thought to be most significant.

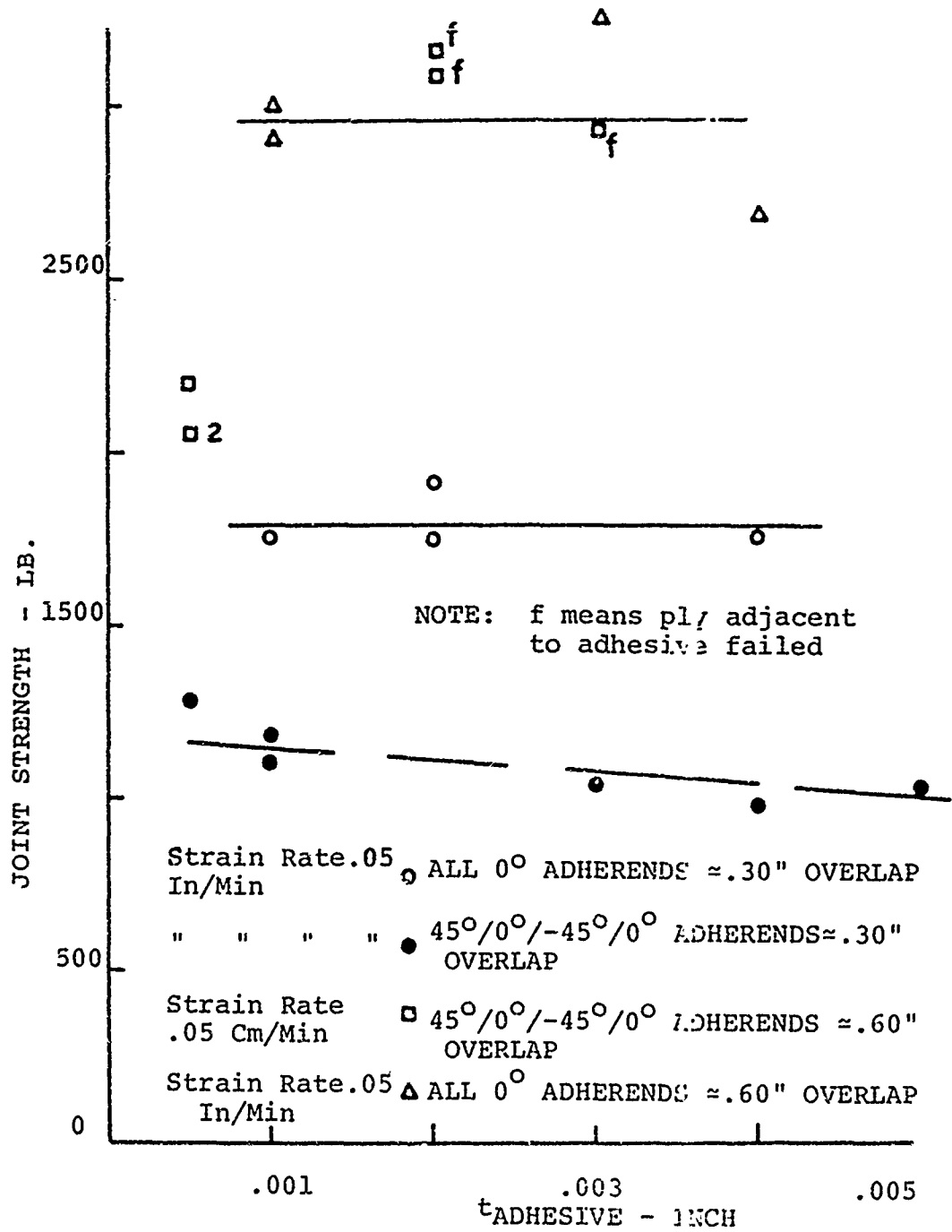


FIGURE (5-9) JOINT STRENGTH VS. ADHESIVE THICKNESS

Figure (5-9) displays the influence of adhesive thickness on joint strength. No obvious trends are evident over the rather narrow range of adhesive thicknesses covered. However, the shear test results of Chapter IV, Figures (4-29) and (4-30) would lead one to believe that the effective moduli should experience an increase in stiffness, thus raising the peak stress as the adhesive thickness increases. A lack of significant adhesive thickness variation as evidenced in Table (5-1) meant at most a small change in the effective moduli and in turn the peak stresses for the specimens tested. Thus, to discern a thickness effect or lack of it, a wider range of adhesive thicknesses should be studied. Moreover, since the shear load vs. deformation curve of Chapter IV, Figure (4-39) is essentially that of an elastic - perfectly plastic body, one wonders if the influence of the initial value of effective shear modulus would influence the ultimate strength of the joint. Again, a properly designed series of tests would answer this question.

Overall, it has been shown that excellent correlation between the analysis predictions of Bond3 (parametric study) vs. the ultimate strength of the single lap joint are possible. While Bond3 is an

elastic analysis, its capability to predict the effects of peak shear and tensile stresses accurately has been shown to be extremely useful in predicting ways to increase the capacity of a single lap joint.

Based on the results presented thus far, it was deemed desirable to attempt to provide one with an ultimate failure design criteria. Fundamentally, there are two distinct modes of failure in a single lap joint: an adhesive failure or an adherend failure. Mathematically, these modes of failure can be stated as follows(22). For an ultimate adhesive failure to occur.

$$\frac{t}{L} F_{tu} \geq \frac{P_{ult}}{L} \geq F_{su} \quad (5-1)$$

For an adherend failure to occur

$$\frac{t}{L} F_{tu} \leq \frac{P_{ult}}{L} \leq F_{su} \quad (5-2)$$

where:

P = ultimate applied axial load (lbs/in)

W = width (1.0 inches in all cases)

L = the overlap length of the joint (inches)

t = thickness of the weaker adherend (inches)

F_{tu} = ultimate tensile strength of the weaker
adherend (PSI)

F_{su} = ultimate shear strength of the adhesive
(PSI).

Since lap joints in which adherends were the initial failure component were not considered in this work, only a correlation between predicting ultimate loads vs. test results will be attempted. One can define the average shear stress in the adhesive at failure as

$$\tau_{avg.} = \beta F_{su} = \frac{P_{ult}}{L} \quad (5-3)$$

thus,

$$\beta = \frac{F_{su}}{\tau_{avg.}} \quad (5-4)$$

Based on the test results in Table (5-1), one can get an average failure stress. Moreover, based on the shear test results of Chapter IV Section C, one found that F_{su} for a strain rate of 0.05 centimeters/minute was 4300 PSI. However, since all the 0° adherend specimens were run at a strain rate of 0.05 inches/minute, and since it has been shown in Reference 22 that Hysol EA951 adhesive is strain rate sensitive, the ultimate shear allowable determined in this reference for a 0.05

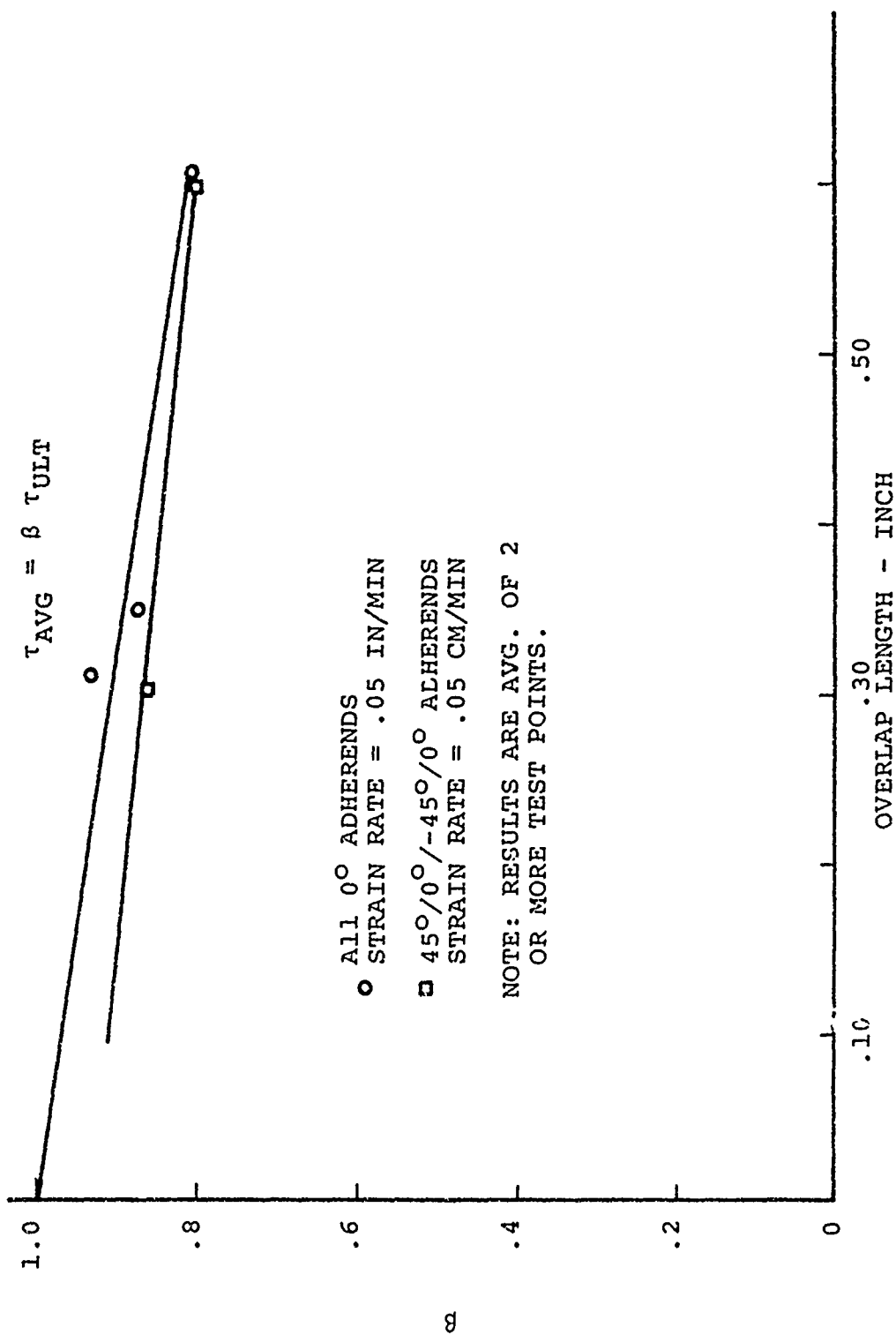


FIGURE (5-10) β VS. OVERLAP LENGTH

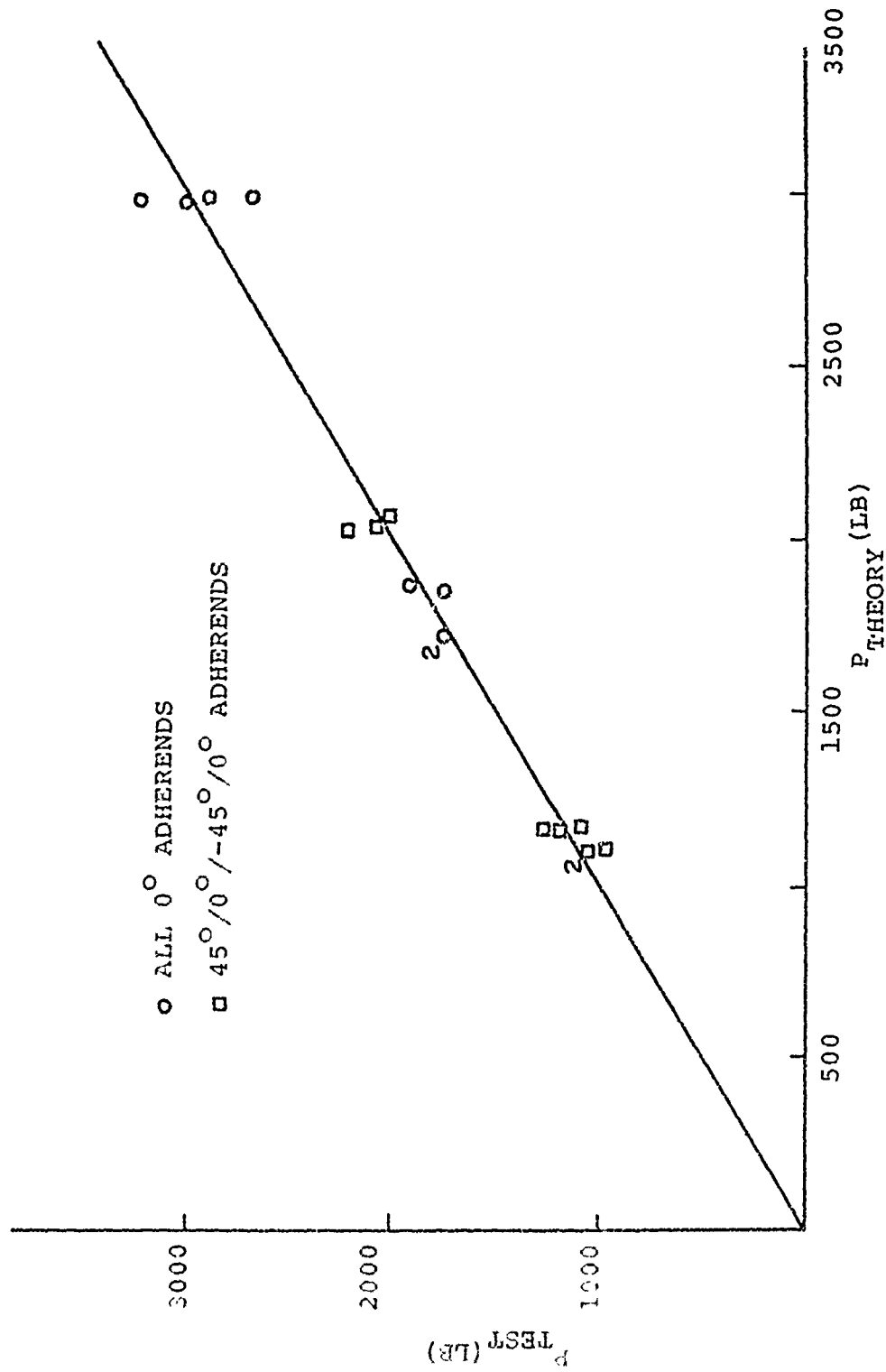


FIGURE (5-11) P_{TEST} VS. P_{THEORY}

TABLE (5-2) SUMMARY OF THEORETICAL VS. TEST ULTIMATE DESIGN LOAD RESULTS

SPEC. NO.	PLY ORIENTATION	F _{su} (PSI)	P _{theory} = (β)F _{su} (L)		P _{test} (LB)	ERROR
			(LB)	(L)		
063025-2	All 0°	6100*	1701		1750	2.90
-9	"	6100*	1701		1750	2.90
063045-2	"	6100*	1900		1760	7.30
-9	"	6100*	1900		1910	.50
066029-2	"	6100*	2977		3000	.80
-9	"	6100*	2977		2900	2.60
066049-2	"	6100*	2970		2675	9.90
-9	"	6100*	2970		3250	9.40
063025-4	45°/0°/-45°/0°	4300	1146		1278	11.50
-7	"	4300	1146		1185	3.40
-15	"	4300	1146		1115	2.70
0630105-3	"	4300	1118		1042	6.80
-8	"	4300	1118		996	10.90

1
0
4
1

Table (5-2) - Continued

SPEC. NO.	PLY ORIENTATION	F _{su} (PSI)	P _{theory} = (β)F _{su} (L) (LB)	P _{test} (LB)	% ERROR
0630105-16	45°/0°/-45°/0°	4300	1118	1047	6.30
066029-4	"	4300	2051	2061	.50
-8	"	4300	2051	2204	7.40
-11	"	4300	2051	2076	1.20

* For .05 in/min Strain Rate
per Reference (22).

inches per minute strain rate was used. This value was 6100 PSI.

Figure (5-10) is a plot of β vs. overlap length. It shows only a marginal difference between the two adherend systems studied, further emphasizing that strain rate was mainly responsible for the discrepancy in Figure (5-8). Employing Figure (5-10) and the basic design equation

$$P_{ult} = \beta F_{su} L \quad (5-5)$$

one is able to predict the ultimate failure load of a single lap joint. Table (5-2) summarizes the values of predicted load, actual test load and the per cent error based on the design load vs. the test results. In general the error between test vs. predicted load is within 10 per cent. This is seen to be excellent correlation. Figure (5-11) is also presented showing the excellent correlation between test and theory.

In summary, therefore, it is concluded that the above approach is very feasible for predicting the ultimate strength of a single lap joint, if the design is adhesive critical. However, the strain rate and its ultimate shear strength must be known.

Conclusions:

Based on a review of the enclosed ultimate test data, the following conclusions can be ascertained.

- A. For the range of geometries tested, the ultimate joint strength increases with an increase in overlap length.
- B. The strain rate at which the specimens were tested is extremely important, Hysol EA951 adhesive being quite strain rate sensitive. Increasing the strain rate increases the ultimate shear strength of the adhesive. This can alter the type of joint failure expected and/or increase the ultimate strength of the joint.
- C. Ply orientation overall, or of the ply adjacent to the adhesive, had a minor effect on joint strength for the range of variables tested.
- D. The Bond3 parametric study of Chapter III proved extremely useful in explaining the ultimate strength trends observed.
- E. The influence of adhesive thickness over the range of values tested had a minimal influence on joint strength, for the range

of variables.

- F. A feasible ultimate test procedure for adhesive critical design, incorporating strain rate effects, was put forth.

Proposed Research.

1. A test program to discern the influence of strain rate on the ultimate shear strength of Hysol PA951 adhesive material and its effect on ultimate joint strength and mode of failure should be performed.
2. A test program involving longer overlap lengths to complete the enclosed ultimate strength vs. overlap length plots should be performed.
3. An adherend critical design criteria should be advanced and substantiated by tests.

B. FATIGUE TEST RESULTS OF BONDED SINGLE LAP
JOINTS

The objective of this section was four fold:

(1) to study the influence of certain geometric variations of the lap joint configuration on the fatigue life of the joint; (2) to discern the relative importance of the shear proportional limit stress on the fatigue behavior of the single lap joint; (3) to establish if possible a certain design procedure for a single lap joint in fatigue and (4) to introduce specific introductory comments on the type of adhesive failure surfaces observed. A more detailed study of these surfaces will hopefully be conducted during the next year.

As reported in the previous section, the lap joint fatigue specimens were fabricated together with the ultimate strength lap joint test pieces. Thus their fabrication and curing factors are identical. The adherends are 1002-S pre-preg tape selected because of its superior fatigue characteristics vs. E-glass (5/1). The adherends were nominally .063 inches thick by 1.0 inches wide. The overall physical dimensions were the same as those of the ultimate strength lap specimens. Again, the adhesive selected was

EA951. The fundamental reason for this is its good shear and tensile ultimate strength properties plus its extremely low stiffness characteristic in tension and shear as evidenced by the shear and tension test results in Chapter IV. It is the soft, ductile nature of the nylon-epoxy adhesive which reduces peak stresses in the adhesive at the discontinuous ends of the joint. In turn, this more uniform transfer of the load results hypothetically in an improved fatigue life of the joint as long as the adhesive is the critical failure component.

The joint tested was an equal adherend configuration. Figure (5-12) defines its general shape and the various nomenclature used in defining pertinent geometrical quantities. A typical part ready to be fatigue tested is shown in Figure (5-13). The test setup and fixtures used in this program made use of a closed-loop servo-controlled hydraulic system with a peak capacity of 6000 pounds. The hydraulic system consisted of an actuator, servo-valve, pump, dump valve and associated industrial hydraulic and electronic control equipment. An instrumented and calibrated load link is mounted in series with the specimen and the friction grip assembly, and serves as the load monitoring device for each specimen. Electronic microswitches deactivate the system when failure occurs.

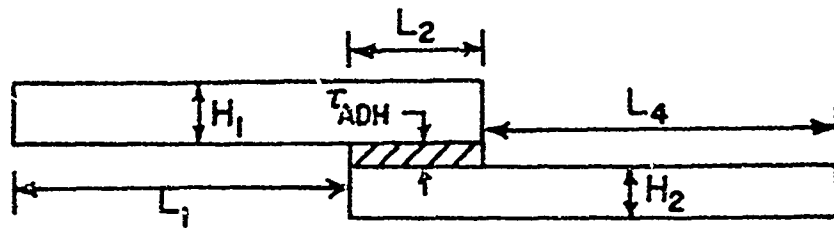


FIGURE (5-12) TYPICAL SINGLE LAP SPECIMEN NOMENCLATURE

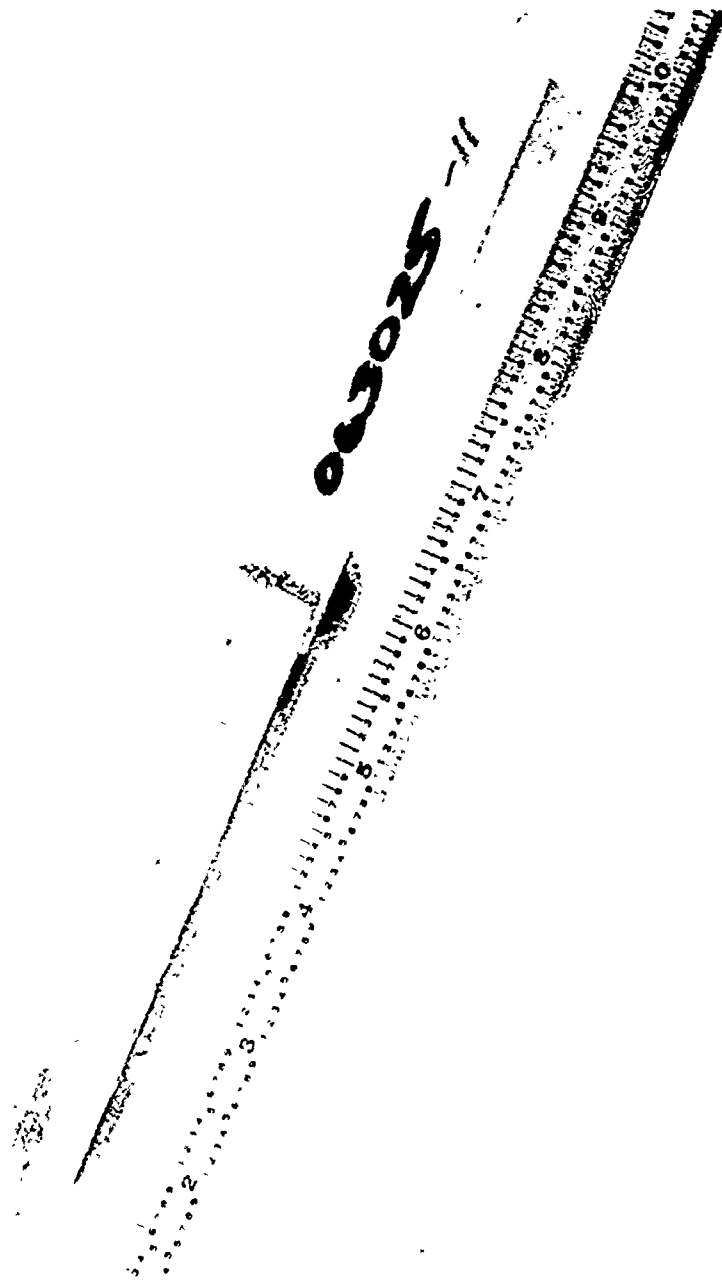


FIGURE (5-13) SINGLE LAP JOINT FATIGUE SPECIMEN

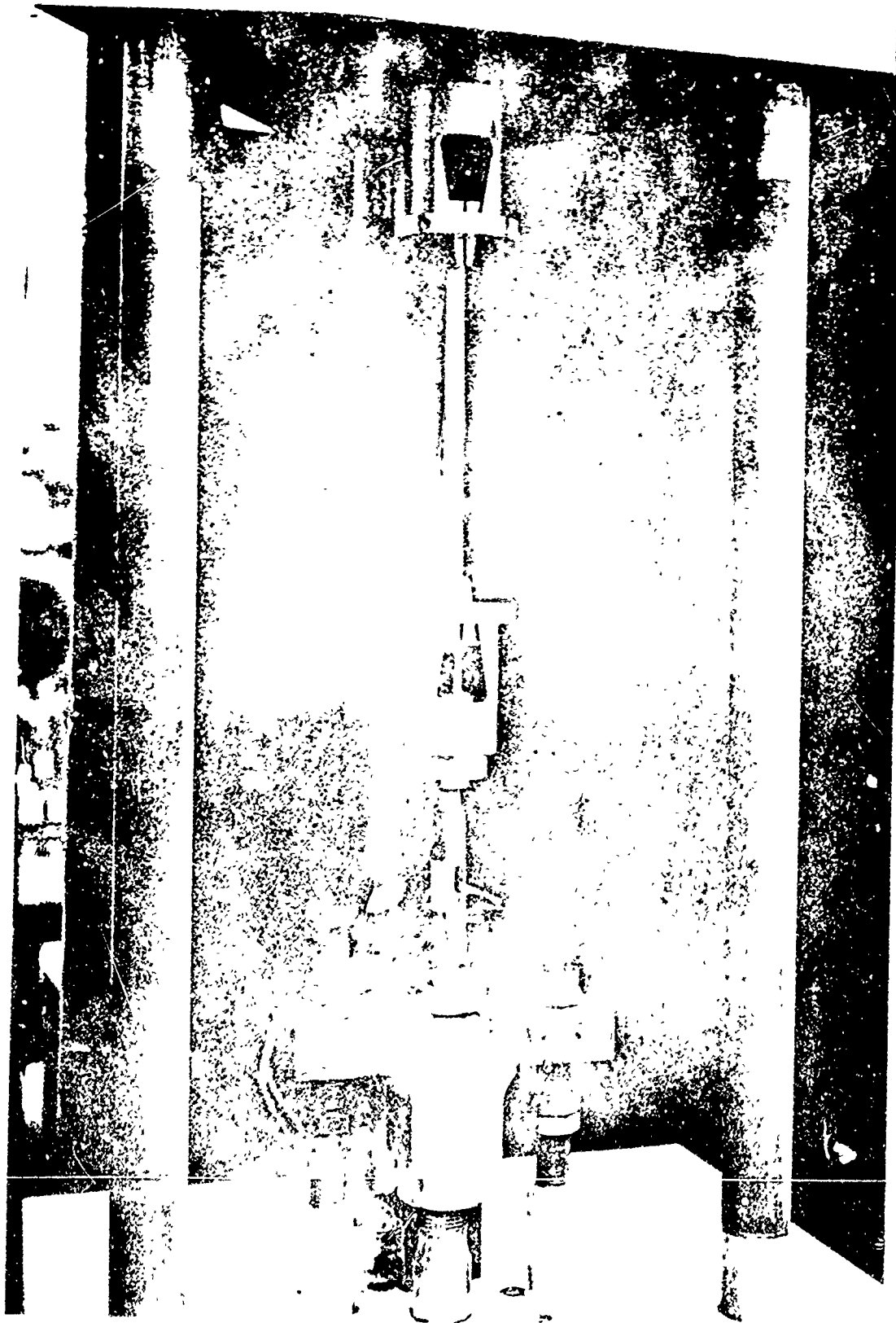


FIGURE 5-14 FATIGUE TEST FIXTURE

Output from the instrumented load link is amplified with an Ellis model BA-13 bridge amplifier with an oscilloscope display. The test frequency for this testing was set at 900 c.p.m. with a Hewlett-Packard oscillator. The upper limit on the test frequency was set at 900 c.p.m. to alleviate any secondary thermal effects which tend to degrade the fiberglass system above this frequency. Figure (5-14) displays the fatigue test set up with a single lap specimen in the grips. The fatigue loading used was of a constant amplitude type. The specimens were loaded at a stress ratio = $\frac{\text{MINIMUM LOAD}}{\text{MAXIMUM LOAD}}$ of + .10. The load was applied as a mean load (i.e. constant amplitude load) + an alternating load (i. e. a variable amplitude load).

A second series of tests is presently proceeding. It involves a multi-step loading pattern to determine the influence of simple variable amplitude loadings on the fatigue life of the joints. In addition a number of single-lap joint specimens with Dupont fiber PRD-49 type II adherends will be tested in an attempt to compare the fiberglass static and fatigue test results to another material system. It is hoped a definite correlation between results will be evident.

The data presented in this Section results from

57 lap joint fatigue tests. Twenty-nine had all zero degree uni-ply orientation while the twenty-eight angle ply specimens had a $45^{\circ}/0^{\circ}/-45^{\circ}/0^{\circ}$ ply orientation pattern. This was one of the parametric variables studied. In addition two different overlap lengths of 0.30 and 0.60 inches, and two adhesive thickness variations of 2.5 and 10 mils were studied. The overlap lengths were restricted to below a ratio of overlap length to a adherend thickness of 12 to precipitate an adhesive failure.

C. ALL 0° ADHEREND FATIGUE TEST RESULTS

The overall results of the all zero degree ply adherends for the thickness and overlap variations are summarized in tables (5-3) and (5-4). The overlap lengths tested were .30, .36 and .62 inches. The adhesive thickness again was a problem in that the nominal 2.5 and 10 mil film thickness, after being cured per the manufacturers recommended procedure, exhibited a significant amount of oozing from the joint. As a result, the adhesive thicknesses were between 1 and 3 mils with the bulk of the thicknesses being approximately 2 mils. Therefore, any effort to discern a correlation between adhesive thickness and fatigue life was not possible.

Pertinent adherend dimensions are recorded in the tables as are the range of temperature and relative humidity the test pieces were exposed to during their time of test. The temperature is seen to be quite uniform while the relative humidity did fluctuate somewhat.

As stated earlier, one of the primary objectives of this test program was to determine the influence of the shear proportional limit stress of the adhesive on the

TABLE (5-3) SUMMARY OF FATIGUE TEST RESULTS - ALL 00 ADHERENDS

SPEC. NO.	OVER LAP (in)	t _{adh} (in)	TEMP. RANGE (°F)	REL. HUM. RANGE (%)	MEAN ±ALT LOAD (LB)	MAX* LOAD % OF ULT. LOAD	MAX** SHEAR STRESS @ MEAN LOAD	MAX** NORMAL STRESS @ MEAN LOAD	SHEAR S.C.F. @ MAX LOAD	CYCLES X 10 ⁶	TYPE FAILURE
063025-1	.31	.0018	75	22-30	55±45	5.7	-	-	-	4.74	Test Stopped
-3	.31	.002	75	25-27	165±135	17.2	-	-	-	4.781	" "
-4	.31	.002	75	27-38	220±180 275±225	23.0 28.5	- 1017	- 877	-	1.000 1.152	" "
-5	.30	.0018	75	26	330±270	34.4	-	-	-	.838	Band evident CoHes-Adh
-6	.30	.0015	75	15-17	330±270	34.4	-	-	-	.288	Band evident CoHes-Adh
-7	.30	.001	76	17	330±270	34.4	-	-	-	.518	Band Evident CoHes-Adh
-8	.30	.0012	75	15-32	275±225	28.5	1017	877	-	2.301	Band Evident CoHes-Adh
-10	.31	.0012	75	39-41	247±202	25.7	930	785	1.1	4.530	Test Stopped
-11	.30	.0015	76	42-48	247±202	25.7	930	785	1.1	6.144	Test Stopped

Table (5-3) - Continued

SPEC NO.	OVER LAP (In)	t _{adh} (In)	TEMP. RANGE (OF)	REL. HUM. RANGE (%)	MEAN ±ALT LOAD (L/B)	MAX* LOAD % OF ULT. LOAD	MAX** SHEAR STRESS @ MEAN LOAD	MAX** NORMAL STRESS @ MEAN LOAD	SHEAR S.C.F. @ MAX LOAD	CYCLES X 10 ⁶	TYPE FAILURE
063045-1	.37	.004	75	20-32	330±270	32.7	-	-	-	1.580	Adh-Bands Starting
-3	.37	.003	75	32	330±270	32.7	-	-	-	.897	CoHes-Adh Bands Starting
-4	.36	.0025	75	32-34	330±270	32.7	-	-	-	2.901	CoHes-Adh Bands Starting
-5	.36	.0025	74	13-32	275±225	27.3	1017	877	1.16	4.753	Adh- No Bands
-6	.36	.002	75	12-19	275±225	27.3	1017	877	1.16	4.689	Test Stopped
-7	.35	.002	75	12-14	275±225	27.3	1017	877	1.16	5.044	CoHes-Adh- Bands Starting

* Based on .05 in/min strain rate
shear ultimate test results of Chapter IV

ADHEREND - 1002-S, PRE-PREG TAPE
ADHESIVE - EA951 Film
All Spec. ~.95 inches wide
R = +.10

** Per Bond3 Analysis

TABLE (5-4) SUMMARY OF FATIGUE TEST RESULTS - ALL 0° ADHERENDS

SPEC. NO.	OVER LA.2 (In)	t _{adh} (In)	TEMP. RANGE (°F)	REL. HUM. RANGE (%)	MEAN ±ALT LOAD (LB)	MAX*		MAX**		SHEAR S.C.F. @ MAX LOAD	CYCLES X 10 ⁶	TYPE FAILURE
						LOAD % OF ULT. LOAD	OF LOAD	MAX** SHEAR STRESS @ MEAN LOAD	MAX** NORMAL STRESS @ MEAN LOAD			
066029-1	.60	.0025	76	12-20	550±450	34.0	-	-	-	-	.116	CoHes-Adh- Bands Evident
-3	.625	.002	75	19	550±450	34.0	-	-	-	-	.129	CoHes-Adh-Bands Evident on ends
-4	.625	.0025	75	19-20	495±405	30.5	-	-	-	-	.303	CoHes-Adh-Bands Evident on ends
-5	.625	.002	75	14-29	330±270	20.4	731	800	1.36	4.102	Test Stopped	
-6	.620	.002	75	28-48	330±270	20.4	731	800	1.36	4.009	"	
-7	.610	.0015	75	24-31	330±270	20.4	731	800	1.36	4.133	"	
-8	.610	.0015	75	45-48	385±315	27.0	-	-	-	3.327	CoHes-Adh-Bands Evident on ends	
-10	.610	.0017	75	45-50	385±315	27.0	-	-	-	5.703	Runout	
066049-3	.620	.0022	74	20-22	440±360	30.5	-	-	-	.439	CoHes-Adh Bands Evident on Ends	

Table (5-4) Continued

SPEC. NO.	OVER LAP (In)	t _{adh} (In)	TEMP. RANGE (°F)	REL. HUM. RANGE (%)	MEAN ±ALT LOAD (LB)	MAX* LOAD % OF ULT. LOAD	MAX** SHEAR STRESS @ MEAN LOAD	MAX*** NORMAL STRESS @ MEAN LOAD	SHEAR S.C.F. @ MAX LOAD	CYCLES X 10 ⁶	TYPE FAILURE
066049-4	.620	.0025	74	24-26	385±315	23.6	-	-	-	1.294	CoHes-Adh Bands Evident on ends
-5	.610	.003	74	25-26	385±315	23.6	-	-	-	1.052	CoHes-Adh Bands Faintly Evident on ends
-6	.620	.0025	75	26-41	330±270	20.2	731	800	1.36	4.616	Test Stopped
-7	.610	.0025	75	26-45	330±270	20.2	731	800	1.36	1.306	Failure Due Inadvertent Mach.Overload (Adh)
-8	.610	.002	75	20-30	330±270	20.2	731	800	1.36	4.033	Test Stopped

* Based on .05 in/min strain rate
shear ultimate test results of Chapter IV

** Per Bond3 Analysis

ADHEREND - 1002-S, PRE-PREG TAPE
ADHESIVE - EA951 Film
All Spec.±.95 inches wide
R = +.10

fatigue life of the joint. To accomplish this, coincident with the development of the Bond3 stress analysis program and the determination of the proportional limit stress in the shear test program of Chapter IV, a trial and error procedure was adopted to determine at what load level no visible damage to the specimen had occurred. Then, using the results from the proportional limit shear tests, in conjunction with the Bond3 analysis program, one could observe if any correlation exists between the shear proportional limit stress and a lack of damage to a specimen loaded in fatigue for a specified number of cycles.

It was arbitrarily decided that fatigue runout for these tests (i.e. the number of cycles at which you stop the test) would be defined as 4.0×10^6 cycles. Based on this criteria, fatigue runout was achieved at a mean load of 247 lbs. for the .30 inch overlap specimens, at 275 lbs., for the .36 inch overlap specimens and at 330 lbs. for the .62 inch overlap specimens.

The Bond3 analysis was then conducted using the proportional limit values determined in the shear tests of Chapter (IV) and the mean loads at which runout was achieved. Table (5-5) tabulates these results. The correlation seems quite good. In essence it states that

TABLE (5-5) COMPARISON OF THE THEORETICAL MAXIMUM SHEAR STRESS
AT RUNOUT VS. SHEAR PROPORTIONAL LIMIT STRESS

SPEC. NO.	MAX SHEAR* PROPORT. LIMIT STRESS (PSI)	MAX SHEAR** STRESS FOR MEAN LOAD AT RUNOUT (PSI)
063025	1015	930
063045	990	1017
066029	590	731
066049	590	731

*From Shear Test Results in Chapter IV, Table (4-6)

**From Bond3 Analysis

TABLE (5-6) ULTIMATE TEST RESULTS OF FATIGUE RUNOUT SPECIMENS

SPEC NO.	L ₁ (In)	L ₂ (In)	L ₃ (In)	H ₁ (In)	H ₂ (In)	t _{adh} (In)	WIDTH (In)	SURF. AREA (In ²)	FAILURE LOAD		AVG. ADH. STRESS (PSI)	LOAD-CYCLES TYPE FAILURE
									(#)	% OF ULT.		
063025-1	4.21	.31	4.21	.067	.068	.00175	.940	.2914	1485	(85)	5096	55±45 4.74 x 10 ⁶ Adhes-No Bands
-3	4.21	.31	4.21	.066	.069	.002	.945	.2930	1528	(89)	5215	165±135 4.78x 10 ⁶ Adhesive no bands
-4	4.21	.31	4.21	.069	.066	.002	.95	.2945	1320	(76)	4482	220±180 @ 1 x 10 ⁶ and 275±225 @ 1.15 x 10 ⁶ Adhesive no bands
063045-6	4.16	.36	4.15	.069	.069	.002	.946	.3405	905	(49)	2658	275±225 459 x 10 ⁶ Cohes - Adhes. Bands starting on one end
066029-5	3.94	.625	3.94	.072	.067	.002	.953	.5956	1985	(67)	3332	330±270 4.1 x 10 ⁶ Cohes - Adhes Band one end

Table (5-6) - Continued

SPEC. NO.	L ₁ (In)	L ₂ (In)	L ₃ (In)	H ₁ (In)	H ₂ (In)	t _{adh} (In)	WIDTH (In)	SURF AREA (In ²)	FAILURE LOAD		AVG. ADH. STRESS (PSI)	LOAD-CYCLES TYPE FAILURE
									(#)	% OF ULT.		
066029-5	3.94	.62	3.94	.072	.067	.002	.950	.589	2920	(99)	4957	330±270 4.01 x 10 ⁶ Adhesive-no band
-7	3.94	.61	3.94	.073	.067	.0015	.945	.5764	2540	(86)	4406	330±270 4.13 x 10 ⁶ CoHes-Adhes Bands starting
066049-6	3.92	.62	4.02	.069	.070	.0025	.952	.5902			Bad Data	330±270 CoHes-Adhes 4.616 x 10 ⁶ No bands
-8	3.94	.61	4.02	.368	.071	.002	.950	.5795	860	(29)	1484	330±270 4.03 x 10 ⁶ Adhesive No Bands

*Based on ultimate test results
of Section A.

ADHEREND - 1002-S PRE-FREG TAPE
ADHESIVE - EA951 FILM
PLY ORIENTATION All 0°

if the peak shear stress in the adhesive at mean load is kept below the shear proportional limit stress of the adhesive, a marked increase in fatigue life of the joint can be achieved, assuming an adhesive failure is the critical mode. In this series of tests, in which 100 lb. load increments were used, an increase in life of the joint of 5 times or more could reasonably be expected. Moreover, referring to table (5-6) one sees that for those specimens in which runout was attained anywhere from 50 to 99 per cent of the ultimate strength of the joint remained. This in turn indicates that a much longer life for those parts which achieved runout could have been achieved if the fatigue testing had continued. Again, referring to table (5-3) it is seen that the maximum load (mean + alternating) at which fatigue runout occurred was a definite function of lap length. Runout for the .30 and .36 inch overlap specimens was at approximately 26 per cent of the ultimate load results of the previous section. The .62 inch specimens achieved runout at 20 per cent of ultimate load. However, these results are strain rate sensitive as the ultimate results of the previous section indicate.

Based on these results a plot of cycles to failure vs. maximum fatigue design load is presented in Figure

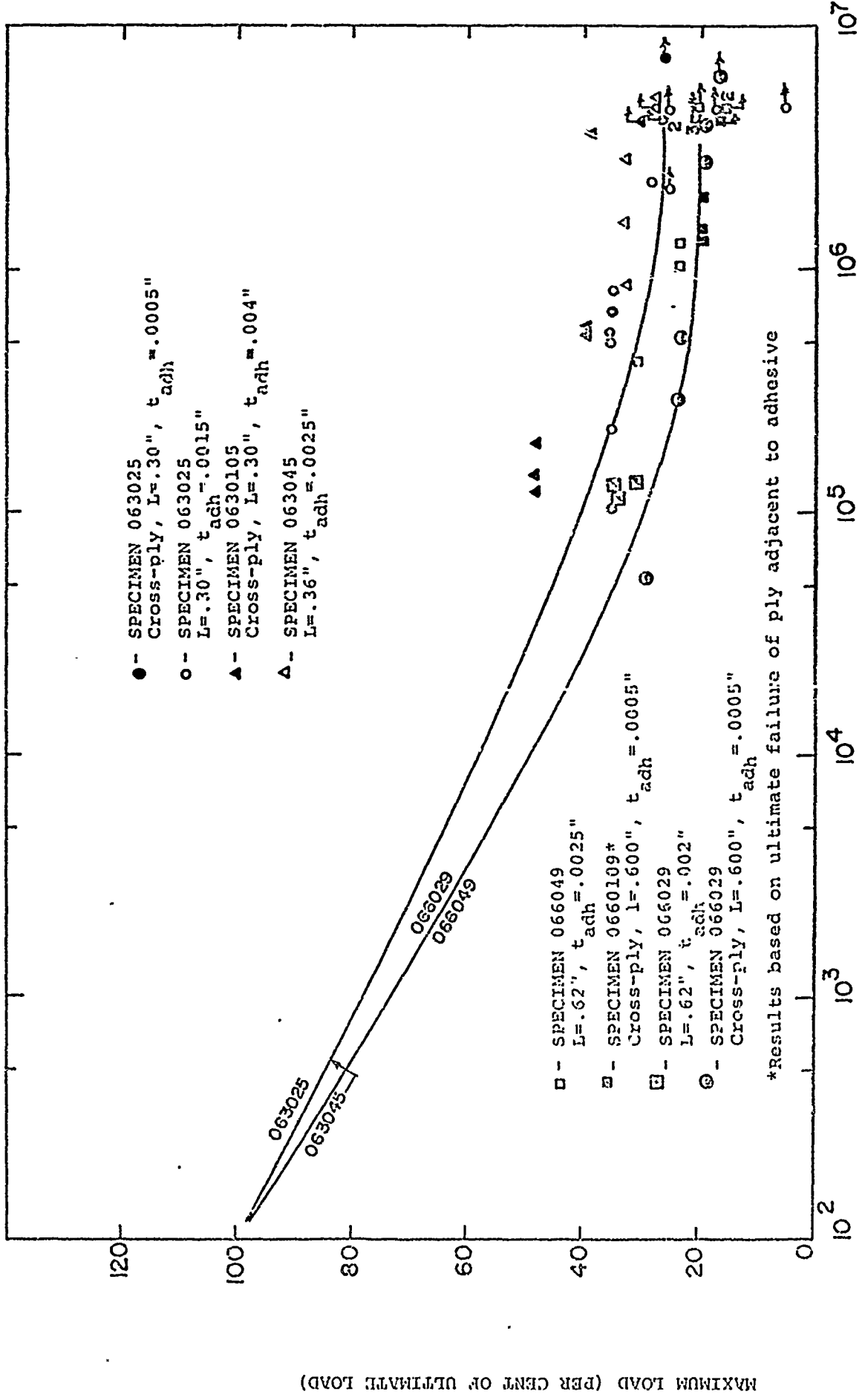


FIGURE (5-15) MAXIMUM DESIGN FATIGUE LOAD FOR SINGLE LAP JOINT VS. CYCLES TO FAILURE

(5-15). Using these results and the ultimate design procedure outlined in the previous Section a fatigue design procedure can be adopted. Thus knowing the ultimate design load per the previous Section's design methodology one can, for a given number of cycles and overlap length, determine the maximum design fatigue load for a given lap joint. However, one must realize that for different adhesive systems, unequal adherends, environmental effects and varying strain rates (Figure (5-15) would need to be revised. However, the fundamental design methodology is unalterable.

It is hypothesized that this significant increase in fatigue life with respect to staying below the proportional limit stress of the adhesive, is primarily due to the retention of an elastic medium which has experienced very little plastic flow. This in turn usually means a slower propagation of cracks within the adhesive to the critical crack length whereby failure suddenly occurs.

Figures (5-16) and (5-17) present a possible alternate design approach. Based on a maximum alternating load criteria and the Bond3 analysis program, Figure (5-16) is a plot of peak adhesive shear stress vs. fatigue life. Figure (5-17) plots the peak adhesive tensile

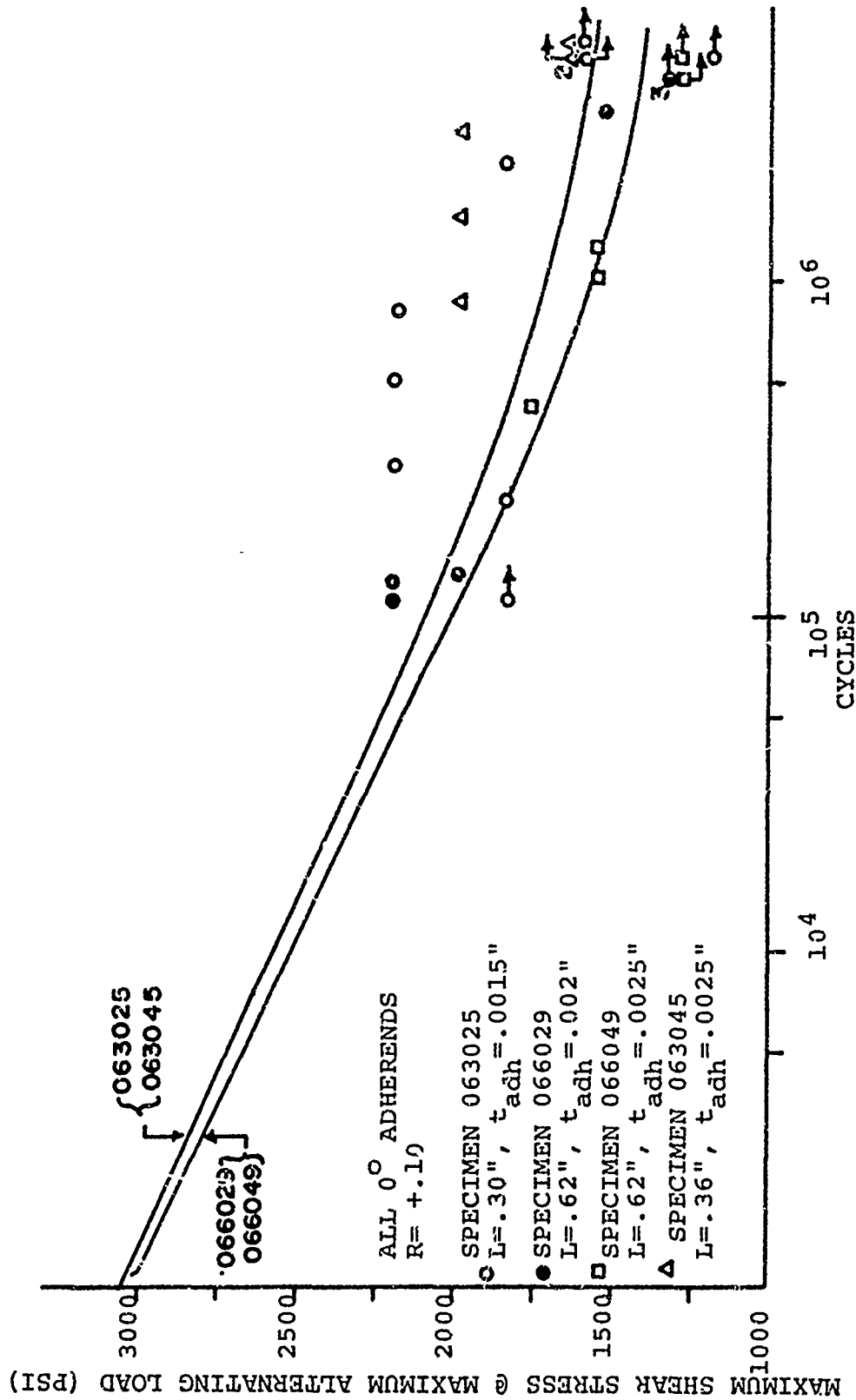


FIGURE (5-16) MAXIMUM SHEAR STRESS IN ADHESIVE VS. CYCLES TO FAILURE

0

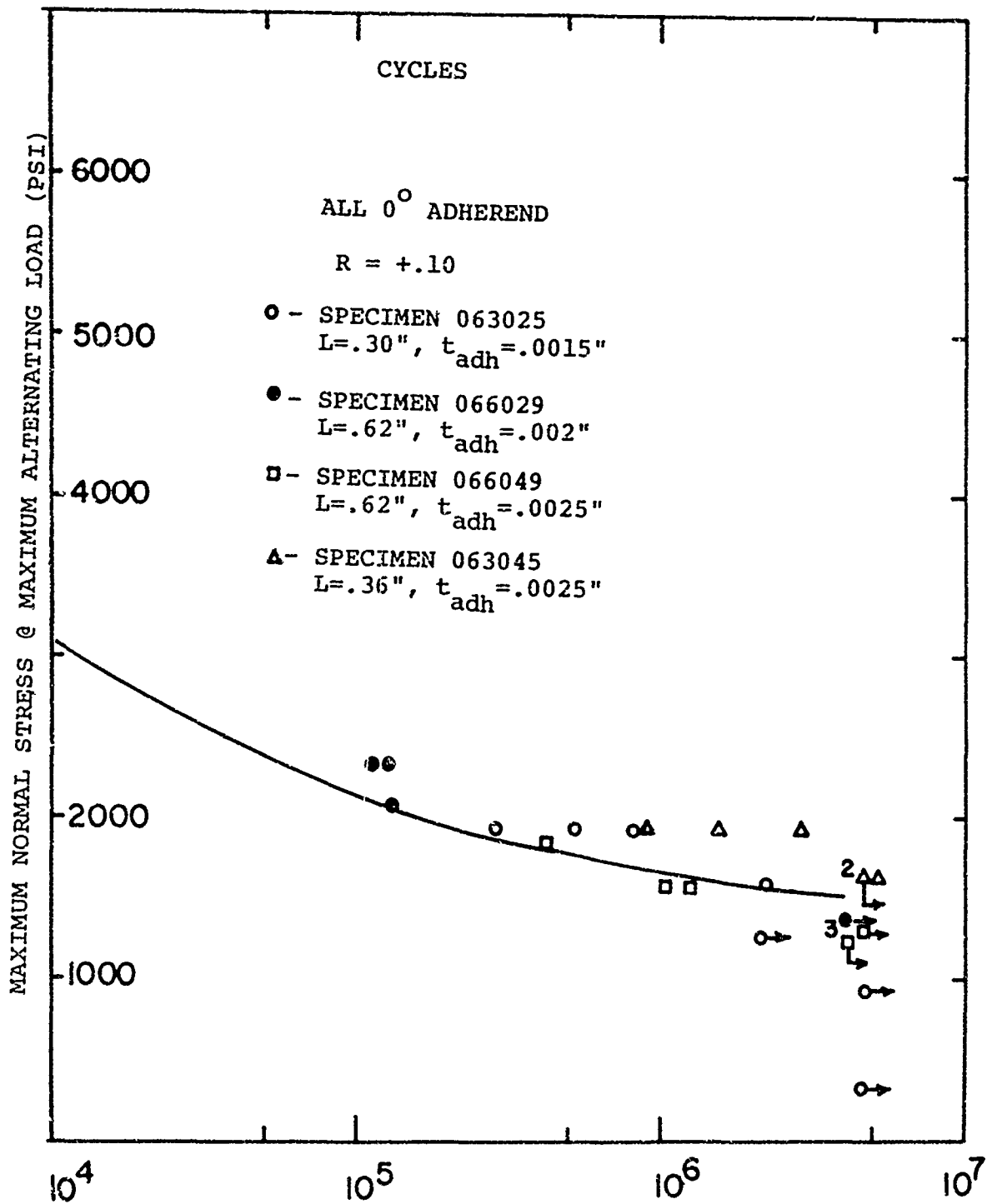


FIGURE (5-17) MAXIMUM NORMAL STRESS IN THE ADHESIVE VS. CYCLES TO FAILURE

stress vs. fatigue life. Reflecting on these results one can discern that the fatigue life of the part achieved runout when the maximum alternating load peak tensile and shear stresses were approximately 1500 PSI. That this equality of shear and tensile stresses is other than coincidence can not be ascertained at this time. However, by looking at other adhesive systems and their peak stress levels at runout vs. their maximum alternating load, one could clarify this gray area.

Based on the results presented thus far, several suggestions on ways to improve the fatigue life of a lap joint designed to fail in the adhesive can be ascertained.

1. An adhesive with extremely low moduli which tends to reduce peak stresses in the adhesive is desirable.
2. An adhesive with a high shear proportional limit stress will most likely increase the life of the joint.
3. Reducing the unsupported lengths, L_1 and L_3 in Figure (5-12) would reduce the peak stresses in the adhesive by reducing the moment induced at the discontinuous ends of the overlap.

4. An optimum overlap length, as yet undetermined, most likely would increase the fatigue life of the lap joint.

An initial examination of the fatigue failure surfaces for the all zero degree adherends has been made. A more detailed study of these surfaces will be made during the next year.

Of those specimens which exhibited failure prior to four million cycles, all exhibited an adhesive-cohesive failure as detailed in tables (5-3) and (5-4), and Figures (5-18) and (5-19). Typically, the failed surfaces displayed distinct bands as shown in Figure (5-20). The bands were harder to discern in the thicker adhesives and in numerous instances were uneven in their width over the width of the joint. The bands at each loaded end of the joint were similar and seemed to be smooth and of a cohesive nature while the center region displayed a failed surface analogous to that of an ultimately failed specimen. It is assumed that the smooth nature of the outer bands was due to the minute motion of the adhesive within its thickness after cracking had occurred. Further it is believed the cracks initiated from the ends of the overlap, moving inward until the next section of the remaining



Fatigue Failure Surface

Ultimate Failure Surface

Figure (5-18) All 0° Adherends



Fatigue Failure Surface

Ultimate Failure Surface

Figure (5-19) All 0° Adherends

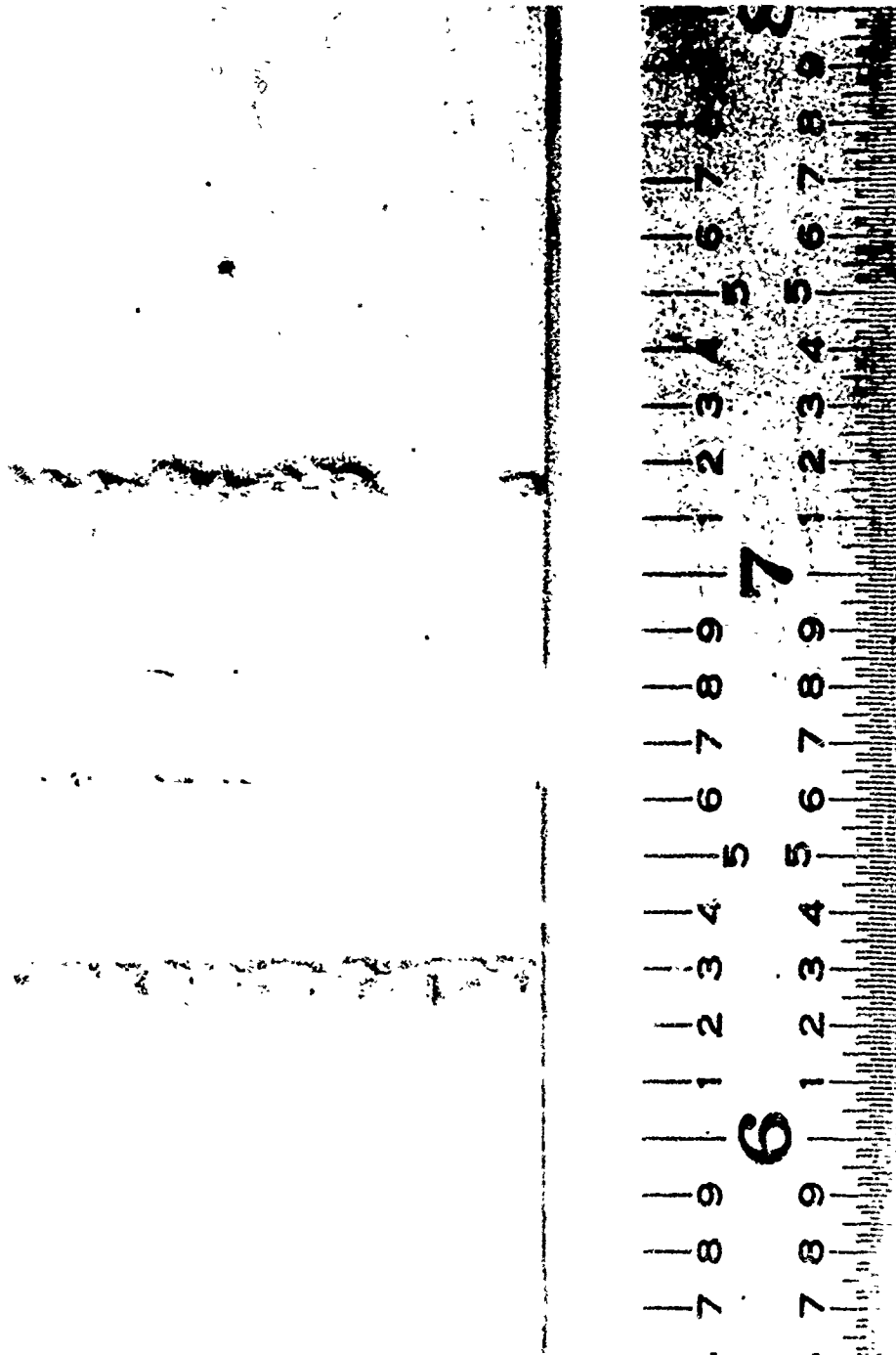


Figure (5-20) Typical Fatigue Bands of All 0°
Adherend Failure Surfaces

Reproduced from
best available copy.



adhesive, which was uncracked could not withstand the applied load in an ultimate manner. Such growth of the bands is believed realistic for two reasons. (1) Peak tensile stresses occur at the end of the overlap supplying a mode I capability for crack growth. This form of crack growth has been substantiated by Jemian (References 63-65) (2) Of those specimens in which runout was attained and which were then statically tested to failure, small initial smooth bands are evident emanating from the ends of the overlap. The center region which exhibited a more coarse failure surface tended to duplicate the characteristic failure surface of the ultimate tested lap joints.

The overall mode of failure in fatigue can be hypothesized as follows. Initially a crack forms at the end of the overlap due to an initial flaw in the adhesive which is propagated by the peak stresses at the end of the joint (i. e. primarily the tensile stresses). As the crack grows the effective length of the joint is reduced, the peak tensile and shear stresses moving inward just ahead of the crack. This effectively alters the geometry of the joint. Moreover, Salkind (57), has demonstrated that under fatigue stress levels of 6-12 thousand PSI cracking in the matrix of adherend can

occur. This reduces the stiffness of the adherend, increasing the peak stresses in the joint (i.e. see Figure (3-13) of the parametric study). Thus since the average adherend stress level in the fatigue test pieces was 9000 PSI it is conceivable that the geometry of the part was altered collectively by the growth of the crack in the adhesive and the softening of the adherend. Therefore, the original part must withstand the increased peak stresses brought about by the effectively shorter overlap length and softer adherends. As was shown in the parametric study of Chapter III in Figures (3-11), (3-12) (3-13) and (3-14), all these parameters tend to raise the peak shear and tensile stresses in the adhesive. Eventually, the ultimate strength of the adhesive is reached and a sudden ultimate type failure is observed.

In Chapter III, referring to Figure (3-3) comment was made that possibly a correlation between the band widths and where the normal stress became compressive did exist. Table (5-7) is an attempt to correlate the two. However, examination would suggest that no correlation does exist between the two. Moreover, the results do suggest that in all cases where failure in fatigue did occur, the band widths did exceed the initial point where the normal stress became compressive. This in turn would

TABLE (5-7) SUMMARY OF BAND WIDTHS ON ADHESIVE
FAILURE SURFACES VS. WIDTH OF TENSILE NORMAL STRESS ZONES

SPEC. NO.	OVER LAP (IN)	AVG. MEAS. BAND WIDTH (IN)	CYCLES X 10 ⁶	REMARKS ON BAND WIDTH	DIST. FROM* EDGE WHERE COMPRESS. NORMAL STRESS BEGINS (IN)	MEAN ±ALT LOAD (LB)
063025-5	.30	.09±.11	.838	Widths slightly un- even over width part	.07	330±270
-6	.30	.11±.125	.288	Widths slightly un- even over width part		330±270
-7	.30	.06±.11	.518	Widths slightly un- even over width part		330±270
-8	.30		2.301	Widths slightly un- even over width part		275±225
063045-6	.36	.09	4.69 (Run- out)	Band Forming on one end	.07	275±225
-7	.36	.0125	5.044 (Run- out)	Even width bands		275±225

Table (5-7) - Continued

SPEC. NO.	OVER LAP (IN)	AVG. MEAS. BAND WIDTH (IN)	CYCLES X 10 ⁶	REMARKS ON BAND WIDTH	DIST. FROM* EDGE WHERE COMPRESS. NORMAL STRESS BEGINS (IN)	MEAN ±ALT. LOAD (LB)
066029-1	.62	.11±.125	.116	Uneven over width part	.09	550±450
-3	.62	.19±.25	.129	Even width bands		550±450
-4	.62	.19±.25	.303	Uneven over width part		495±405
-5	.62	.125 & .005	4.102 (Runout)	Bands starting to form		330±270
-7	.62	.09	4.133 (Runout)	Bands forming on one end		330±270
066049-3	.62	.11±.15	.439	Even band widths	.09	440±360
-4	.62	.19	1.294	Even band widths		385±315
-5	.62	.19±.25	1.052	Even band widths		385±315

* Per Bond3 Analysis

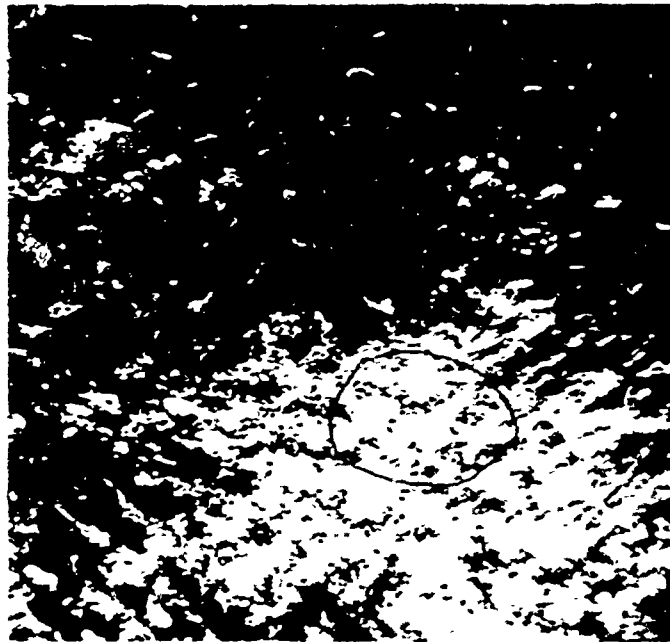


Figure (5-21) Smooth Band Area of Adhesive Fatigue Surface



Figure (5-22) 122 x Magnification of Area Circled in Figure (5-21)



Figure (5-23) 125 Magnification of Area Circled in Figure (5-22)

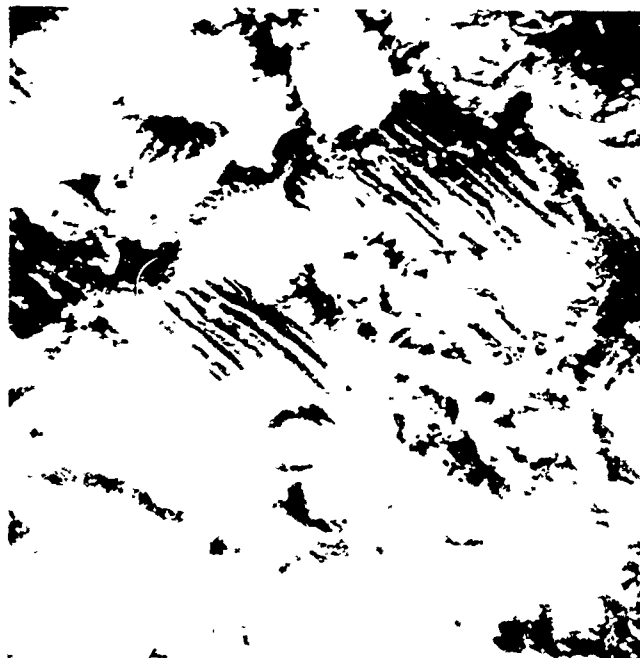


Figure (5-24) 125 x Magnification of Adhesive in Center of Overlap

suggest that the peak stresses move inward as the crack moves inward in accordance with the earlier stated mode of progressive failure.

Using the electron scanning microscope in the Mechanical and Aerospace Engineering Department at the University of Delaware, photographs of the smooth band areas on the ends of the overlap and the center jagged region were made. Figure (5-21) depicts a segment of the smooth band area on one end of the overlap at 24 x magnifications. It is a rather smooth undulating surface. In the lower left hand corner the fibrous nature of the scrim is evident. A blow-up of the area circled is shown in Figure (5-22). Again, the generally smooth landscape with slight ridges and valleys is evident. A further magnification of the area circled in Figure (5-22) is displayed in Figure (5-23). Note is made of the ripples over the surface. These ripples are normal to the crack extension direction and may be associated with the ductile nature of the EA951 adhesive.

The center region of a typical fatigue failed surface is shown in Figure (5-24). The white areas are the residual adhesive material, while the striated regions are the glass adherend material. Figure (5-25) displays

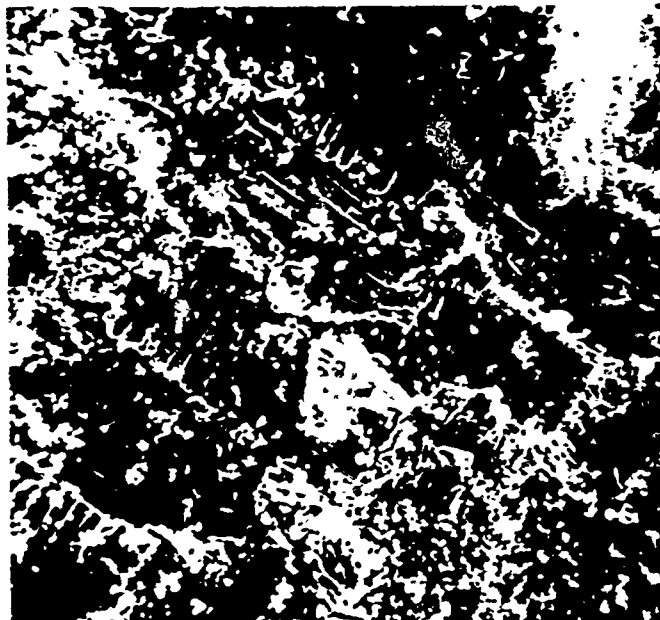


Figure (5-25) 138 x Magnification of Adhesive Ultimate Failure Surface

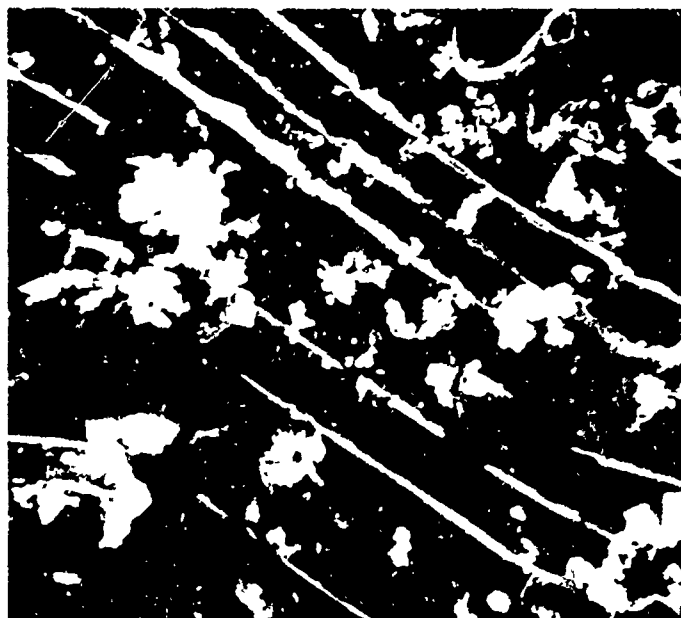


Figure (5-26) 680 x Magnification of Adhesive Ultimate Failure Surface



Figure (5-27) 2700 x Magnification of Adhesive Ultimate Failure Surface

a similar failed surface. It is that of an ultimate failure specimen. Thus, the similarity is unmistakable, making the idea that the fatigue specimen fails ultimately in next section seem very plausible. Figures (5-26) and (5-27) are magnifications of Figure (5-25). The fiberglass fibers and the residual adhesive attached to the strands is evident.

D. ANGLE-PLY (45/0/-45/0) FATIGUE TEST RESULTS

Analogous to the all uni-directional fiberglass adherends, the objectives of this section were to study the influence on fatigue life of certain parametric variables. These were overlap length, thickness of the adhesive and the influence of the $45^{\circ}/0^{\circ}/-45^{\circ}/0^{\circ}$ lamina orientation of the adherends. In addition the influence of the adhesive proportional limit stress, design recommendations and the types of failures observed will also be discussed. A summary of the fatigue test results is tabulated in Tables (5-8) and (5-9). In all instances the ply lay-up pattern was $45^{\circ}/0^{\circ}/-45^{\circ}/0^{\circ}$. The overlap lengths were .30 and .60 inches. The adhesive thicknesses were from .5 to 5 mils thick. Again, the lack of efficient bond line thickness control is evident. The tests were conducted at 75° Fahrenheit, while the relative humidity fluctuated from 20 to 44 per cent. All tests were run at a stress ratio of +.10. Fatigue runout (i.e. 4.0×10^6 cycles) for the 063025 specimens was at a mean load of 165 pounds. Specimens 0630105, 066020 and 0660109 achieved runout at 165 pounds, 200 pounds and 275 pounds respectively.

TABLE (5-8) SUMMARY OF FATIGUE TEST RESULTS - 45°/0°/-45°/0° ADHERENDS

SPEC. NO.	OVER LAP (in)	t _{adh} (in)	TEMP RANGE (°F)	REL. HUM. RANGE (%)	MEAN ±ALT LOAD (LB)	MAX LOAD % OF ULT. LOAD	MAX** SHEAR STRESS @ MEAN LOAD	MAX** NORMAL STRESS @ MEAN LOAD	SHEAR S.C.F. @ MAX LOAD	CYCLES X 10 ⁶		TYPE FAILURE
063025-1	.30	.0005	75	31-35	220±180	34.5	-	-	-			.107 Bands forming Cross-ply failed
	-2 .30	.001	75	30	220±180	34.5	-	-	-			.676 Bands forming Cross-ply failed
	-3 .30	.0005	75	39-45	220±180	34.5	-	-	-			.513 Bands forming Cross-ply failed
	-5 .30	.0005	75	44	165±135	26.0	675	767	1.28	6.267		Runout
	-6 .315	.0005	75	33-44	165±135	26.0	675	767	1.28	4.168		Runout
0630105-1	-8 .315	.001	75	37-43	165±135	26.0	675	767	1.28	4.246		Runout
	.300	.004	75	43	220±180	39.0	-	-	-	3.632		Cross-ply failed Adh Raised
	-2 .301	.004	75	42-44	275±225	48.5	-	-	-	.194		Cross-ply failed Adh Raised
	-4 .301	.003	75	43-48	220±180	39.0	-	-	-	.551		Cross-ply failed Adh Raised

Table (5-8) - Continued

SPEC NO.	OVER LAP (In)	t_{adh} (In)	TEMP. RANGE (°F)	REL. HUM. RANGE (%)	MEAN ±ALT LOAD (LB)	MAX LOAD % OF ULT. LOAD	MAX** SHEAR STRESS @ MEAN LOAD	MAX** NORMAL STRESS @ MEAN LOAD	** SHEAR S.C.F. @ MAX LOAD	CYCLES X 10 ⁶	TYPE FAILURE
0630105-5	.300	.004	75	41-43	220±180	39.0	-	-	-	.576	Adhesive Failure Raised Adh
-6	.300	.005	75	35	275±225	48.5	-	-	-	.141	Cross-ply failed Adh raised
-7	.300	.004	75	33-37	275±225	48.5	-	-	-	.123	Cross-ply failed Adh raised
-9	.300	.004	75	48-52	165±135	29.4	-	-	-	5.02	Runout
-10	.300	.004	75	45-47	165±135	29.4	-	-	-	4.12	Runout

** Per Bond3 Analysis

ADHEREND - 1002-S PRE-PREG TAPE
 ADHESIVE - EA951 FILM
 ALL SPEC ≈ 1.0 INCHES WIDE
 R = +.10

1 396 1

TABLE (5-9) SUMMARY OF FATIGUE TEST RESULTS - 45°/0°/-45°/0° ADHERENDS

SPEC. NO.	OVER LAP (In)	t _{adh} (In)	TEMP. RANGE (°F)	REL. HUM. RANGE (%)	MEAN ±ALT LOAD (LB)	MAX LOAD % OF ULT. LOAD	MAX** SHEAR STRESS @ MEAN LOAD	MAX** NORMAL STRESS @ MEAN LOAD	** SHEAR S.C.F. @ MAX LOAD	CYCLES X 10 ⁶	TYPE FAILURE
066029	-1.586	.001	75	34	330±270	28.5	-	-	-	.055	Bands formed Cross-ply failed
-2	.586	.001	75	34	275±225	23.6	-	-	-	.298	Bands formed Cross-ply failed
-3	.591	.0005	75	22-43	192±158	16.6	590	1010	1.8	6.176	Runout
-5	.604	.0005	75	30-33	220±180	19.0	678	1070	1.8	4.092	Runout
-6	.604	.0005	75	25-31	220±180	19.0	-	-	-	2.80	Bands formed Cross-ply failed
-7	.600	.001	75	20-28	275±225	23.6	-	-	-	.526	Bands formed Cross-ply failed
0660109	-1.601	.003	75	34	330±270	19.6#	-	-	-	1.318	Resin in cross-ply layer adj to Adh failed - no bands
-2	.601	.003	75	23-42	330±270	19.6	-	-	-	2.002	Resin in cross-ply layer adj to Adh failed - no bands

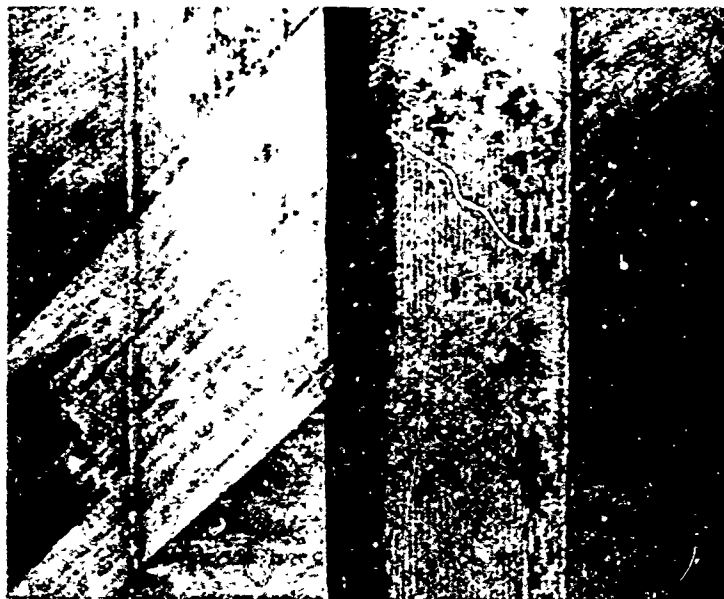
Table (5-9) - Continued

SPEC. NO.	OVER LAP (in)	t _{adh} (in)	TEMP RANGE (OF)	REL. HUM. RANGE (%)	MEAN ±ALT LOAD (LB)	MAX LOAD % OF ULT. LOAD	MAX** SHEAR STRESS @ MEAN LOAD	MAX** NORMAL STRESS @ MEAN LOAD	** SHEAR S.C.F. @ MAX LOAD	CYCLES X 10 ⁶	TYPE FAILURE
0660109-3	.601	.002	75	23-24	330±270	19.6	-	-	-	1.453	Resin in cross ply layer adj to Adh failed no bands
-4	.601	.002	75	25-43	275±225	16.3	428	671	1.45	4.164	Runout
-5	.601	.002	75	35-44	275±225	16.3	428	671	1.45	4.281	Runout
-6	.601	.001	75	34-35	275±225	16.3	428	671	1.45	4.393	Runout

Based on ultimate failure results of cross ply in Chapter IV, Section (C)

ADHEREND - 1002-S PRE-PREG TAPE
 ADHESIVE - EA951 Film
 All Spec = 1.0 inches wide
 R = +.10

** Per Bond3 Analysis



Fatigue Failure Surface

Ultimate Failure Surface

Figure (5-28) $45^{\circ}/0^{\circ}/-45^{\circ}/0^{\circ}$ Adherends



Fatigue Failure Surface

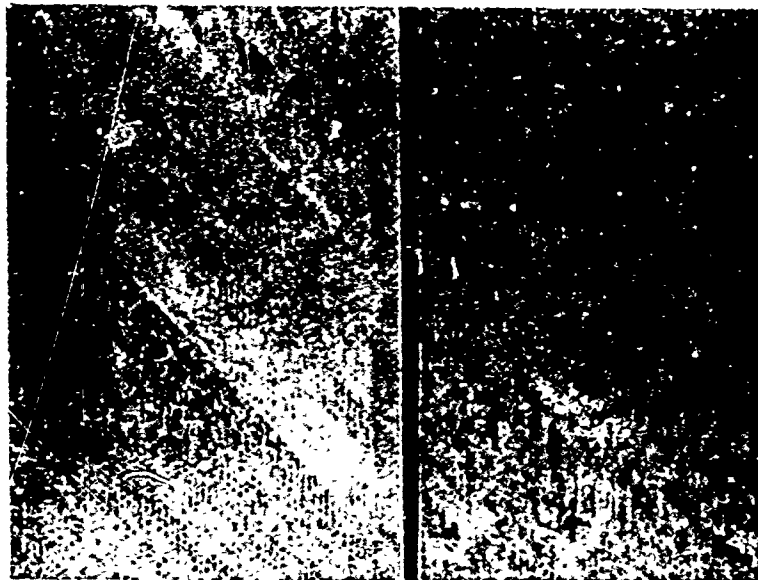
Ultimate Failure Surface

Figure (5-29) $45^{\circ}/0^{\circ}/-45^{\circ}/0^{\circ}$ Adherends

The general appearance of the fatigue failed surfaces vs. their ultimate test counterparts were as follows. Figure (5-28) displays the fatigue and ultimate failure surfaces of specimen configuration 063025.

Basically the ultimately loaded specimens failed in shear. In some instances part of the 45° ply adjacent to the adhesive did fail. This is believed to be a secondary effect. Moreover, the critical fatigue failure displayed the initial failure to be in the 45° ply adjacent to the adhesive. Resin degradation has occurred and the fibers are starting to break normal to their direction. This is thought to be the result of high interlaminar shear (τ_{12}) and normal stresses in the resin. This will be discussed in more detail later.

Figure (5-29) displays the fatigue and ultimate failure surfaces of specimens 0630105. They are different from the previous specimens in that their adhesive thickness is approximately 4 mils vs. .5 mils for specimens labeled 063025. Their ultimate failure mode is seen to be in the adhesive. The adhesive has been raised up. This may indicate a tearing away by normal stresses of the adhesive from the adherend. The fatigue failure mode also displays this raising up of the adhesive as



Fatigue Failure Surface Ultimate Failure Surface

Figure (5-30) $45^{\circ}/0^{\circ}$ - $45^{\circ}/0^{\circ}$ Adherends



Fatigue Failure Surface Ultimate Failure Surface

Figure (5-31) $45^{\circ}/0^{\circ}$ / $-45^{\circ}/0^{\circ}$ Adherends

is evident in the ultimate mode of failure. However, the actual fatigue failure is believed to be the result of resin degradation in the 45 degree ply adjacent to the adhesive. Again the breaking of the fibers normal to their direction is evident. Reflecting on the failed surfaces of specimens 063025 and 0630105 the primary difference in the appearance of the failed surfaces seems to be the lifting of the adhesive evident in the thicker adhesive part. This effect may also be present in the .5 mil specimens once it is put under an electron microscope. However, no increase in fatigue strength was noticed, regardless of the adhesive thickness.

Figure (5-30) compares specimens of group 066029. They are similar to specimens 063025 except their overlap length is twice as long (.60 vs. .30 inches). This set of test pieces behaved most analogous to the all zero degree adherend specimens. They failed in the adhesive when tested to ultimate failure. Moreover, the fatigue items failed almost simultaneously in the adhesive, where the bands were evident, and in the 45 degree ply adjacent to the adhesive.

Figure (5-31) displays the ultimate and fatigue failure surfaces of group 0660109. These are similar to

specimens 0630105 except that the overlap length is twice as long (.60 vs. .30 inches) and the adhesive thickness is about half as much (2 vs. 4 mils). The ultimate mode of failure is totally in the 45 degree ply adjacent to the adhesive. The fatigue mode again was in the ply adjacent to the adhesive, displaying a general breakdown of the resin around the fiber and a breakage of fibers normal to their direction.

In summary, the type of fatigue failure observed seemed to be independent of the overlap lengths and to a minor degree sensitive to the adhesive thickness used. Moreover, the ply orientation effect is definitely a factor in the type of fatigue failure one observes. Whereas the all zero degree adherend items failed in the adhesive, displaying definite bands attributed to the growth of cracks in the adhesive and related to the shear proportional limit stress of the adhesive, the 45/0/-45/0 degree items failed in the 45° ply adjacent to the adhesive due to resin degradation and fiber breakage. Finally, in referring back to Tables (5-8) and (5-9) it is readily discernable that the mean load increased as the length of overlap increased.

In an effort to further justify the shear

TABLE (5-10) COMPARISON OF ADHESIVE SHEAR AT RUNOUT

PLY ORIENT.	SPEC. NO.	SHEAR PROPORT* LIMIT STRESS (PSI)	MAX SHEAR** STRESS FOR MEAN LOAD (PSI)	MEAN LOAD (#)
45°/0°/-45°/0	063025	925	675	165
45°/0°/-45°/0	0630105	950	612	165
45°/0°/-45°/0	066029	480	615	200
45°/0°/-45°/0	0660109	480	428	275

*From Shear Test Results in Chapter IV, Table (4-5)

**From Bond3 Analysis

proportional limit of the adhesive being a critical life parameter in fatigue a comparison of the shear proportional limit stress as determined in Chapter (IV) vs. the maximum shear stress for the mean load at which runout occurred was made. Table (5-10) details these results. Basically, it stipulates that the peak shear stresses of specimens 063025 and 0630105 never attained their proportional limit stress allowables. Thus an adhesive failure would not be expected. It did not occur. Further, specimen 066029 which failed almost simultaneously in adhesive shear and ply degradation did in fact exhibit maximum shear stresses in excess of its proportional limit stress. A shear and ply type failure did occur. Finally, specimen 0660109 is shown to have not exceeded its proportional limit stress, thus leading one to expect failure of the ply adjacent to the adhesive to occur. It did. Moreover, the results are mixed when comparing the type of failure vs. adhesive thickness in Tables (5-8) & (5-9). Results seem to indicate that for longer overlaps and thinner adhesive thicknesses an adhesive failure is possible.

Table (5-11) summarizes the ultimate strength of those fatigue test items which achieved runout. In

TABLE (5-11) ULTIMATE TEST RESULTS OF FATIGUE RUNOUT SPECIMENS

SPEC. NO.	L ₁ (In)	L ₂ (In)	L ₃ (In)	H ₁ (In)	H ₂ (In)	t _{adh} (In)	WIDTH (In)	SURF. AREA (In ²)	FAILURE LOAD		AVG. ADH. STRESS (PSI)	LOAD CYCLES TYPE FAILURE
									(#)	%OF* ULT.		
063025-5	4.20	.30	4.20	.069	.069	.0005	1.000	.300	1210.	(101)	4033	165±135 6.267 x 10 ⁶ Adhesive failed
-6	4.20	.315	4.20	.069	.069	.0005	1.018	.3206	250	(21)	779	165±135 4.168 x 10 ⁶ Adhesive failed
-8	4.20	.315	4.18	.070	.070	.001	1.000	.315	475	(40)	1508	165±135 4.246 x 10 ⁶ Cross-ply failed
0630105-9	4.21	.30	4.20	.070	.070	.004	1.004	.3012				
-10	4.21	.30	4.19	.070	.070	.004	1.007	.3021				
066029-3	3.90	.591	3.90	.067	.068	.0005	1.002	.5922	1875	(89)	3166	192±158 6.176 x 10 ⁶ Adhes. Cross-ply Starting to fail
-5	3.91	.604	3.91	.069	.070	.0005	1.007	.6082	1500	(71)	2466	220±180 4.092 x 10 ⁶ Adhes. Failure Bands Forming

Table (5-11) - Continued

SPEC NO.	L ₁ (In)	L ₂ (In)	L ₃ (In)	H ₁ (In)	H ₂ (In)	t _{adh} (In)	WIDTH (In)	SURF. AREA (In ²)	FAILURE LOAD		AVG. ADH. STRESS (PSI)	LOAD CYCLES TYPE FAILURE
									% OF*	ULT.		
0660109-4	3.90	.601	3.90	.070	.070	.002	1.010	.6070	3200 (104)		5272	275±225 4.164 x 10 ⁶ Cross-ply failure
-5	3.90	.6015	3.90	.071	.071	.002	1.005	.6045	3200 (104)		5293	275±225 4.281 x 10 ⁶ Cross-ply failure
-6	3.90	.6015	3.90	.071	.071	.001	1.008	.6063	3100 (102)		5113	275±225 4.393 x 10 ⁶ Cross-ply failure

- 407 -

* Based on ultimate test results of
Section A

ADHEREND - 1002-S PRE-PREG TAPE
ADHESIVE - EA951 FILM
PLY ORIENTATION 45/0/-45/0

general their ultimate strength after undergoing 4×10^6 cycles or more was between 40 and 104 per cent. In specimens 063025 an adhesive failure occurred with signs of resin failure commencing. In specimens 066029 an adhesive failure occurred and the bands common on the all 0° adherend specimens were beginning to form. All other specimens failed in the 45° ply adjacent to the adhesive.

In an effort to discern a viable design methodology for fatigue items of other than all zero degree lamina orientation, one is again referred to Figure (5-15). The results of the $45^\circ/0^\circ/-45^\circ/0^\circ$ fatigue tests have been plotted vs. the maximum fatigue load as a per cent of the ultimate load of the part. The results would indicate that the angle-ply had a negligible effect on the per cent of design ultimate one can design for in fatigue. In fact at first glance it seems that one pays no penalty in fatigue for an angle-ply adherend. Definitely, this is not true. The fact is that the ultimate allowables of the angle-ply specimens are less than those of the uni-ply ones. It seems however, that the fatigue life of an item is nearly a constant percentage of the ultimate strength of the item and depends on the number of cycles one is designing the fatigue item for. Therefore,

TABLE (5-12) EFFECT OF LAMINA ORIENTATION ON FATIGUE LIFE

SPEC. NO.	PLY ORIENT.	MEAN LOAD AT RUNOUT	PER CENT REDUCTION
063025	45/0/-45/0	165	
063025	0	247	33
0630105	45/0/-45/0	165	
063045	0	275	40
066029	45/0/-45/0	200	
066029	0	330	40
0660109	45/0/-45/0	275	
066049	0	330	17

ADHERENDS - 1002-S PRE-PREG TAPE
ADHESIVE - EA951 FILM
R = +.10

if one follows the ultimate design methodology elaborated on earlier in this chapter, an adequately designed fatigue item should be had.

Moreover, to dispel any idea that the fatigue life of a specimen is unaltered by the orientation of the plys, one need only look at table (5-12). From this it is evident that a 20-40 per cent reduction in fatigue strength for 4.0×10^6 cycles was observed when the 45/0/-45/0 degree ply orientation was employed vs. the all 0 degree ply orientation.

Having observed the critical degradation of the 45 degree ply adjacent to the adhesive, leading to a premature failure of the lap joint vs. an adhesive failure, one must ask why and how did this occur. In capsule form it is believed the 45 degree ply adjacent to the adhesive failed prematurely because of severe normal and shear stresses in the resin itself between lamina. These are not of appreciable magnitude in a zero degree ply.

Recalling that the x-y axes are the geometrical axes of the part being loaded and the 1-2 axes run parallel to and normal to the fiber orientation respectively, an explanation of the failure mechanism in a 45 degree ply will be made. Observation of the failed surfaces indi-

cated that the 45 degree ply's initial damage occurred at the loaded edge of the overlap (Figure (5-31)). Therefore it was decided to look at the differences in the peak stresses and stiffnesses of a 45 degree ply adjacent to the adhesive vs. a zero degree ply adjacent to the adhesive. The Bond3 analysis program was used for this comparison. The results are summarized in table (5-13).

Critical stress comparisons were made for an all 0° adherend and a $45^\circ/0^\circ/-45^\circ/0^\circ$ adherend. All other properties were identical, including the loads. Observing the peak shear stresses in the adhesive one sees very little difference, and only a modest difference in the peak normal stresses which would accelerate the crack growth rate in the adhesive, if it were so disposed. Therefore, one looks further and readily discerns very significant changes in the interlaminar shear stress (τ_{12}) and the normal stress (σ_2) perpendicular to the fiber direction. The interlaminar shear stress goes from 0 for a 0° ply orientation to approximately 3500 PSI for a 45° ply orientation. However, even more startling is the threefold increase in the tensile stress on the resin in the two direction. Moreover, this is at mean load, reaching much higher values at peak alternating load.

TABLE (5-13) COMPARISON OF 0° AND 45° PLY STRESSES

SPEC. NO.	PLY ORIENT.	OVER LAP		t _{adh} (In)	45° Layer Adj. to Adhes.		MEAN LOAD			LAYER ADJ. TO ADHESIVE				TYPE FAILURE
		(In)	(In)		A ₆₁ =A ₆₂ (#/In)	D ₁₆ =D ₂₆ (In-#)	MAX* ADHES SHEAR STRESS (PSI)	MAX* ADHES NORMAL STRESS (PSI)	MEAN LOAD (#)	τ_{12}^* (PSI)	σ^* 2 (PSI)	σ^* 3 (PSI)		
063025	45/0/- 45/0	.315	.0005	10412 (0) Lam- inate	7.65 (13.48)	0	0	581	623	165	3505	9515	654	45° ply adj to Adhes failed- No Bands
0630105	45/0/- 45/0	.315	.004	10412 (0) Lam- inate	7.65 (13.48)	0	0	512	518	165	3889	10529	455	45° Ply Adj to Adhes Failed- No Bands
0630105	0	.315	.004	0	0	0	0	583	378	165	0	3770	334	CoHes- Adhes Failure- Bands Evident

Table (5-13) - Continued

Table (3-13) - Continued													
SPEC. NO.	PLY ORIENT.	OVER LAP (In)	t _{adh} (In)	45° LAYER ADJ TO ADHES.		MEAN LOAD		LAYER ADJ. TO ADHESIVE**					TYPE
				A ₆₁ =A ₆₂ (#/In)	D ₁₆ =D ₂₆ (in-#)	MAX* ADHES SHEAR STRESS (PSI)	MAX* ADHES NORMAL STRESS (PSI)	MEAN LOAD (#)	τ_{12}^* (PSI)	σ_2^* (PSI)	σ_3^* (PSI)		
066029	45/0/- 45/0	.615	.0005	10412 (0) Lam- inate	7.65 (13.48) Laminate	610	1029	200	2975	8106	853	Bands formed-45° ply adj.to Adhes.failed 1st twice, Adhes.failed 1st once,ply damaged	
066029	0	.615	.0005	0	0	531	854	200	0	2653	718	CoHes- Adhes fail- ure-Bands Evident	
0660109	45/0/- 45/0	.615	.002	10412 (0) Lam- inate	7.65 (13.48) Laminate	575	890	275	3544	9631	778	45° ply failed ini- tially twist- ing evident- no bands	
0660109	0	.615	.002	0	0	536	742	275	0	3406	656	CoHes- Adhes failure Bands evident	

*Per Bond3 Analysis

**Stresses at .005" from loaded edge of overlap

Compounding the situation even further is the introduction of secondary effects. These effects are caused by the appearance of the A_{16} , A_{26} , D_{16} , D_{26} terms from the extensional stiffness and flexural stiffness matrices respectively. While in 0° and the $45^\circ/0^\circ/-45^\circ/0^\circ$ laminate they have at best a minor influence, in the 45 degree ply adjacent to the adhesive they play a significant role. Recalling that A_{ij} , which is the in-plane extensional stiffness matrix, relates axial loads and strains per

$$[\epsilon^\circ] = [A^{-1}] [N] \quad (5-6)$$

and that D_{ij} , the flexural stiffness matrix relates moment and curvature effects per

$$[\kappa] = [D^{-1}] [M] \quad (5-7)$$

one can discern the effect of the A_{16} , D_{16} terms on our specimens.

Given an applied load and moment, N_x and M_x respectively, it can be shown using equations (5-6) and (5-7) that a shear strain

$$\gamma_{xy} = A_{16}^{-1} N_x \quad (5-8)$$

and a curvature

$$\kappa_{xy} = D_{16}^{-1} M_x \quad (5-9)$$

are introduced. In this particular case A_{16} is far more dominate and is believed to account for the significant

increase in the shear stress in the 1-2 plane.

Furthermore it is believed this induced shear effect and the induced warpage, to a lesser degree, are responsible for the fibers of the 45 degree ply being broken normal to their direction.

Having established that high stresses do indeed exist within the 45° ply at the loaded end of the overlap, one wonders if the resin can sustain such stress levels. Evidence is scarce here and test results exhibit a wide scatter but generally indicate that the resin in 1002S material cannot take stress levels comparable to those calculated and summarized in Table (5-13).

In retrospect, it would seem the critical mode of failure in the 45° ply was primarily tensile stress in the 2-direction.

An initial investigation of the details of the failure surfaces of the $45^{\circ}/0^{\circ}/-45^{\circ}/0^{\circ}$ specimens has been performed. Using the electron microscope in the Mechanical and Aerospace Engineering Department Figures (5-32) to (5-35) were made. Figure (5-32) is a 32 x magnification of the 45° ply, adhesive boundary of a fatigue specimen. It shows how the fibers sheared parallel to themselves.

Reproduced from
best available copy.



Figure (5-32) 32 x Magnification of Adhesive Cross-Ply Failure Surface



Figure (5-33) 158 x Magnification of Ridge Areas

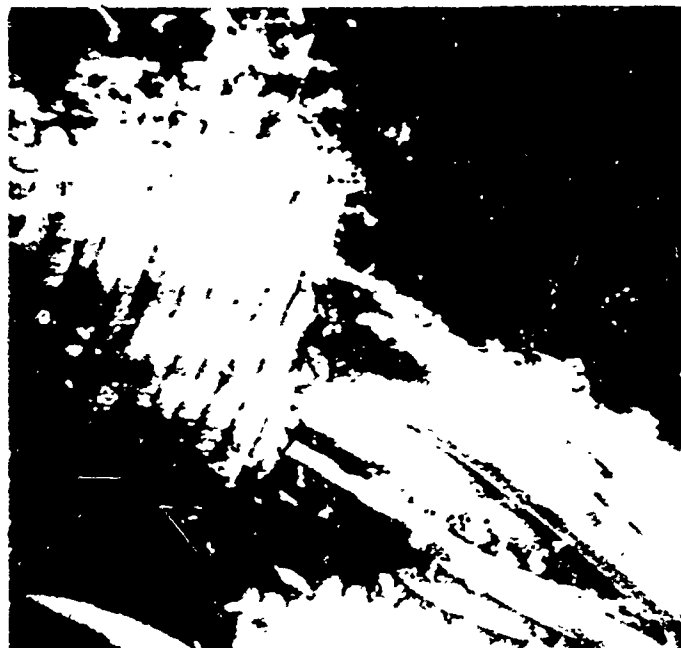


Figure (5-34) 800 x Magnification of Circled Area in Figure 5-34

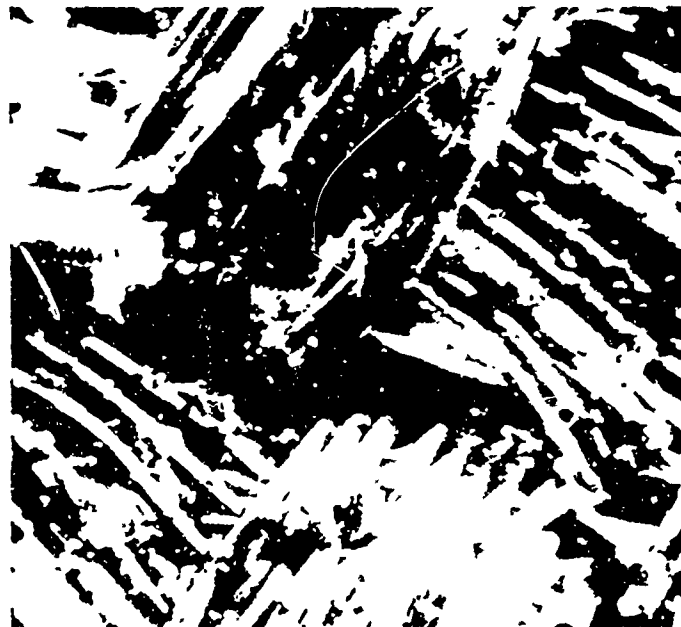


Figure (5-35) 820 x Magnification of a $45^{\circ}/0^{\circ}/-45^{\circ}/0^{\circ}$ Adhesive Ultimate Failed Surface

The fibers are to the left. The top surface has a scrim cloth on it. More important, however, are the high ridges of the adhesive normal and near the loaded edge of the overlap. These are the regions of the adhesive that were lifted up as if torn suddenly by peeling forces. Figure (5-33) is a 158 x magnification of these ridge areas. They look granular and if one looks closely broken fibers in the adhesive can be seen. In the lower left hand corner the angle ply failure boundry is evident.

Figure (5-34) is an 800 x magnification of the area circled in Figure (5-33). Broken pieces of adhesive can be seen lying on the fibers of the adhesive. Moreover, the transversely failed surfaces of the adhesive fibers is evident in the upper left hand corner.

Figure (5-35) is an 820 x magnification of an ultimate tested adhesive surface. The similarity between it and the fatigue specimen surface in Figure (5-34) enforces the fact that the angle ply adjacent to the adhesive was indeed the critical failure mode in the fatigue specimen, the adhesive being failed as an aftermath in an ultimate mode.

A continuing study of all failure surfaces will proceed throughout the coming year. In addition variable

load fatigue tests now being conducted will be reported
on as will tests with PRD-49 type II material.

Conclusions

- A. A relationship between the mean load and the shear proportional limit of the adhesive is evident.
- B. The fatigue life of all specimens increased with an increase in lap length.
- C. For a fatigue life of 4×10^6 cycles a maximum design load of 26 per cent of ultimate load for a lap length of .30 inches and of 20 per cent of ultimate load for a lap length of .60 inches was attained. This was independent of ply orientation.
- D. The strongest fatigue specimen was an all 0° adherend one with a .60 inch overlap, and being bonded by a "soft" adhesive.
- E. A fatigue design methodology was advanced.
- F. The ideal adhesive in fatigue is one of low tensile and shear moduli, possessing a high proportional limit stress and possessed with high shear and tensile ultimate strength. EA951 film is such a desirable adhesive.
- G. No distinct effect on fatigue life vs. adhesive thickness was ascertained.

- H. Failure of the adhesive in fatigue was due to an ultimate failure of the uncracked material, once the critical crack length was reached.
- I. Failure in the 45° ply was due to excessive in-plane stresses normal to the fiber direction in the resin. Avoid such a ply adjacent to the adhesive. Perhaps a 0° would be helpful next to the adhesive in a $0^{\circ}/45^{\circ}/0^{\circ}/-45^{\circ}$ pattern.
- J. A 20-40 per cent penalty in load level vs. run-out (4.0×10^6 cycles) was observed, for a $45^{\circ}/0^{\circ}/-45^{\circ}/0^{\circ}$ specimen vs. an all 0° one.

Proposed Research

- A. Study the influence of extending the overlap length beyond .60 inches on the fatigue life of the joint.
- B. Study the effect of unequal adherends on the fatigue life of the joint.
- C. Study the influence of "thick" vs. "thin" adhesive films on the fatigue life of the joint.

- D. Study various ways of decreasing the eccentricity effect which induces adverse stresses in both the adherend and the adhesive.
- E. Study the effect of a $0^{\circ}/45^{\circ}/0^{\circ}/-45^{\circ}$ lay up pattern on the type of bonded joint failures observed.

REFERENCES

1. Crandall, S. H. and Mark, W. D., Random Vibrations Academic Press, 1963.
2. Liu, H. W. and Corten, H. T., "Fatigue Damage During Complex Stress Histories", University of Illinois, NASA TN D-256, November 1959.
3. Lin, Y. K., Probabilistic Theory of Structural Dynamics, McGraw-Hill, 1967.
4. Swanson, S. R., "Random Load Fatigue Testing - State of the Art Survey", Materials Research and Standards, April 1968.
5. "A Guide for Fatigue Testing and the Statistical Analysis of Fatigue Data", ASTM Special Technical Publication No. 91 A.
6. Boller, K. H., "Fatigue Tests of Glass - Fabric - Base Laminates Subjected to Axial Loading", Forest Products Lab. Report No. 1823, May 1952.
7. Boller, K. H., "Supplement to Fatigue Tests of Glass - Fabric - Base Laminates Subjected to Axial Loading", Forest Products Lab. Report No. 1823-A, April 1954.
8. Boller, K. H., "Supplement to Fatigue Tests of Glass - Fabric - Base Laminates Subjected to Axial Loading", Forest Products Lab. Report No. 1823-B, August 1956.
9. Kimball, K. E., "Fatigue Tests of Glass - Fabric - Base Laminates Subjected to Axial Loading", Forest Products Lab. Report No. 1823-C, October 1958.
10. Stevens, G. H. and Boller, K. H., "Effect of Type of Reinforcement on the Fatigue Properties of Plastic Laminates", WADC-TR-59-27, September 1958
11. Stevens, G. H., "Fatigue Test of Phenolic Laminate at High Stress Levels and Elevated Temperatures", Forest Products Lab. Report No. 1884, August 1961

12. Boller, K. H. "Fatigue Properties of Plastic Laminates Reinforced with Unwoven Glass Fibers", ASD-TDR-62-464, March 1962.
13. Boller, K. H., "Resume of Fatigue Characteristics of Reinforced Plastic Laminates Subjected to Axial Loading", ASD-TDR-63-768, December 1963.
14. Stevens, G. H., "Fatigue Strength of Phenolic Laminates from one to ten Million Cycles of Repeated Load", Forest Products Lab. Report No. 027, January 1964.
15. Boller, K. H., "Effect of Tensile Mean Stress on Fatigue Properties of Plastic Laminates Reinforced with Unwoven Glass Fibers", ML-TDR-64-86, June 1964.
16. Boller, K. H., "Fatigue Characteristics of Two New Plastic Laminates Reinforced with Unwoven "S" Glass Fibers under Cyclic Axial or Shear Loading", AFML-TR-66-54, March 1966.
17. Boller, K. H., "Effect of Single-Step Change in Stress on Fatigue Life of Plastic Laminates Reinforced with Unwoven "E" Glass Fibers, AFML-TR-66-220, September 1966.
18. Dally, J. W. and Broutman, L. J., "Frequency Effects on the Fatigue of Glass Reinforced Plastics", Journal of Composite Materials, October 1967.
19. Hofer, K. E., "An Investigation of Fatigue Behavior of Reinforced Plastics", I. I. T. Research Institute, Chicago, Illinois, March 1969.
20. Wang, Douglas Y., "Influence of Stress Distribution on Fatigue Strength of Adhesive-Bonded Joints", Experimental Mechanics, June 1964.
21. Szepe, Ferenc, "Strength of Adhesive Bonded Lap Joints with Respect to Change of Temperature and Fatigue", Experimental Mechanics, May 1966.
22. Lehman, G. M., Hawley, A. V. et.al., "Investigation of Joints in Advanced Fibrous Composites for Aircraft Structures", AFFDL-TR-69-43, Volumes I and II, June 1969.

23. Goland, M. and Reissner, E., "The Stresses in Cemented Joints", Journal of Applied Mechanics, March 1944.
24. DeBruyne, N. A. and Houwink, R., Adhesion and Adhesives, Elsevier Publishing Company, 1951.
25. Cornell, R. W. "Determination of Stresses in Cemented Lap Joints", Journal of Applied Mechanics, 20, No. 3 pp. 355-364, September 1953.
26. Eickner, H. W., "Basic Shear Strength Properties of Metal Bonding Adhesives as Determined by Lap-Joint Stress Formulas of Volkersen and Goland and Reissner", Forest Products Lab. Report No. 1850, August 1955.
27. Sherrer, R. E. "Stresses in a Lap Joint with Elastic Adhesive", Forest Products Laboratory Report No. 1864, September 1957.
28. Hahn, K. F. and Houser, D. F., "Methods of Determining Stress Distribution in Adherends and Adhesives", Journal of Applied Poly. Sci., 6, pp. 145-149, 1962.
29. Goodwin, J. F., "Research on Thermomechanical Analysis of Brazed or Bonded Structural Joints", ASD-TDR-63-447, September 1963.
30. Kutscha, D., "Mechanics of Adhesive Bonded Lap type Joints", Survey and Review, ML TDR-64-298, October 1964.
31. Calcote, L. R. and Grimes, G. C., "Investigation of Structural Design Concepts for Fibrous Aircraft Structures", Vol. II - Technology Appraisal, Southwest Institute, AFFDL-TR-67-29, January 1967.
32. Halpin, J. C. and Polley, H. W., "Observations on the Fracture of Viscoelastic Bodies", Journal of Composite Materials, Vol. 1. 1967.
33. "Structural Airframe Application of Advanced Composite Materials", 14th Monthly Progress Report, General Dynamics, Fort Worth Division, AF 33615-5257, August 1967.
34. Cole, B. W., Wang, J. P. and Courtney, A. L., "Development of the Shim Joint Concept for Composite Structural Members", The Bendix Corporation, AFFDL-TR-67-116, August 1967.

35. Hawley, A. V. Ashizawa, M., et.al., "Investigation of Joints and Cutouts in Advanced Fibrous Composites for Aircraft Structures", 1st and 2nd and 3rd Quarterly Progress Reports, Douglas Aircraft Co., Contract No. F33615-67-C-1582, 1967.
36. "Investigation of Advanced Filament Wound Aircraft Landing Gear Structures", 1st Quarterly Progress Report, Douglas Aircraft Co., Contract No. F33616-67-C-1717, August 1967.
37. Nadler, M. A. and Yoshino, S. Y., "Adhesive Joint Strength as a Function of Geometry and Material Parameters", SAE Paper No. 670856, 1967.
38. Schwartz, R. T. and Schwartz, H. S., "Fundamental Aspects of Fiber Reinforced Plastic Composites", Section I.3, Interscience Publication, 1968.
39. Tsai, S. W., Halpin, J. C. and Pagano, N. J., "Composite Materials Workshop", Section on "Characterization and Design of Composite Materials", Technomic Publishing Co., 1968.
40. Grimes, G. C., "Investigation of Structural Design Concepts for Fibrous Aircraft Structures", Vol. I - Technology Appraisal, Southwest Research Institute, AFFDL-TR-67-29, February, 1968.
41. "Advanced Composite Wing Structures - Preliminary Analysis and Optimization Methods", AFML TR-AC-SM-7843, August 1968.
42. "Structural Design Guide for Advanced Composite Applications" Southwest Research Institute, AF 33615-68-C-1241, November 1968.
43. "Fabrication Techniques for Advanced Composite Attachments and Joints", Final Report for Contract F 33615-67-C-1802, Columbus Division of North American Rockwell Corporation, 1968.
44. Kutscha, D. and Hofer, K. E. Feasibility of Joining Advanced Composite Flight Vehicle Structures, AFML-TR-68-391, January 1969.

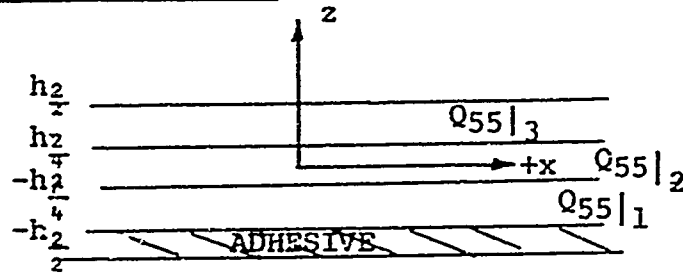
45. "Advanced Composite Wing Structures", Grumman Aircraft Engineering Corporation, Bethpage, New York, Contract F 33615-68-C-1301, February 1969.
46. Lehman, George M., "Fundamentals of Joint Design for composite Airframes", Technical paper presented at the 1969 Western Metal and Tool Conference and Exposition, March 1969.
47. "Engineering with Adhesives" Course Notes by G. C. Grimes at Conference on Concepts and Principles of Bonded Joint Design, March 1969.
48. "Structural Design Guide for Advanced Composite Applications", Department of the Air Force, Air Force Materials Laboratory, Wright-Patterson Air Force Base, Ohio.
49. Grimes, G. C., "Static and Fatigue Design Allowables Criteria for Fiber Reinforced Thermosets", Southwest Research Institute, presented at the Conference on Fatigue and Impact Resistance of Plastics, September 1969.
50. Tetelman, A. S., "Fracture Processes in Fiber Composite Materials", A.S.T.M. Special Technical Publication No. 460.
51. "Ductile Fracture of Anisotropic Materials--Theoretical and Experimental Evaluation of Dugdale Model Applied to Anisotropic Materials", Paper No. 1729, Society of Experimental Stress Analysis, October 18-22, 1970.
52. "Experimental Aspects of Adhesive Bonded Joints", G. C. Grimes, Society of Aerospace Material and Process Engineering, Second National Technical Conference, October 1970 Proceedings.
53. Erdogan, F. and Ratwani, M., "Stress Distribution in Bonded Joints", Journal of Composite Materials, July 1971.
54. "Development of an Understanding of the Fatigue Phenomena of Bonded and Bolted Joints in Advanced Filamentary Composite Materials", Contract No. F33615-70-C-1302, Lockheed-Georgia Co.

55. Hamel, D. R., Korbacher, G. K. and Smith, D. M., "Fatigue Strength Optimization of Bonded Joints", Journal of Basic Engineering, Transactions of the American Society of Mechanical Engineers, December 1971.
56. "Stress, Strain Behavior of Adhesives in a Lap Joint Configuration", by Tiezzi and Doyle, Journal of Macromolecular Sciences, Series A - Chemistry Volume A3, June 1969.
57. Salkind, M. J., "Fatigue of Composites", Composite Materials, Testing and Design, Second Conference, American Society of Testing Materials STP 497.
58. Pajoja, Murlidhar H., "Stress Analysis of an Adhesive Lap Joint Subjected to Tension, Shear Force and Bending Moments", T. & A. M. Report No. 361, University of Illinois, Urbana, Illinois, August 1972.
59. Hughes, Edward J. and Rutherford, John L., Study of Micromechanical Properties of Adhesive Bonded Joints", Technical Report 3744, Aerospace Research Center, General Precision Systems, Inc., Little Falls New Jersey, August 1968.
60. Cuthrell, R. E., "Macrostructure and Environment - Influenced Surface Layer in Epoxy Polymers", Journal of Applied Polymer Science, Volume 11, pp. 949-952, 1967.
61. Kuenzi, E. W., Stevens, G. H. Forest Products Laboratory Report No. FPL-011, September 1963.
62. "Development of a Non-Destructive Test Method for Elastic Properties", AFML-TR-68-233.
63. Jemian, Wartan A. and Ventrice, Marie B., "The Fracture Toughness of Adhesive - Bonded Joints", The Journal of Adhesion, Volume 1, July 1969.
64. Wilcox, Roy C. and Jemian, Wartan A., "Scanning Electron Fractography of Lap-Shear Joints", Polymer Science and Engineering, Volume 13, No. 1, January 1973.

65. Wilcox, Roy C. and Jemian, Wartan A., "Fracture Surface Features of Epoxy Bonded Joints", Department of Mechanical Engineering, Auburn University, Auburn Alabama

APPENDIX A

Example - 3-Ply Laminate



Given: A 3-ply laminate with properties $Q_{55}|_1$, $Q_{55}|_2$ and $Q_{55}|_3$ with thicknesses as given in the above sketch, orientation of the plys is arbitrary. The top surface of layer 3 will be assumed stress free as in our lap joint problem, thus,

$$\sigma_z(x, \frac{h_2}{2})_3 = 0 \quad (1)$$

Using equation (2.33) on page 50 one obtains

$$0 = [-\frac{h_2}{8}] \frac{d\tau_0}{dx} + [-\bar{Q}_{55}|_3 \frac{h_2}{3} - \frac{h_2}{2} b_{55}|_3] \frac{d\phi_{x2}}{dx} + d_3(x) \quad (2)$$

Therefore, one must obtain $d_3(x)$ by using equation (2.39) to obtain $d_3(x)$ in terms of $d_1(x)$ and $d_2(x)$. $d_1(x)$ comes from the boundary condition

$$\sigma_z(x, -\frac{h_2}{2}) = \sigma_{oL} \quad (3)$$

$$d_1(x) = \sigma_{oL} - \frac{3h_2}{8} \frac{d\tau_o}{dx} - \bar{Q}_{55}|_1 \frac{h_2}{3} \frac{d\phi_{x_2}}{dx} \quad (4)$$

Using the boundary condition for continuity of normal stresses between adjacent lamina, namely:

$$\sigma_z(x, H_{M+1})_M = \sigma_z(x, H_{M+1})_{M+1} \quad (5)$$

One can determine $d_2(x)$ and $d_3(x)$. They are

$$d_2(x) = \frac{11}{48} h_2 \frac{d\phi_{x_2}}{dx} [\bar{Q}_{55}|_1 - \bar{Q}_{55}|_2] - b_{55}|_2 \frac{h_2}{4} \frac{d\phi_{x_2}}{dx} + d_1(x) \quad (6)$$

$$d_3(x) = [\bar{Q}_{55}|_3 - 2\bar{Q}_{55}|_2 + \bar{Q}_{55}|_1] \frac{11}{48} h_2 \frac{d\phi_{x_2}}{dx} - b_{55}|_2 \frac{h_2}{2} \frac{d\phi_{x_2}}{dx} + d_1(x) \quad (7)$$

Substituting equations (7) and (4) into (2) the resulting expression for the normal stress on the top surface of the laminate is

$$0 = -\frac{h_2}{2} \frac{d\tau_o}{dx} + [-\frac{5}{48} h_2 \bar{Q}_{55}|_3 - \frac{11}{24} \bar{Q}_{55}|_2 h_2 - \frac{5h_2}{48} \bar{Q}_{55}|_1$$

$$- b_{55}|_2 \frac{h_2}{2} \frac{d\phi_{x_2}}{dx} + \sigma_{oL} \quad (8)$$

Making use of expressions (2.253) and (2.260) on page 139 a relation for σ_o is obtained.

$$\sigma_{oL} = \frac{h_2}{2} \frac{d\tau_o}{dx} + K_5 \frac{d\phi_{x_2}}{dx} \quad (9)$$

Substituting this relation in equation (8) a relation for K_5 is obtained which must be satisfied if $\sigma_z(x, \frac{h_2}{2}) = 0$ is to be satisfied.

$$K_5 = \frac{5}{48} h_2 \bar{Q}_{55}|_3 + \frac{11}{24} h_2 \bar{Q}_{55}|_2 + \frac{5}{48} h_2 \bar{Q}_{55}|_1 + b_{55}|_2 \frac{h_2}{2} \quad (10)$$

Per the definition of K_5 given on page 81 for our 3-ply laminate one obtains

$$K_5 = \sum_{K=1}^3 \left\{ \bar{Q}_{55}|_K \left(z - \frac{4z^3}{3h_2^2} \right) \begin{vmatrix} H_K \\ H_{K+1} \end{vmatrix} + b_{55}|_K z \begin{vmatrix} H_K \\ H_{K+1} \end{vmatrix} \right\} \quad (11)$$

Expanding this expression and combining similar terms one obtains

$$K_5 = \frac{5}{48} Q_{55}|_1 h_2 + \frac{11}{24} Q_{55}|_2 h_2 + \frac{5}{48} Q_{55}|_3 h_2 + b_{55}|_2 \frac{h_2}{2} \quad (12)$$

Comparing this to (10) we see that they are identical.

Thus, $\sigma_{z|_K}(x, \frac{h_2}{2}) = 0$ is satisfied independent of lamina orientation.